

Summer 8-10-2011

The Nucleocytoplasmic Shuttling Functions of P68 in Cancer Cell Migration and Proliferation

Haizhen Wang
Georgia State University

Follow this and additional works at: https://scholarworks.gsu.edu/biology_diss

Recommended Citation

Wang, Haizhen, "The Nucleocytoplasmic Shuttling Functions of P68 in Cancer Cell Migration and Proliferation." Dissertation, Georgia State University, 2011.
https://scholarworks.gsu.edu/biology_diss/113

This Dissertation is brought to you for free and open access by the Department of Biology at ScholarWorks @ Georgia State University. It has been accepted for inclusion in Biology Dissertations by an authorized administrator of ScholarWorks @ Georgia State University. For more information, please contact scholarworks@gsu.edu.

THE NUCLEOCYTOPLASMIC SHUTTLING FUNCTIONS OF P68 IN CANCER CELL
MIGRATION AND PROLIFERATION

by

HAIZHEN WANG

Under the Direction of Zhi-Ren Liu

ABSTRACT

P68 RNA helicase (p68), as a DEAD family protein, is a typical RNA helicase protein. P68 functions in many other biological processes, which include the regulations of the gene transcription, cell proliferation and cell differentiation. In our group, Y593 phosphorylated p68 was found to have a function in the epithelial mesenchymal transition, which is an important process for cancer metastasis. In the present study, we found that p68 is a nucleocytoplasmic shuttling protein. The protein carries two functional nuclear exporting signal sequences and two nuclear localization signal sequences. Calmodulin, a calcium sensor protein, is well known to play roles in cell migration by regulating the activities of its target proteins at the leading edge. Calmodulin interacts with p68 at the IQ motif of p68. However, the biological function of this interaction is not known. In this study, we found that the p68/calmodulin protein complex functions as a microtubule motor in migrating cells. The shuttling function of p68 along with the motor function of p68/calmodulin causes the leading edge distribution of calmodulin in migrating cells. Disruption the interaction between p68 and calmodulin inhibits cancer cell metastasis in an established mouse model. On the other hand, Y593-Y595 double phosphorylated p68 were found to interact with PKM2, an important tumor isoform of pyruvate kinase. The

shuttling function of p68 is reasoned to promote the dimer formation of PKM2 and transport the PKM2 to the cell nucleus. The nuclear PKM2 was found to function as a protein kinase to promote cell proliferation. In specific, the nuclear PKM2 phosphorylates and activates Stat3, an important transcription factor functions in cell proliferation. Overall, p68 is found to have functions in both cell migration and cell proliferation, and these two functions depend on the nucleocytoplasmic shuttling activity and the post-translational modification of p68.

INDEX WORDS: P68 RNA helicase, Calmodulin, PKM2, Nucleocytoplasmic shuttling, Cell migration, Cell proliferation

THE NUCLEOCYTOPLASMIC SHUTTLING FUNCTIONS OF P68 IN CANCER CELL
MIGRATION AND PROLIFERATION

by

HAIZHEN WANG

A Dissertation Submitted in Partial Fulfillment of the Requirements for the Degree of

Doctor of Philosophy

in the College of Arts and Sciences

Georgia State University

2012

Copyright by
Haizhen Wang
2012

THE NUCLEOCYTOPLASMIC SHUTTILING FUNCTIONS OF P68 IN CANCER CELL
MIGRATION AND PROLIFERATION

By

HAIZHEN WANG

Committee Chair: Dr. Zhi-Ren Liu

Committee: Dr. Jenny Jie Yang

Dr. Shi-Yong Sun

Dr. Ritu Aneja

Electronic Version Approved:

Office of Graduate Studies

College of Arts and Sciences

Georgia State University

May 2012

ACKNOWLEDGEMENTS

This dissertation would not have been possible without the help and support of many people. First and foremost, I would like to acknowledge Dr. Zhi-Ren Liu provided me the chance to study in his lab and gave me great instructions and supports in the past seven years. With his great support, so I can achieve the Ph.D. degree in China in 2007. With his great advice, so I can accomplish another Ph.D. program in Georgia State University in 2012. I am very grateful to my doctoral committees for their great advices and help in my research. Dr. Jenny Jie Yang afforded excellent supports and conveniences in my research project. Thanks also go to her great help to my family by providing a lot useful information for my son's education. I appreciate Dr. Shi-Yong Sun gave me great help in the IHC staining and great suggestions for my research. I would like to thank Dr. Aneja for her kind support for the animal experiments, including gifting the cell line.

I would like to acknowledge Dr. Xueliang Gao for his great help and suggestion in my research and my life. I could not continue the Ph.D. program in GSU without his great support and contributions. I would like to thank my old labmates: Liuqin Yang (Luke), Chunru Lin (Ruth), Christee Carter, Heena Dey, Lu Yin and Lixia Wei for their wonderful help during my study. Thanks also go to the new labmates: Xiaowei Liu, Liangwei Li, Chiayi Liu, Yin Wei, Bing Xu and Ravi. I would like to thank Nancy, Yanyi Chen, Gina, Jie Jiang, Alice and other members from Jenny's lab for their many detail technical assistances. I would like to thank Dr. Prasanthi Karna from Dr. Aneja's lab and Dr. Bo Li from Dr. Sun's lab for their great helps in my research work.

In the end, I would like to thank my parents and my parents in law for giving me great supports to let me accomplish my Ph.D. study.

TABLE OF CONTENTS

ACKNOWLEDGEMENTS	iv
LIST OF TABLES	xv
LIST OF FIGURES	xvi
LIST OF ABBREVIATIONS	xix
CHAPTER 1 INTRODUCTION	1
1.1 Cell migration and cancer metastasis	1
1.1.1 <i>Cell migration</i>	1
1.1.1.1 Molecular mechanism of process of cell migration	1
1.1.1.2 Major signaling pathways and regulations for cell migration	3
1.1.1.3 Ca²⁺/calmodulin in cell migration	4
1.1.2 <i>Cancer metastasis</i>	6
1.1.3 <i>The relationship between cell migration and cancer metastasis</i>	7
1.1.4 <i>Clinical significance of colon cancer metastasis and model for the colon cancer metastasis</i>	8
1.2 Cell proliferation	10
1.2.1 <i>Cell proliferation and tumor growth</i>	10
1.2.2 <i>Major signaling pathways in cell proliferation</i>	10
1.3 Tumor metabolism and metabolism adjustment	12
1.3.1 <i>Tumor metabolism</i>	13
1.3.2 <i>Metabolism adjustment in tumor</i>	13
1.4 Nuclear import and nuclear export	14
1.4.1 <i>Nuclear localization signal (NLS)</i>	15

1.4.2 <i>Nuclear exportation signal (NES)</i>	16
1.4.3 <i>The process of nucleocytoplasmic shuttling</i>	16
1.4.4 <i>The function of nucleocytoplasmic shuttling of proteins</i>	18
1.5 P68 RNA helicase (p68)	18
1.5.1 <i>General function of p68 as a member of DEAD-box protein</i>	18
1.5.2 <i>Biological function of p68</i>	20
1.5.3 <i>Posttranslational modification of p68</i>	21
1.5.4 <i>P68 and cancer</i>	22
1.5.5 <i>Cytoplasmic p68 and cancer</i>	23
1.6 Calmodulin	24
1.6.1 <i>Calmodulin is a conserved Ca²⁺ sensor protein</i>	24
1.6.2 <i>Calmodulin binding proteins</i>	25
1.6.3 <i>Calmodulin translocation in the cells</i>	25
1.7 PKM2	27
1.7.1 <i>PKM2 and tumor</i>	27
1.7.2 <i>Localization of PKM2</i>	28
1.8 Microtubule motor	29
1.8.1 <i>General information about microtubule and microtubule motor</i>	29
1.8.2 <i>The functions of microtubule motor and motor as an antitumor target</i>	30
1.8.3 <i>The functions of microtubule motors in cell migration</i>	31
1.9 Aims of the dissertation	32
CHAPTER 2 GENERAL MATERIALS AND METHODS	35
2.1 Nucleic acids related techniques	35

2.1.1 <i>Mini preparation for DNA</i>	35
2.1.2 <i>Midi preparation for DNA</i>	35
2.1.3 <i>Agarose gel electrophoresis and gel extraction of DNA</i>	36
2.1.4 <i>Quantification of DNA or RNA</i>	36
2.1.5 <i>Polymerase chain reaction (PCR) method</i>	37
2.1.6 <i>Restriction enzyme digestion and plasmids construction</i>	37
2.1.7 <i>Site-directed mutation method</i>	38
2.1.8 <i>Ethanol purification of DNA</i>	38
2.1.9 <i>RNA extraction from tissue</i>	39
2.1.10 <i>Reverse transcription PCR</i>	40
2.2 Bacterial techniques	40
2.2.1 <i>JM109 competent cell preparation</i>	40
2.2.2 <i>Bacterial culture and storage</i>	40
2.2.3 <i>Transformation</i>	41
2.3 Protein and peptide techniques	42
2.3.1 <i>HA-p68 protein expression and purification</i>	42
2.3.2 <i>Recombinant p68-CaM fusion protein expression and purification</i>	42
2.3.3 <i>Protein quantification</i>	43
2.3.4 <i>Sodium dodecyl sulfate polyacrylamide gel electrophoresis (SDS-PAGE)</i>	44
2.3.5 <i>Coomassie blue staining</i>	44
2.3.6 <i>ATPase assay</i>	45
2.3.7 <i>Motor assay</i>	46
2.3.8 <i>Microtubule pellet down assay</i>	46

2.3.9 Peptide purification	46
2.4 Mammalian cell techniques	47
2.4.1 Mammalian cell culture and storage	47
2.4.2 Transient transfection method	48
2.4.3 Stable cell line establishing	48
2.4.4 RNA interference	49
2.4.5 Growth factor treatment	50
2.4.6 Monolayer scratch treatment	50
2.4.7 Whole cell lysate preparation (both RIPA buffer and grind method)	50
2.4.8 Nuclear extract and cytoplasmic extract preparation	51
2.4.9 Immunoprecipitation (IP) and co-immunoprecipitation (Co-IP)	51
2.4.10 Calmodulin beads pull-down and GST beads pull-down	52
2.4.11 Western Blot	52
2.4.12 Boyden chamber assay	53
2.4.13 Recombinant adenovirus generation and infection in mammalian cells	54
2.4.14 Cell proliferation assay	55
2.4.15 Living cell imaging and fixed cell imaging	56
2.5 Animal experiment	57
2.5.1 Tumor implanting (subcutaneous tumor injection)	57
2.5.2 Tumor size measurement and tumor weight measurement at the end point	57
2.5.3 Tumor splenic metastasis examination	57
2.5.4 Tissue staining	58
2.6 Materials	58

CHAPTER 3 P68 IS A NUCLEOCYTOPLASMIC SHUTTLING PROTEIN	69
3.1 Abstract	69
3.2 Introduction	69
3.3 Results	70
3.3.1 P68 RNA helicase shuttles between the nucleus and the cytoplasm	70
3.3.2 Identification of NLSs and NESs of p68	71
3.3.3 P68 shuttles via a RanGTPase dependent pathway	74
3.4 Discussion	75
3.5 Materials and methods	78
3.5.1 Reagents, antibodies, and cells	78
3.5.2 Plasmids construction	78
3.5.3 Expression and purification of recombinant GST-p68	79
3.5.4 Interactions between p68 and importins	79
3.5.5 Heterokaryon analyses and immunofluorescence imaging	79
3.5.6 Computational homology structure modeling the helicase core of p68	80
CHAPTER 4 P68 RNA HELICASE AND CALMODULIN INTERACTION REGULATES CELL MOTILITY BY ACTING AS A MICROTUBULE MOTOR	95
4.1 Abstract	95
4.2 Introduction	95
4.3 Results	97
4.3.1 A peptide from p68 (a.a. 549 – 568) and GFP fusion of the peptide inhibit cancer metastasis	97

4.3.2	<i>The IQ peptide interrupts p68-calmodulin interaction that is essential for cell migration</i>	98
4.3.3	<i>The p68 and calmodulin interaction affect the localization of both calmodulin and p68 to the cytoplasm and to the leading edge of the migrating cells</i>	101
4.3.4	<i>P68 RNA helicase exhibits a calmodulin-dependent microtubule motor activity</i>	103
4.4	Discussion	107
4.5	Materials and methods	109
4.5.1	<i>Scratch-wound treatments</i>	109
4.5.2	<i>Microtubule pull- down</i>	109
4.5.3	<i>Microtubule gliding assay</i>	109
CHAPTER 5 PYRUVATE KINASE M2 REGULATES GENE TRANSCRIPTION BY ACING AS A PROTEIN KINASE		
5.1	Abstract	142
5.2	Introduction	142
5.3	Results	143
5.3.1	<i>Nuclear PKM2 activates transcription of MEK5 by phosphorylating stat3</i>	143
5.3.2	<i>Dimeric PKM2 is the active protein kinase</i>	148
5.3.3	<i>Expression of R399E increased stat3 phosphorylation in cells and promoted cell proliferation</i>	152
5.3.4	<i>PKM2 protein kinase substrates bind to the ADP binding site</i>	153
5.3.5	<i>Reciprocal regulation of protein kinase and pyruvate kinase activities of PKM2 by tyrosine phosphor-proteins</i>	154

5.4 Discussion	159
5.5 Materials and methods	161
5.5.1 Reagents, cell lines, antibodies, and plasmids construction	161
5.5.2 Expression and purification of recombinant PKM2 and PKM1	162
5.5.3 In vitro protein kinase and pyruvate kinase assays	162
5.5.4 Gel-mobility shift and super-shift assays	163
5.5.5 Size-exclusion chromatography and non-denaturing gel electrophoresis	164
5.5.6 PKM2 and peptide interaction	165
5.5.7 Nude mice xenograft	165
CHAPTER 6 CONCLUSION AND DISCUSSION	206
6.1 Shuttling and translocation of p68 in cell migration	206
6.1.1 P68 is a nucleocytoplasmic shuttling proteins and calmodulin binding regulates the nuclear exportation of p68 in migrating cells	206
6.1.2 Working model for the cytosol translocation of p68 through binding with Ca²⁺-calmodulin	207
6.1.3 Nucleocytoplasmic shuttling p68 facilitates the translocation of its binding proteins	209
6.1.3.1 P68 shuttles calmodulin out of nucleus and functions in cell migration	210
6.1.3.2 P68 shuttles beta-catenin and PKM2 to the nucleus	212
6.2 P68/calmodulin functions as a microtubule motor in migrating cells	213
6.2.1 P68/calmodulin functions as a motor in migrating cells	213
6.2.2 The leading edge transportation of calmodulin by motor unit of p68/calmodulin	

	214
6.2.3 <i>The putative signaling pathway in regulation the interaction between p68 and calmodulin</i>	215
6.2.4 <i>Other putative cytoplasmic function of p68</i>	218
6.3 Colon tissue array and mouse xenograft model for cancer metastasis	218
6.3.1 <i>Colon tissue array</i>	218
6.3.2 <i>Mouse xenograft model for cancer metastasis</i>	220
6.3.2.1 The subcutaneous implantation to study the colon cancer metastasis to spleen is a suitable system	220
6.3.2.2 Microscopic spleen metastasis was detected in spleen	221
6.3.2.3 About the structure of SW620 generated tumor	223
6.3.2.4 IQ peptide inhibited the cytosol translocation of p68 and tumor growth	224
6.4 Cell proliferation is contributed by the shuttling function of phosphorylated p68	226
6.5 Phosphorylated p68 may promote the dimer transformation of PKM2 and regulate the metabolism in the cancer cells	227
REFERENCES	229
APPENDICES	245
A. THE RECOMBINANT β SUBUNIT OF C-PHYCOCYANIN INHIBITS CELL PROLIFERATION AND INDUCES APOPTOSIS	245
A.1 Abstract	245
A.2 Introduction	245
A.3 Materials and methods	247

<i>A.3.1 Cell lines and culture</i>	247
<i>A.3.2 Plasmid construction</i>	247
<i>A.3.3 Expression, purification, concentration and refolding of the recombinant C-PC/β</i>	247
<i>A.3.4 Proliferation of cancer cells and non-cancer cells</i>	248
<i>A.3.5 Immunofluorescent confocal microscopy</i>	248
<i>A.3.6 Apoptosis, caspases activities, and cell cycle analyses</i>	249
<i>A.3.7 GST pull-down and co-immunoprecipitation</i>	249
<i>A.3.8 Soluble and assembled tubulin / actin</i>	250
<i>A.3.9 Subcellular localization of GAPDH</i>	251
A.4 Results	251
<i>A.4.1 Expression and purification of recombinant C-PC/β in E. coli</i>	251
<i>A.4.2 The C-PC/β inhibited cell proliferation</i>	252
<i>A.4.3 Recombinant C-PC/β induces apoptosis and cell cycle arrest</i>	252
<i>A.4.4 Recombinant C-PC/β was accumulated on the plasma membrane</i>	253
<i>A.4.5 C-PC/β interacted with β -tubulin in the cell membrane promoting depolymerization of microtubules</i>	254
<i>A.4.6 C-PC/β interacted with GAPDH and promoted GAPDH redistribution</i>	255
A.5 Discussion	256
A.6 References	257
B. P68 IS A POTENTIAL SUBSTRATE OF CASPASE 3	268
B.1 Materials and methods	268
<i>B.1.1 Apoptosis induction of SW480 cells by Oxiplantin</i>	268

B.1.2 <i>Plasmids construction and truncates of p68 expression</i>	268
B.2 Results	269
B.2.1 <i>Three putative cleavage sites of p68 by Caspase 3</i>	269
B.2.2 <i>P68 can be cleaved by Caspase 3</i>	269
B.2.3 <i>Expression of F4 truncate of p68 activates Caspase 3 in cells</i>	269
C. P68/CAM MAY HAVE A FUNCTION IN PC-12 DIFFERENTIATION	275
C.1 Material and method	275
C.2 Result	275
C.2.1 <i>P68 and calmodulin colocalized at the leading edge of the dendrites in PC-12 cells</i>	275

LIST OF TABLES

Table 1 The setup for HPLC pump	47
Table 2 Antibodies and proteins	58
Table 3 Primers	60
Table 4 Mammalian cell lines	65
Table 5 Chemicals	66
Table 6 Experimental kits	68

LIST OF FIGURES

Figure 3.1 Phosphor-p68 promotes β-catenin nuclear localization in SW620 cells	81
Figure 3.2 P68 shuttles between the nucleus and the cytoplasm	83
Figure 3.3 NLSs of p68	85
Figure 3.4 NESs of p68	87
Figure 3.5 NESs and NLSs of p68	89
Figure 3.6 P68 nucleocytoplasm shuttling is RanGTPase pathway dependent	91
Figure 3.7 P68 interacts with importins <i>in vitro</i>	93
Figure 4.1 Pep IQ inhibited the cancer metastasis	111
Figure 4.2 P68 and calmodulin interactions	113
Figure 4.3 P68 and calmodulin interaction is essential for cell migration and for localization of calmodulin to the leading edge of migrating cells	115
Figure 4.4 Cytosol localization of p68 in the migrating cells among the tumor tissues	119
Figure 4.5 P68 and calmodulin interact with microtubule	121
Figure 4.6 Microtubule stimulates the ATPase activity of p68	124
Figure 4.7 P68-calmodulin has a microtubule dependent motor activity	126
Figure Supplement 4.1	128
Figure Supplement 4.2	130

Figure Supplement 4.3	132
Figure Supplement 4.4	134
Figure Supplement 4.5	136
Figure Supplement 4.6	138
Figure Supplement 4.7	140
Figure 5.1 PKM2 regulates MEK5 transcription	166
Figure 5.2 PKM2 upregulates MEK5 transcription via activation of Stat3	169
Figure 5.3 PKM2 upregulates MEK5 transcription by promoting Stat3 DNA interaction and phosphorylation of Stat3	171
Figure 5.4 Phosphorylation of GST-Stat3 by the rPKM2	174
Figure 5.5 Dimeric PKM2 is active protein kinase and expression of the R399E mutant promotes cell proliferation	176
Figure 5.6 The effects of PKM2 protein kinase activity on tumor growth	179
Figure 5.7 Tyrosine phosphorylated p68 interacts with PKM2	181
Figure 5.8 Tyrosine phosphor-protein/peptide reciprocally regulates protein kinase and pyruvate kinase activity of PKM2	184
Figure 5.9 Growth stimulation activates protein kinase activity of PKM2	187
Figure Supplement 5.1	189

Figure Supplement 5.2	191
Figure Supplement 5.3	194
Figure Supplement 5.4	196
Figure Supplement 5.5	198
Figure Supplement 5.6	200
Figure Supplement 5.7	202
Figure Supplement 5.8	204
Figure 6.1 Working model about p68 cytosol exportation under the binding of Ca²⁺-calmodulin	209
Figure 6.2 Putative signaling pathway in the regulation of the interaction between p68 and calmodulin	217
Figure A.1	260
Figure A.2	261
Figure A.3	262
Figure A.4	264
Figure A.5	266
Figure B.1 Three putative cleavage sites of p68 by active Caspase 3	270
Figure B.2 P68 was cleaved by activated Caspase 3	271
Figure B.3 Truncates of p68 activated Caspase 3	273
Figure C.1 P68 and calmodulin colocalized at the leading edge of the dendrites in PC-12 cells	276

LIST OF ABBREVIATIONS

GAPDH: Glyceraldehyde-3-phosphate dehydrogenase

P68: P68 RNA helicase

PKM2: Pyruvate kinase M2

NES: Nuclear exporting signal

NLS: Nuclear localization signal

ECM: Extracellular matrix

HIF: Hypoxia-inducible factors

CHAPTER 1

INTRODUCTION

1.1 Cell migration and cancer metastasis

1.1.1 *Cell migration*

Cell migration refers to the translocation of cell from one site to another site. It has functions in regular biological processes including wound healing, embryonic development and immune response; cell migration is also involved in different disease processes such as tumor formation, cancer metastasis, mental retardation and vascular disease. There are two major schemes for the cell migration (Bretscher 1996): First, extension of the cell in the front by polymerization of the actin filaments at the leading edge (polarized actin cycle); Second, extension of the cell surface by exocytosis at the leading edge (polarized endocytic cycle). In the polarized actin cycle scheme, the actin filament ahead of the nucleus is constantly depolymerized to provide actin monomers; the actin monomers diffuse to the front of the cell and polymerize there, which pushes the leading edge forward. In the polarized endocytic cycle, a lipid flow in the plasma membrane is generated when endocytosis occurs at the front of the cell surface. The cell is pushed forward when the lipid flow pushes on substratum-attached feet.

1.1.1.1 Molecular mechanism of process of cell migration

In general, the process of cell migration is considered to involve several steps: polarization, protrusion and adhesion, translocation of the cell body and retraction of the rear (Bretscher 1996).

Polarization in the process of cell migration refers to the molecular and functional differences between the front and back in cells (Ridley, Schwartz et al. 2003). The cell can polarize with or without the extracellular asymmetric stimulation (Wedlich-Soldner and Li 2003). Polarization may be caused by adhesion to the substratum or the formation of lateral contacts

with other cells. A polarized influx of extracellular signal may determine the asymmetric recruitment or activation of signaling proteins in the cell. The consequence of this influx will create morphological and functional asymmetry. The gradients of stimuli, including chemoattractants, induce the polarized signals and generate a protrusion at the front of cell which faces to the highest concentration of the gradient (Iglesias and Devreotes 2008). Monolayer scratch assay can also generate cell polarization towards the scratch area (Goulimari, Kitzing et al. 2005). The composition of the plasma membrane may reflect the functional polarization in some cases. Interestingly, cells can be induced into polarization even when the chemoattractants are loaded in a non-polarized and homogeneous manner (called chemokinesis) (Verkhovsky, Svitkina et al. 1999). The front area may be generated first in the polarizing process; while the rear area may be created before the front area has been established. Chemoattractants generate the asymmetry by activating some specific receptors, such as G-protein coupled receptor (GPCR) (Cotton and Claing 2009; Swaney, Huang et al. 2010), which is considered to be evenly distributed on the cell membrane in the resting cells. The small difference in gradient between the front and the rear regions of the cell leads to the asymmetrical activation of the receptor. This small gradient difference can be amplified by activation of receptor, as the receptor will recruit and activate the signaling adaptors and their downstream targets. The cells will then be polarized, and protrusion can be achieved after the polarization.

Protrusion usually involves the polymerization and depolymerization of the actin. The growth of the actin filaments pushes the leading edge to move forward. The extension of cellular membranes is also involved in the protrusion process. The leading edge protrusion faces the direction of movement in most cells. Protrusions usually respond to chemoattractants. When there is no directional extracellular stimulation, cells may probe and explore the surrounding

environment by forming the protrusion. Several cellular processes are required to form the protrusions. The dynamic polymerization of the actin pushes the membrane forward. The trafficking and the fusion of membrane-containing vesicles support the membrane expansion. At the same time, the protrusion needs to adhere to the basement to prevent the membrane moving backward. Cell body translocation is driven by the contraction of the actomyosin cytoskeleton in a harmonized way. The detailed mechanism is not well understood.

In order to retract the rear part of the cell, contraction of the actin filaments and disassembly of the adhesion at the rear edge are required. There are several mechanisms to promote adhesion disassembly. In brief, the contraction of actomyosin generates the force against the adhesion to disassemble adhesions (Chrzanowska-Wodnicka and Burridge 1996); microtubules play an important role in the disassembly of the adhesion (Kaverina, Krylyshkina et al. 1999); the endocytosis of integrins also facilitates the dissociation of the adhesion (Gomes, Jani et al. 2005); and the cleavage of the focal adhesion proteins helps in the retraction of the rear (Chan, Bennin et al. 2010). All these mechanisms facilitate the retraction of the rear part of the cell.

1.1.1.2 Major signaling pathways that regulate cell migration

Cells migrate in a specific direction in response to different stimuli, such as growth factors, chemokines or ECM molecules. The cell surface receptors are engaged by these factors. The receptors will initiate a series of cellular events. Briefly, G protein coupled receptors and receptor tyrosine kinases are activated, while GEFs are stimulated to activate CDC42. The lipid kinases are in activated form, and the activated Rac is then recruited. Along with the activation of Rac and/or Cdc42 in the local region, other regulators, including WASP/WAVE family proteins and Arp2/3 complex, are stimulated to branch actin filament at the leading edge (Cory

and Ridley 2002) (Ridley, Schwartz et al. 2003). A protrusion in the direction of migration is formed. The growth of the actin filament is regulated by the proteins that sever the existing filaments, cap the growing filaments, and control the availability of the monomeric actins. Activation of Rac and Cdc42 at specific area will decrease the activity of Rho and enhance the activity of PI3K, which then lead to the production of PIP3 at the leading edge (Devreotes and Janetopoulos 2003). The reorientation of the MTOC facing the leading edge that leads to the growth of microtubules and transport vesicles to the leading edge is also mediated by Cdc42 (Etienne-Manneville and Hall 2003). Adhesion proteins including integrins are activated by PI3Ks, PKCs, and Rap. Those adhesion proteins stabilize the cell protrusion by connecting the actin filaments to the leading edge structure. The adhesion molecules recruit additional integrins and form adhesions by signaling to Rac. The activity of Rac, Cdc42, and PI3K is reinforced by recruitment of these additional integrins. Sensitization of the receptors at the leading edge during the cell polarization favors the continuous movement in the same direction. The cycle of cell migration is completed when the adhesions are disassembled and the rear is retracted (Ridley, Schwartz et al. 2003). FAK, ERK, Src, and the protease calpain are important molecules to signal the disassembly of adhesions (Alahari, Reddig et al. 2002; Brahmabhatt and Klemke 2003). Microtubule dynamics play an additional role in disassembling of the adhesions. Rho kinase, with low activity at the leading edge and high activity at the rear, plays an important role in retraction at rear side of cells in a myosin dependent manner (Ridley, Schwartz et al. 2003).

1.1.1.3 Ca²⁺/calmodulin in cell migration

Ca²⁺/calmodulin is an important factor in regulating cell migration. Regulation of cell migration by Ca²⁺/calmodulin is demonstrated in many signaling pathways in multiple processes.

Importantly, Ca^{2+} /calmodulin is known to regulate many molecules that participate in the major signaling pathways of cell migration.

G protein coupled receptors (referred to as GPCR) are transmembrane receptors that sense the migration signals through the extracellular domain and subsequently activate intracellular domain to activate G proteins. G protein coupled receptor kinases (refers to GRKs) phosphorylate the GPCR at the specific site to regulate the activity of GPCR. Calmodulin is found to regulate the activity of a number of GRKs, such as GRK5, in a Ca^{2+} -dependent manner (Pronin, Satpaev et al. 1997).

IQGAP1 is a RasGAP-related protein that functions as a scaffold protein and plays a role in cell migration. IQGAP1 is known to interact with the cytoskeleton, and bind to actin, Rho family members, and E-cadherin. Interestingly, binding of calmodulin to IQGAP1 regulates its association with Cdc42 and actin (Ho, Joyal et al. 1999). On the other hand, calmodulin regulates the binding of E-cadherin to IQGAP and consequently affects the cell-cell adhesion (Li, Kim et al. 1999).

The Arp2/3 complex controls the rate of actin polymerization to induce membrane protrusion, which is important in cell migration. Caldesmon, presented in the membrane ruffles, slows down the Arp2/3-induced actin polymerization. Interestingly, Ca^{2+} /calmodulin reverses this inhibitory effect (Yamakita, Oosawa et al. 2003).

PI3-kinase has multiple functions in cell migration as the activation of PI3-kinase has been linked to actin rearrangement, tubulin binding, and membrane ruffling (Ridley 1994; Wennstrom, Hawkins et al. 1994; Kapeller, Toker et al. 1995; Martin, Haruta et al. 1996). Importantly, calmodulin is found to be able to activate PI3-kinase (Joyal, Burks et al. 1997).

All those examples illustrate that Ca^{2+} /calmodulin is an important regulator in the process of cell migration. Since many regulating events by Ca^{2+} /calmodulin occur at the leading edge, translocation of calmodulin to the leading edge is very important.

1.1.2 *Cancer metastasis*

Cancer metastasis is an event about the spreading of cancer cells to the nearby/distant site(s) that are not immediately adjacent to the primary tumor site. Cancer cells may spread by invasion through blood vessels and/or lymph vessels. The cancer cells may also spread by penetration into the body cavity or the places surrounding the organs. The process of metastasis includes local invasion, intravasation, transport, extravasation, formation of micrometastases, and colonization (Steeg 2006). The initiation process for metastasis is the cancer cell invasion. During the invasion step, the adherence junctions between cells, and between cell and the extracellular matrix (ECM), undergo dramatic changes. These changes allow cancer cells to detach from the primary tumor. The cells gain the capability of migration through the tissues. Integrins are important transmembrane proteins that mediate the adhesion between tumor cells and ECM (Friedl and Wolf 2003); while cadherins are important proteins for the cell-cell adhesion. Inside the cell, the cadherins can signal to catenins and actin cytoskeleton in order to regulate the movement of the cell (Cavallaro and Christofori 2004). The movement of most tumor cells during invasion is dynamic. The tumor cells adhere to the ECM at the leading edge of the cells. At the trailing edge, tumor cells detach from the ECM. Thus, the cell will move forward. Growth factor and chemokines can stimulate tumor cell migration.

During the process of intravasation, the tumor cells invade through the basal membrane and get into the lymphatic or blood vessels. When the tumor cells get into the blood stream, the tumor cells must survive and avoid immune attack. The factors that affect the survival of the

tumor cells are: velocity-induced shear forces, lack of a substratum, and the existence of immune cells (Steeg 2006). In order to extravasate from the blood circulation, the tumor cells need to be arrested at the specific area in the circulatory system. The tumor cells may be arrested by nonspecifically binding to the coagulation factors, thereby the cells may be restricted in the capillary beds because of the size of the cells. In certain cases, tumor cells may specifically adhere to the surface of endothelial cells (Weiss, Grundmann et al. 1986). When the endothelial retraction is induced, tumor cells attach to the subendothelial ECM and the capillary is reformed after the tumor cells extravasate from the blood circulation.

When the tumor cells get into the new distant organ by invasion through the vessel wall, they form micrometastases at the beginning, and they may grow progressively to form macrometastases. This process is termed metastatic colonization. This process involves the interaction between tumor cells and the surrounding cells in this distant organ. However, the colonization efficiency is very low. During the process of cancer metastasis, only 2.5% of cancer cells that survived in blood circulation extravasate to form micrometastasis. And only 1% of the micrometastasis can grow to form macroscopic metastasis, as some of the metastasized cells may get into the dormant situation (Luzzi, MacDonald et al. 1998).

1.1.3 The relationship between cell migration and cancer metastasis

Cell migration is considered as the first step of the cancer metastasis (Steeg 2006), as the tumor cells need to invade (migration) through the surrounding tissue at the primary site to spread the cells to the distant organ. Successful invasion (including migration) is required for the tumor cells metastasize to the distant organ. Theoretically, cancer metastasis can be stopped if the cell migration is inhibited.

However, the process of cancer metastasis is more complicated than the process of cell migration. Many microenvironmental factors (including surrounding non-cancer cells) are involved in promoting metastasis. These factors are constantly changed when the cancer cells spread to the different locations. Instead, the study of the cell migration is often performed using the simplified *in vitro* system. We only consider one factor or several combined factors in studying the mechanism of the cell migration. Therefore, animal model for cancer metastasis is often applied to further test the mechanism that has been illustrated in *in vitro* system.

1.1.4 *Clinical significance and model of colon cancer metastasis*

The second leading cause of death in the U.S. is cancer (Death: Preliminary data for 2009 from National Vital Statistic Reports). About 90% of cancer patient death is due to metastasis. Therefore, elucidation of the molecular mechanism that regulates the migratory activity of cancer cells is very important.

Colon cancer is the second leading cause among all cancer types in the United States (from National Cancer Institute at the National Institutes of Health). Over half of the colon cancer patients develop metastasis. Around 50% of patients suffer from liver metastasis, and around 15% of the patients produce lung metastasis (Chambers, Groom et al. 2002).

There are very few models of colon cancer metastasis except the locally invasive models, even though there are many genetic mouse models of benign adenoma. Unlike in humans, there are no genetic mouse models which can spontaneously form tumors in the intestines, become invasive and metastasize to the other organs. Since most of the colon cancer mortality is due to the cancer metastasis, it is very important to study the colon cancer metastasis. The transplantation (xenograft) models are therefore becoming the suitable model to study the colon cancer metastasis at the current stage (Taketo and Edelman 2009). The xenograft models of the

colon cancer used to study the colon cancer metastasis include intrarectal implantation of the colon cancer cells (Tsutsumi, Kuwano et al. 2001), orthotopic implantation of the tumor tissue (Sun, Sasson et al. 1999) or tumor cells (Cespedes, Espina et al. 2007), and subcutaneous implantation of tumor cells. However, every model has its own benefits and shortcomings. For intrarectal implantation, the tumor cells can only metastasize to the nearby lymph nodes but not to the distant organs. For orthotopic implantation of the human tumor tissue or tumor cells, even though the cancer cells metastasize to the distant organ, the procedure is quite complicated (may not be suitable for the experiment with many mice). Meanwhile, research shows that injection of SW620 cells at the orthotopic site (intracaecal) does not generate liver metastasis as examined by gross inspection and histological examination 10 weeks after tumor cell injection. The growth of SW620 tumors at the orthotopic sites appears much slower than that at the subcutaneous site (Hewitt, McMarlin et al. 2000). On the other hand, the procedure is quite simple for the subcutaneous implantation of the colon cancer cells. Even though the distant organ metastasis of the tumor is not directly observed (not macrometastasis), trace amount of the tumor cells metastasis to the spleen has been successfully detected by RT-PCR technique (micrometastasis).

There are other systems that have been generated to study the colon cancer metastasis. For example, colon cancer cells are injected into the blood circulation through tail vein (Cambien, Karimdjee et al. 2009) or cardiac ventricle (Ma, Rong et al. 2008). Those methods are good systems to study extravasation and colonization. However, those methods skipped the invasion and intravasation steps of cancer metastasis. They are not good systems if the target molecules play major roles in the invasion step of cancer metastasis.

1.2 Cell proliferation

1.2.1 Cell proliferation and tumor growth

Cell proliferation refers to the increase in the cell number by cell division. The function of cell proliferation is to maintain the cell amount to a certain level. The cell proliferation rate is determined by cell division rate (cell cycle) and cell apoptosis rate. Cell proliferation proceeds through the following steps: first, growth factors bind to the receptors on the cell surface; second, the receptors are linked to the signaling molecules and convey the message into the nucleus; third, transcription factors bind to DNA to turn on/off the corresponding genes; fourth, the above events will lead to the cell division. Any changes in step during cell proliferation will lead to the change of the cell proliferation rate. The induction of tumor is the consequence of the cell proliferation being out of control. In tumors, factors that involve signaling pathways of cell proliferation are altered due to accumulation of genetic and epigenetic alterations. The alterations of signaling factors lead to the alteration of cell cycle and apoptosis. As a consequence, cell proliferation is altered (Evan and Vousden 2001).

1.2.2 Major signaling pathway in cell proliferation

The cell proliferation process is complicated. It involves multiple signaling pathways and interconnects with other biological processes including apoptosis (Sears and Nevins 2002). One central player in the cell proliferation is the retinoblastoma tumor suppressor protein (Rb). In this pathway, the D-type G1 cyclins and the associated kinases (Cdk4 and Cdk6) initiate the phosphorylation of Rb and Rb family proteins (p130 and p170) to inactivate their binding to E2F transcription factors (E2F1, E2F2, and E2F3a). This event leads to the accumulation of E2F member proteins and activation of the transcription of a number of genes. Transcriptions of those genes are required for cell cycle progression and DNA replication. Meanwhile, phosphorylation

of Rb and p130 can disrupt its interaction with other E2F member proteins (E2F3b, E2F4, and E2F5), which play a role in the repression of transcription of the S phase genes (Sears and Nevins 2002). Rb can be further phosphorylated and inactivated by the E2F target genes cyclin E and the associated kinase Cdk2, which will lead to continual inactivation of Rb. On the other hand, small protein inhibitors CKIs (including p21, p27 and p16) negatively regulate the activity of the G1 Cdk. All these proteins participate in the Rb/E2F pathway that plays a central role in regulating cell proliferation.

Myc proteins are demonstrated to play an essential role in normal cell function. Several target genes for Myc have been identified. Expression of these genes promote cell proliferation (Dang 1999). Myc can directly activate the transcription of cyclin D1 and D2, Cdk4 (cyclin D partner), and Cdc25A (phosphatase in removing negative regulatory phosphates from the Cdk). These transcription activities activate the G1 cyclin-dependent kinase. In the Myc induced cell proliferation, the activity of cyclin E/Cdk2 is induced when Myc is expressed (Beier, Burgin et al. 2000). Myc expression leads to the down regulation of p27 CKI as well as the sequestration of p27 (Rudolph, Saffrich et al. 1996; Bouchard, Thieke et al. 1999). Interestingly, Myc directly contributes to the activation of E2F proteins (E2F1, E2F2 and E2F3), which can induce G1 to S phase transition (Leone, DeGregori et al. 1997; Sears, Leone et al. 1999; Adams, Sears et al. 2000).

The Ras proto-oncogene has a critical function in cell growth. The function of Ras in cell growth is mediated by Ras effector molecules. The Raf/MEK/ERK kinase cascade is one of the Ras effector that is primarily involved in signaling from plasma membrane to nucleus (Seeger and Krebs 1995). The Ral GTPase signaling pathway, another Ras effector pathway, is involved in G1 to S phase progression (Gille and Downward 1999; Marshall 1999). The third Ras effector

signaling pathway, the PI3-K/AKT pathway, is mainly involved in cell survival signaling (Kennedy, Wagner et al. 1997). All these three Ras effector pathways are activated by Ras-GTP and are involved in initiating cyclin D1 gene transcription and activating cyclin D1/Cdk4 kinase (Robles, Rodriguez-Puebla et al. 1998). These three Ras effector pathways act cooperatively in cell proliferation.

1.3 Tumor metabolism and metabolism adjustment

1.3.1 *Tumor metabolism*

The metabolism in cancer cells is not the same as that in normal cells (Merida and Avila-Flores 2006). Normal cells utilize the oxidative phosphorylation to generate energy, and glycolysis in normal cells is tightly regulated as the glycolysis is inhibited in the presence of oxygen. Cancer cells prefer to metabolize glucose by glycolysis to produce energy even in the presence of sufficient oxygen (Warburg 1956; Kondoh, Lleonart et al. 2007).

Interestingly, the efficiency of producing ATP by the glycolysis process is much lower than that by the oxidative phosphorylation. In the glycolysis, one molecule of glucose generates two molecules of pyruvate and two molecules of ATP. Pyruvate, as the product of glycolysis, has different fates in mammalian cells. Pyruvate can be catalyzed into lactate by lactate dehydrogenase when the oxygen level is low. This process is called anaerobic glycolysis. Pyruvate can also be converted into acetyl coenzyme A by the pyruvate dehydrogenase complex when the oxygen level is high. In the citric acid cycle, acetyl coenzyme A is used to generate electrons in the mitochondria. The electrons create an electron gradient which leads to the generation of a pH gradient across the inner mitochondrial membrane. The pH gradient can lead to the generation of ATP by ATP synthase. This process is named as aerobic oxidative phosphorylation. One acetyl CoA molecule can produce two molecules of NADH, one molecule

of FADH₂, and eight molecules of electrons in the citric acid cycle. By the oxidative phosphorylation process, one molecule of glucose can be completely degraded into H₂O and CO₂ and produce 38 molecules of ATP. Clearly, the generation of ATP is more efficient by the oxidative phosphorylation than by the glycolysis.

1.3.2 Metabolism adjustment in tumor

Why cancer cells prefer glycolysis instead of oxidative phosphorylation to generate ATP is not well understood. Interestingly, there are a lot of phosphointermediates generated in the glycolysis. The phosphointermediates can be used by the cancer cell to synthesize macromolecules including lipids, proteins, and nucleic acids, which may facilitate the tumor growth. This may be the most important reason for the switch of the metabolism pathways in cancer cells. On the other hand, the switch to the glycolysis may avoid the apoptosis of the cancer cells as activation of the oxidative phosphorylation may promote cancer cell apoptosis (Bonnet, Archer et al. 2007). Finally, employing the glycolysis pathway may support cancer-specific signaling. Since specific metabolite (such as lactate) from glycolysis might be concentrated in the tumor cells and allow the tumor cells to engage in metabolite-mediated autocrine and paracrine signaling that does not occur in the normal tissues.

There are two possible ways to alter the metabolism in cancer cells. First, the tumor microenvironment drives changes in metabolism. As the tumor expands, the local blood supply is limited. This can lead to hypoxia and stabilize the hypoxia-inducible transcription factor (HIF). The activation of HIF leads to the overexpression of glycolytic enzymes as well as glucose transporters. Nearly all glycolysis enzymes, including hexokinase, phosphofructokinase, aldolase, pyruvate kinase and lactate dehydrogenase, are upregulated by activation of HIF-1 (Semenza 2007). More energy can be provided to cancer cells as the overexpression of those glycolytic

enzymes increase the rate of glycolysis. Meanwhile, activation of HIF stimulates angiogenesis as HIF induces VEGF expression from cancer cells. Second, several important oncogenes and tumor suppressor genes are known to regulate glycolysis in cancer cells and induce the shift to the glycolysis. Those genes include AKT, c-Myc, AMPK, Ras and p53. Akt is a serine/threonine kinase and is amplified in different cancers. Akt regulates glycolysis through several mechanisms, such as upregulation of glucose transporter to increase glucose uptake (Plas, Talapatra et al. 2001), stimulation of the hexokinase activity to convert glucose to glucose-6-phosphate (Rathmell, Fox et al. 2003), and regulation of phosphofructokinase activity to control glycolysis rate (Deprez, Vertommen et al. 1997). C-Myc is a nuclear oncoprotein which is constantly active in many malignant tumors (Elliott, Ge et al. 2000). C-Myc regulates transcription of many glycolysis-related genes, including glucose transporters, hexokinase, phosphofructokinase and pyruvate kinase (Gordan, Bertout et al. 2007). AMP-activated protein kinase (AMPK), is a master regulator for controlling energy metabolism. AMPK is reported to regulate glucose consumption by controlling the transcription of glucose transporter and translocation of this transporter to the cell surface (Russell, Bergeron et al. 1999). P53 is an important tumor suppressor. P53 is inactivated in more than half of cancers (Hainaut and Hollstein 2000). Activation of p53 causes the downregulation of transcription of several glycolytic enzymes, such as phosphoglycerate mutase and glucose transporters (Schwartzenberg-Bar-Yoseph, Armoni et al. 2004).

1.4 Nuclear import and nuclear export

Eukaryotic cells have nuclear envelope that creates two distinct cellular compartments in the cells. Even though these two separated compartments have unique functions by themselves, their functions are interconnected. In order for the nuclear and cytoplasmic processes to act in

concert, communication between the nucleus and the cytoplasm by exchange of proteins and other molecules are needed. The nuclear import refers to the process by which specific molecules move into the nucleus, and the nuclear export refers to the process by which specific molecules come out from the nucleus. The nuclear pore complexes (NPC), which is a large protein complex that crosses the nuclear envelope, is the place that allows the exchange components to get in/out of the nucleus (Alber, Dokudovskaya et al. 2007). Nucleoporins are the major proteins that make up the nuclear pore complex (NPC). About half of the nucleoporins have a typical alpha solenoid or beta-propeller fold structure. The other half is a group of very flexible proteins due to its native unfolded characteristic. The components of the NPC allow the pore to be dilated to around 26 nanometers wide from 9 nanometers at the opening status.

1.4.1 Nuclear localization signal (NLS)

NLS is a short stretch of amino acids that mediates the transportation of proteins into the nucleus. Typically, NLS consists of one or more short sequences of positively charged lysines or arginines. Some NLSs are glycine-rich with few positive charged residues (Bonifaci, Moroianu et al. 1997). The NLSs can be divided into classical NLSs and non-classical NLSs. Classical NLSs can be divided into two types: monopartite and bipartite (Boulikas 1994). Typically, the monopartite motif has a cluster of basic residues preceded by a helix-breaking residue. The bipartite motif has two clusters of basic residues with 9-12 non-charged residues in between. Classical NLSs can be recognized by importin- α . Interestingly, most of the non-classical NLSs can be recognized by importin- β (considered as import mediate). Studies show that quite a lot of NLS motifs bind to DNA (Cokol, Nair et al. 2000).

1.4.2 Nuclear exportation signal (NES)

NESs have a very important function in regulating the subcellular location of proteins. Subcellular translocation of proteins affects the transcription and other nuclear processes. The well known NESs are leucine-rich sequence motifs. The first NESs were identified in 1995 in the human immunodeficiency virus type 1(HIV-1) Rev protein (Fischer, Huber et al. 1995) and cAMP-dependent protein kinase inhibitor (PKI) (Wen, Meinkoth et al. 1995). NESs are now extended to the motifs that contains multiple hydrophobic amino acids residues including L, V, I, and M. CRM1 has been illustrated to be the export receptor for proteins containing the leucine rich NESs. The transport mediated by CRM1 can be effectively inhibited by the fungicide leptomycin B (LMB) (Fornerod, Ohno et al. 1997), as LMB can covalently bind to a cysteine residue in CRM1 (Kudo, Matsumori et al. 1999). RanGTP and proteins with leucine-rich NESs are considered to bind cooperatively to CRM1 and form a ternary CRM1-RanGTP-NES complex (la Cour, Kiemer et al. 2004). This complex can be diffused to the cytoplasm, where GTP is hydrolysed and the NES-cargo protein is released. CRM1-RanGDP will diffuse back to the nucleus and be reused. CRM1 mediated export is a tightly regulated process, as not all NES substrates can be exported constitutively from the nucleus. The NES-dependent export is regulated by several mechanisms: masking/unmasking of NESs (Craig, Zhang et al. 2002), phosphorylation (Brunet, Kanai et al. 2002), and forming a disulfide bond (Kuge, Arita et al. 2001).

1.4.3 The process of nucleocytoplasmic shuttling

Nucleocytoplasmic shuttling refers to the transport of water-soluble molecules across the nuclear envelope by a back and forth manner. The transported water-soluble molecules include RNA, ribosomes, proteins, carbohydrates, and signal molecules. Some of them are transported in

a one-way manner, such as RNA moves from the nucleus to the cytoplasm (Rodriguez, Dargemont et al. 2004). Others can be transported out and into the nucleus. Many proteins (Rehberg, Lischka et al. 2002; Lahaye, Lespinasse et al. 2010) have been reported to shuttling between the nucleus and the cytoplasm. Although small molecules (<30 kDa) cross the NPC by simple diffusion, large molecules may need to carry a specific signal sequence (NLS and/or NES) with the help of the nucleoporins to get through the nuclear envelope.

Ras-related nuclear protein (Ran) is a small 25 kDa protein that is known to be transported into and out of the cell nucleus during interphase (Moore and Blobel 1994; Dasso and Pu 1998). Ran is a GTP binding protein. Ran exists in the cell in GDP-bound and GTP-bound forms. With the action of RCC1 (RanGEF, Ran Guanine nucleotide Exchange Factor), RanGDP can be converted to RanGTP. The GTPase activity of Ran can be activated by interaction with Ran GTPase activating protein (RanGAP). The conversion of RanGTP to RanGDP is through the activation of the Ran GTPase. Since RCC1 is located inside of the nucleus and RanGAP is bound to the cytoplasmic side of the nuclear pore complex, the ratio of RanGTP to RanGDP is high inside the nucleus and low outside the nucleus. Meanwhile, the protein concentration of Ran is higher in the nucleus than that in the cytoplasm. The nucleocytoplasmic gradient of RanGTP powers the import cycle. Ran interacts with karyopherins (act as importin or exportin) and changes their ability to bind or release cargo molecules, therefore facilitates the transport of proteins across the NPC. When the cargo proteins carry NLS(s), the proteins bind to importin and are transported into the nucleus. In the nucleus, RanGTP binds to the importin and the imported cargo protein are released. Importin will then be diffused back to the cytoplasm and used for another cycle. When the cargo proteins carry NES(s), the proteins

bind to the exportin together with RanGTP. When GTP is hydrolyzed to GDP outside of the nucleus, the exported cargos are released.

1.4.4 *The function of nucleocytoplasmic shuttling of proteins*

After the demonstration of nucleolin as the first nucleocytoplasmic shuttling protein in 1989 (Borer, Lehner et al. 1989), many different nucleocytoplasmic shuttling proteins have been identified. They are many RNA binding proteins (Nakielny and Dreyfuss 1999; Shyu and Wilkinson 2000), cell cycle regulators (Yang and Kornbluth 1999), transcription factors (Cartwright and Helin 2000), transport receptors and adaptors (Gorlich and Kutay 1999; Nakielny and Dreyfuss 1999), and steroid hormone receptors (Hache, Tse et al. 1999). The nucleocytoplasmic shuttling proteins can translocate between the cytoplasm and the nucleus. Therefore, shuttling proteins can be factors for conveying information between nucleus and cytoplasm in the cells. The nucleocytoplasmic shuttling proteins have multiple functions depending on the nature of the proteins. Studies have shown that nucleocytoplasmic shuttling protein have a function in signal transduction because of their cellular location (Gama-Carvalho and Carmo-Fonseca 2001). The translocation of proteins can regulate the cell cycle progression and proliferation (Kau and Silver 2003). Shuttling proteins may also have a function in coupling nuclear and cytoplasmic mRNA metabolism. Misregulation of the subcellular location was shown to be involved in cancers (Takai, Tan et al. 2005).

1.5 p68 RNA helicase (p68)

1.5.1 *General function of p68 as a member of DEAD-box protein*

The DEAD box family proteins have a core segment of eight conserved motifs including a Asp(D)-Glu(E)-Ala(A)-Asp(D) box (Linder, Lasko et al. 1989). The DEAD box proteins share similar functions of RNA-dependent ATPase activity, and many of them exhibit RNA helicase

activity. According to the previous studies, the DEAD box proteins play many important roles in RNA metabolism, including ribosome biogenesis, pre-mRNA splicing, and translation (Fuller-Pace 1994; de la Cruz, Kressler et al. 1999).

DEAD box proteins play important roles in a wide range of cellular processes through interaction with specific RNA molecules. Interestingly, several DEAD box proteins, such as rck/p54 and DDX1, have been implicated in both growth regulation and tumor development (Godbout and Squire 1993; Akao, Marukawa et al. 1995; Nakagawa, Morikawa et al. 1999). P68 is a member of the DEAD box family of RNA helicases, its ATPase and RNA helicase are demonstrated (Hirling, Scheffner et al. 1989; Iggo and Lane 1989). P68 was originally identified through a cross reaction with an antibody for simian virus 40 (SV40) large T antigen (Lane and Hoeffler 1980). The amino acid sequence of p68 RNA helicase core has a striking homology to the other RNA helicase of DEAD box proteins, such as vasa, eIF-4A, Dhhlp, and UAP56. The definition of p68 as a DEAD box family protein is due to its homology sequence to eIF-4A (Ford, Anton et al. 1988). P68 is highly conserved through evolution. The mouse and human p68 are 98% identical (Lemaire and Heinlein 1993), and the sequence of IQ motif at the C-terminal of p68 is exactly same in both mouse and human.

As a member of DEAD box family, p68 binds to both double- and single-stranded RNA. The binding of p68 to RNA stimulates its ATPase activity. The released energy can be used to unwind RNA duplexes in both directions (Huang and Liu 2002; Lee 2002). The function of p68 is mainly involved in RNA metabolism, such as pre-mRNA and pre-rRNA processing, alternative splicing, and mRNA decay. Importantly, p68 plays a role in cell proliferation.

1.5.2 Biological function of p68

Even though most functions of p68 are related to RNA, new functions of p68 have been uncovered in recent years. Expression of p68 is regulated by cell growth and development, which strongly indicate that p68 may play a role in cell proliferation (Lane and Hoeffler 1980; Stevenson, Hamilton et al. 1998). Interestingly, p68 is found to be essential for the development. Specifically, DDX5 knockout embryos die at day 11.5 (Fukuda, Yamagata et al. 2007). On the other hand, p68 has functions in organ maturation during development. P68 is overexpressed in the differentiated adipocyte and skeletal muscle cells (Kitamura, Nishizuka et al. 2001; Caretti, Schiltz et al. 2006).

Recently, p68 is found to regulate gene transcription. This transcription function of p68 is found often linked with p72. P68 and p72 are homologous and can form homo- or hetero-dimer (Janknecht 2010). P68 interacts with RNA polymerase II, and the ubiquitous transcriptional cofactors including CBP, p300 and PCAF (Rossow and Janknecht 2003). CBP, p300 and PCAF are acetyltransferase that can acetylate lysine residues of histone tail to activate the gene transcription (Yang, Ogryzko et al. 1996; Janknecht 2002; Lee and Workman 2007). Interestingly, p68 also binds to histone deacetylase (HDAC) that can repress the gene transcription (Wilson, Bates et al. 2004). Thus, p68 can act as transcription co-activator or repressor depending on the associated protein contents. P68 is known to function as transcriptional co-activator for transcription factors. Interestingly, the RNA helicase activity of p68 is not required for the transcriptional co-activator function. For example, the RNA helicase of p68 is not required when it functions as a coactivator for p53 tumor suppressor (Bates, Nicol et al. 2005), Runx2 (Jensen, Niu et al. 2008) and MyoD (Caretti, Schiltz et al. 2006). RNA

helicase activity, however, is required for p68 to function as the transcription cofactor for cyclin D1 and c-myc (Yang, Lin et al. 2007).

1.5.3 Posttranslational modification of p68

Posttranslational modification is the chemical modifications after a protein has been translated. The posttranslational modifications can change the structure, activity, and stability of a protein. P68 was found to be phosphorylated by PKC *in vitro*. However, the phosphorylation site has not been confirmed. It is proposed that the serine/threonine within IQ motif may harbor the phosphorylation site. Phosphorylation of p68 by PKC inhibits the ATPase activity (Buelt, Glidden et al. 1994). Meanwhile, binding to single-stranded RNA by the C-terminal region of p68 is inhibited (Yang, Yang et al. 2004). P68 is also phosphorylated at Y593 by c-Abl upon the stimulation of PDGF in colon cancer cells. The phosphorylation of p68 at Y593 is required for its interaction with beta-catenin. This interaction can translocate beta-catenin from the cytoplasm to the nucleus to induce the epithelial-mesenchymal transition (Yang, Lin et al. 2006; Lin and Arlinghaus 2008). Interestingly, double phosphorylation of p68 at Y593 and Y595 leads to resistance to the trail-induced apoptosis of T98G glioblastoma cells (Yang, Lin et al. 2007). In addition, p68 is phosphorylated by p38 MAP kinase (Yang, Lin et al. 2005). The phosphorylation site(s) and its biological function are currently unknown.

P68 is also highly poly-ubiquitylated in colon cancers. In principle, ubiquitylation of p68 should lead to degradation of p68 (Causevic, Hislop et al. 2001). Whether ubiquitylation of p68 has other function and which lysine residue(s) is ubiquitylated are open questions.

The lysine residue (K53) at the N-terminus of p68 is demonstrated to be sumoylated (Mooney, Grande et al. 2010). The sumoylation of p68 can stabilize the protein. It increases the

interaction between p68 and HDAC1 and affects the potential of p68 as a transcription co-activator (Jacobs, Nicol et al. 2007).

1.5.4 P68 and cancer

It is well known that p68 has important functions in cell proliferation and survival (Kahlina, Goren et al. 2004; Yang, Lin et al. 2007). The expression level of p68 is correlated with the growth status of cells. P68 exhibits tissue specific expression (Stevenson, Hamilton et al. 1998). P68 is suggested to be a proto-oncogene, as ectopic expression in fibroblast cells (NIH3T3 and NC3H10) can induce the tumor formation in nude mice (Wei and Hu 2001). Overexpression of p68 in cells leads to the resistance to the cancer therapy (Cohen, Geva-Zatorsky et al. 2008).

The protein level of p68 is upregulated in colorectal tumors (Causevic, Hislop et al. 2001; Shin, Rossow et al. 2007). Immunohistochemical analyses show that the expression of p68 is increased with the progression of the tumor from hyperplastic polyps to adenomas and adenocarcinomas (Shin, Rossow et al. 2007). Interestingly, the aberrant activation of beta-catenin is associated with colon carcinogenesis (Segditsas and Tomlinson 2006). P68 can bind to beta-catenin and activate beta-catenin dependent gene transcriptions including cyclin D1 and c-myc (Yang, Lin et al. 2007). The upregulation of p68 may lead to and/or target the activated beta-catenin to promote gene transcriptions, which results in colorectal tumorigenesis.

P68 is reported to be over expressed in the breast tumor as well (Mooney, Grande et al. 2010). Around 70% of the breast tumors are ER α positive (Yager and Davidson 2006). P68 is transcription coactivator of ER α (Endoh, Maruyama et al. 1999). Overexpression of p68 may activate the ER α dependent gene transcriptions, and subsequently lead to the induction of the breast tumor. P68 is upregulated in prostate tumor (Clark, Coulson et al. 2008). Formation of the

prostate tumor may be resulting from activating androgen receptor dependent gene transcription by p68 (Clark, Coulson et al. 2008).

1.5.5 *Cytoplasmic p68 and cancer*

P68 is consistently overexpressed in colorectal cancer cells when compared with the corresponding normal cells. The mRNA level of p68 has no significant difference between tumor and normal cells (Causevic, Hislop et al. 2001). Therefore, posttranslational modifications such as sumoylation, may stabilize p68 and consequently lead to the upregulation of p68 in the tumor cells (Mooney, Grande et al. 2010). On the other hand, overexpression/ubiquitylation of p68 is observed in both pre-invasive and invasive lesions (Causevic, Hislop et al. 2001), indicating that p68 or the ubiquitylation levels may connect to the tumor growth but not relevant to the invasion of tumor cells.

P68 was first demonstrated to be localized in the nucleus by using antibodies against SV40 large T antigen that cross-reacts p68 (Iggo and Lane 1989; Iggo, Jamieson et al. 1991; Nicol, Causevic et al. 2000). Later on, p68 is also found in the cytoplasm using the antibodies raised against the C-terminal of p68. Specifically, p68 is found in the cytoplasm of ovarian and breast cancer cells (Rossow and Janknecht 2003). In fact, the results of colon cancer tissue staining shows that p68 exist in the cytoplasm of the colon cancer cells in 2001 using the antibodies against p68 (Causevic, Hislop et al. 2001). Interestingly, analysis of HCT-116 and SW620 colon cancer cells reveals that p68 is present in the cytoplasm and the cell nucleus, whereas normal CCD-841-CoN colon cells display exclusive nuclear localization pattern (Shin, Rossow et al. 2007). All these observations suggest that cytoplasmic p68 may have important functions in cancer development and progression.

Y593 phosphorylated p68 is proposed to translocate to the cytoplasm. The cytoplasmic p68 dissociated Axin by binding to beta-catenin. The beta-catenin will therefore translocate to the nucleus to act on the expression of a number of mesenchymal promoting genes. This process leads to the epithelial mesenchymal transition (EMT) of the tumor cells (Yang, Lin et al. 2006). EMT is one critical step for cancer cell metastasis.

1.6 Calmodulin

1.6.1 *Calmodulin is a conserved Ca^{2+} sensor protein*

Calmodulin is a small protein with the molecular weight of around 16 kDa. Calmodulin is an acidic protein. It has four EF-hand motifs, and Ca^{2+} is bound by those EF-hand motifs. Calmodulin consists of two symmetrical domains connected by a long α -helix. Two Ca^{2+} ions bind to each domain. The long helix involves the interaction of calmodulin with many proteins (Motohashi 1991).

Calmodulin is expressed in all eukaryotic cells and is highly conserved among different species. Calmodulin is a typical Ca^{2+} sensor, as the conformation of calmodulin will change in the presence of Ca^{2+} (Ikura 1996). Specifically, the structure of calmodulin can be changed from random coil (without Ca^{2+}) to a dumbbell shape structure (with Ca^{2+}). Calmodulin is able to respond to an intracellular Ca^{2+} concentration change. The range of intracellular Ca^{2+} concentrations is 10^{-7}M to 10^{-6}M in most cells. The affinity of calmodulin for Ca^{2+} falls in the range of $5 \times 10^{-7}\text{M}$ to $5 \times 10^{-6}\text{M}$, which matches well with the range of intracellular Ca^{2+} concentration.

The total amount of calmodulin (10^{-6}M to 10^{-5}M) in cells constitutes over 0.1% of the total proteins. The expression level of calmodulin can be upregulated in rapidly growing cells and the cells under differentiation.

1.6.2 Calmodulin binding proteins

Calmodulin itself has no intrinsic enzymatic activity, while it has the capability to regulate biological activities of many cellular proteins as well as transmembrane proteins. Calmodulin binding proteins can be classified into at least six groups based on their model of regulation in the presence of absence of Ca^{2+} . In group I, the effectors bind to calmodulin irreversibly in a Ca^{2+} independent manner. However, the effector/calmodulin complex may be activated in the presence of Ca^{2+} . In group II, the effectors bind to calmodulin in the absence of Ca^{2+} , but dissociate in the presence of Ca^{2+} . In group III, the effectors form low affinity and inactive complexes with calmodulin at low concentration of Ca^{2+} ; while at high concentration of Ca^{2+} , these effectors engage in a high-affinity and active complex with calmodulin. In group IV, the effectors bind to calmodulin in the presence of Ca^{2+} , and calmodulin inhibits their function. In group V, effectors are activated by Ca^{2+} -calmodulin, which is a more conventional behavior. In group VI, effectors bind to Ca^{2+} -calmodulin. The formed complex will be further regulated by another calmodulin-regulated kinase (Chin and Means 2000).

P68 is known to interact with calmodulin. Interestingly, two groups showed that the interaction between p68 and calmodulin is Ca^{2+} dependent, and another showed that this interaction is Ca^{2+} independent. However, the functional relevance of the interaction is unknown. *In vitro* experiments showed that the RNA-dependent ATPase of p68 was regulated by the binding to calmodulin.

1.6.3 Calmodulin translocation in the cells

The concentration and location of calmodulin appear to play important roles in regulating its biological activity. The local concentration of calmodulin may have significant influence as various calmodulin targeting proteins are regulated by different concentration of free calmodulin

(10^{-12} ~ 10^{-16} M) (Chin and Means 2000). Interestingly, the majority of calmodulin is observed to be freely diffusible, as shown in the experiment with serum-deprived Swiss 3T3 fibroblasts. Calmodulin is immobilized under the stimulation of serum (Gough and Taylor 1993). Most calmodulin is Ca^{2+} bound in unstimulated smooth-muscle cells. This information indicates that calmodulin is not always freely diffusible inside the cells. Mechanism that regulates the calmodulin translocation may exist. Understanding the mechanism by which the calmodulin translocates in the cells is important, as translocation of the calmodulin appears to be required for many of its biological functions.

Interestingly, calmodulin is observed to be redistributed from the cytosol to the nucleus in response to a rise of Ca^{2+} in cells (Luby-Phelps, Hori et al. 1995). The movement of calmodulin to the nucleus is also observed in the neuron cells under the stimulation (Deisseroth, Heist et al. 1998). In hormone-treated pancreatic acinar cells, calmodulin is accumulated slowly in the nucleus (Craske, Takeo et al. 1999). Due to the small size of the calmodulin (16.8 kDa), calmodulin has a similar pattern of accumulation in the nucleus with 20 kDa fluorescein-dextran. It is speculated that accumulation of calmodulin in the nucleus is the result of the passive diffusion of calmodulin into the nucleus (Liao, Paschal et al. 1999). However, whether all the calmodulin nucleus translocation depends on the passive diffusion is not conclusive. Interestingly, Richard Thorogate and co-workers found that the majority of calmodulin nuclear entry occurs by the facilitated mechanism in both Ca^{2+} dependent and Ca^{2+} independent manners (Thorogate and Torok 2004). Since calmodulin has important function in the cytosol, the nuclear calmodulin needs to be redistributed to the cytoplasm and to a specific area. However, the mechanism governing this redistribution is unclear. The diffusion as well as the redistribution of calmodulin may be slowed down by many other factors in the cells including macromolecular

crowding and cytoskeleton. The elevated Ca^{2+} can also slow down the diffusion of calmodulin in the presence of calmodulin kinase II (Kim, Heinze et al. 2004). Therefore, redistribution of calmodulin by active mode seems very likely.

1.7 PKM2

1.7.1 PKM2 and tumor

Cancer cells employ glycolysis to generate energy and phosphointermediates which is different from the normal tissue. Glycolysis is a metabolic pathway that converts glucose into pyruvate and ATP. Glycolysis involves ten reactions. There are three regulation points in the pathway: hexokinase, phosphofructokinase, and pyruvate kinase. Pyruvate kinase (PK) is the third rate-limiting enzyme in glycolysis. The transfer of phosphoryl group from phosphoenolpyruvate (PEP) to ADP to produce pyruvate and ATP is catalyzed by pyruvate kinase. There are four isoforms of pyruvate kinases (L type, R type, M1 type, and M2 type) in mammalian cells. PKM2 is one isoform of pyruvate kinase which is expressed in highly proliferating tissues including fetal tissue and tumor tissues. During tumorigenesis, M2 type of pyruvate kinase is expressed while other tissue specific form of PK is completely down-regulated (van Berkel, de Jonge et al. 1974; Miwa, Nakashima et al. 1975; Etiemble and Boivin 1976; Marie, Kahn et al. 1976). The expression of M2 type of pyruvate kinase can change the glycolysis rate to produce more phosphoryl intermediates for cell growth.

PKM2 has three structural forms: monomer, dimer, and tetramer. Each monomer of PKM2 has four domains: A domain, B domain, C domain and N domain. Two monomers bind to each other at the A domain interface to form a dimeric structure. Two dimers form a tetramer through binding at the A domain and C domain interface (Dombrackas, Santarsiero et al. 2005). A domain is the core structure of the monomer. The active site of PKM2 is located in the cleft

constructed by A domain and B domain. The FBP binding site for PKM2 is positioned at the C-domain. Lysine 433 at the C-domain is important for the binding of FBP to PKM2, and this site is important for PKM2 binding to the tyrosine phosphorylated peptides (Christofk, Vander Heiden et al. 2008; Spoden, Morandell et al. 2009). Tetrameric PKM2 has a higher affinity for its glycolysis substrate PEP than dimeric PKM2 does.

Interestingly, there are more dimeric PKM2 in cells during tumorigenesis. The existence of high portion of dimeric PKM2 is reasoned to be beneficial for cell growth and proliferation. This is because the low affinity of dimeric PKM2 to PEP decreases the glycolysis rate, and more phosphor intermediates is then produced. The phosphor intermediates can be used to synthesize lipids, amino acids and some other macromolecules which are essential for cell proliferation.

Studies show that pp60V-src kinase and HPV-16E7 proteins directly interact with PKM2, and help the conversion of dimeric form from tetrameric form (Zwerschke, Mazurek et al. 1999). However, how the tetrameric PKM2 converts to dimeric PKM2 is not well studied. Interestingly, PKM2 is a phosphor tyrosine binding protein, and the binding of these peptides can decrease its enzymatic activity (Christofk, Vander Heiden et al. 2008).

1.7.2 Localization of PKM2

As a pyruvate kinase, PKM2 is dominantly located in the cytoplasm. Interestingly, PKM2 is also found in the nucleus under certain situations. Under the stimulation of interleukin 3 (IL-3), more PKM2 localizes to the nucleus to regulate cell proliferation in hematopoietic cell, Ba/F3 (Hoshino, Hirst et al. 2007). PKM2 interacts with several nuclear proteins, such as Oct-4 and PIAS3 (Lee, Kim et al. 2008). Sumoylation changes protein properties including transcription, nuclear-cytosolic localization as well as protein stability. The overexpression of PIAS3 increases the sumoylation of PKM2, which leads to the accumulation of nuclear PKM2 (Spoden,

Morandell et al. 2009). Somatostatin, a neuropeptide hormone and its anti-cancer analogues, TT-232, interact with pyruvate kinase in COS-7 cells. The interaction induces the nuclear accumulation of PKM2 from the cytoplasm to trigger cell apoptosis (Stetak, Veress et al. 2007). Moreover, UV and H₂O₂ cause PKM2 nuclear accumulation independent of its kinase activity to induce cell apoptosis (Stetak, Veress et al. 2007). Even though the nuclear location of PKM2 has been observed, the putative function of nuclear PKM2 is a paradox. Furthermore, the mechanism in regulating the translocation of PKM2 to the nucleus is not known.

1.8 Microtubule Motor

1.8.1 *General information about microtubule and microtubule motor*

Microtubule is one important part of cytoskeleton. The structure of microtubule is dynamic in the cells. Microtubules grow from the microtubule-organizing center (MTOC) towards the plasma membrane. Microtubules at the MTOC are the minus end where microtubules are more stably tethered. The end of microtubule which faces to the plasma membrane is the plus end where microtubule can grow dynamically (Valiron, Caudron et al. 2001). Two major well known microtubule motors have been found, kinesins and dyneins. Kinesin super family contains up to 45 members (Miki, Okada et al. 2005). Most kinesin members move toward the plus end of microtubule. Different kinesins have variations in the accessory subunits and cargo binding domain which lead to the specific transportation of individual cargos. Dynein is the major motor that moves toward the minus end of the microtubule.

Conventional kinesin (kinesin-1) has two heavy chains and two light chains. Each heavy chain has an ATP-binding motor domain (globular structure) at the N-terminus. The motor heads move kinesin along the microtubule. The stalk domains of two heavy chains interact to form a

coiled coil structure. The stalk domain connects the globular head and the tail. The two light chains bind at the tail regions of the two heavy chains. C-terminal domain of kinesin light chains carry several tetrapeptide repeats which are involved in the binding of cargos (Dietrich, Sindelar et al. 2008).

1.8.2 The function of microtubule motor and motor as an antitumor target

Microtubule motor proteins are a class of molecular motors that can move along the surface of the microtubules. They utilize the energy that is generated by the hydrolysis of ATP (Schnitzer and Block 1997). The general functions of the motors are active transport of the associated protein(s) and vesicles (may include mitochondria and Golgi bodies) in the cytoplasm (Vale 2003). They also have functions in the formation of spindle apparatus and separation of the chromosomes during mitosis/meiosis. The microtubule motors also have functions in anchoring the microtubule to the actin filaments, which stabilize/destabilize the microtubule structures, and bundling of the microtubules (Gatlin and Bloom 2010).

The formation of tumor is due to the uncontrolled proliferation of the tumor cells. Therefore, the process of mitosis is an important target to prevent cell proliferation (Janssen and Medema 2011). There are a variety of anti-mitotic drugs that are successfully used in the clinic. Most approved antimitotic drugs target the spindle microtubules. These drugs lead to mitotic arrest and apoptosis by interfering with spindle dynamics. However, these drugs have side effects including neurotoxicity. In the recent years, the mitotic kinesins or mitotic motors have drawn attention. Since the mitotic kinesins have their specific function during mitosis, those proteins are becoming the alternative mitotic drug targets (Mayer, Kapoor et al. 1999). Because of the specific function of the mitotic kinesins in mitosis, the side effect profile will be improved if the drugs specifically target these proteins. On the other hand, the resistance to the microtubule

targeting drugs may be overcome by applying the kinesin inhibitors (Huszar, Theoclitou et al. 2009).

1.8.3 *The functions of microtubule motors in cell migration*

Cell migration is a multistep process that has important functions in normal physiological processes such as embryonic morphogenesis, tissue repair and regeneration. Cell migration also plays important roles in pathogenic conditions, including cancer, arthritis, and mental retardation (Ridley, Schwartz et al. 2003).

The popular model for cell migration is the formation and rearrangement of actin filaments at the leading edge, which induce the protrusion. Microtubule is also proposed to function in vesicle transport to provide membrane and proteins at the leading edge to promote the protrusion of the cells. The microtubule growth into the leading edge which leads to the transport of the molecules to the leading edge is important in initiating/maintaining the protrusion (Ridley, Schwartz et al. 2003).

There are three groups of cytoskeleton associated motors: myosins, kinesins, and dyneins. The major function of these proteins is the transport of macromolecular complexes and membranous vesicles inside the cells. Interestingly, multiple motors have been suggested to have functions in cell migration. Myosins, such as myosin II, play a role in the migration of fibroblasts and neurons (Krendel and Mooseker 2005). Interestingly, myosin II is suggested to push the nucleus forward from behind in migrating cells. Cytoplasmic dynein is also indicated plays a role in directed cell movement. Both myosin II and dynein are proved to have function in soma translocation in migrating cells (Vallee, Seale et al. 2009). Surprisingly, the extension of the leading edge is not affected when dynein HC is knocked down. This indicates that other microtubule motors may be involved in the extension of the leading edge.

Cell migration can be divided into 4 steps: polarization, protrusion, traction, and retraction. Before the formation of the lamellipodium at the front area, the cell must be polarized. This means some of the molecules must be unevenly distributed, and this may need the facilitation of the microtubule motor to distribute the molecules to the front area. How the motor senses the difference of the front area and tail area is not well understood.

1.9 Aims of the dissertation

P68 is previously found to be predominantly located in the nucleus. Many functional studies of p68 are focused in the nucleus. Due to its homology with other RNA helicases, many functions of p68 related to RNA metabolism have been discovered. P68 was found to exist in the cytoplasm of the cancer cells (Causevic, Hislop et al. 2001). A number of research laboratories also found the existence of p68 in the cytoplasm of cultured colon cancer cells as well as colon cancer tissues (Jacobs, Nicol et al. 2007). The previous studies in our lab indicate that Y593 phosphorylated p68 can be exported to the cytoplasm and carry beta-catenin back to the nucleus (Yang, Lin et al. 2006). However, it is not known why and how p68 is translocated to the cytoplasm. **Therefore, the first aim of this study is to identify whether p68 is a nucleocytoplasmic shuttling protein.**

Even though several groups have found the existence of p68 in the cytoplasm, the biological function of p68 in the cytoplasm is unknown. Meanwhile, what is the regulating mechanism behind the export of p68 to the cytoplasm is not known. Our laboratory revealed that the cytoplasmic tyrosine phosphorylated p68 can translocate cytoplasmic beta-catenin into the nucleus under the stimulation of PDGF (Yang, Lin et al. 2006). Interestingly, high level of p68 are found in the cytoplasm of the highly metastatic tumor cells but not in the normal cells (Shin, Rossow et al. 2007), which indicate the potential role of cytoplasmic p68 in colon cancer

motility. Therefore, we used the cultured colon cancer cells as a study system to try to elucidate the function of cytoplasmic p68 in cell migration.

P68 interacts with calmodulin in the presence of calcium (Buelte, Glidden et al. 1994). However, the biological function of this interaction in the cell is unknown. Previous study has successfully illustrate the function of two interacting proteins by fusing ubiquitin to the C-terminal of the target protein (Lee, Wang et al. 2005). We adopted the similar system to investigate the function role of the interaction by fusing calmodulin to the C-terminal of p68. Interestingly, expression of this fusion protein promotes the cell migration. Specifically, p68-calmodulin fusion protein is located in the cytoplasm and in the regions of the leading edge. Along with the previous observations that p68 is up-regulated in the highly metastatic cells, **we speculated that the interaction between p68 and calmodulin may have function in cell migration, and the binding between p68 and calmodulin may have an important function in the cytoplasmic translocation of p68 and calmodulin.**

Calmodulin has important functions in cell migration. The function of calmodulin in cell migration is mainly regulated by binding the target proteins in cells at specific region. The active redistribution of calmodulin is important as calmodulin is not always freely diffusible. The nuclear translocation of calmodulin by binding to other proteins is quite well known. How the calmodulin is redistributed to the cytosol, however, is unknown. Since p68 is a nucleocytoplasmic shuttling protein, and p68-calmodulin fusion protein is located to the cytoplasm, **we speculated that the interaction between p68 and calmodulin may facilitate the cytoplasmic translocation of calmodulin.**

PKM2 plays important roles in tumor progression as PKM2 is the isoform of pyruvate kinase expressed in cancer cells. PKM2 binds to the tyrosine phosphorylated peptide. Our study

demonstrated that the Y593/595 double phosphorylated peptide from p68 binds PKM2. Since Y593 phosphorylated p68 is able to translocate to the cytoplasm and carry its associated beta-catenin back to the nucleus, **we hypothesized that PKM2 might be transported to the nucleus by associating with Y593/595 phosphorylated p68.** The nuclear PKM2 is dominantly in dimeric structure. The nuclear accumulation of PKM2 was found to alter the cancer cell growth by promoting the growth or by inducing apoptosis. Therefore, **the function of dimeric PKM2 on the tumor growth was tested in this study.**

CHAPTER 2

GENERAL MATERIALS AND METHODS

2.1 Nucleic acids related techniques

2.1.1 *Mini preparation for DNA*

QIAprep® Spin Miniprep Kits (QIAGEN, Cat. No. 27106) was used to purify the plasmid from E. coli. Simply, 2-3 ml of overnight cultured E.coli in LB medium was centrifuged and the pellet was collected. The pellet cells were then suspended in 250 µl of Buffer P1. 250 µl of Buffer P2 was added and the mixture was inverted for 6 times till the mixture become clear. 350 µl of Buffer N3 was then added and the mixture was inverted for 6 times till the solution became cloudy. The mixture was then centrifuged for 10 minutes at 13,000rpm. The supernatant was collected and the QIAprep spin column was used and was centrifuged for 1 minute. The flow-through was discarded. The QIAprep spin column was washed by adding 0.5 Buffer PB and centrifuge for 1 minute. The flow-through is discarded. The column was further washed by adding 0.75ml of Buffer PE and was centrifuged for 1 minute. The flow-through was discarded, and the column was centrifuged for additional one minute. The column was then moved to a new microcentrifuge tube. 30 µl of water was used to elute DNA by standing for 1 minute and centrifuging for 1 minute at 13,000 rpm. The eluted DNA was confirmed by either running gel electrophoresis and/or sending for DNA sequencing.

2.1.2 *Midi preparation for DNA*

Bacteria carrying DNA plasmid were cultured in 1ml of LB medium supplemented with antibiotics (50ng/ml Kanamycin or Ampicillin). Then, the bacteria culture was transferred into 150ml warm LB medium and cultured overnight at 37°C to amplify bacteria together with plasmid DNA. On the second day, the bacteria were collected by centrifuging at 6,000rpm for 8

minutes. 3ml of resuspension buffer was used to suspend the cell pellet, and 3 ml of lysate buffer was used to lysis the bacteria. The lysate was neutralized by adding 3 ml of neutralization buffer and inverting the mixture. Then, the solution was centrifuged at 15,000 for 25 minutes and the supernatant was carefully collected into a 50 ml conical tube. 10 ml of DNA purification resin provided with the kit was added to the same tube and mixed gently. The mixture was loaded to a mini preparation column and the vacuum equipment was applied to remove supernatant. The resin beads bounded with DNA plasmids were washed with washing buffer twice (10ml each time) by using the vacuum equipment. 300 μ l of pre-warmed ddH₂O (~70°C) was added into the dehydrated resin. Then, DNA plasmid was eluted from the column by centrifuging at 13,200 rpm for 1 minute. The plasmid DNA may be further purified with phenol/Chloroform/Ethanol method and the concentration of the DNA was measured with spectrometry at OD260nm.

2.1.3 Agarose gel electrophoresis and gel extraction of DNA

A double stranded DNA binding dye, Ethidium Bromide, can be used to visualize plasmid DNA or DNA fragments under a UV transilluminator. 1% agarose gel was prepared by adding 1g of agarose into 100ml of TAE buffer. The mixture was heated with microwave to completely dissolve agarose. The solution was cooled down to 50-60°C with a water bath before adding 6 μ l of ethidium Bromide into it. The solution was then poured into a gel casting apparatus. Well inserts was set up to make suitable well. 8~10 μ l of DNA ladder was loaded into one well to indicate the molecular weight of DNA fragments. The gel ran at constant voltage of 120V until the DNA/DNA fragment was separated and visualized under the UV transilluminator.

2.1.4 Quantification of DNA or RNA

The concentration of nucleic acids was measured in a spectrophotometer (UV-1700 spectrophotometer, Shimadzu Co.) at OD260nm. The DNA concentration was determined by the

formula: DNA concentration ($\mu\text{g/ml}$) = $(\text{OD}_{260\text{nm}}) \times (\text{diluted factor}) \times (50 \mu\text{g DNA/ml}) / (1 \text{ OD}_{260\text{nm}} \text{ unit})$. The purity of DNA was determined by the ratio of the absorbance of $\text{OD}_{260\text{nm}}/\text{OD}_{280\text{nm}}$. The purity of DNA was acceptable when the ratio is between 1.8 and 2.0.

2.1.5 Polymerase chain reaction (PCR) method

PCR method was applied to amplify a target sequence from DNA including plasmid DNA. PCR method also can be used to mutate specific nucleic acids of a plasmid vector. In general, 0.5 μg of template DNA was mixed with 1mM of dNTP, 0.5 μg of both forward and reverse primers, and 1-2 unit of Pfu polymerase in 1X reaction buffer. The reaction mixture was denatured at 95°C for 2 minutes and then was followed by 25-35 cycles: 95°C denaturation for 30 seconds, 57-62°C annealing for 45 seconds, 72°C elongation for 45seconds (the elongation time can be adjusted based on the length of the target sequence). An additional elongation step at 72°C for 10 minutes was performed to stabilize the double strands. The PCR product was examined by agarose gel electrophoresis.

2.1.6 Restriction enzyme digestion and plasmids construction

CDNA of target gene needs to be constructed into the vector in order to exogenously introduce proteins into the cells. The plasmid needs to be chosen based on the purpose of the research. The sequences of the vectors are available from the companies. The primers incorporating the digestion site(s) used for cloning the target gene would be very carefully designed. The restriction enzymes have optimum conditions therefore the right buffer reaction system is critical to make the digestion successful. The restriction digestion could be carried by using one restriction enzyme one time or by using two restriction enzymes one time. In general, in the final digestion system, 1 μg of the plasmid DNA or 30 μl of PCR product and 1 μl of the specific enzyme was used. The mixtures were then incubated at the recommended temperature

for 2 hours or even longer. Agarose gel electrophoresis was used to separate the digested PCR product or digested vector. T4 DNA ligase was applied to ligase the digested DNA into the digested vector. The 3'-OH of one nucleic acid and 5' phosphate of the other nucleic acid can be joined by T4 DNA ligase. The recommended ratio of the DNA to plasmid vector was around 3:1. The ligation process was performed in 1X ligation buffer with 1-2 μ l of T4 DNA ligase. The mixture was incubated at 4°C overnight or at room temperature for 30 minutes. The ligation product containing the ligated vector was transformed into competent bacteria on the second day.

2.1.7 Site-directed mutation method

QuikChange II XL site-directed mutagenesis kit (stratagene) was used to perform a site-directed mutation. The primer for the mutation can be designed on-line (The Quikchange primer design program). 0.5 μ g of primers was applied to PCR reaction mixture. 2 μ l of DpnI enzyme (20U) was added to the reaction system to digest the parental plasmid vector. The digestion reaction was performed at 37°C water bath for 2 hours. The mutated plasmid vectors were transformed into XL-1 Blue competent cells after the DNA was purified. The transformed XL1-Blue cells were coated on the agar plate containing an appropriate antibiotic overnight at 37°C. On the second day, several colonies were picked and were cultured in 2ml of LB medium overnight at 37°C. DNA plasmid was isolated by mini-prep from the bacteria. DNA sequence technique at the core facility of GSU was used to identify the mutated DNA sequences.

2.1.8 Ethanol purification of DNA

Ethanol purification was performed to remove salt or protein in DNA samples. At first, DNA solution was added and mixed well with 1/10 volume of 3M sodium acetate. The mixture was then added and mixed well with 2 volumes of ice-cold 100% ethanol. The mixture was centrifuged at full speed for 10 minutes at 4°C to pellet DNA. The supernatant was removed and

the DNA was washed with ice-cold 70% ethanol twice and centrifuge at 4°C for 5 minutes. The supernatant was removed and then the DNA pellet was dried by air at room temperature until the pellet becomes transparent. The concentration of the DNA was determined at OD_{260nm} in spectrophotometer after the DNA pellet was dissolved in ddH₂O.

2.1.9 RNA extraction from tissue

Whole spleens from mice were collected and submerged into 1.5ml of the RNAlater RNA stabilization reagent (QIAGEN, Cat. 76104). The tumor was cut into small pieces (0.5 cmX0.5cmX0.5cm) and was consequently put into the same amount of the reagent. The samples were kept at 4°C for overnight and were then moved to -20°C (for less than 4 weeks). 1/3 of the spleen was collected, and the total mRNA was isolated by the mini-plus kit (including the shredder column). In detail, the spleen tissue (~30mg) was homogenized in Buffer RLT which had been added with B-mercaptoethanol. The tissue lysates were then added into the QIAshredder spin column (QIAGEN, Cat. 79654). Then the lysate were centrifuged for 3 minutes at the maximum speed. The supernatant was transferred into a gDNA Eliminator spin column and centrifuged for 30s at 10,000rpm. The flow-through in the tube was added with 1 volume of 70% ethanol and mixed by pipetting. The mixture was transferred to an RNeasy spin column and centrifuged for 30s at 10,000rpm. The flow-through was discarded. 700 µl of Buffer RW1 was added into the RNeasy spin column and the flow-through was discarded after centrifuging. 500 µl of Buffer RPE was added into the column. The flow-through was discarded after centrifuging. And this step was repeated once. The trace amount of Buffer RPE was removed by centrifuging the column in a new tube for 1 minute at the full speed. The total RNA was eluted into the collection tube from the column by adding 30-50 µl of H₂O into the column and centrifuging the column for 1 minute.

2.1.10 Reverse transcription PCR

The generation of cDNA from mRNA can be performed by reverse Transcription PCR. 1 µg of total RNA extract and 1 µl of oligo dt15 was mixed in a final volume of 5 µl by adding RNase-free H₂O. The mixture was incubated at 25°C for 5 minutes. The mixture was then incubated at 70°C for 5 minutes. After that, the mixture was incubated on ice for 5 minutes. Among each reaction, 1 µl of reverse transcriptase, 1 µl of RNase inhibitor, 4 µl of MgCl₂ (25mM) and 4 µl of 5X reaction buffer were added together and mixed thoroughly. The mixture was incubated at 25°C for 5 minutes, 45°C for 1hour and 70°C for 15 minutes. The final RT-PCR products were then stored at -80°C.

2.2 Bacterial Techniques

2.2.1 JM109 competent cell preparation

5 µl of JM109 was added into 50ml of pre-warmed, antibiotic free LB medium. The culture solution was put in incubator for 1 hour (optional). The solution was then shaken for 2 hours till the absorbance at 600nm reaches 0.5-1. The amplified bacteria were transferred to 2 centrifuge tubes and the solutions were centrifuged at 3000-5000rpm for 8 minutes at 4°C. The supernatant was discarded and the pellet cells were re-suspended in 20ml of ice cold, sterile 50mM CaCl₂. The cell suspension was incubated on ice for 20 minutes. Then the cell suspension was centrifuged again at 3000-5000rpm for 8 minutes at 4°C. The supernatant was discarded and the pellet cell was re-suspended in 4ml of ice cold, sterile 50mM CaCl₂ and 15% glycerol. Then 100 µl of the aliquots in eppendorf tube were stored at -80°C.

2.2.2 Bacterial culture and storage

The E.coli strains, such as JM109, XL1-blue, BL-21 were used for plasmid DNA construction, amplification or recombinant protein expression. E.Coli strain was inoculated in

autoclaved Luria Broth (LB) medium containing 1% bacto-tryptone w/v, 0.5% bacto-yeast-extract w/v and 1% NaCl w/v. 50 µg /ml of Ampicillin or Kanamycin was added into LB medium for antibiotic resistant strains selection. The bacteria were cultured in shakers (culture medium) or incubators (agar plates) at 37°C. Agar plates were prepared in LB medium with the addition of 1.5% Agar prior to autoclaving. 50 µg /ml of Ampicillin/Kanamycin was added in when the autoclaved LB medium containing agar was cooled down to around 50°C. The transformed bacteria was added with sterile 30% glycerol w/v and preserved at -80°C in order to store the bacteria for long term.

2.2.3 Transformation

For DNA plasmid amplification, E.coli JM109 can be used to transform the plasmid into it. The bacteria together with the plasmid can be amplified by this way. JM109 competent cells with 100 µl of the volume were thawed on ice. 1 µg of plasmid DNA was added into the tube and incubated with JM109 competent cells for 30 minutes on ice. Heat shock was applied to the mixture at 42°C for 90 seconds. The mixture was chilled on ice for additional 2 minutes and 200 µl of the pre-warmed LB were added into the tube. Then the tube was incubated at 37°C in a shaker with 220rpm for 1 hour. The bacteria solution were then spread onto the agar plates containing appropriate antibiotics and incubated at 37°C overnight. On the second day, colonies were picked with sterile plastic sticks separately from the agar plates and dipped into 2ml of LB medium containing antibiotics for single colony amplification. The mini-culture was then used for large scale amplification (100ml-150ml) of the plasmid.

2.3 Protein and peptide Techniques

2.3.1 HA-p68 protein expression and purification

pHM6-p68 vector (or HA-p68-calmodulin expression vector) was transiently expressed in HEK cells for two days. The cells were collected and the whole cell lysate was used to purify HA-p68 proteins. The cells were suspended in 1XPBS (with protease inhibitor cocktails) and were sonicated to break the cells. The supernatant was collected. 20 µl of the poly anti-HA antibodies were added into the supernatant, which were collected from one dish. And the mixture was incubated for 3 hours to overnight at 4°C. The washed G-agarose was added into the mixture solution and incubated for additional 2 hours. The G-agarose was collected and washed for 5 times, and the G-agarose were additionally washed by washing buffer (20mM Tris-HCl, 0.5M NaCl, pH7.5) for ~20 volumes of the G-agarose to remove the proteins which were associated with p68. The HA-p68 proteins on G-agarose was released by incubating with the elution buffer (20mM Tris-HCl, 0.1M NaCl, 0.1mM EDTA, pH7.5) containing 1mg/ml of HA-peptide (Sigma) for 15 minutes at 37°C. The HA peptide was removed by dialysis and HA-p68 protein was concentrated by centrifuging of the solution in Amicon Ultra Centrifugal Filter Devices (Millipore, Cat No. UFC800308).

2.3.2 Recombinant p68-calmodulin fusion protein expression and purification

His-p68-calmodulin fusion protein encoding DNA fragment was constructed into pET30a bacteria expression vector. BL-21 bacteria were transformed with pET30a-p68-calmodulin vector and were cultured in LB medium containing 50ng/ml Kanamycin. Single clone of the transformed BL-21 was cultured in 50ml of LB, and the culture was transferred into 1L pre-warmed LB medium and shook at 220 rpm at 37°C until OD600nm of the culture mixture reached between 0.4 and 0.6. Isopropyl-B-D-thiogalactoside (IPTG) was added to LB medium to

a final concentration at 1mM to induce recombinant protein expression. 4 hours later, bacteria were collected with centrifuging at 5,000rpm at 4°C for 10 minutes. Bacteria pellet were washed with ice cold PBS twice and lysed in lysis buffer containing 1mg/ml lysozyme. The bacteria lysate was sonicated for 1 minute on ice and centrifuged at 17,000rpm for 20 minutes. The expression of recombinant His-p68-calmodulin was examined in SDS-PAGE gel. Most recombinant His-p68-calmodulin protein was expressed in inclusion bodies. The pellet was washed with washing buffer (0.5M Urea and 50mM phosphorylate buffer, pH 7.4). The inclusion body was lysated at room temperature for 1 hour and was centrifuged at 16,000rpm for 30 minutes. The supernatant was collected and diluted dropwise with 50 mM phosphorylated buffer till Urea was diluted to 0.5 M. Recombinant His-p68-calmodulin protein was purified with HiTrap column using Akta purifier 100 FPLC system. Recombinant His-p68-calmodulin protein was gradient eluted with 0.5M imidazole. The eluted protein was collected and dialyzed in buffer (50mM Tris, pH 7.5, 0.1 M KCl, and 20% glycerol). His-p68-calmodulin protein solution was added with 25mM DTT and consequently dialyzed in the refolding buffer (50mM Tris, pH 8.0, 0.1M KCl, 20% glycerol, 0.1M EDTA, 1mM DTT).

2.3.3 Protein quantification

Biorad protein assay was used to determine the concentration of soluble proteins. The standard curve was generated based on a serial of different concentration of Bovine serum Albumin (BSA) from 0 to 0.01 $\mu\text{g} / \mu\text{l}$. The standard curve was generated according to the absorption values of BSA. 1-2 μl of sample solution was added into ddH₂O till the final volume 800 μl . 200 μl of BioRad dye solution was added. The OD was obtained in a spectrophotometer at a wavelength of 595nm. The protein concentration was calculated according to the absorption values. The equation for the standard curve was used.

2.3.4 Sodium dodecyl sulfate polyacrylamide gel electrophoresis (SDS-PAGE)

SDS-PAGE gel was applied to separate denatured proteins according to their molecular weight. The electrophoresis apparatus was assembled according to the manufacture's instructions. SDS-PAGE gel consists of separating gel and stacking gel. Separating gel (375mM Tris-HCl, 0.1% SDS, and pH 8.8) was prepared as the following method. The mixture was prepared in a 100ml glass beaker and poured into two glass plates. Around 500 μ l of isopropanol was added on the top of separating gel to get rid of air bubbles. In rough, it took 45 minutes for separating gels to be polymerized. After the separating gel was polymerized, isopropanol was rinsed away by ddH₂O gently. 4% stacking gel mixture (125mM Tris-HCl, 0.1% SDS, and pH 6.8) was prepared and poured on the top of the separating gel when there is no ddH₂O. An appropriate comb was inserted into the stacking gel to generate wells before the stacking gel is polymerized. The prepared SDS-PAGE gels were kept in 1X SDS-PAGE running buffer (25mM Tris, 250mM Glycine, 0.1% SDS, and pH 8.3) at 4°C for few days. Protein samples were mixed with 5X loading buffer (50mM Tris-HCl at pH 6.8, 2% SDS, 10% glycerol, 1% beta-Mercaptoethonal, 0.02% Bromophenol Blue and 12.5mM EDTA) and boiled at 95°C for 8 minutes. The boil-denatured protein samples were then loaded into the well. Both the inner chamber and the outer chamber was filled with SDS-PAGE running buffer before the protein samples were loaded. The gel was run at 60V until the dye just reached the separating gel and then the voltage was switched to 120V until the blue dye running out of the gel.

2.3.5 Coomassie blue staining

Coomassie blue stain was used to visualize the high amount of proteins (>1 μ g) on SDS-PAGE gel. The gel was washed with ddH₂O for few minutes. Then, the gel was stained with Coomassie blue solution (0.1% Coomassie Brilliant Blue, 20% Methanol, and 10% Acetic Acid)

for 30 minutes. The gel was destained with the destaining buffer (40% Methanol and 10% Acetic Acid) to remove extra Coomassie blue dyes which did not bind to the proteins.

2.3.6 ATPase assay

A direct colorimetric assay was used to measure the ATPase activities through measuring the released inorganic phosphate during ATP hydrolysis. The method is based on the change in absorbance ($A_{623 \text{ nm}}$) of malachite green-molybdenum complex with or without inorganic phosphate. In general, ATPase assay was carried out in 50 μl reaction volumes, containing 20 mM Tris-HCl, pH 7.5, 200 mM NaCl, 1 mM MgCl_2 , 5 mM DTT, $\sim 1\text{--}2 \mu\text{g}$ of appropriate RNA, 40 units of RNasin, 4 mM NTP, and 10 μl of helicase. The ATPase reactions were incubated at 37 °C for 30 minutes. After incubation, 1 ml of malachite green-molybdenum reagent was added to the reaction mixture, and reactions were further incubated at room temperature for exactly 5 minutes. The absorption (A) at 630 nm was then measured. The concentrations of inorganic phosphate were determined by matching the $A_{630 \text{ nm}}$ in a standard curve of $A_{630 \text{ nm}}$ versus known phosphate concentrations. In order to generate a Standard curve of P_i , 1-0.1mM of $\text{Na}_2\text{HPO}_4 \cdot 7\text{H}_2\text{O}$ was used. If the proteins were purified before testing the ATPase activity, RNasin is not required. Reagent for phosphorus determination: 1) ammonium molybdate: 28.6g of ammonium molybdate was dissolved in 500 ml of 6N HCl. 2) Polyvinyl alcohol: 11.6g of polyvinyl alcohol was dissolved in 500 ml of boiling water. 3) Malachite green: 0.812g of malachite green was dissolved in 1000 ml of deionized water. 4) Mixed reagent: 2x 3)+ 1x 1)+ 1x 2)+ 2x deionized water (prepared on the day of use, room temperature for 30 minutes until it turned golden yellow.)

2.3.7 Motor assay

The protein HA-p68-calmodulin, HA-p68, or His-p68-calmodulin (10 μ l) was loaded into a glass slide. The slide was then blocked with the blocking buffer. For the slide loaded with HA-p68, 10 μ l of calmodulin with 0.5 mM of Ca²⁺ was added into the slide and was incubated for 10 minutes. The slide was consequently washed with the wash buffer added with Ca²⁺ in order to remove the unbound proteins. The pre-prepared Rodamine labeled microtubules were then loaded into the slide. The same wash buffer containing Ca²⁺ was used to remove unbound microtubules. The movement of microtubules was then recorded by the confocal microscope after the wash buffer was replaced with the buffer containing ATP.

2.3.8 Microtubule pellet down assay

The commercial microtubule was reconstituted in the warm PM buffer (15 mM Pipes pH 7.0, 1 mM MgCl₂) which were added with taxol as instructed by the vendor. The microtubules were ready to use after 15-minute of incubation at room temperature. The proposal protein(s) was incubated with the reconstituted microtubules under specific conditions. The microtubules with the associated proteins were separated from the incubation solution by centrifugation at 100,000g for 30 minutes. The precipitated microtubules were re-suspended in 50 μ l of 2 x SDS PAGE loading buffer and were heated at 85 °C for 10 minutes and were subsequently analyzed by western blot.

2.3.9 Peptide purification

The crude peptide was dissolved into ddH₂O to a final concentration around 1mg/100 μ l. HPLC equipment (Agilent Technologies 1200 series) was used. C-18 reverse phase semi-prepare column (10mmx25cm, ultrasphere) was used. The buffer A was 0.1% TFA in H₂O. The buffer B was 0.1% TFA in Acetone Nitrial (ACN). 3ml/minute of the flow rate was used.

The pump was set as follows:

Flow: 3.0ml/minute A: 95% H₂O

Stop time: 60 minutes B: 5% CAN Max: 400Bar

Table 1 The setup for HPLC pump

	Time (minute)	%B	Flow
1	0	0	3.0
2	3	5.0	3.0
3	17	40.0	3.0
4	18	40.0	3.0
5	19	95.0	3.0
6	25	0	3.0
7	30	0	3.0
8	31	0	0
9	60	0	0

The peptide fraction was collected during 14.6-15.2 minutes. The peptide was then dehydrated.

The weight of the dehydrated peptide was measured. The fraction of the peptide was confirmed by running MS.

2.4 Mammalian cell techniques

2.4.1 Mammalian cell culture and storage

Cell lines including LN686, M4C1, SW480, SW620, WM115, WM266, T98G, U87MG, H146 and H460 were purchased from ATCC. The culturing methods of the cells follow the vendor's instructions provided by ATCC. In order to freeze cells, the confluences of the cells were maintained around 60-70%, T75 flasks may be used to amplify the cells. The cells were released from the flask by trypsinization, and cell numbers were counted by using hemocytometer. Cells were harvested by centrifuging at 800 rpm for 5 minute. The supernatants were removed and cell pellets were resuspended in freezing medium (10% v/v DMSO, 90% of culture medium contained 10% of FBS). The reuspended cells were aliquoted into freezing

vials (5×10^6 cells/vial). The vials were stored in a freezing container at -80°C overnight. The next day, the freezing vials were transferred to a liquid nitrogen reservoir for long storage.

2.4.2 Transient transfection method

In order to exogenous express a specific protein, mammalian cells can be transiently transfected the protein encoding plasmids by adding with Fugene-HD reagent (Roche). The instruction of manufacture which was provided by the Roche was followed. Mammalian cells were seeded in corresponding medium in 6-well plates. The trasfection were performed on the second day, and 70-90% confluence of the cell density was preferred. The mixture of plasmids DNA and Fugene-HD was prepared in polystyrene transfection tubes. 2 μg of plasmid DNA was added into 100 μl of Opti-MEM medium and mixed thoroughly. Then, 5 μl of Fugen-HD reagent was added into the tube and mixed with plasmid DNA thoroughly. The mixtures were incubated for 20 minutes at room temperature. During the time, the wells in the plates were washed with fresh normal medium twice and fed back with 1ml corresponding medium. Then, 100 μl of the transfection mixture was added to each well gradually. Then the solutions in the plates were mixed well by rocking back and forth for several times. The cells were then cultured in an incubator with/without 5 % CO_2 at 37°C for additional 48-72 hours before harvesting. For immuno-staining experiments, the transfected cells were reseeded in chambers 24 hours later.

2.4.3 Stable cell line establishing

SW480 cells or SW620 cells were seeded into the tissue culture dishes with around 50% confluency. The cells were transiently transfected with eGFP/eGFP-IQ/eGFP-MA/HA-PKM2/HA-399E respectively. The medium was replaced on the next day, and cells were reseeded into the new dishes with around 10% confluency. The selective medium (containing 0.4mg/ml of G418) was applied when the cells have adhered to the dishes. The selective medium

was replaced every two days till the clones have been formed. For the eGFP expression cells, fluorescent microscope was applied to examine the stable expression of the GFP proteins. 24 clones for each construction were picked up by using the autoclaved discs. Each clone was cultured in each well of the 24-well plate. The clones of cells were gently pipetted to disassociate the cells. After the cells had adhered to the bottom of the plates, the discs were removed and the selective medium (0.2mg/ml of G418) was replaced as previously. The fluorescent microscope and western blot were used to confirm the stable expression of the proteins after the cells has been amplified.

2.4.4 RNA interference

The expression level of endogenous protein can be down regulated by RNA interference technique. 30-50 % confluence of cells was seeded to into a 6-well plate in corresponding culture medium one day before the performance of knockdown experiment. On the second day, the wells in the plates were washed by 2ml of Opti-MEM medium to remove FBS. siRNA duplex for p68 was purchased from Dharmacon RNA Technologies. RNA duplex was dissolved in DEPC-treated H₂O to 40 pmol/ μ l. 200 pmol of siRNA duplex was diluted in 250 μ l of Opti-MEM medium. 5 μ l of transfection reagent, lipofectamine RNAiMAX (invitrogen), was added into 250 μ l of Opti-MEM medium. These two solutions were added together and the mixture was incubated for 30 minutes at room temperature. 0.75ml of Opti-MEM medium was added into each well. Then, the mixture was added into each well gradually. Fresh medium might be added into each well on the second day. In order to re-express the corresponding wide type or mutant proteins in the cells, those knockdown cells were transfected the corresponding plasmid using FuGene 24 hours later. Cells were released from the wells by scratching or trypsinization after additional 48 hours and were then harvested by centrifuging at 1,000 rpm for 10 minutes at 4 °C.

2.4.5 Growth factor treatment

In order to stimulate the cells get into the migration status, certain growth factors including EGF and HGF were tested. Mammalian cells were starved for 6-12 hours with Opti-MEM medium before the addition of the growth factor. Growth factors were dissolved in Opti-MEM medium. The starved cells were cultured in growth factor containing Opti-MEM medium for a given amount of time (3-5hours). Opti-MEM was used as a control. The cells were harvested once the treatment has done and the cell lysate was stored at -80 °C. For the images assay, the cells were fixed after the treatment of the growth factors.

2.4.6 Monolayer scratch treatment

A scratch or multiple scratches using pipette tips were introduced into a 6 well cell culture plate. The cells were further cultured under serum starvation for 30 minutes, and were subsequently cultured for an additional indicated time. The scratch-treated cells were either directly visualized by microscopes or the cells were fixed and subsequently examined by immunostaining. Alternatively, the cells were collected and lysized. The prepared cellular extracts were then used for other analyses.

2.4.7 Whole cell lysate preparation (both RIPA buffer and grind method)

Mammalian cells were washed twice with cold 1X PBS and were collected by centrifuging at 1,000 rpm for 10 minutes at 4°C. 1X RIPA buffer (50 mM Tris-HCl, pH7.4, 150 mM NaCl, 0.25 % deoxycholic acid, 1 % NP-40 and 1 mM EDTA) supplemented with Protease Inhibitors Cocktail (PIC) (Sigma) and phosphatase inhibitors cocktail (Pierce) was used to lysis the collected cells at 4°C for few hours. The volume of the RIPA depends on the amount of the cells needs to be lysized. A rotary plate at 4 °C was used to incubate the lysing cells. Then, cell

lysis solution was centrifuged at 13,200 rpm for 10 minutes at 4°C to spin down the cell debris. The supernatant was collected carefully and stored at -80 °C for later applications.

2.4.8 Nuclear extract and cytoplasmic extract preparation

A nuclear extraction kit from Active Motif. Nuclear can be used to isolate cytosolic proteins and nuclear proteins from mammalian cells. The collected cells were washed with cold 1X PBS added with PIC twice to remove culture medium. The centrifuge was used to spin down the cells and 1,500 rpm for 10 minutes at 4 °C was applied. In general, 1 ml of 1X hydrophobic buffer supplemented with PIC was used to resuspend 1×10^6 cells and the cells were incubated on ice for 15 minutes. Then, 50 µl of detergent was added into the suspended cells to break the cytoplasmic membrane and the tube was vortexed at maximum speed for 30 seconds. The supernatant was collected after the cell suspension was spin down. The supernatant was stored at -80 °C up to 2 months. The cold 1XPBS was used to wash the pellet, which contains the nucleus, for twice to get rid of the cytoplasmic protein. Then, AM1 lysis buffer containing PIC and 1 mM DTT was used to resuspend the nuclear pellet and the mixture was incubated at 4 °C for 1hour. Next, the tube was centrifuged at 13,200 rpm for 10 minutes at 4 °C to collect the supernatant which was the nuclear extracts. The nuclear extract was collected and stored at -80°C for further applications.

2.4.9 Immunoprecipitation (IP) and co-immunoprecipitation (Co-IP)

IP and Co-IP experiments were performed in 1X NET buffer (150 mM NaCl, 50 mM Tris-HCl [pH 7.5], 5 mM EDTA, 0.05 % NP-40) supplemented with 1X PIC (EDTA free) and phosphatase inhibitors (1mM SoV, 5mM NaF). 500 µg of whole cell lysate or subcellular extract were incubated with appropriate primary antibody in 1X NET buffer overnight at 4°C. The next day, 50 µl of protein G agarose bead slurry was washed five times with NET buffer and was then

added into the reaction tube and incubated on a rotating platform for additional 2 hours at 4 °C. The tubes were centrifuged at 1,000 rpm for 5 minute at 4 °C. The immuno-complex samples were denatured in 30 µl of 2X SDS-PAGE loading buffer by heating at 100 °C for 10 minutes. The supernatant which contains the immuno precipitated proteins were separated in SDS-polyacrylamide gel electrophoresis (PAGE) and the specific protein bands were detected by using the corresponding antibodies.

2.4.10 Calmodulin beads pull-down and GST beads pull-down

Calmodulin beads (50 µl /assay) were washed with the NET buffer for 4 times. 500 µg of the whole cell lysate was added to the washed calmodulin bead (around 25 µl). Ca^{2+} or EGTA was added into the mixture accordingly. The mixture was incubated for 3 hours at 4°C, and the calmodulin beads were then collected at 5000rpm, 4°C for 1 minute. The beads were washed with the corresponding buffer for 3 times with the same setting. The washed beads were finally loaded with 30 µl of 2X SDS loading buffer and heated at 100°C for 8 minutes. The supernatant was collected and was analyzed by the Western-blot technique.

The method for the GST beads pull-down assay is similar to the calmodulin beads pull down assay. The difference for the GST beads pull-down assay is that the beads pulled down the GST tagged protein (or protein complex) instead of the calmodulin binding proteins. Different buffer was used based on the purpose of the experiment.

2.4.11 Western Blot

Protein samples, including the recombinant proteins, whole cell lysate, subcellular lysate or immuno-complex, were added with 5X SDS-PAGE loading buffer. The protein samples were denatured by heating at 100 °C for 10 minutes. Multiple proteins were separated in 8~10% SDS-PAGE according to the molecular weight of proteins and were transferred to nitrocellular

membranes. Nitrocellular membranes, sponges and filter papers were soaked in transfer buffer (Tris-HCl, pH8.3, Glycine and 40 % methanol) for 10 minutes. The transfer sandwich was assembled as the manufacturer's instructions indicated. The transferring was carried out at 105 mA for 3 hour. The transfer sandwich was disassembled after the transferring has done. The nitrocellular membranes was stained with Pancrea S dye for 10 seconds and destained with ddH₂O for 1 minute to remove extra dye. Multiple protein bands would be visualized on the membranes. The membranes can be cut into several strips based on the molecular marker. The strips of the membrane were washed with TBST for 10 minutes to remove Panceau S dye and the strips can be blocked with 5% BSA for 30-60 minutes. The membranes were incubated with primary antibody in 2% BSA-TBST buffer at 4 °C for 2 hours to overnight. The next day, the membranes were washed with TBST buffer for three times. The time for the washing would be around 5 -10 minutes each time. Then, the strips were incubated with the secondary antibody (1:2,000 dilutions in 2% BSA-TBST buffer) for 2 hours at room temperature. The strips were then washed for three times again to remove the non-specific binding of the antibodies. The strips were incubated with SuperSignal West Dura Extended Duration Substrate (Pierce) for 2 minutes and the western blotting signals were detected in a UVP machine.

2.4.12 *Boyden chamber assay*

CHEMICON® QCM™ 24-well Cell Migration Assay (ECM508) was used to measure the migration capability of the epithelial cells including SW480 and SW620 cells. The capability of cell migration was examined when the cells were knocked down with endogenous p68 and /or transfected with corresponding vectors. The treated cells were collected and counted. Around 3×10^5 of the cells were seeded into the inserted wells in FBS free medium (L-15). The lower chamber was loaded with FBS free medium in order to let the cells to starve for 5 hours. 5 hours

later, the medium in the lower chamber was changed to 10% FBS medium. The cells were then incubated in the incubator for 16 hours (overnight) to let the transmigration through the membrane occur. 225 μ l of prewarmed cell detachment solution was prepared and loaded into new well in the 24-well plate. The insert well with the cells was carefully washed twice and the medium was removed completely. The insert was then moved to the new wells with the prewarmed cell detachment solution. The incubation of the insert in the detachment solution took 30 minutes. The detachment solution in the well was added with 225 μ l of lysis buffer after the insert was removed. 300 μ l of the mixture were reloaded into the 96-well plate. The absorbance was obtained.

2.4.13 Recombinant adenovirus generation and infection in mammalian cells

The DNA sequences of four truncated p68 were cloned from pHM6-p68 vector. Recombinant adenoviruses expressing four truncates of p68 were constructed according to the method generated by Dr. Tong-Chuan He (Luo J et al, Nature protocols, 2007, 2(5), 1236-1247). Briefly, truncated p68 DNA sequences were cloned into a shuttle vector pAdEasy-1 with EcoRI and NotI restriction endonuclease sites respectively. The resultant plasmid was digested with PmeI and transformed into competent AdEasier cells containing the adenoviral backbone plasmid pAdEasy-1 by electroporation method (BJ5183-AD-1, Stratagene). Recombinants were selected for kanamycin resistance and further confirmed by restriction endonuclease analyses. The confirmed plasmid with the truncated p68 DNA was digested with PacI restriction endonuclease and transformed into HEK-293 cells expressing adenovirus E1 (Stratagene). The production of recombinant adenoviruses in HEK-293 cells was examined with GFP expression under fluorescent microscope. The amplified virus was released from HEK-293 cells by four freeze-thaw-vortex cycles. Cell debris was removed by centrifugation at 500 rpm at 4 °C for 15

minutes. The recombinant adenoviruses were amplified three rounds in HEK-293 cells to get higher titers. Titers were measured with GFP expression in HEK-293 cells with a series of 10 folds dilutions of virus lysate. The titer in the initial lysate was around 1.43×10^9 pfu/ml. After three rounds of amplification the titer reached 1.09×10^{13} pfu/ml. All viral lysates was stored in -80 °C for further applications. To infect cells, cells were seeded in 48-well plates to 70~80 % confluence one day before infection. 50 μ l of viral lysate (1.09×10^{13} pfu/ml) was added to each well of a 48-well plate and incubated with cells for 3-5 hours. For 24-well and 6-well plates, the scales were increased according to the plate sizes. Fresh medium was changed 3~5 hours later. The expression of HA tagged truncated p68 proteins were examined by Western blot 48 hours later.

2.4.14 Cell proliferation assay

Cell proliferation was measured by counting the cells or was measured with BrdU cell proliferation assay (Calbiochem). In brief, cells were seeded into a 96 well culture plate (1×10^4 cells/well). Cells were treated with the growth factor or IQ peptide. 24 hours post treatment, BrdU was added in a working solution with fresh culture medium. 20 μ l of working solution was added into each well and the plate was put in a cell culture incubator. 24 hours later, culture medium was removed and cells were fixed with 50 μ l of Fixative/Denaturing solution. 20 μ l of anti-BrdU antibodies was then added into the well. The cells were incubated for 1 hour at room temperature. The cells were washed with the washing buffer, and the secondary antibody conjugated with HRP was added into the wells and incubated with cells for 30 minutes at room temperature. The plates were washed with ddH₂O and the cells were incubated with substrate solution for 15 minutes. A spectrophotometric plate reader (Wallac 1420 multilabel counter) at

wavelengths of 450-540nm was used to measure the absorbance after each well was added with 50 μ l of stop solution.

2.4.15 Living cell imaging and fixed cell imaging

When the cells were exogenously expressed with fluorescent protein or fluorescent tagged protein (including DsRed and GFP proteins), the fluorescent signal can be detected under fluorescent microscope or Confocal microscope in living cells. The confluency of the cell in the chamber can be 30%-50%. A special chamber was used to observe the living cells under confocal microscope with high resolution. Phenol red free medium may improve the detection of fluorescent signals.

Immunostaining technique was used to examine the location of a specific protein in the cells. Immunostaining are often done in the fixed cells. In simple, cells in a specific chamber were washed by pre-warmed 1XPBS buffer twice. The cells were then fixed in pre-warmed 3.7% formaldehyder for 10 minutes. The cells were washed with 1X PBS for three times. The cells were treated with 0.2% Triton-100 for 5 minutes. The cells were washed by 1X PBS for three times. The cells were incubated with signal enhancer solution for 30 minutes. The cells were rinsed with 1X PBS. The first antibody to a specific protein was added into 1X PBS contains 2.5% BSA. And the cells were incubated withthe first antibody for 60 minutes at room temperature. The cells were washed with 1X PBS for three times. The second antibody which conjugated with fluorescent signal was added into 1X PBS containing 2.5% BSA. The cells were incubated in the second antibody solution for 30 minutes. The cells were loaded with the oil containing DAPI to stain the nucleus after the cells were washed with 1X PBS. The slide was then covered with a slide and the samples were ready to be observed under confocal microscope.

2.5 Animal experiment

2.5.1 Tumor implanting (subcutaneous tumor injection)

Cells from four 175 cm² flasks were trypsinized with 4ml of trypsin and neutralized by adding 10ml of the 10% FBS added L-15 medium. The cells were then collected in the tube by centrifuging at 850rpm for 5 minutes. The cells were washed for three times with 40ml of pre-chilled HBSS. The total amount of the cells was counted. 6×10^7 of the cells (for 6 mice) was collected in two eppendorf tubes respectively. The cells were centrifuged and resuspended in 200 μ l of HBSS (total volume was around 300 μ l). 300 μ l of the BD matrigel was added and swirled with the cell suspensions. Then 100 μ l of the cell mixture were subcutaneously implanted into the nude mouse at the right flank. Need to mention that, all the needle and pippet and HBSS needs to be pre-chilled before being used. In this experiment, 6 mice were used for each group.

2.5.2 Tumor size measurement and tumor weight measurement at the end point

The volume of the tumor was measured and calculated after the nude mice were subcutaneously implanted with tumor cells for 5 days. The width/ length/height of the tumor were measured every two days. The formula: $4p/3 \times (\text{width}/2)^2 \times (\text{length}/2)$ was used to calculate the volume of the tumors. After around one month later (4-5 weeks), the mice were euthanized. The tumors were isolated from the mice and the weights of the tumor were measured.

2.5.3 Tumor splenic metastasis examination

The mRNA level of human keratin was detected in the spleen of mice by RT-PCR. The mice spleens were collected and submerged into the RNAlater RNA stabilization reagent (Cat. 76104). For the tumor fraction with the size 0.5 cmX0.5cmX0.5cm was put into the reagent. The samples were kept at 4°C for overnight, and the samples were then moved to -20°C (for less than 4 weeks). 1/3 of the spleen was used, and the total mRNA was isolated by the RNeasy Plus mini

kit (Cat. 74134, including the QIAshredder column, Cat. 79654). For the RT-PCR, 10 μ g of the total mRNA was used. Primers for mouse b-actin, human b-actin, and human keratin 18 were used (The cDNA which was generated from 10 μ g of the total mRNA may need to be purified before the PCR.). In order to examine the green fluorescent signal from the spleen of mouse, the UVP machine with 488nm of the wavelength of the filter was used. Tumor grew from eGFP stable cells was used as a positive control.

2.5.4 Tissue staining

The tumors were isolated from the euthanized mice. The tumors were buried in Cryo-gel and were frozen in liquid Nitrogen till the gel freeze to form a white solid cubic. The samples were stored in -80°C . Frozen tissue was then cut by cryostat. The cut splice (10 μ m) was fixed by the 100% cold Acetone (-20°C) for 9 minutes. The slice was stained with the specific antibodies using the regular cell immunostaining method as described previously. DAPI was used to stain the nucleus. The confocal was used to examine the expression of the corresponding of proteins as well as the location of the proteins.

2.6 Materials

Table 2 Antibodies and proteins

Name	Source	Company	Cat #
P68	Rabbit	Georgia State University, Animal center facility	RGG#4
P68-RGG	Mouse	Auburn University Hybridoma Facility	6G7C8A2
Anti-HA	Mouse	Roche	12CA5
Anti-HA Fluorescein, high affinity (3F10)	Mouse	Roche	1 988 506
Anti-HA poly	Rabbit	Georgia State University, Animal center facility	--
His-Tag mAb	Mouse	Cell signaling	27E8
CRM1	Rabbit	Abcam	Ab3459
GAPDH	Mouse	Chemicon	MAB374
Lamin A/C	Rabbbit	Cell Signaling	2032

Beta-Actin	Rabbit	Cell signaling	4967
Calmodulin	Rabbit	ZYMED	61-8500
Calmodulin	Mouse	ZYMED	13-6900
Calmodulin	Rabbit	Abcam	Ab45689-100
Calmodulin	Mouse	Abcam	Ab38841-200
Kinesin [KN-01]	Mouse	Abcam	Ab9097-100
Dynein intermediate chain 1	Mouse	Abcam	Ab6304-100
Alpha-tubulin, clone DM1A	Mouse	Sigma	T9026
Beta-tubulin, clone TUB2.1	Mouse	Sigma	T4026
GFP	Rabbit	Abcam	Ab6556-25
GFP	Rabbit	Cell signaling	2555
His tag [HIS.H8]	Mouse	Abcam	Ab18184-100
DDX17	Rabbit	Abcam	Ab52826-100
GRB2 [Y237]	Rabbit	Abcam	Ab32037
Kinesin HC motor domain protein	---	Cytoskeleton	KR01
Karyopherin-a2	---	CALBIOCHEM	420370
Karyopherin-b1	---	CALBIOCHEM	420375
Calmodulin	---	Abcam	Ab53982-1
Beta-catenin	Mouse	Upstate	8E4
Stat3	Mouse	Cell signaling	124H6
γ -tubulin	Rabbit	Abcam	Ab11317-100
Jak2	Rabbit	Cell signaling	D2E12
Phospho-Stat3	Rabbit	Cell signaling	D3A7
Eg5	Rabbit	Abcam	Ab38095-200
Lamin B1	Rabbit	Abcam	Ab16048-100
MAP2K5 antibody	Mouse	Abnova	1B4
MAP2K5(pSer311/Thr315)	Rabbit	AnaSpec	29770
NTF97/importin β	Mouse	Abcam	Ab2811
PKM2	Rabbit	Georgia State University, Animal center facility	---
Phosphotyrosine	Mouse	Abcam	PY20
Phosphotyrosine	Mouse	Cell signaling	P-Tyr-100
Caspase-3 (3G2)	Mouse	Cell signaling	9668

Cleaved Caspase-3 (Asp 175)	Rabbit	Cell signaling	9661S
Caspase-8 (1C12)	Mouse	Cell signaling	9746

Table 3 Primers

Construction	Primers (5'-3')	Vector
NLS3 deletion	GGGGATGGGTGGCCTGCCATGGGT GGGGGTTTCCACAAAAACAATGGTTTTATT	PCDNA3.1- eGFP-p68
NLS4 deletion	GGGGGTGGATTTAATACCTTTAGAG GGGACCTGAACCTCTGTCTTCGAC	PCDNA3.1- eGFP-p68
Mutation 1	GGCCTTATCTGGAAAGGAGTTTGGAAACCCTGGG	pHM6-p68
Mutation 2	GGAAACCCTGGGGAGAAATTAGTTAAAGAGAAGT GGAATCTT	pHM6-p68
Mutation 3	CCCTGATTTGGCTAGGGCCACAGCACAAAGAGGTG	pHM6-p68
Mutation 4	CACAAGAGGTGGAAACATACAGAGCAAGCAAGG AAATTACAGTTAGAG	pHM6-p68
Mutation 5	CCATTGTTTTTGTGGAAACCAAAGCAAGATGTGAT GAGCTTACCAGA	pHM6-p68
Mutation 6	TGATGAGCTTACCAGAAAAATGGCGAGAGATGGG TGGCCT	pHM6-p68
Mutation 7	CATTGTTTTTGTGGAAACCAAAGCAGCATGTGATG AGCTTACCAGAAAAATG	pHM6-p68
Mutation 8	ATGTGATGAGCTTACCAGAGCAATGGCGAGAGAT GGGTGG	pHM6-p68
Mutation NES2	GGATCTGGGAAAACATTGTCTTATGCGCTTCCTGC CGCTGCCACATCAATCATCAGCCA	pHM6-p68
Mutation NES5-1	CAAAGAAGTAAGACAGCTTGCTGAAGATGCCGC GAAAGACTATATTCATATAAACATTGGTG	pHM6-p68
Mutation NES5-2	AGACTATATTCATATAAACATTGGTGCAGCTGAAC TGAGTGCAAACCACA	pHM6-p68
Mutation NES5-3	AGATGCCGCGAAAGACTATATTCATGCAAACATT GGTGCAGCTGA	pHM6-p68
Mutation NES8-1	CTAATAACATAAAGCAAGTGAGCGACGCTGCCTC TGTGCTTCGTGAAGCTAATCAAG	pHM6-p68
Mutation NLS4-1	GGTTCAGGTCGTTCCGCGGGTAGAGGAGGCAT	pHM6-p68
Mutation NLS4-2	GCATGAAGGATGACCGTGCGGACAGATACTCTGC	pHM6-p68
Mutation NLS4-3	CGGGACAGATACTCTGCGGGCGCAAGGGGTGGAT TTAATACC	pHM6-p68

NLS-1 forward And reverse	AATTCGGATGAAGAAGTTTGGAAACCCTGGGGAG AAATTAGTTAAAAAGAAG GATCCTTCTTTTAACTAATTTCTCCCCAGGGTTTC CAAACCTCTT CATCGG	DsRed
NLS-2 forward And reverse	AATTCGGATGAGGCGCACAGCACAAGAGGTGGAA ACATACAGAAGAAGCAAG GATCCTTGCTTCTTCTGTATGTTTCCACCTCTTGTG CTGTGCGCCT CATCGG	DsRed
NLS-3 forward And reverse	AATTCGGATGAAAAGAAGATGTGATGAGCTTACC AGAAAAATGAGG GATCCCTCATT TTTCTGGTAAGCTCATCACATCTTC TTTTCATCGG	DsRed
NLS-4 forward And reverse	AATTCGGATGCGTTCCAGGGGTAGAGGAGGCATG AAGGATGACCGTCGGGACAGATACTCTGCGGACA AAAGG GATCCCTTTTGTCCGCAGAGTATCTGTCCCGACGG TCATCCTTCATGCCTCTCTACCCCTGGAACGCAT CGG	DsRed
NLS3-M	AATTCGGATGAAAGCAGCATGTGATGAGCTTACC AGAGCAATGGCGAGG GATCCCTCGCCATTGCTCTGGTAAGCTCATCACAT GCTGCTTTCATCGG	DsRed
NLS4-M	AATTCGGATGCGTTCCGCGGGTAGAGGAGGCATG AAGGATGACCGTGCGGACAGATACTCTGCGGGCG CAAGG GATCCCTTGCGCCCGCAGAGTATCTGTCCGCACGG TCATCCTTCATGCCTCTCTACCCGCGGAACGCAT CGG	DsRed
Putative NES-1	AATTCGGATGCAGGGATGGCCAGTTGCTCTAAGT GGATTGGATATGGTTGGAGTGGCG GATCCGCCACTCCAACCATATCCAATCCACTTAGA GCAACTGGCCATCCCTGCATCGG	DsRed
Putative NES-2	AATTCGGATGTCTGGGAAAACATTGTCTTATTTGC TTCTTGCCATTGTCCACATCCAG GATCCTGGATGTGGACAATGGCAGGAAGCAAATA AGACAATGTTTTCCAGACATCGG	DsRed
Putative NES-3	AATTCGGATGAAGGGACCACAAATACGTGATTTG GAGAGAGGTGTGGAAATCTGTATTGCG GATCCGCAATACAGATTTCCACACCTCTCTCCAAA TCACGTATTTGTGGTCCCTTCATCGG	DsRed
Putative NES-4	AATTCGGATGCTTGATATGGGCTTTGAACCCAAA TAAGGAAGATTGTGGATCAAATAAGG GATCCCTTATTTGATCCACAATCTTCCTTATTTGGG GTTCAAAGCCCATATCAAGCATCGG	DsRed
Putative NES-5	AATTCGGATGTGGCCAAAAGAAGTAAGACAGCTT GCTGAAGATTTCTGAAAGACTATATTCATATAAA	DsRed

	CATTGGTGCACCTTGAACCTGGGG GATCCCCCAGTTCAAGTGCACCAATGTTTATATGA ATATAGTCTTTCAGGAAATCTTCAGCAAGCTGTCT TACTTCTTTTGGCCACATCGG	
Putative NES-6	AATCCGATGGCAAACCACAACATTCTTCAGATTG TGGATGTGTGTCATGACGTAGAG GATCCTCTACGTCATGACACACATCCACAATCTGA AGAATGTTGTGGTTTGGCCATCGG	DsRed
Putative NES-7	AATCCGATGGCCTCCAGAGGGCTAGATGTGGAA GATGTGAAATTTGTCATCCAG GATCCTGGATGACAAATTCACATCTTCCACATCT AGCCCTCTGGAGGC CATCGG	DsRed
Putative NES-8	AATCCGATGACACCTAATAACATAAAGCAAGTG AGCGACCTTATCTCTGTGCTTCGG GATCCCGAAGCACAGAGATAAGGTCGCTCACTTG CTTTATGTTATTAGGTGTCATCGG	DsRed
NES2-M	AATCCGATGTCTGGGAAAACATTGTCTTATGCGC TTCTGCGCTGCCACATCCAG GATCCTGGATGTGGGCAGCGGCAGGAAGCGCATA AGACAATGTTTTCCAGACATCGG	DsRed
NES5-M	AATCCGATGTGGCCAAAAGAAGTAAGACAGCTT GCTGAAGATGCCGCGAAAGACTATATTCATGCAA ACATTGGTGCAGCTGAACTGGGG GATCCCCCAGTTCAGCTGCACCAATGTTTGCATGA ATATAGTCTTTCGCGGCATCTTCAGCAAGCTGTCT TACTTCTTTTGGCCACATCGG	DsRed
NES8-M	AATCCGATGACACCTAATAACATAAAGCAAGTG AGCGACGCTGCCTCTGTGCTTCGG GATCCCGAAGCACAGAGGCAGCGTCGCTCACTTG CTTTATGTTATTAGGTGTCATCGG	DsRed
Primer for sequencing NLS4+NES8	GGAAAAGCTCCTATTCTGATTG	---
Primer for sequencing NES 2	CAAGGAAATTACAGTTAGAGGTC	---
Primer for sequencing NES5	CAATCTGAGAAGAACAACCTAC	---
DII-forward And reverse	GGGGGTGGATTTAATACCTTTAGAG GGGACCTGAACCTCTGTCTTCGAC	PCDNA3.1- eGFP
175+500 -1	GTTTGGTGCTGGCACCAACTCGGGAAGTGGC	pHM6-p68
175+500 -2	GGACAGATACTCTGCGGGCAAAGGGGTGGATTT A	pHM6-p68

Delete NLS3	AGGAGAATAAAACCATTGTTTTTGTGGAAACCGA TGGGTGGCCTGCCATGGGTATCCA TGGATACCCATGGCAGGCCACCCATCGGTTTCCAC AAAAACAATGGTTTTATTCTCCT	pHM6-p68
Delete NLS4	CAGTTGCTTCAGTTGGTTCGAAGACAGAGGTTTCAG GTGGTGGATTTAATACCTTTAGAGACAGGG CCCTGTCTCTAAAGGTATTAATCCACCACCTGAA CCTCTGTCTTCGACCAACTGAAGCAACTTG	pHM6-p68
NLS3-M	AATCCGATGAAAGCAGCATGTGATGAGCTTACC AGAGCAATGGCGAGG GATCCCTCGCCATTGCTCTGGTAAGCTCATCACAT GCTGCTTTCATCGG	DsRed
NLS4-M	AATCCGATGCGTTCGCGGGTAGAGGAGGCATG AAGGATGACCGTGCGGACAGATACTCTGCGGGCG CAAGG GATCCCTTGCGCCCGCAGAGTATCTGTCCgcACGG TCATCCTTCATGCCTCTCTACCCGCGGAACGCAT CGG	DsRed
NES2-M	AATCCGATGTCTGGGAAAACATTGTCTTATGCGC TTCTGCCGCTGCCACATCCAG GATCCTGGATGTGGGCAGCGGCAGGAAGCGCATA AGACAATGTTTTCCAGACATCGG	DsRed
NES5-M	AATCCGATGTGGCCAAAAGAAGTAAGACAGCTT GCTGAAGATGCCGCGAAAGACTATATTCATGCAA ACATTGGTGCAGCTGAACTGGGG GATCCCCCAGTTCAGCTGCACCAATGTTTGCATGA ATATAGTCTTTCGCGGCATCTTCAGCAAGCTGTCT TACTTCTTTGGCCACATCGG	DsRed
NES2 mutation	GGATCTGGGAAAACATTGTCTTATGCGCTTCCTGC CGCTGCCACATCAATCATCAGCCA	pHM6-p68
NES5 mutation	CAAAGAAGTAAGACAGCTTGCTGAAGATGCCGC GAAAGCATATATTCATATAAACATTGGTG AGACTATATTCATATAAACATTGGTGCAGCTGAAC TGAGTGCAAACCACA AGATGCCGCGAAAGACTATATTCATGCAAACATT GGTGCAGCTGA (this primer based on above two)	pHM6-p68
NES8 mutation	CTAATAACATAAAGCAAGTGAGCGACGCTGCCTC TGTGCTTCGTGAAGCTAATCAAG	pHM6-p68
NES8-M	AATCCGATGACACCTAATAACATAAAGCAAGTG AGCGACGCTGCCTCTGTGCTTCGG GATCCCGAAGCACAGAGGCAGCGTCGCTCACTTG CTTTATGTTATTAGGTGTCATCGG	DsRed
Primer for fragment 1	GGGAAGCTTATATTCGAGTGACCGAGACCG GGGCGGCCGCTTAGTCTGCTTCATCAAGGACAAG G	pHM6

Primer for fragment 2	GGGAAGCTTAAGAATGCTTGATATGGGCTTTG GGGCGGCCGCTTAATCTTCCACATCTAGCCCTCT	pHM6
Primer for fragment 3	GGGAAGCTTAGTGAAATTTGTCATCAATTATGAC GGGCGGCCGCTTAGTCCCGACGGTCATCCTTC	pHM6
Primer for fragment 4	GGGAAGCTTACGATACTCTGCGGGCAAAGG GGGCGGCCGCTTATTGGGAATATCCTGTTGGCATT	pHM6
N-terminal of p68	TGGCCATCCCTGAGCTTGA GTCTAGAGGGCCCGTTTAAA	PCDNA3.1-eGFP
Truncate before NLS-3	GGTTTCCACAAAAACAATGGTT GTCTAGAGGGCCCGTTTAAA	PCDNA3.1-eGFP
Truncate after NLS-3	GATGGGTGGCCTGCCATG ATATCTGCAGAATTCTGACTTG	PCDNA3.1-eGFP
C-terminal of p68	CGTGAAGCTAATCAAGCAATTA ATATCTGCAGAATTCTGACTTG	PCDNA3.1-eGFP
(DIII)D2 (a.a.0-a.a.126) Reverse primer	TGGCCATCCCTGAGCTTGA	PCDNA3.1-eGFP
D3 (a.a.0-a.a.350) Reverse primer	GGTTTCCACAAAAACAATGGTT	PCDNA3.1-eGFP
Forward CaM	GGGGGTACCATGGCTGACCAGCTTACTGAA	pHM6
Reverse CaM	GGGGCGGCCGCTCTACTTCGCTGTCATCATTG	pHM6
Sequencing primer for CaM	CAATGGTATGAACCAACAGGC	---
His-p68-CaM fusion protein Forward and reverse primers	GGGGGATCCGTCCCAGACTACGCTGGA GGGGCGGCCGCTCTACTTCGC	PET-30 vector

Table 4 Mammalian cell lines

Name	Company	Origin	Culture medium
SW480	ATCC	Human colorectal adenocarcinoma cells	Leibovitz L-15 +10% FBS
SW620	ATCC	Human colorectal adenocarcinoma cells derived from metastatic site: lymph node	Leibovitz L-15 +10% FBS
WM115	ATCC	Human skin melanoma cells	MEM + 10% FBS
WM266	ATCC	Human skin metastatic melanoma cells	MEM + 10% FBS
H460	ATCC	Human primary lung	DMEM + 10% FBS
H146	ATCC	Human metastatic lung	DMEM + 10% FBS
T98G	ATCC	Human brain glioblastoma cells	MEM + 10% FBS +1mM pyruvate kinase +1mM non-essential amino acid
U-87 MG	ATCC	Human brain astrocytoma cells	MEM +10%FBS +1mM pyruvate kinase +1mM non-essential amino acid
HEK293	ATCC	Human kidney epithelial cells immortalized by adenovirus 5 DNA	DMEM+ 10% FBS
HEL 299	ATCC	Human lung normal fibroblast cells	MEM + 10% FBS
NIH/3T3	ATCC	Mouse embryo fibroblast cells	DMEM + 10% FBS
4T1 (Luciferase)	Gifted from Dr. Aneja Ritu	Mouse breast cancer cells	DMEM+10% FBS

Table 5 Chemicals

Name of chemical	Company
α -Cyano-4-hydroxycinnamic acid	Agilent Tech, Santa Clara
2-Mercaptoethanol	Sigma Aldrich, St. Louis
Acetic acid	VWR International, West Chester
Acetone	VWR International, West Chester
Acrylamide/bisacrylamide solutions	Fisher BioReagent, Fairlawn
Agar	Sigma-Aldrich, Saint Louis
Agarose	MP Biomedicals, Aurora
Ammonium persulfate	Sigma-Aldrich, Saint Louis
Anhydrous acetonitrille	Applied Biosystems, Foster City
Bacto Yeast Extract	BD Bioscience, Spark
Bacto Tryptone	BD Bioscience, Spark
Bovine serum albumin	Promega, Madison
Bromophenol Blue	EMD Biosciences, San Diego
Coomassie blue	Sigma-Aldrich, Saint Louis
Deep purple total protein stain	Amersham Biosciences, Piscataway
Dithiothreitol	Shelton Scientific, Shelton
Ethanol	AAPER Alcohol & Chemical, Shelbyville
Ethidium bromide	Sigma-Aldrich, Saint Louis
Ethylenedinitro-tetraacetic acid (EDTA)	Sigma-Aldrich, Saint Louis
Fetal calf serum	HyClone, Logan
Formaldehyde	Calbiochem, San Diego
Formic acid	EMD Biosciences, San Diego
FuGENE 6 Transfection Reagent	Roche Applied Science, Indianapolis
GelCode Blue Stain Reagent	Pierce, Rochford
Glycine	MP Biomedicals, Aurora
HiTrap affinity columns	Amersham Biosciences, Piscataway
Hydrochloric acid	VWR International, West Chester
Imidazole	Sigma-Aldrich, Saint Louis
Isopropyl- β -D-thiogalactopyranosid	Sigma-Aldrich, Saint Louis
Isopropanol	VWR International, West Chester
Kanamycin solution	Teknova, Hollister
Lipofectamine 2000	Invitrogen, Carlsbad
Lipofectamin RNAiMAX	Invitrogen, Carlsbad
Lysozyme	Sigma-Aldrich, Saint Louis
Magnesium Chloride	Fisher Biotech, Fairlawn
Methanol	VWR International, West Chester
Molecular weight marker (DNA)	MBI Fermentas, Hanover
Molecular weight marker (protein)	MBI Fermentas, Hanover
N- (2-hydroxyethyl) piperazine-N`-(2-ethanesulfonic acid) (HEPES)	Sigma-Aldrich, Saint Louis
Nickel-nitrilotriacetic acid (Ni-NTA) agarose	Qiagen, Hilden

Ni-TED™ Silica	Active Motif, Carlsbad
N, N, N', N'-Tetramethylethylenediamine	Promega, Madison
Nonidet P40	Roche Applied Science, Indianapolis
Normal goat serum (10%)	KPL, Gaithersburg
Phenol/Chloroform	Promega, Madison
Phenylmethylsulfonyl fluoride	Fluka, Switzerland
Phosphatase inhibitor cocktail	Sigma-Aldrich, Saint Louis
Poly-L-lysine solution	Sigma-Aldrich, Saint Louis
Ponceau S	Sigma-Aldrich, Saint Louis
Protease inhibitor cocktail tablets	Roche, Germany
Protein G agarose	Upstate, Charlottesville
Protein G sepharose 4 fast flow	Amersham Biosciences, Piscataway
Sephadex G-25	Amersham Biosciences, Piscataway
Superdex 200 HR 10/30	Amersham Biosciences, Piscataway
Sodium acetate	Promega, Madison
Sodium azide	Fluka, Switzerland
Sodium bicarbonate	Sigma-Aldrich, Saint Louis
Sodium chloride	Fisher BioReagent, Fairlawn
Sodium dodecyl sulfate	Fisher BioReagent, Fairlawn
Sodium fluoride	Fluka, Switzerland
Sodium hydroxide	Fisher BioReagent, Fairlawn
Sodium orthovanadate	EMD Biosciences, San Diego
Sodium pyruvate	Cellgro, Herndon
Triton X-100	Sigma-Aldrich, Saint Louis
Trypan Blue	Sigma-Aldrich, Saint Louis
Trypsin proteomics grade	Sigma-Aldrich, Saint Louis
Tween-20	Sigma-Aldrich, Saint Louis
Urea	Fisher Biotech, Fairlawn
X-tremeGene siRNA Transfection Reagent	Roche, Germany
RNA stabilization reagent	Qiagen

Table 6 Experimental kits

Name	Company
Glucose Assay Kit	BioVision, Mountain View
BrdU cell proliferation assay	Calbiochem,
Pyruvate Assay Kit	BioVision, Mountain View
Kinesin/dynein Motility Kit	Cytoskeleton
Tubulin Polymerization Assay	Cytoskeleton
Improm-II Reverse Transcription System	Promega, Madison
MinElute PCR Purification Kit	Qiagen, Valencia
Nuclear Extract Kit	Active Motif, Carlsbad
ProteoSliver Plus Sliver Stain Kit	Sigma-Aldrich, Saint Louis
Shredder column	Qiagen, Valencia
RNeasy Plus Kit	Qiagen, Valencia
Qiaprep Spin Mini-Prep	Qiagen, Valencia
Qiaquick Gel Extraction Kit	Qiagen, Valencia
QuickChange II XL site-directed Mutagenesis Kit	Stratagene, La Jolla
Trypsin Profile IGD kit for in-gel digests	Sigma-Aldrich, Saint Louis

CHAPTER 3

P68 RNA HELICASE IS A NUCLEOCYTOPLASMIC SHUTTLING PROTEIN

3.1 Abstract

P68 RNA helicase is a prototypical DEAD box RNA helicase. The protein plays a very important role in early organ development and maturation. In consistence with the function of the protein in transcriptional regulation and pre-mRNA splicing, p68 was found to predominately localize in the cell nucleus. However, recent experiments demonstrate a transient cytoplasmic localization of the protein. We report here that p68 shuttles between the nucleus and the cytoplasm. The nucleocytoplasmic shuttling of p68 is mediated by two nuclear localization signal (NLS) and two nuclear exporting signal (NES) sequence elements. Our experiments reveal that p68 shuttles via a classical RanGTPase dependent pathway.

3.2 Introduction

In eukaryotic cells, the nucleus is separated from the cytoplasm. Maintenance of cellular functions requires trafficking of many bio-macromolecules into and out of the nucleus. Proteins that are targeted to the nucleus are marked by one or more sequence elements termed Nuclear Localization Signal (NLS) (Goldfarb, Garipey et al. 1986; Schneider, Schindewolf et al. 1988), while the proteins that are transported out of the nucleus carry one or more Nuclear Exporting Signal (NES) sequence tags (Wen, Meinkoth et al. 1995). Nucleocytoplasmic trafficking occurs via the nuclear pore complex (NPC). Most protein transportation through the NPC is mediated by specific cargo and a nuclear receptor system, importins and exportins (Gorlich and Kutay 1999; Nakielny and Dreyfuss 1999; Hill 2009). Interestingly, many proteins often carry both NLS and NES signals. This characteristic usually leads to shuttling of these proteins between the nucleus and the cytoplasm (Lusk, Blobel et al. 2007). The nuclear p68 RNA helicase (hereafter

referred to as p68) is a prototypical member of the DEAD box family of RNA helicases (Lane and Hoeffler 1980; Crawford, Leppard et al. 1982). As an early example of a cellular RNA helicase, the ATPase and the RNA unwinding activities of p68 RNA helicase were previously documented (Ford, Anton et al. 1988; Hirling, Scheffner et al. 1989; Iggo and Lane 1989). Expression of p68 correlates with cell proliferation and early organ maturation (Stevenson, Hamilton et al. 1998). We have previously reported that p68 is phosphorylated at multiple amino acid residues, including serine/threonine and tyrosine (Yang and Liu 2004; Yang, Lin et al. 2005). Tyrosine phosphorylation of p68 correlates with tumor progression (Yang, Lin et al. 2005). Phosphorylation of p68 at Y593 mediates the effects of growth factors in promoting epithelial-mesenchymal-transition (EMT). The phosphor-p68 promotes EMT by facilitating β -catenin nuclear translocation (Yang, Lin et al. 2006). In the present study, we demonstrate that p68 shuttles between the nucleus and the cytoplasm. P68 shuttling is mediated by two NLSs and two NESs sequence elements. Our data show that p68 shuttles via the classical RanGTPase dependent pathway.

3.3 Results

3.3.1 *P68 RNA helicase shuttles between the nucleus and the cytoplasm*

We previously reported that Y593 phosphorylated p68 facilitates cytoplasmic β -catenin nuclear translocation by displacing the cytoplasmic β -catenin anchor protein axin (Yang, Lin et al. 2006). P68 RNA helicase has been shown to predominantly localize in the nucleus (Nicol, Causevic et al. 2000). Thus, an interesting question is how p68 translocates to the cytoplasm. We reasoned whether phosphorylation of p68 at Y593 facilitated p68 cytoplasmic translocation. To test this possibility, we employed a panel of cell lines; SW620, a metastatic colon cancer cell, SW480 and HT-29, non-metastatic colon cancer cell lines, and T98G, a cell line derived from

glioblastoma. P68 is not phosphorylated at tyrosine residues in HT-29 cells (Yang, Lin et al. 2006) but is phosphorylated at high levels in T98G cells (Yang, Lin et al. 2007). P68 is highly phosphorylated at tyrosine residue in SW620 cells and low levels in SW480 cells (Fig. 3.1A, and data not shown). Consistent with our previous observations, high levels of β -catenin were detected in the nucleus of SW620 cells. Nuclear β -catenin was significantly reduced in the cells in which the endogenous p68 was replaced by the Y593F mutant, suggesting that phosphorylation of p68 at Y593 contributed to β -catenin nuclear localization in SW620 cells (Fig. 3.1B). Immuno-staining using the antibody p68-RGG showed that p68 was almost completely localized in the nucleus in all four cell lines (Fig. 3.1C), indicating that phosphorylation of p68 did not change the predominant nuclear localization of the protein. Another possibility for the cytoplasmic localization is that p68 shuttles between the nucleus and the cytoplasm. A number of nuclear localized proteins have been shown to be nucleocytoplasm shuttles (Cartwright and Helin 2000; Zhu and McKeon 2000). We thus employed a heterokaryon assay (Fan and Steitz 1998) using SW620 cells and NIH3T3 cells to test whether p68 shuttles between the nucleus and the cytoplasm. HA-tagged p68s were exogenously expressed in SW620. After fusing the SW620 with NIH3T3 cells, the HA-p68s were detected in the nucleus of NIH3T3 cells (Fig. 3.2, upper panel). As a negative control, the non-shuttling protein MS2-DEK (Shibuya, Tange et al. 2004) expressed in SW620 cells could not be detected in the nucleus of NIH3T3 cells (Fig. 3.2, bottom panel). The experimental results suggest that p68 is a nucleus – cytoplasm shuttling protein with a much longer residence time in the nucleus.

3.3.2 Identification of NLSs and NESs of p68

Most nucleocytoplasm shuttling proteins carry sequence elements of both NLS and NES. We analyzed the amino acid sequence of p68 and found a number of sequence segments that

resemble NLSs and NESs (Fig. 3.3A and 3.4A). To test the functionality of these putative NLSs and NESs in p68, we first fused each individual putative NLS or NES with a fluorescent protein DsRed. The fusion proteins were expressed in SW620 cells. It was clear that only NLS3 and NLS4 led to a substantial nuclear accumulation of the fluorescent protein (Fig. 3.3B). On the other hand, fusion of NES2 and NES5 with the fluorescent protein resulted in high levels of cytoplasmic fluorescent protein (Fig. 3.4B). Interestingly, fusion of NES8 with DsRed led to slightly higher levels of fluorescent protein localization in the cytoplasm (Fig. 3.4B), indicating that NES8 is a weak nuclear export signal. Treatment of cells with leptomycin B (LMB) abolished the cytoplasmic localization patterns of DsRed fusion proteins (NES2, NES5, and NES8) (Fig. 3.4C). The results suggest that NLS3 and NLS4 potentially function as nuclear localization signals, and NES2, NES5 and NES8 potentially function as nuclear export signals of p68. To verify the functionality of NLS3 and NLS4, we made mutations in NLS3 (R352A, R353A, K360A, and R362A) or NLS4 (R484A, R494A and K501A) in the context of full length p68. The HA-tagged mutants were expressed in SW620 cells. Immunostain of the exogenously expressed HA-p68, wild type and mutants, indicated that nuclear localization of the HA-mutants was dramatically reduced (Fig. 3.3C). Quantification of fluorescence intensity in the nucleus and the cytoplasm of a random group of cells confirmed the reduction of nuclear HA-p68 (the mean average of Cyto/Nu fluorescence intensity ratio were 0.038 +/- 0.026 for wt, 1.477 +/- 0.029 for NLS3-M, and 1.489 +/- 0.097 for NLS4-M). The results suggested that NLS3 and NLS4 indeed functioned as nuclear localization signals of p68. To further test the functions of nuclear localization signals and nuclear export signals of p68, we constructed several p68 deletion mutants (Fig. 3.5A). These deletion mutants were expressed in SW620 cells either as HA-tag proteins or eGFP-fused proteins (due to small sizes of truncates). Locations of each putative

NLSs and NESs of p68 in the p68 truncation proteins are indicated. The localizations of these p68 truncates were analyzed by immunostaining with anti-HA antibody or imaging of eGFP. DII and DIII localized to the nucleus, indicating that NLS4 is a functional NLS, while the NES1 and NES 7-8 are not functional NES. Strong cytoplasmic DIV and DV were observed, suggesting that one or more of NES 2 – 6 are functional NES. The stronger fluorescence in DV than that of DIV and certain levels of cytoplasmic localization of DVI indicate function of NLS3. In summery, these results supported that NLS3 and NLS4 may function as nuclear localization signals of p68 while NES2 and NES5 may function as nuclear exporting signals of p68. Consistent with our experimental results, NLS3 is located in an exposed helical secondary structure while NLS4 is located in an exposed loop that is flanked by two α -helixes in a computer simulated p68 model structure (Fig. 3.5B). Both NES5 and NES8 are also located on the exposed surface in the model structure, while NES2 is buried under an α -helix in the model structure. This structure model provided additional support for the identification of the NLSs and NESs of p68. We next mutated both NLS3 and NLS4 by the same mutations described above (hereafter referred to as NLS-M). The mutant was expressed in SW620, T98G, and SW480 cells. Immunofluorescence staining demonstrated that no significant levels of p68 mutant localized in the cell nucleus (Fig. 3.3D). The results were further verified by immunoblot analyses of exogenously expressed HA-p68s (wt and the mutant) in the cytoplasmic and nuclear extracts made from HA-p68s expressing T98G cells (Fig. 3.3E). It was also clear that the mutant no longer shuttled between the nucleus and the cytoplasm as demonstrated by the heterokaryon assay (Fig. 3.2, 2nd panel from top). The distribution pattern did not change significantly when the heterokaron cells were treated with LMB (data not shown). In our structure model, NES5 and NES8 are well exposed, while NES2 is buried. Thus, we constructed the p68 NES mutant by

mutations at both NES5 and NES8, F293A, L294A, L298A, L305A, L456A, and I457A (hereafter referred to as NES-M). Immuno fluorescence staining of SW620 cells that expressed the mutant showed an exclusive nuclear localization of the mutant (Fig. 3.4D). Heterokaryon assay demonstrated that the nucleocytoplasmic shuttling of p68 was almost completely abolished by the mutations (Fig. 3.2, 3rd panel from top). In contrast, mutations separately on either NES5 or NES8 (same mutations) did not completely abolish but certainly reduced the shuttle of HA-p68 to the NIH3T3 cell nucleus (Fig. 3.2, 4th and 5th panels from top). Our mutational analyses confirmed that the NLS3/NLS4 and NES5/NES8 were functional NLSs and NESs, and these NLSs and NESs were required for p68 nucleocytoplasmic shuttling.

3.3.3 P68 shuttles via a RanGTPase dependent pathway

CRM1 is an export receptor mediating nuclear export of proteins that carry leucine-rich nuclear exporting signals (Fornerod, Ohno et al. 1997; Watanabe, Fukuda et al. 1999). We demonstrated that p68 RNA helicase carries NLSs and NESs sequences that mediate nucleocytoplasmic shuttling. We reasoned whether overexpression of CRM1 would affect the localization of p68. We exogenously expressed CRM1 in SW620 cells (Fig. 3.6A). Immunoblot of p68 indicated that there were significantly higher levels of cytoplasmic p68 after CRM1 was exogenously expressed in the cells, and the increases in cytoplasmic p68 were inhibited by LMB treatment (Fig. 3.6B). Increases in cytoplasmic p68 by expression of CRM1 were not observed with p68 mutant that carries mutations at both NES5 and NES8 (Fig. 3.6C). The results suggest that p68 RNA helicase was exported from the nucleus mediated by exportin pathway. The effects of exogenous expression of CRM1 on p68 export were further confirmed by immunostaining analyses. It was evident that staining of p68 in the cytoplasm was significantly increased upon the expression of CRM1, and the increases were inhibited by LMB (Fig. 3.6D). To further verify

that the p68 nucleocytoplasmic shuttling is mediated by RanGTPase pathway, we tested whether p68 interacts with importin *in vitro*. We used a commercially available his-tag importin $\alpha 2$. When his-importin $\alpha 2$ was incubated with recombinant GST-p68, GST-p68 could not be pulled-down by his-importin $\alpha 2$ (Fig. 3.7A). It is known that importin $\alpha 2$ functions as a hetero-dimer with importin β (Lindsay, Plafker et al. 2002; Goldfarb, Corbett et al. 2004). Therefore, we added another commercially available recombinant importin $\beta 1$. It was clear that GST-p68 coprecipitated with his-importin $\alpha 2$ when importin $\beta 1$ was also present, but the p68 NLS mutant (NLS-M) did not co-precipitate with his-importin $\alpha 2$ under any condition (Fig. 3.7A). We also carried out co-precipitation experiments with immunopurified HA-p68 from HEK293 cells. The His-importin $\alpha 2$ /importin $\beta 1$ co-immunoprecipitated with the purified HA-p68 using anti-HA antibody. However, the importins did not immunoprecipitate with HA-p68 NLS mutant (Fig. 3.7B). The observations suggested that p68 interacts with the importin $\alpha 2/\beta 1$ dimer, providing additional support for the nucleocytoplasmic shuttling of p68 via the RanGTPase pathway.

3.4 Discussion

P68 RNA helicase was shown to predominately localize in the cell nucleus (Nicol, Causevic et al. 2000). However, recent experiments carried out in Janknecht's and our laboratories showed a transient cytoplasmic localization of the protein (Rossow and Janknecht 2003). In this report, we presented data demonstrating the nucleocytoplasm shuttling of p68 RNA helicase. Our experiments showed that p68 shuttling is mediated by two NLSs and two NESs sequence elements. The p68 nuclear export and import follow a RanGTPase dependent pathway. Interestingly, a number of DEAD/DExH box RNA helicases have also been shown to shuttle between the nucleus and cytoplasm, including eIF-4AIII, An3, and RNA helicase A (Askjaer, Bachi et al. 1999; Shibuya, Tange et al. 2004; Aratani, Oishi et al. 2006).

However, the functional role of the shuttling of these RNA helicase is not well known. The cellular function(s) of the p68 RNA helicase nucleocytoplasmic shuttling is an open question. In general, proteins that shuttle between the nucleus and the cytoplasm usually have distinct cellular functions in these two separated sub-cellular compartments. They often relocate to the nucleus or the cytoplasm to fulfill specific functional role(s) in response to a particular cellular signal stimuli (Kau, Way et al. 2004; Xu and Massague 2004). Alternatively, nucleocytoplasmic shuttling of a protein can function as a 'chaperons' to help nuclear import or export of other proteins or RNAs. (Fried and Kutay 2003; Loyola and Almouzni 2004). Cellular functions of p68 helicase in the cell nucleus are well documented. The protein is functionally involved in gene transcription (Endoh, Maruyama et al. 1999; Bates, Nicol et al. 2005; Buszczak and Spradling 2006; Yang, Lin et al. 2007), pre-mRNA (Liu 2002; Lin, Yang et al. 2005), pre-rRNA, and premiRNA processing (Fukuda, Yamagata et al. 2007; Davis, Hilyard et al. 2008). Whether p68 RNA helicase has any potential function(s) in the cytoplasm is currently not very clear. Hong et al. detected the interaction of p68 with HCVNS5B in the cytoplasm in the viral infected or NS5B expressing 293 cells and the interaction is essential for viral replication (Goh, Tan et al. 2004). In another independent study, D. Harris and co-workers found that the 3'-nontranslated region of HCV interact with p68 in an RNA affinity capture experiments with the cytoplasmic extracts of 293 cells that express viral replicon (Harris, Zhang et al. 2006). These observations are consistent with our experimental results indicating that p68 localizes both in the nucleus and the cytoplasm. However, despite the demonstration of the function of p68 in HCV replication in the cytoplasm of virus infected cells, the evidence that suggest the involvement of p68 in any cellular process in the cytoplasm is currently lack. We have observed a significant increases in cytoplasmic p68 levels upon treatment of cells with several growth factors and

chemokines (Yang, Lin et al. 2006), indicating that p68 may function in the cytoplasm under specific cellular conditions, such as abnormal growth or cell migration in response to growth factor or chemokine stimulations.

Localization of p68 is intriguing. The protein is shuttling between the nucleus and the cytoplasm, while the protein predominantly resides in the cell nucleus, and is nearly undetectable outside of the nucleus by immunostaining or by immunoblot analyses of cytoplasmic extracts. The phenomenon suggests that the function of the NESs of p68 is tightly regulated. It is possible that an interacting partner(s) in the nucleus masks the p68 NES sequences. Nuclear export of p68 depends on the dissociation of the interaction partner(s). Our data demonstrated that p68 has three sequence elements that potentially function as NESs. On the other hand, structural modeling of p68 helicase core showed that one of the potential NES (NES2) is buried under an α -helix. Therefore, it is possible that a specific post-translational modification drives conformational changes which subsequently expose this buried NES sequences for p68 export (Wrighton, Lin et al. 2009). Very similar regulatory mechanisms were observed in nuclear exporting and importing of Dok1 and NF-AT1 (Okamura, Aramburu et al. 2000; Niu, Roy et al. 2006). In consistent with this notion, we observed a substantially increased cytoplasmic p68 levels in cells when the cells were treated with several growth factors and chemokines (Yang, Lin et al. 2006), suggesting a possibility that the growth factors and chemokines treatments trigger the exposure of the NES sequences for nuclear export of p68.

There are two NLS sequences. Mutation of either NLS reduced nuclear localization (increased cytoplasmic p68, Fig. 3.3C), indicating that both NLSs contribute partly to nuclear localization of p68.

3.5 Materials and methods

3.5.1 Reagents, antibodies, and cells

Leptomycin B (LMB), PEG3350, cycloheximide, HA peptide, and protease inhibitor cocktail were purchased from Calbiochem, Sigma, and Roche respectively. Antibodies against HA and His tags, phospho-tyrosine, GAPDH, Lamin A/C, β -actin, and Histone 2A were purchased from Roche, Cell signaling, Upstate, and Chemicon respectively. Cell lines SW480, SW620, HT29, NIH3T3, and T98G were purchased from ATCC and cultured by following the vendor's instructions.

3.5.2 Plasmids construction

The HA-tagged p68s expression plasmids (wild type, and Y593F, Y595F, LGLD, and NLS-M mutants) were constructed in pHM6 vectors as previously reported (Yang, Lin et al. 2006). The vectors for expression of eGFP and DsRed fusion proteins were constructed using eGFP-pcDNA-3.1(+) or pDsRed1-N1 vectors. Full length p68 or deletion mutants of p68 variants were sub-cloned into the vector by EcoR321 and NotI restriction sites. The p68 or deletion mutants were fused at the C-terminal of the fluorescent protein tag. Different putative NLSs or NESs tagged DsRed were constructed by cloning into pDsRed-N1 vectors at 5' (BamHI and EcoRI sites) with the addition of a starting methionine at the N-terminal of each NLS or NES respectively. Site directed mutagenesis was performed using QuikChange® Multi Site-Directed Mutagenesis Kit (Stratagene). All the DNA clones and mutations were verified by auto-DNA sequencing at GSU. The procedures for transfection of expression vectors of HA-p68, fluorescent proteins, and Crm1 and duplex RNAi were similar to our previous reports (Yang, Lin et al. 2006).

3.5.3 Expression and purification of recombinant GST-p68

Recombinant GST-p68 was expressed and purified as described in our previous report (Huang and Liu 2002).

3.5.4 Interactions between p68 and importins

Recombinant GST-p68 (8 μ g) was incubated with commercial his-importin α 2 (8 μ g) and/or importin β 1 (Calbiochem) overnight at 4°C in 500 μ l in PBS buffer. After incubation, the protein complex was pulled-down by Ni-TED silica beads. The pull-down proteins were separated by 10% SDS-PAGE, and were analyzed by immunoblot using anti-GST or anti-his-tag antibodies. The presence of importin β 1 was visualized by ponceau S staining. For coimmunoprecipitation of HA-p68 with importin α 2, HA-p68s, wt or mutant, were expressed in HEK cells and were immunoprecipitated using 30 μ l anti-HA antibody. Protein G agarose (50 μ l) was added to the mixture. After extensive washing, HA-p68s were eluted from the beads by competition using HA peptide (100 μ g/ml). The eluted HA-p68s were dialyzed against PBS. The recombinant importin α 2 and/or β 1 was incubated with the purified HA-p68 in PBS for 4 hours. The protein mixtures were immunoprecipitated using anti-HA antibody. The precipitated complex was separated in 10% SDS-PAGE followed by immunoblot using anti-his-tag antibody. The presence of HA-p68 was detected by immunoblot using the antibody p68-rgg.

3.5.5 Heterokaryon analyses and immunofluorescence imaging

The experimental procedures for immunofluorescence staining and imaging were similar to our previous reports (Wang, Liu et al. 2007). For heterokaryon analyses, SW620 cells were first transfected with HA-p68s (wt or mutants) or MS2-DEK. The cells were mixed with an equal number of mouse NIH3T3 cells 24 hour post-transfection and reseeded in 4-well chambers. Subsequently, 50 μ g/ml of cycloheximide was added to the culture medium to inhibit protein

synthesis. After 3h, the co-cultured cells were fused using 50% PEG3350 for 2 minutes, washed, and incubated with the medium containing 75 µg/ml cycloheximide for 3 hours. The treated cells were then fixed and immunostained as described above. Rabbit polyclonal anti-MS2 antibody was employed to stain MS2-DEK, followed by Alex Fluor 555 goat anti-rabbit IgG antibody. In a random group of 30 cells, the numbers of cells with both NIH3T3 and SW620 nucleus and with HA-p68 in NIH3T3 nucleus or in the cytoplasm of fused cells were counted. The percentage of HA-p68 in the nucleus or cytoplasm of fused cells equals fused cells with HA-p68 in NIH3T3 nucleus or cytoplasm / total fused cells with expression of HA-p68.

3.5.6 Computational homology structure modeling the helicase core of p68

The sequence alignment of p68 RNA helicase core with homologous RNA helicase cores of several DEAD box family proteins (e.g. vasa, eIF4A, Dhhlp, and UAP56) was performed by the program ClustalW. The secondary structure elements were predicted based on the consensus analysis using computational programs JPRED, PHD, and PSIPRED (Cuff, Clamp et al. 1998; McGuffin, Bryson et al. 2000). The homology modeling of the p68 RNA helicase structure was constructed using the homology-modeling server SWISS-MODEL based on X-ray crystal structure of *Drosophila* vasa (Sengoku, Nureki et al. 2006), which has the highest alignment score with p68 RNA helicase core. The putative NLSs and NESs were indicated in the modeling structure.

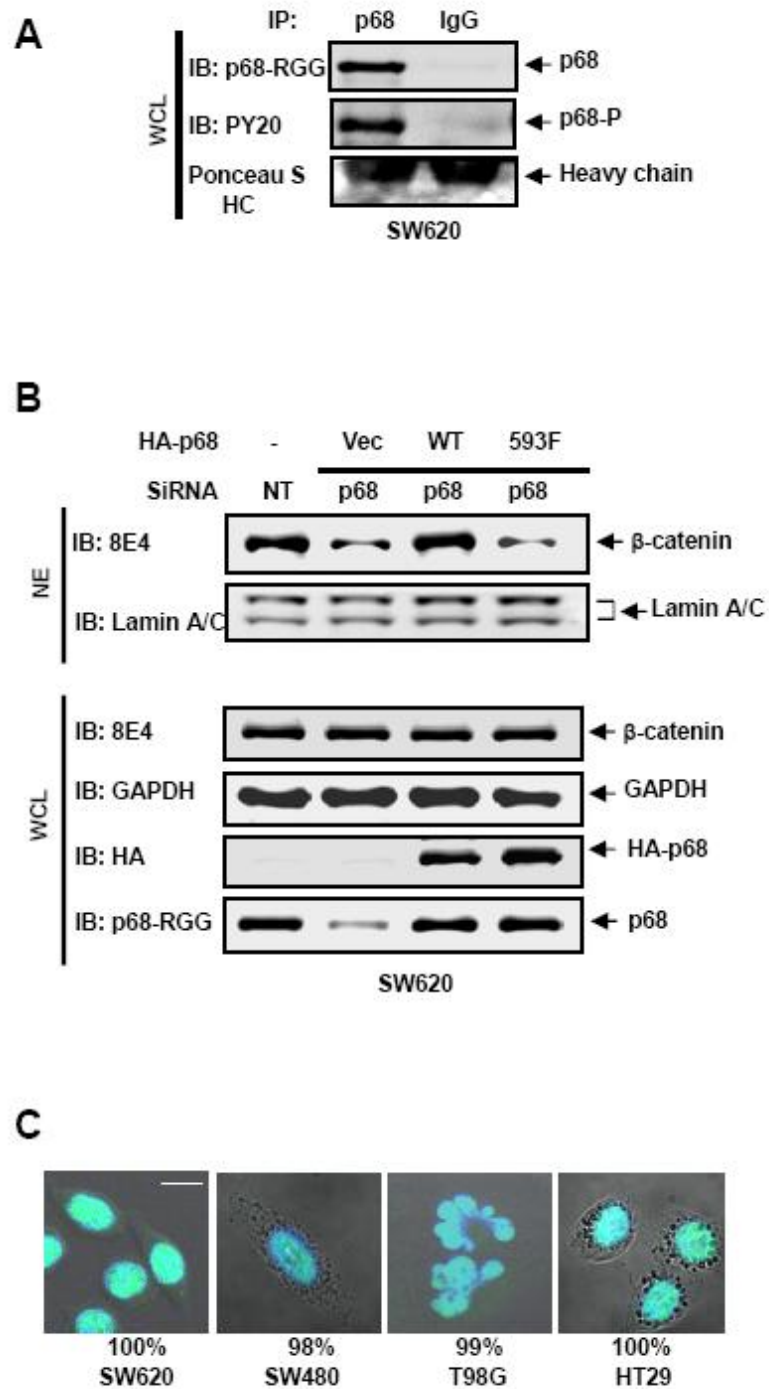


Figure 3.1 Phosphor-p68 promotes β -catenin nuclear localization in SW620 cells

(A) Tyrosine phosphorylation of p68 RNA helicase in SW620 cells. P68 was immunoprecipitated (IP) from whole cell lysate using Pab-p68 or rabbit IgG, followed by immunoblot (IB) with appropriate antibody (indicated). The IBs with antibody p68-rgg are the loading controls. Ponceau S staining IgG heavy chain is a loading control (Ponceau S:HC). (B) Nuclear β -catenin was examined by IB of nuclear extracts made from p68 knockdown (SiRNA(p68)/NT) SW620 cells. HA-p68s (WT or Y593F, Vec means vector alone) were expressed in p68 knockdown cells. The cellular levels of p68 were shown by IB using antibody p68-rgg (IB:p68-rgg). The cellular levels of HA-p68s were shown by IB using anti-HA antibody (IB:HA). Cellular levels of β -catenin were IB of β -catenin in 10% of whole cell extracts (IB:8E4). The IB of LaminA/C and GAPDH in the extracts were loading controls. All the immunoblot experiments were repeated three times and similar results were obtained. (C) Representative images of immunostaining of p68 RNA helicase using antibody p68-rgg in different cell lines (indicated). The green signal represents staining of p68. The blue signal represents staining of DNA. The images are an overlay of green and blue stains. The numbers are percentage of cells showing similar (nuclear or cytoplasm) staining pattern in a random group of 50 cells.

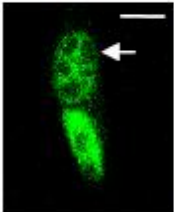
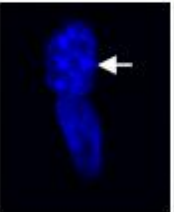

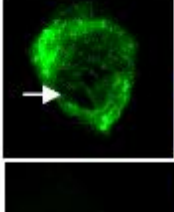
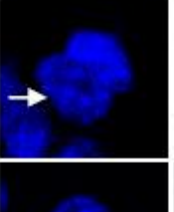
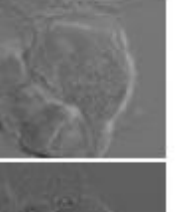
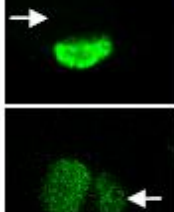
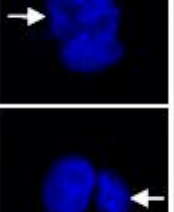
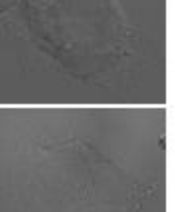
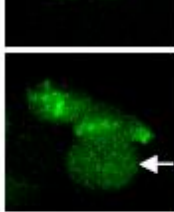
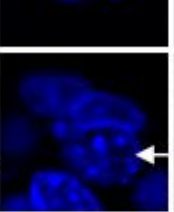
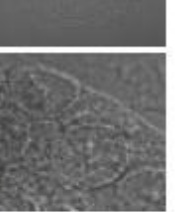
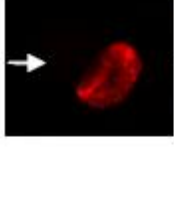
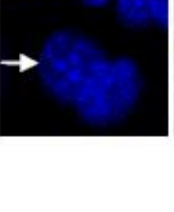




		Ab	DAPI	Phase	3T3 Nu	Cytoplasm
HA-p68	WT				90%	---
	NLS-M				---	87%
	NES-M				3%	---
	NES5-M				23%	---
	NES8-M				57%	---
Control	MS2-DEK				3%	---

Figure 3.2 P68 shuttles between the nucleus and the cytoplasm

Representative images of SW620 cells expressing HA-p68s (WT, NLS-M, NES-M, NES5-M, and NES8-M). After fusion with NIH3T3 cells, the HA-p68s were immunostained using anti-HA antibody (Ab). The green signal represents staining of HA-p68s. DAPI stains DNA in the cell nucleus of the fused cells (DAPI). The same treated cells were also revealed by phase contrast microscopy (Phase). MS2-DEK (immunostained by antibody against MS2) was a negative control for nucleocytoplasm shuttling assays. Arrows indicate the nucleus of mouse NIH3T3 cells. The numbers on the right side of images are the percentages cells with the HA-p68s detected in NIH3T3 nucleus (HA-3T3/NE) or in the cytoplasm (HA-Cyto) of the fusion cells based on counting a random group of 30 cells.

A

Putative NLSs	Amino acid sequence
NLS1	32-KKFGNPGEKLVKKK-45
NLS2	67-RRTAQEVETYRRSK-80
NLS3	351-KRRCDELTRKMRR-363
NLS4	482-RSRGRGGMKDDRRDRYSAGKR-502

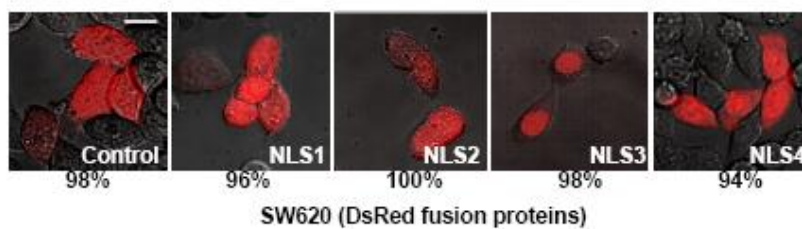
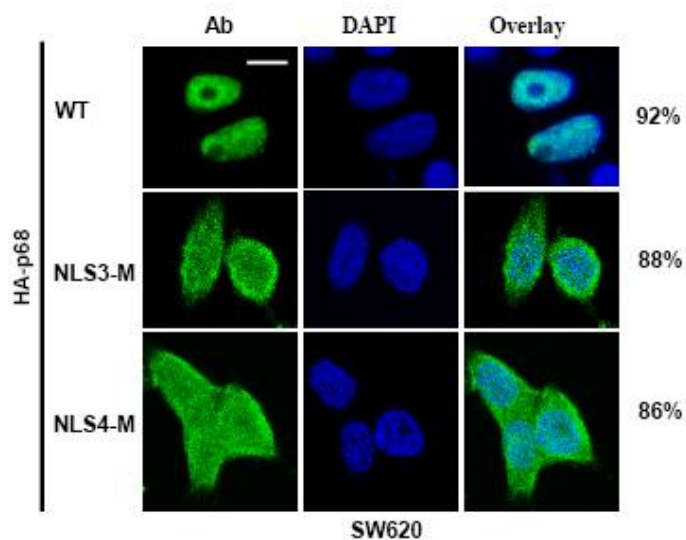
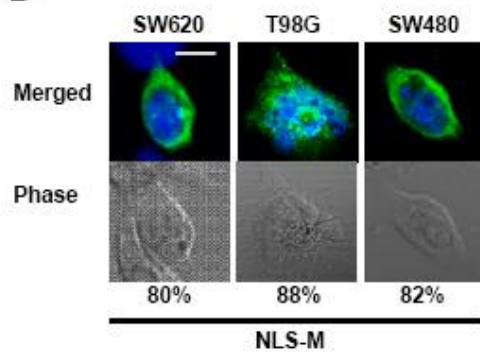
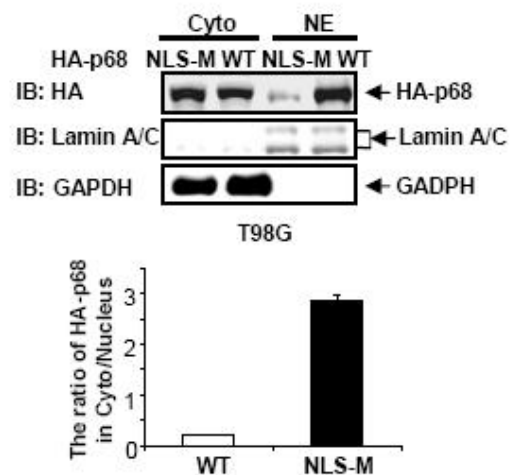
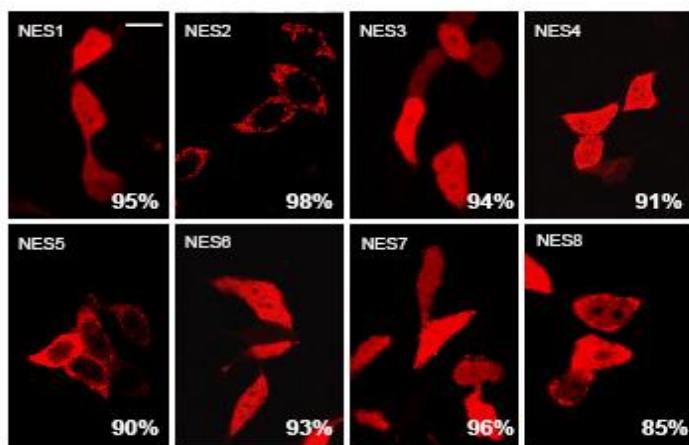
B**C****D****E**

Figure 3.3 NLSs of p68

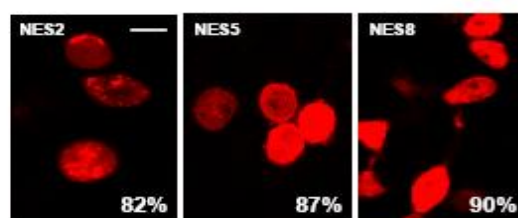
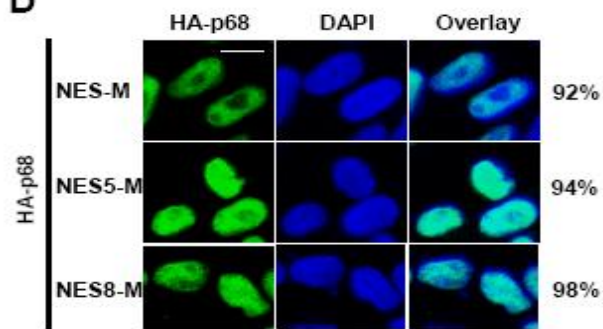
(A) Putative sequence segments of p68 that resemble NLS. (B) Representative of confocal fluorescent microscopy images show the localizations of p68 putative NLSs (N-terminal NLS1, NLS2, NLS3, NLS4) fused with DsRed in SW620 cells. The fused proteins were expressed in the cells. The red signal represents the expressed fusion proteins. The control is the expressed DsRed protein without the NLS fusion. (C) Examples of confocal images show sub-cellular localizations of the exogenously expressed HA-p68s in SW620 cells by immunostaining using anti-HA antibody (HA-p68). The green signal represents staining of HA-tag. The blue signal represents staining of DNA. HA-p68s, wild-type (WT) NLS mutant (NLS3-M, NLS4-M), were expressed in the cells. The right panels are overlay of anti-HA and DAPI stains. (D) HA-p68 NLS mutant (NLS-M) was expressed in different cell lines (indicated). Examples of confocal images of the cells show sub-cellular localizations of the NLS-M by immunostaining using anti-HA antibody. The top panel is the overlay of anti-HA and DAPI stains. The bottom panel is the phase contrast image of the stained cells. In (B), (C), and (D), the numbers are percentage of cells showing similar image pattern (nuclear vs cytoplasm staining) in a random group of 50 cells. (E) The levels of exogenously expressed HA-p68s, wild type (WT) or NLS-Mutant (NLSM) in the extracts made from the cytoplasm or the nucleus of T98G cells were examined by immunoblot using anti-HA antibody (IB:HA) (upper panel). The IBs with antibodies against lamin A/C and GAPDH are the loading controls. The bottom panel is the quantization of an average four separate experiments of the IB signals and presented as ratio of cytoplasmic over nuclear HA-p68s (WT or NLS-M).

A

Putative NESs	Amino acid sequence
NES1	123-QGWPVALSGLDMVGVA-138
NES2	142-SGKTLSYLLPAIVHIN-156
NES3	207-KGPQIRDLERGVEICIA-223
NES4	253-MLDMGFEPQIRKIVDQIR-270
NES5	282-WPKEVRQLAEDFLKDYIHINIGALELS-308
NES6	309-ANHNILQIVDVCHDVE-324
NES7	401-ASRGLDVEDVKFVIN-415
NES8	446-TPNNIKQVSDLISVLR-461

B

SW620 (DsRed fusion proteins)

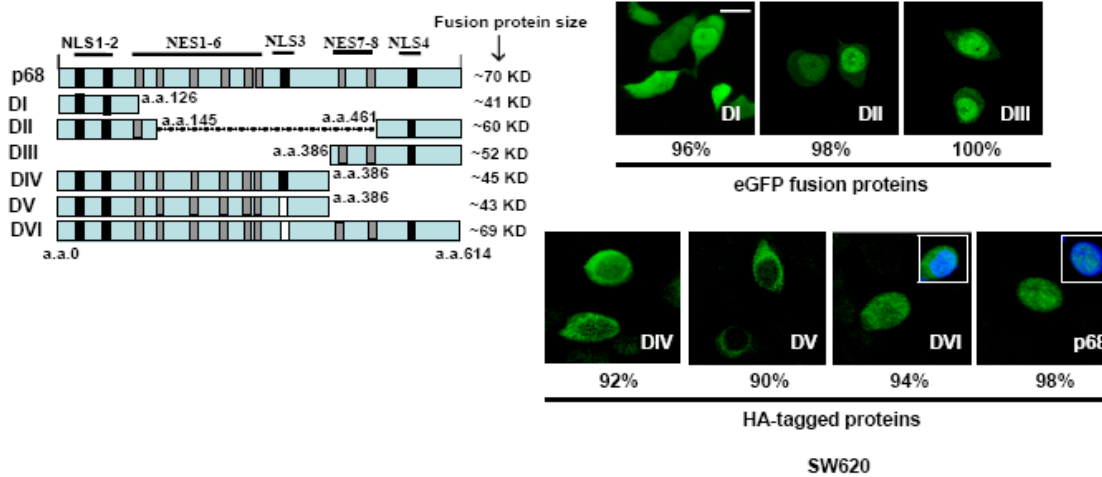
CSW620 (DsRed fusion proteins)
3-hour post LMB treatment**D**

SW620

Figure 3.4 NESs of p68

(A) Putative sequence segments of p68 that resemble NES. (B) Examples of confocal fluorescent microscopy images of SW620 cells show localizations of p68 putative NESs (N-terminal fusion) fused DsRed. The fused proteins were expressed in the cells. The red signals are the fluorescence of the expressed fusion proteins. (C) Inhibition of the exporting of selected putative p68 NESs (NES2, NES5, and NES8) fused with DsRed protein by LMB. The fusion proteins were expressed in SW620 cells. The cells were treated with LMB 24 hrs post fusion protein expression. The confocal fluorescence images were taken 3 hours post drug treatments. (D) Examples of confocal fluorescent microscopy images of SW620 cells show the sub-cellular localizations of the p68 NES mutants (NES-M, NES5-M, and NES8-M) in by immunostaining using anti-HA antibody. The green signal represents staining of HA-tag. The blue signal represents staining of DNA. In (B), (C) and (D), the numbers are percentage of cells showing similar localization pattern in a random group of 50 cells.

A



B

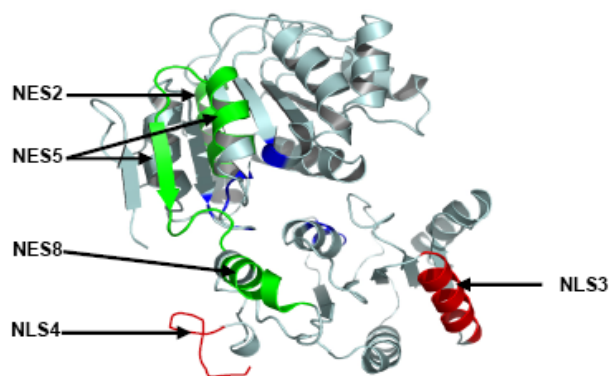


Figure 3.5 NESs and NLSs of p68

(A) P68 truncates (illustrated in the **left panel**) containing different putative NLSs and NESs either fusion C-terminal flank eGFP or N-terminal HA-tag were expressed in SW620 cells. The numbers indicate the molecular weight of each fusion protein. The black bars indicate the location of NLSs. The gray bars indicate NESs. The white bars indicate that the corresponding NLSs were deleted. (**right panel**) Examples of confocal fluorescent microscopy images show the localizations of eGFP fused or HA-tagged p68 truncates in SW620 cells. The HA-tagged p68 truncates in SW620 cells were immunostained with anti-HA antibody (Green). The numbers are percentage of cells showing similar localization pattern in a random group of 50 cells. (B) Model structure of p68 RNA helicase core domain. The model structure was constructed based on the X-ray crystal structure of another DEAD box RNA helicase *drosophila vasa*. The positions of NLS3 and NLS4, NES2, NES5, and NES8 are indicated by arrows.

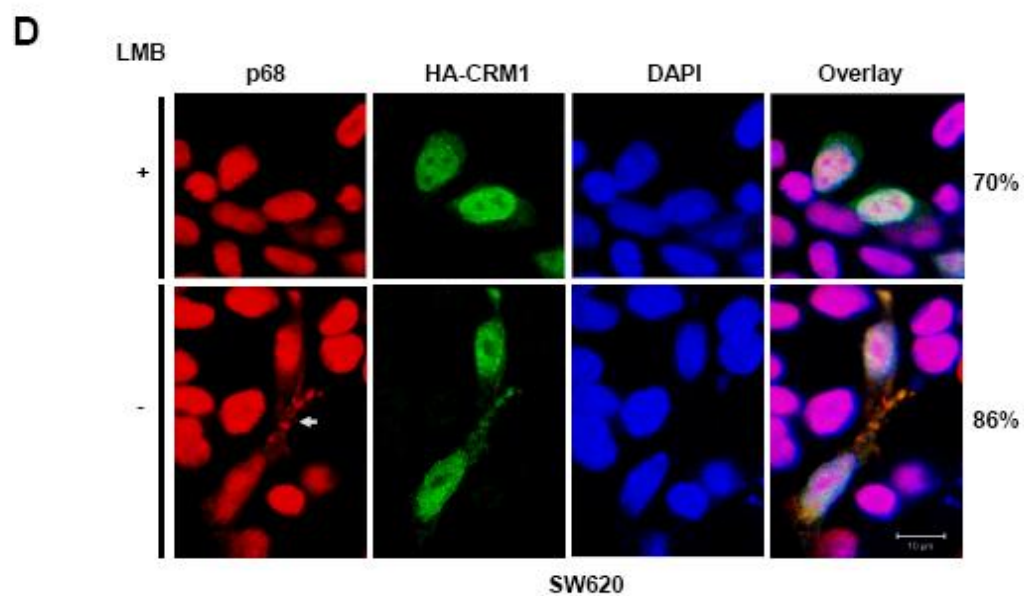
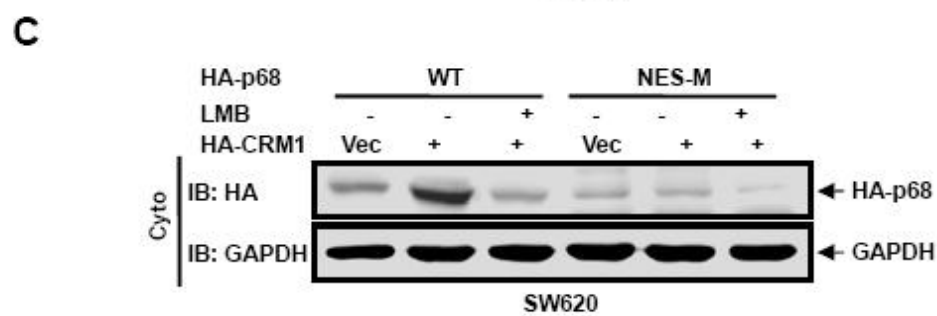
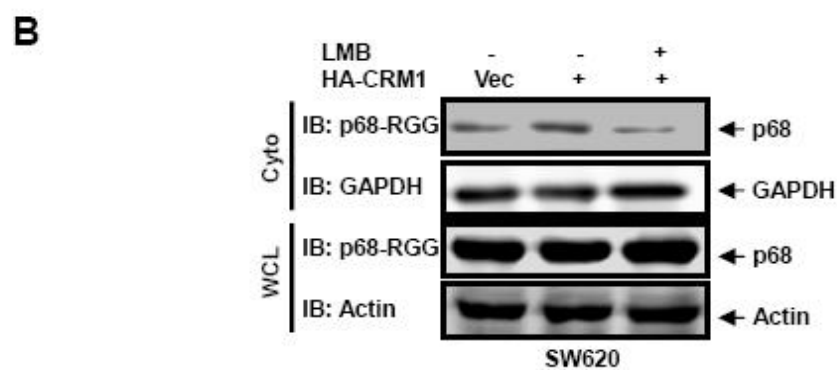
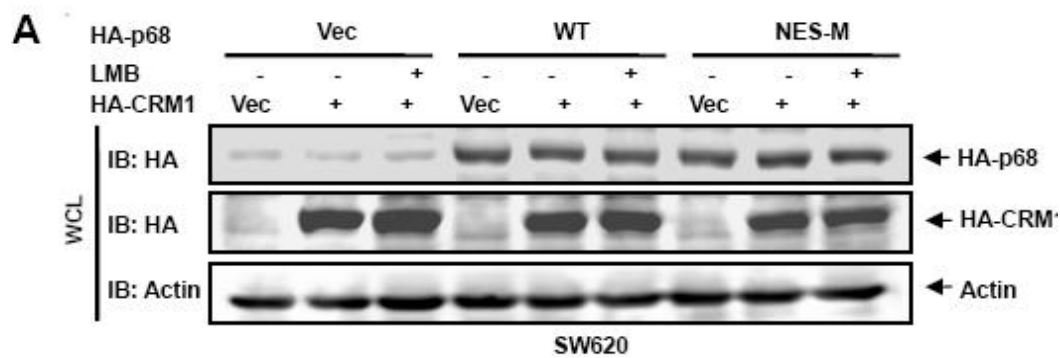


Figure 3.6 P68 nucleocytoplasm shuttling is RanGTPase pathway dependent

(A) Exogenous expression of HA-p68s, wild-type (WT) and mutant (NES-M), and HA-CRM1 in SW620 cells were analyzed by immunoblot of whole cell lysate (WCL) using anti-HA antibody (IB:HA). (B) Cytoplasmic (Cyto) p68 levels of SW620 cells were analyzed by immunoblot using the antibody p68-rgg (IB:p68-RGG). Immunoblots of p68 in whole cell lysate (IB:p68-RGG) indicate cellular levels of p68. (C) The cytoplasmic (Cyto) levels of exogenously expressed HAp68s (WT and NES-M) were analyzed by immunoblot of cytoplasmic extracts using anti-HA antibody (IB:HA). In (A), (B), and (C), IBs of β -actin (IB:actin) and GAPDH (IB:GAPDH) are loading controls. The SW620 cells were transfected with vector alone (Vec), the vector for CRM1 (HA-CRM1), and the vector for CRM1 plus treatment with LMB (HA-CRM1 + LMB). (D) Examples of confocal fluorescent microscopy images of SW620 cells show the cellular localizations of endogenous p68 (P68) and exogenously expressed HA-CRM1 (HA-CRM1). The cells were treated (+) or untreated (-) with LMB. Red signals are staining p68. The green signal represents staining of HA-tag. The blue signal represents staining of DNA. Overlay images are overlay of staining of p68, HA-CRM1, and DNA. The numbers are percentage of cells showing similar image pattern in a random group of 50 cells.

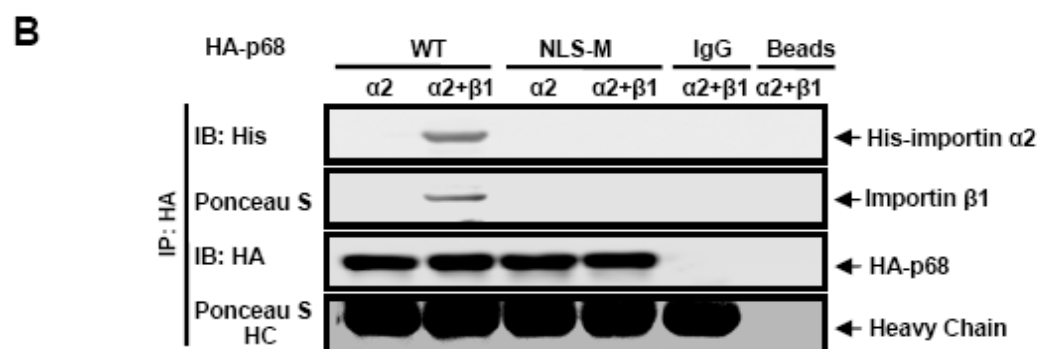
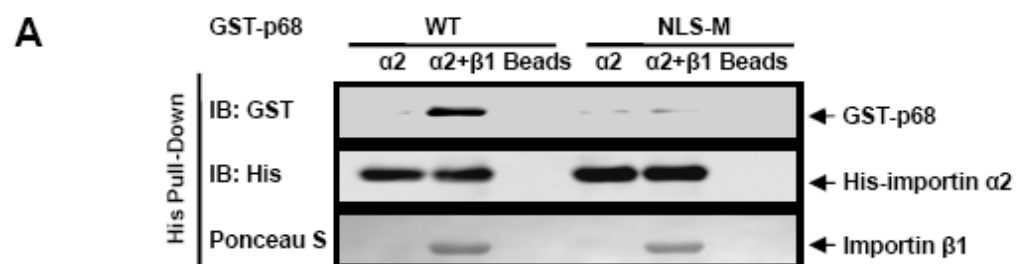


Figure 3.7 P68 interacts with importins *in vitro*

(A) Immunoblot analyses of GST-p68 (IB:GST) and his-importin $\alpha 2$ (IB:His) in His-pull-down proteins (His Pull-down) from a protein mixture of GST-p68 wild-type (WT) or GST-p68 NLSM with; his-importin $\alpha 2$ ($\alpha 2$), his-importin $\alpha 2$ and importin $\beta 1$ ($\alpha 2+\beta 1$), and Ni-TED beads alone (Beads). **(B)** Immunoblot analyses of his-importin $\alpha 2$ (IB:His) and HA-p68 (IB:HA) in coimmunoprecipitates (IP:HA) from a protein mixture of HA-p68 wild-type (WT), HA-p68 mutant NLS-M (NLS-M), rabbit IgG (IgG), or protein G beads (Beads) with; his-importin $\alpha 2$ ($\alpha 2$), his importin $\alpha 2$ and importin $\beta 1$ ($\alpha 2+\beta 1$). Ponceau S staining IgG heavy chain (Ponceau S:HC) is a loading control. In **(A)** and **(B)**, importin $\beta 1$ is visualized by ponceau S staining (Ponceau S).

CHAPTER 4

P68 RNA HELICASE AND CALMODULIN INTERACTION REGULATES CELL MOTILITY BY ACTING AS A MICROTUBULE MOTOR

4.1 Abstract

P68 RNA helicase is a prototypical RNA helicase. The RNA unwinding activity is well documented. The protein has been implicated in various cellular processes. In this report, we present evidence to show that p68 plays a role in cell migration by interacting with Ca²⁺-calmodulin. A peptide that interrupts the interaction between p68 and calmodulin abolishes cell migration. The peptide strongly inhibits cancer metastasis in animal model, suggesting an important physiological function of the p68-calmodulin interaction. Our results indicate that the p68-calmodulin interaction is essential for the formation of lamellipodia and filopodia structures in the migrating cells. P68 upon binding to calmodulin functions as a microtubule motor to transport calmodulin to the leading edge of migrating cells. P68 interacts with microtubule in the presence of calmodulin. Our experiment shows that p68 ATPase activity is initiated by interacting with microtubule. Further, microtubule gliding assays demonstrate that p68 may function as a microtubule motor. Our study uncovered a new molecular microtubule motor which specifically functioned in the migrating cells.

4.2 Introduction

Migration is an essential characteristic of cells in numerous fundamental biological processes (Ridley, Schwartz et al. 2003; Vicente-Manzanares, Webb et al. 2005; Bretscher 2008; Kurosaka and Kashina 2008; Montell 2008; Zoller 2009). Cell migration is accomplished by a series of highly organized cyclic processes. First, the cells polarize and extend protrusion towards the direction of migration stimuli. The polarization and protrusion is led by lamellipodia

or spike-shaped filopodia structures (Le Clainche and Carlier 2008). Accompanying the protrusion, an extensive rearrangement of cell adhesions to the extracellular matrix stabilizes the protrusion and functions as an anchor for traction during migration (Webb, Parsons et al. 2002; Le Clainche and Carlier 2008). Following the protrusion, the cell adhesion at the rear side detaches from the extracellular matrix, and the cell moves forward (Horwitz and Webb 2003). It is believed that the formation of migration leading edges (lamellipodia or filopodia structures) is driven by microfilament polymerization (Pollard and Borisy 2003; Mattila and Lappalainen 2008; Pollard and Cooper 2009). A number of proteins have been shown to play a role in regulating the cytoskeleton rearrangement during cell migration (Le Roy and Wrana 2005). Another important feature accompanying the cell migration is that many important molecules that play critical role(s) in cell migration re-distribute to the migration leading edge (de Curtis 2001; Insall and Machesky 2009). It is believed that transporting along the microtubule structure by a family of microtubule motor molecules is the main mechanism by which proteins and organelles translocate toward directions of migration (Hirokawa, Noda et al. 2009; Lowery and Van Vactor 2009; Vallee, Seale et al. 2009; Verhey and Hammond 2009).

Calmodulin is a calcium binding protein with four EF-hand structure modules. The protein activates a wide range of cellular targets to regulate multiple important processes in response to Ca^{2+} signals (Clapham 2007). One important molecular mechanism that contributes to the capability of calmodulin in regulating many cellular processes is the rapid redistribution of calmodulin to subcellular compartments in response to various signal stimuli (Shariat-Madar, Goldsmith et al. 1997; Pezzella-D'Alessandro, Le Moal et al. 2001). It is well recognized that calmodulin is a major player in connecting Ca^{2+} signaling to cell motility of many cell types (Hinrichsen 1993; Chin and Means 2000). Migration signals trigger spatiotemporal redistribution

of calmodulin to the leading edge of the migrating cell, which is essential for cell motility (Evans and Falke 2007; Collins and Meyer 2009; Wei, Wang et al. 2009). Although, redistribution of calmodulin has long been recognized as an important mechanism that regulates complex cellular Ca^{2+} signals, little is known about how redistribution of calmodulin to subcellular compartments is accomplished.

4.3 Results

4.3.1 A peptide from p68 (aa 549–568) and GFP fusion of the peptide inhibit cancer cells metastasizing to spleen

P68 interacts with calmodulin in the cells is well known. However, what is the function of this interaction in the cells is unknown. In this study, we tried to figure out the biological function of this interaction. As we did not know what the mechanism leads to the interaction between p68 and calmodulin, therefore we tried to disrupt the interaction between those two proteins to study the potential function of this protein complex in tumor. The region at aa 549 – 568 at the C-terminal of p68 is responsible for the interaction between p68 and calmodulin. Therefore we designed a peptide generated from that region to competitively disrupt the interaction between p68 and calmodulin (ref to as Pep IQ) to study its biological function. A scramble peptide (ref to as Pep scramble) which contains the same component of amino acid residues but in a random order was used as control peptide. These two peptides were fused with TAT cell permeable sequence at the N-terminal (Fig. 4.1A). The peptides were used to treat the nude mice xenograft of SW620 cells at dose of 30ug/100ul (daily dose for two weeks). It is well known that nude mice xenograft of SW620 will metastasize to spleen. Interestingly, the cancer metastasis was dramatically inhibited by the PepIQ (Fig. 4.1B) but not by the scramble peptide. The tumor proliferation rate was not significantly affected by the treatment with any of the

peptides as demonstrated by the size of the tumors (Fig. 4.1C). We further verified the effects of the IQ peptide on the cancer metastasis by stable expression of an eGFP-IQ peptide fusion protein in SW620 cells (Fig. S4.1A). Expression of the eGFP-IQ greatly reduced cancer metastasis to spleen with the SW620 xenograft tumor, while the metastasis reduction was not observed with expression of eGFP. A fusion protein with mutations at IQ motif was used as a control (Fig. S4.1B). The reduction of the cancer metastasis was not due to changes in tumor growth upon the expression of fusion proteins (Fig. S 4.1C).

4.3.2 *The IQ peptide interrupts p68-calmodulin interaction that is essential for cell migration*

To understand the molecular mechanism by which the IQ peptide inhibited cancer metastasis, SW620 cells were treated by the PepIQ or a control peptide. Cell proliferation and cell migration were analyzed. Clearly, the PepIQ did not affect cell proliferation, while cell migration was almost completely abolished under the peptide treatment (Fig. 4.1D and Fig. 4.1E). Similarly, cell migration was also dramatically inhibited by stable expression of the eEGF-IQ in SW480 cells (Fig. S34.2A). We questioned why the peptide PepIQ was so effective in inhibiting cell migration. It was demonstrated that p68 interacts with the calmodulin in a number of *in vitro* binding studies and the IQ motif covered by the PepIQ harbors the p68- calmodulin interaction site (Shen, Valencia et al. 2005; Jang, Guo et al. 2007). Thus, it is possible that the PepIQ competed with p68 to interact with calmodulin in the cells therefore inhibited cell migration. Thus, we sought to test whether the IQ peptide interrupts the p68-calmodulin interaction and consequently inhibits cell migration. We first probed the p68 and calmodulin interaction by carrying out co-precipitation experiments with cell extracts made from colon cancer cells SW480 using calmodulin beads. Clearly, p68 was precipitated down from the cellular extracts by the calmodulin beads, and the interaction was Ca^{2+} dependent (Fig. 4.2A). To test the role of the IQ

motif of p68 in the calmodulin binding, we created a mutant with mutation (IQ – MA, ref to as IQ-M). The calmodulin bead pull-down demonstrated that the mutant interacted with calmodulin with a substantially weak affinity, and the IQ-M: calmodulin interaction was Ca^{2+} independent (Fig. 4.2B). The results indicated that the strong Ca^{2+} -dependent p68-calmodulin interaction is IQ motif-dependent.

Since we observed that the PepIQ greatly inhibited cell migration, we reasoned whether there is a cell migration signal induced p68-calmodulin interaction and the peptide may interrupt the migration induced p68-calmodulin interaction. Thus, we first examined the p68 and calmodulin interaction under various cell migration stimuli. It is well known that treatment of cells with EGF can induce cell migration. Thus, we first carried out co-immunoprecipitation with cellular extracts made from SW480 cells using an antibody against calmodulin. The cells were pre-treated with EGF. There was a strong increase in the p68 and calmodulin co-precipitation upon the EGF treatment (Fig. S4.3A and Fig. S4.3B). Measurement of the changes in cell migrations under the stimulation of EGF revealed a close correlation between the increase in the p68 and calmodulin interaction and cell migration (Fig. S4.1C). We next probed the p68 and calmodulin interaction by the co-immunoprecipitation with cell extracts prepared from SW480 cells that were subjected to multiple scratch-wound treatment. A strong increase in the p68 and calmodulin co-immunoprecipitation was observed and the increase depended upon the number of scratches (Fig. 4.2E). The results suggest cell migration induced p68 and calmodulin interaction. Since the IQ motif is the site for the strong Ca^{2+} -dependent p68 and calmodulin interaction, we asked whether the increase in the p68 and calmodulin interaction induced by cell migration requires the IQ motif. HA-IQ-M was exogenously expressed in SW480 cells in which the endogenous p68 was knocked down. The scratch-wound dependent p68-calmodulin interaction

enhancement was not observed in the IQ-M mutant expressed cells (Fig. S4.3D). To test whether the peptide abolished the inducible p68-calmodulin interaction upon cell migration, we probed the p68-calmodulin interaction in cell lysate prepared from SW480 cells that were transiently expressed with eGFP-IQ. The p68-calmodulin interaction was not strengthened upon migration stimuli in SW480 cells in which the eGFP-IQ was stably expressed (Fig. S4.2B). Clearly, our experiments supported the notion that the cell migration induced p68 and calmodulin interaction, and the IQ peptide interrupted the induced p68-calmodulin interaction thus inhibited cell migration.

Based on the preceding experiments, we suspected that the p68-calmodulin interaction would be critical for cell migration. The hypothesis was tested by both boyden chamber assay and scratch-wound assay. The endogenous p68 was knocked down in SW480 cells and HA-p68s, wt, IQ-M, LGLD (An ATPase activity deficiency mutant (Lin, Yang et al. 2005)), or Y593F (Yang, Lin et al. 2006), was expressed in the cells (Fig. S4.3E). Boyden chamber assays showed that knockdown of p68 resulted in dramatic reduction in cell migration and the cell migration could be fully recovered by reexpression of wt p68, but not by the IQ-M mutant. As a control, the cell migration could also be recovered by expression of a mutant that carries mutation at an irrelevant site (Y595F) (Fig. 4.3A). Interestingly, expression of an ATPase deficiency mutant LGLD in the p68 knockdown cells did not recover cell migration, indicating that the ATPase activity of p68 is required for cell migration (Fig. 4.3A). We further confirmed the functional role of the p68 and calmodulin interaction in cell migration by the scratch-wound assay. Scratch-wound was introduced to the plates that cultured SW480 cells expressing p68 wt, IQ-M, LGLD, or Y593F. The amount of cells expressing IQ-M or LGLD migration to the wound was much less than those of p68 wt and Y593F expressing cells (Fig. 4.3B). Immunofluorescence staining of

HA-tag revealed that no IQ-M and LGLD expressing cells migrated to the wounds, while p68 wt expressing cells migrated to the wound areas normally (Fig. 4.3C). These experiments showed that the p68-calmodulin interaction is required for cell migration.

4.3.3 The p68 and calmodulin interaction affect the localization of both calmodulin and p68 to the cytoplasm and to the leading edge of the migrating cells

In the immunostaining experiments, we noted two interesting phenomenon. (1) We observed a strong cytoplasm p68 staining only in the migration cells. When the cells reached the migration destination, p68 re-localized exclusively back to the cell nucleus (Fig. 4.3D). (2) There were very high levels of p68 staining in the cytoplasm and at the leading edge of the migration cells and this staining pattern was not observed in the non-migration cells (Fig. 4.3C). Since p68 interacted with calmodulin in migration cells, we probed whether p68 and calmodulin would exhibit similar localization patterns. To this end, scratch-wound was introduced to the SW480 cell culture plates. The cells were then analyzed by immunostaining. Clearly, p68 and calmodulin co-localized, especially at the leading edge of the migration cells. In the non-migration cells, p68 localized exclusively in the nucleus, while calmodulin could be detected almost everywhere in the cells. However, there were significant increases in calmodulin levels at the cell migration leading edges and the nucleus in the migration cells compared to that in non-migration cells (Fig. 4.3D). Similar p68 and calmodulin localization patterns in migration cells were also observed with exogenously expressed HA-p68 and endogenous calmodulin (Fig. S4.5A).

We further examined the localization patterns of exogenously expressed HA-p68 mutants LGLD and IQ-M and the effects of their expression on the cellular localization of calmodulin under scratch-wound conditions. The endogenous p68 was knocked down. The HA-p68s, wt,

LGLD, or IQ-M was expressed in p68 knockdown cells. Scratch-wound was subsequently introduced. Immunostaining using anti-HA antibody showed that the exogenously expressed wt HA-p68 localized to the leading edge of migrating cells. The ATPase deficiency mutant LGLD, although detected in the nucleus and the cytoplasm, failed to accumulate at the membrane edge. Interestingly, the IQ-M almost exclusively localized in the cell nucleus (Fig. 4.3E). Immunostaining of the calmodulin in the same HA-p68s expressing cells revealed that calmodulin also failed to accumulate at the membrane edge of the cells that expressed LGLD or IQ-M mutant under the scratch-wound condition (Fig. 4.3E). The results suggested that the p68 and calmodulin interaction and the ATPase activity of p68 were required for the localization of calmodulin to the leading edge during cell migration.

We next examined whether the cytoplasmic localization of p68 indeed occurs in migrating cells in tissue samples. We carried out the IHC analyses with the colon cancer tissue arrays. Since p68 has function in cell differentiation, we analyzed the cytosol p68 level in different stage of the tumors (high stage number indicates more extensive disease in colon cancer) but in the similar differentiation level (same grade). The cancer cells in higher stage tumor have higher capability of cell migration than the cells in lower stage. Interestingly, we found there were more cytosol p68 in higher stage of the tumor than in the lower stage of the tumor (Fig. S4.6A). Specifically, we found that there was more cytosol of p68 in T4N2M0 colon tissue than in T4N1M0 (Fig. 4.4A). To further analyze the cytoplasm localization of p68, we prepared tissue sections of the SW620 xenograft six weeks after implantation. The tissue sections were prepared from edge of the tumors or the middle of the tumors. It was clear that there were dramatically higher cytoplasmic p68 levels in the tissue sections prepared from edge of the tumors than those prepared from middle of the tumors (Fig 4.4B). Interestingly, treatment of the tumor with the

PepIQ dramatically reduced the cytoplasmic p68 (Fig. 4.4B). The results suggested that there is strong correlation between cell migration status and cytoplasmic localization of p68.

4.3.4 P68 RNA helicase exhibits a calmodulin dependent microtubule motor activity

Redistribution of calmodulin to the leading edge areas is essential for cell migration (Pezzella-D'Alessandro, Le Moal et al. 2001; Bolsover 2005). However, the molecular mechanism by which the calmodulin is localized to the leading edge of migrating cells in response to cell migration stimulus is not well understood. Our preceding experiments indicated that the p68 and calmodulin interaction and the ATPase activity of p68 are required for calmodulin to localize to the leading edge of the migration cells. We reasoned whether p68 plays a functional role in translocation of calmodulin to the leading edge in the migrating cells by acting as an unconventional microtubule associated motor (de Curtis 2001; Insall and Machesky 2009). To test this conjecture, we first analyzed whether p68 and/or calmodulin interact with microtubule. The p68/calmodulin and microtubule interaction were first analyzed by the microtubule co-precipitation assay. We carried out co-precipitation experiments with exogenously expressed HA-p68 that was immunopurified from lysates of SW480 cells with/without multiple scratch-wound (20 scratches) treatments. The purified HA-p68 was incubated with microtubule. After precipitation of the microtubule by centrifugation, the presence of the HA-p68 in the microtubule precipitates was examined by immunoblot using an anti-HA antibody. HA-p68 that was purified from cells that were treated by multiple scratch-wound co-precipitated with the microtubule in the presence of calmodulin. On the contrary, HA-p68 immunopurified from SW480 cells that were not treated by scratch-wound did not co-precipitate with the microtubule even in the presence of calmodulin (Fig. 4.5C). The HA-p68 did not co-precipitate with unpolymerized α - and β - tubulin in the presence and absence of Ca^{2+} and

calmodulin (Fig. S4.5B). Interestingly, co-precipitation of HA-p68 with microtubule in the presence of calmodulin was completely Ca^{2+} dependent, while the ATP was dispensable as the HA-p68 co-precipitated with the microtubule in the presence and absence of ATP, and in the presence of non-hydrolysable ATP analogue AMP-PNP (Fig. 4.5B).

The interaction of p68-calmodulin with the microtubule was further examined by binding of rhodamine labelled microtubule to HA-p68 that was fixed on a glass slide. Binding of the microtubule to the glass slide was then visualized by fluorescence microscope. Clearly, the microtubule bound to the HA-p68 purified from scratch-wound treated SW480 cells in the presence of calmodulin and Ca^{2+} . The microtubule did not bind to HA-p68 without addition of calmodulin (Fig. 4.5D). The microtubule also did not bind to HA-p68 that was purified from SW480 cells that were not subjected to multiple scratch-wound treatments (Fig. 4.5D). Binding of p68 to microtubule was further verified by co-immunostaining of p68 and microtubule in SW480 cells with/without scratch-wound treatments. Clearly, the p68 co-localized with microtubule in the migrating cells under scratch-wound treatment, while p68 exclusively localized in the nucleus in the cells without scratch-wound treatment. We further examined the co-localization of exogenously expressed DsRed-p68 with microtubule labeled by eGFP. Under scratch-wound treatment, DsRed-p68 clearly co-localized with eGFP labeled microtubule (Fig. 4.5F). Thus, we could draw the conclusion that p68 interacts with microtubule and the interaction is dependent upon the p68-calmodulin interaction.

If p68 could function as a microtubule motor-like molecule, we would expect that microtubule would stimulate ATPase activity of p68. Thus, ATPase activity of the HA-p68 that was immunopurified from SW480 cells that were treated with multiple scratch-wound was analyzed in the presence of various different possible substrates including RNA and microtubule.

As previously reported (Huang and Liu 2002), HA-p68 exhibited strong RNA-dependent ATPase activity. Interestingly, the protein demonstrated an even stronger microtubule stimulated ATPase activity (Fig. 4.6A), and the microtubule stimulated ATPase activity was Ca^{2+} dependent as addition of EGTA diminished the ATPase activity (Fig. S4.7B). The observed microtubule stimulated ATPase activity came from p68 as the mutation that abolishes p68 ATPase activity (LGLD) also abolished the microtubule stimulated ATPase activity of the protein (Fig. 4.6B).

We next probed whether the p68 has a microtubule motor activity. To this end, we employed the microtubule gliding assay. The HA-p68 was purified from SW480 cells with scratch-wound treatment and attached to a glass slide. Rhodamine labeled microtubule was then added to the glass slide. Migration of the microtubule in the presence and absence of ATP was then recorded using confocal microscope by the time-lapse photography. First, migration of microtubule was clearly visualized with a positive control motor protein kinesin (Fig. 4.7A). Migration of the microtubule on the glass slide with HA-p68 attached was also clearly evident in the presence of calmodulin and Ca^{2+} . In contrary, the migration of the microtubule was not observed on the glass slide with HA-p68 that purified from SW480 cell extracts without scratch-wound treatment. As a negative control, the migration was not observed without addition of ATP (Fig. 4.7A). Statistical analyses indicated that the HA-p68/calmodulin exhibited motor activity on the microtubule very similar to that of a control motor protein kinesin (the number of gliding microtubules, mean gliding speed, and maximum gliding speed in a random selected group of 50 are similar, Fig. 4.7B). One possibility is that the observed HA-p68 motor activity is due to co-purification of residues other cellular motor proteins. We therefore examined the possible co-existence of two very common microtubule associated motor proteins in the purified HA-p68. Immunoblot analyses clearly demonstrated that no microtubule associated motor proteins were

detected in the HA-p68 purifications (Fig. S4.7C). To further exclude the possibility that the motor activity was due to contaminations during purification, we construct a p68-calmodulin fusion protein (Fig. 4.2C). Expression of HA-p68-calmodulin fusion protein in SW480 cells led to greatly increased cell migration rates and the expressed fusion protein localized to the leading edge of the migrating cells (Fig. 4.2D). In fact, expression of the fusion protein promoted formation of the lamellipodia/filopodia structure without scratch-wound treatment (Fig. 4.2D). These observations indicated that the fusion protein functionally resemble the p68-calmodulin interaction induced by cell migration signals. We then expressed and purified the His-p68-calmodulin from bacterial *E. coli*. The gliding assay was performed with this bacterially expressed protein. Clearly, the bacterially expressed His-p68-calmodulin had microtubule motor activity (Fig. 4.7A).

We next examined whether p68 indeed migrated along microtubule in the cells that were induced for migration. P68 fused with DsRed (DsRed-p68) and eGFP labeled α -tubulin were exogenously co-expressed in SW480 cells. Cell migration was induced by scratch-wound treatment in cell culture plate. Movement of the DsRed-p68 along the eGFP-labeled microtubule was recorded using confocal microscope with multi-photon excitation for imaging of living cells with time-lapse photography. The fluorescence images clearly indicated that p68 migrated along the microtubule under cell migration induction. The movements were toward the migration leading edge (Fig. 4.7C). The results strongly suggest that by interacting with calmodulin, p68 RNA helicase can function as a microtubule motor.

4.4 Discussion

In the present report, we demonstrated that the interaction of p68 RNA helicase with calmodulin is required for cell migration. P68 RNA helicase was shown to interact with calmodulin by several independent *in vitro* binding analyses (Buel, Glidden et al. 1994; Shen, Valencia et al. 2005; Jang, Guo et al. 2007). However, the biological function of this interaction is not known. According to the prediction and primary results, we found that p68 has multiple CaM binding sites (a.a.222-246, a.a.466-486, a.a.515-537, and a.a.549-568). The IQ motif CaM binding site is Ca²⁺ dependent and has a function in cell migration. We reasoned that other CaM binding sites are Ca²⁺ independent as the IQ mutant of p68 binds to CaM beads is Ca²⁺ independent. Meanwhile the binding capability of IQ mutant of p68 to CaM in the presence of or without Ca²⁺ is similar. Our experimental results suggested that the p68 and calmodulin interaction at the IQ motif is necessary for the localization of calmodulin to the migration leading edge, which is an essential event during cell migration. P68, by interacting with calmodulin, exhibited a microtubule motor activity. Apparently, this motor activity allows calmodulin to be transported to the leading edge of the migration cells. Based on our current findings, our working model for the functional role of p68 in cell migration is illustrated in Figure 4.6. Interestingly, p68 stays with calmodulin at the leading edge of the migration cells until the cell reaches its migration destination as demonstrated by the immunostaining, indicating possible additional functions of p68 at the migration leading edge during cell migration. One possibility is that the p68 may also play a role in the migrating cell leading edge protrusion, e.g. actinfilament polymerization in the lamellipodia and filopodia.

Calmodulin regulates various cellular processes by targeting over a hundred proteins downstream. A key feature for such functional diversity of calmodulin is temporal and spatial redistribution of the protein under stimulation of various different signaling pathways (Shariat-

Madar, Goldsmith et al. 1997; Pezzella-D'Alessandro, Le Moal et al. 2001). A long standing question is how calmodulin is translocated to a specific subcellular compartment upon the stimulation of various signals. Our experiments demonstrated an excellent example here that p68 interacted with calmodulin upon the cell migration stimulation. This interaction allows p68 to interact with microtubule and subsequently act as a microtubule motor molecule, which consequently transports the bound calmodulin to the leading edge of the migrating cells. An open question is whether a similar mechanism is also used to re-localize calmodulin in other cellular processes that require temporal and spatial redistribution of calmodulin, such as cytokinesis and mitosis.

It is traditionally believed that DEAD box RNA helicase uses RNA as a substrate to stimulate its ATPase activity. The energy derived from ATP hydrolysis is then used to displace duplex RNA or protein that bind the RNA substrate. Along with our previously published report (Yang, Lin et al. 2006), this is the second example that p68 DEAD box RNA helicase can use protein as a substrate to stimulate its ATPase activity. It is conceivable here that the energy derived from ATP hydrolysis can then be used for translocation along the microtubule (motor like protein). However, a typical microtubule motor molecule binds microtubule with two “motor head”. The movement along the microtubule is usually derived by cyclic hydrolysis of ATP at the two heads (Gennerich and Vale 2009). Thus, an open question is how the p68 RNA helicase motor action on microtubule is achieved by one ATP hydrolysis site. One possibility is that the bound calmodulin may function as an anchor, while ATP hydrolysis in p68 powers the movement. This scenario would require that calmodulin interact with microtubule. Nevertheless, the interaction between calmodulin and microtubule is not observed. Alternatively, p68 RNA helicase may travel along the microtubule using a mechanism similar to that used by a DEAD

box RNA helicase that translocates along the RNA substrate. It is reported that DEAD box RNA helicase Ded1 can displace RNA bound protein without RNA unwound. It was suggested that the Ded1 can act like an RNA motor to remove the bound protein during translocation along the RNA chain by its motor action (Fairman, Maroney et al. 2004). It is plausible that p68 may adapt a similar mechanism. However in this case, the microtubule instead of RNA chain is used as substrate.

4. 5 Materials and methods

4.5.1 *Scratch-wound treatments*

A scratch or multiple scratches using pipette tips were introduced into a 6 well cell culture plate. The cells were further cultured under serum starvation for 30 minutes, and were subsequently cultured for an additional indicated time. The scratch-treated cells were either directly visualized by microscopes or the cells were fixed and subsequently examined by immunostaining. Alternatively, the cells were collected and lysized. The prepared cellular extracts were then used for other analyses.

4.5.2 *Microtubule pull-down*

Microtubule purchased was reconstituted in warm PM buffer (15 mM Pipes pH 7.0, 1 mM MgCl₂) with the addition of taxol as instructed by the vendor. The MTs were ready to use after 15 minutes incubation at room temperature. The test protein(s) was incubated with the reconstituted MTs under various conditions. The MTs with the bound proteins were separated from the incubation solution by centrifugation at 100,000g for 30 minutes. Co-precipitates with the MTs were re-suspended in 50 µl of 2 x SDS PAGE loading buffer and heated to 85 °C for 10 minutes and subsequently analyzed by immunoblots.

4.5.3 *Microtubule gliding assay*

The protein HA-p68, His-p68-calmodulin (10 μ l) or Kinesin was loaded onto a glass slide. The slide was blocked with the blocking buffer. For the slide loaded with HA-p68, 10 μ l of calmodulin with 0.5 mM of Ca^{2+} was added to the slide and was incubated for 10 minutes. After loading the slide was washed with the Ca^{2+} containing wash buffer to remove the unbound proteins. The prepared Rhodamine labeled microtubules were then loaded onto the slide. The same Ca^{2+} containing wash buffer was used to remove unbound microtubules. The movement of microtubules was then recorded by the confocal microscope when the ATP containing buffer was added.

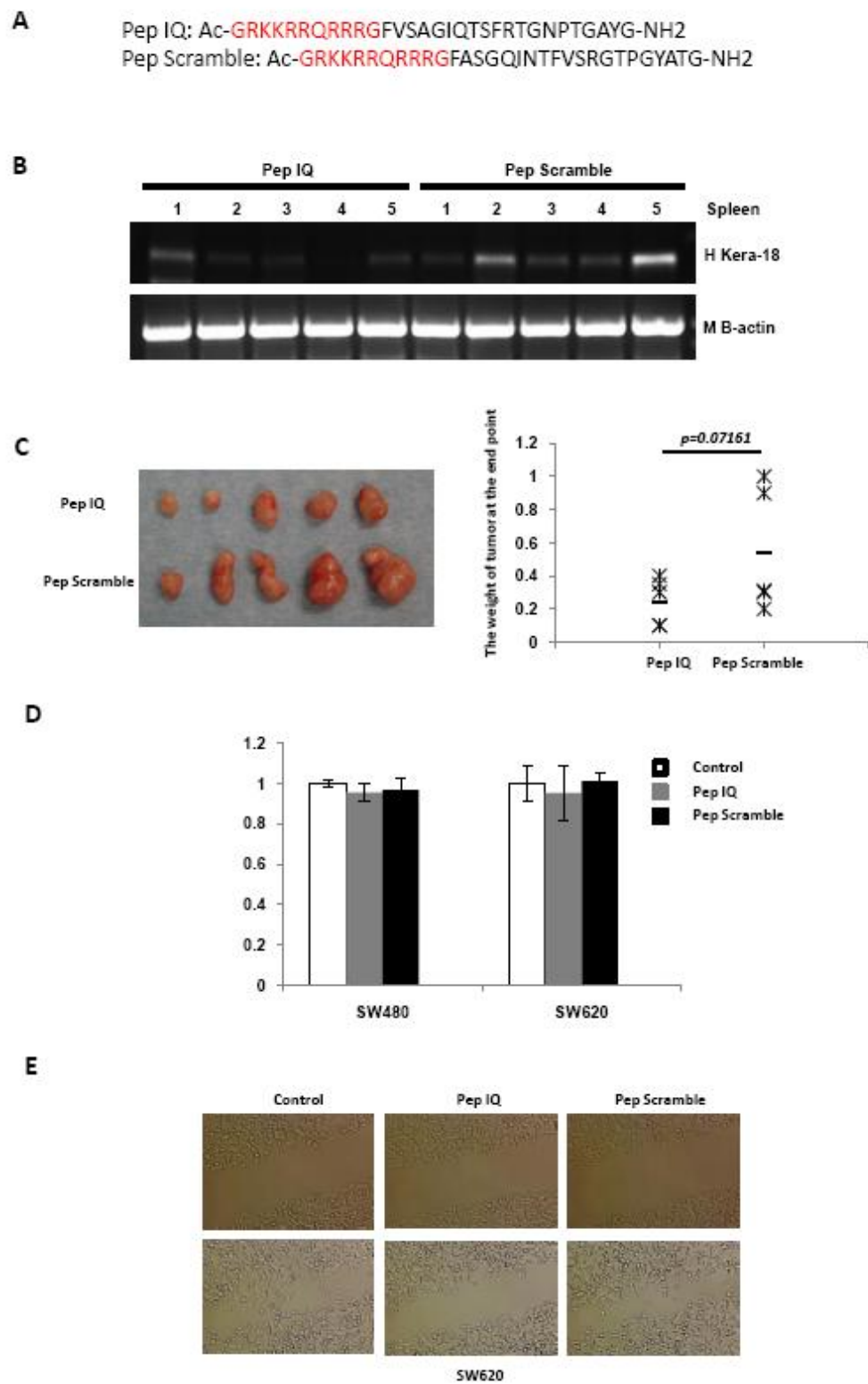


Figure 4.1 Pep IQ inhibited the cancer metastasis

(A) The sequences for Pep IQ and Pep scramble. (B) RT-PCR method was used to detect the trace amount of human colon cancer SW620 cells. Human Keratin-18 (H Kera-18) is the marker protein for human colon cancer cells, which was used to indicate the amount of the SW620 cells migrated to the spleen. Mouse beta-actin (M b-actin) was used as the RNA loading control. (C) The sizes of the subcutaneously implanted tumor at the end point. The left image was the SW620 tumors at the end point; the right graph is the tumor weight at the end point. And the tumor mass was statistically analyzed by the T-test. The cell proliferation of SW480 cells and SW620 cells were not significantly affected when the cells were incubated with Pep IQ or Pep scramble for 24 hours (D). The scratch induced migration of SW620 cells was significantly inhibited when the cells were incubated with Pep IQ (E).

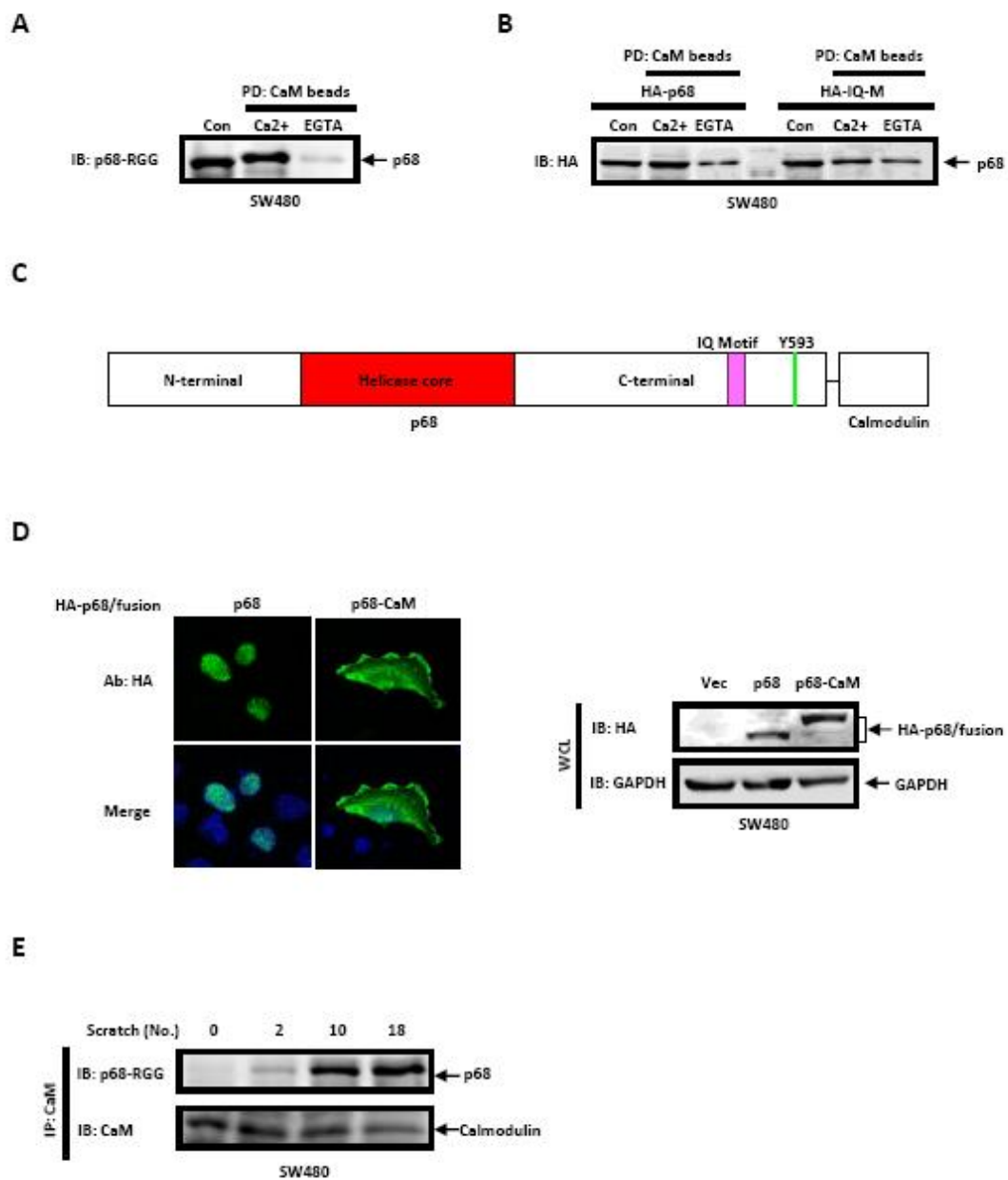
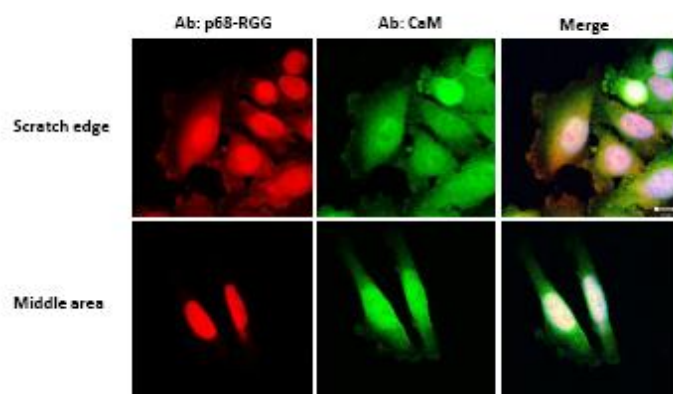


Figure 4.2 P68 and Calmodulin interactions

Interaction of endogenous p68 (A) and exogenously expressed HA-p68s, wt and IQ mutant, (B) with calmodulin in the presence of 2 mM CaCl₂ (Ca²⁺) and 5 mM EGTA (EGTA) was probed by calmodulin beads pull-down (PD: calmodulin beads) followed by immunoblot using antibody against p68 (IB:p68-RGG) or anti-HA antibody (IB:HA). Cons are the control immunoblot of the cellular extracts using indicated antibody without calmodulin beads pull-down. (C) Schematic illustration of the p68 and calmodulin fusion protein. Specific sequence motifs in p68 are highlighted in colors. (D) (left panel) Representative images of SW480 cells expressing HA-p68 (p68) and HA-p68-calmodulin (p68-CaM). The HA-p68 and HA-p68-calmodulin were immunostained using anti-HA antibody (Ab:HA, green). DAPI stains (blue) DNA in the cell nucleus of the HA-p68s expression cells. Merge is overlay of the images of Ab:HA stains and DAPI stains. (right panel) The levels of exogenously expressed HA-p68 (WT) or HA-p68-calmodulin (p68-CaM) in p68 knockdown SW480 cells were examined by immunoblot of whole cell lysate (WCL) using anti-HA antibody (IB:HA). Immunoblot of GAPDH is a loading control. Vec is the cells transfected with the empty vector. (E) P68 and calmodulin interaction in extracts prepared from SW480 cells that were subjected to multiple scratch-wound treatment (number of scratches was indicated) was analyzed by immunoprecipitation of calmodulin (IP:CaM). The extracts were prepared three hours after scratches. P68 co-precipitated with the IP calmodulin was examined by immunoblot using the antibody p68-RGG (IB:p68-RGG). Immunoblot analyses of precipitated calmodulin (IB:CaM) indicated amounts of calmodulin that were precipitated from each IP reaction.

D



E

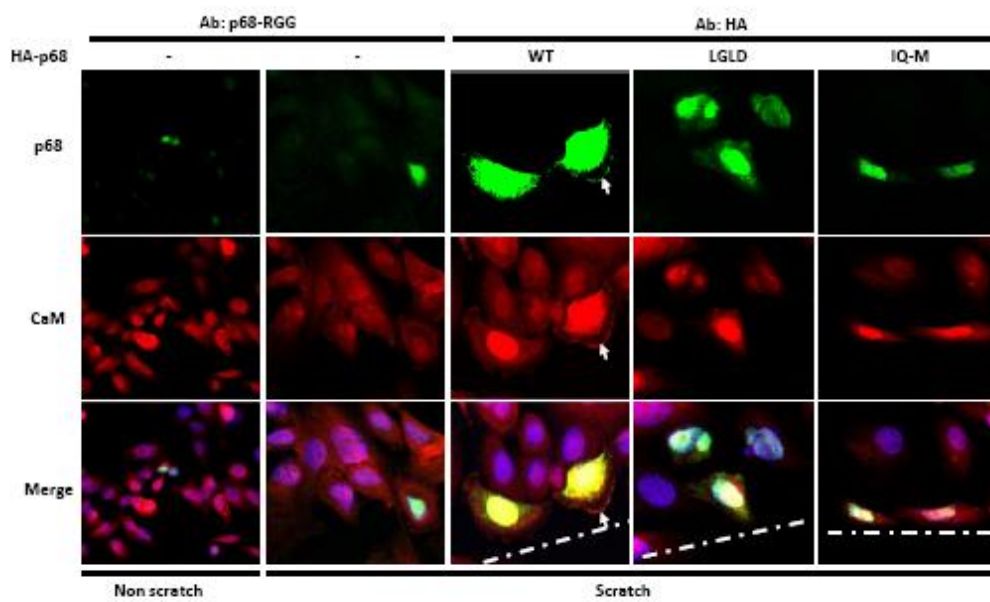
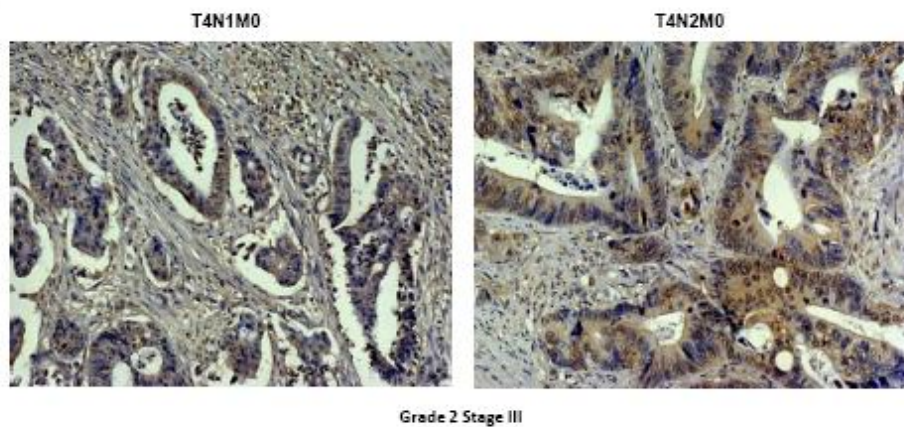
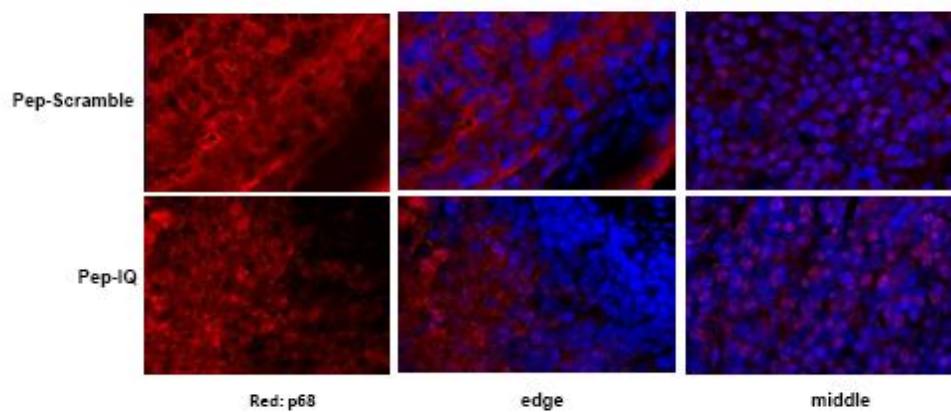
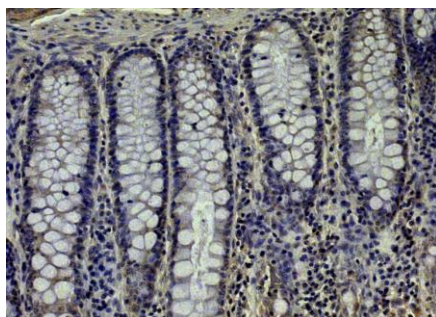


Figure 4.3 P68 and calmodulin interaction is essential for cell migration and for localization of calmodulin to the leading edge of migrating cells

(A) Migration of SW480 cells in which endogenous p68 was knocked down by RNAi (SiRNA) and HA-p68s, wild type (WT) and mutants (indicated), were exogenously expressed was analyzed by boyden chamber assays. The number of cells migrated to the lower chamber was measured and presented as relative migrated cell number by defining the number of migrating cells in which p68 was knocked down and the empty vector was transfected as 1. (B) (Upper panel) Migration of SW480 cells in which endogenous p68 was knocked down by RNAi (SiRNA) and HA-p68s, wild type (WT) and mutants (indicated), were exogenously expressed was revealed by phase contrast microscopy 0 hour (0h) and 12 hours (12h) after scratch-wound was introduced into the cell culture plates. (Lower panel) Quantization of the cells in a fixed microscopic areas that migrated to the scratch areas. (C) Representative images of SW480 cells in which endogenous p68 was knocked down by RNAi (SiRNA) and HA-p68s, wild type (WT) and mutants (indicated), were exogenously expressed. The HA-p68 and HA-p68-calmodulin were immunostained using anti-HA antibody (Ab:HA, green). Endogenous p68 was stained with the antibody p68-RGG (Ab:p68-RGG). DAPI stains (blue) DNA in the cell nucleus of the HA-p68s expression cells. Merge is overlay of the images of Ab:HA (or Ab:p68-RGG) stains and DAPI stains. (D) Immunofluorescence staining of p68 (red) and calmodulin (green) in SW480 cells using antibodies against p68 (Ab:p68-RGG) and calmodulin (Ab:CaM). The cells were treated by a scratch-wound in the culture plate. The left panel focused on the cells that located on the scratch edges, while the right panel focused on the middle of scratch wound areas. (E) Immunofluorescence staining of p68 (Ab:p68-RGG, green) or exogenously expressed HA-p68s (Ab:HA, green), wild type (WT) or mutants (indicated), and calmodulin (Ab: CaM, red) in

SW480 cells. The endogenous p68 was knocked down by RNAi. The cells were treated by a scratch-wound (Scratch) or no scratch-wound (No scratch) in the culture plate. The merges in **(D)** and **(E)** are overlays of the images of calmodulin and p68 staining. Error bars in **(A)** and **(B)** are standard deviations of three independent measurements. Vec is the cells transfected with the empty vector. NT represents the cells treated with non-target RNAi.

A**B****C**

Surrounding normal colon tissue

Figure 4.4 The localization of p68 in colon cancer tissues and xenograft tumor tissues

(A) IHC staining of p68 in the colon cancer tissues isolated from the colon cancer patients who were diagnosed at Grade 2 stage III. The brown color was the staining of p68; the blue spots was the staining of nuclei of cells. (B) Immunofluorescent staining of p68 (Red) in the tumor tissues which grew from the subcutaneously implanted SW620 cells. Blue staining (DAPI) indicated the location of the nuclei. Edge refers to the out layer of the tumor; Middle refers to the center layer of the tumor. (C) IHC staining of p68 in the surrounding normal colon tissue.

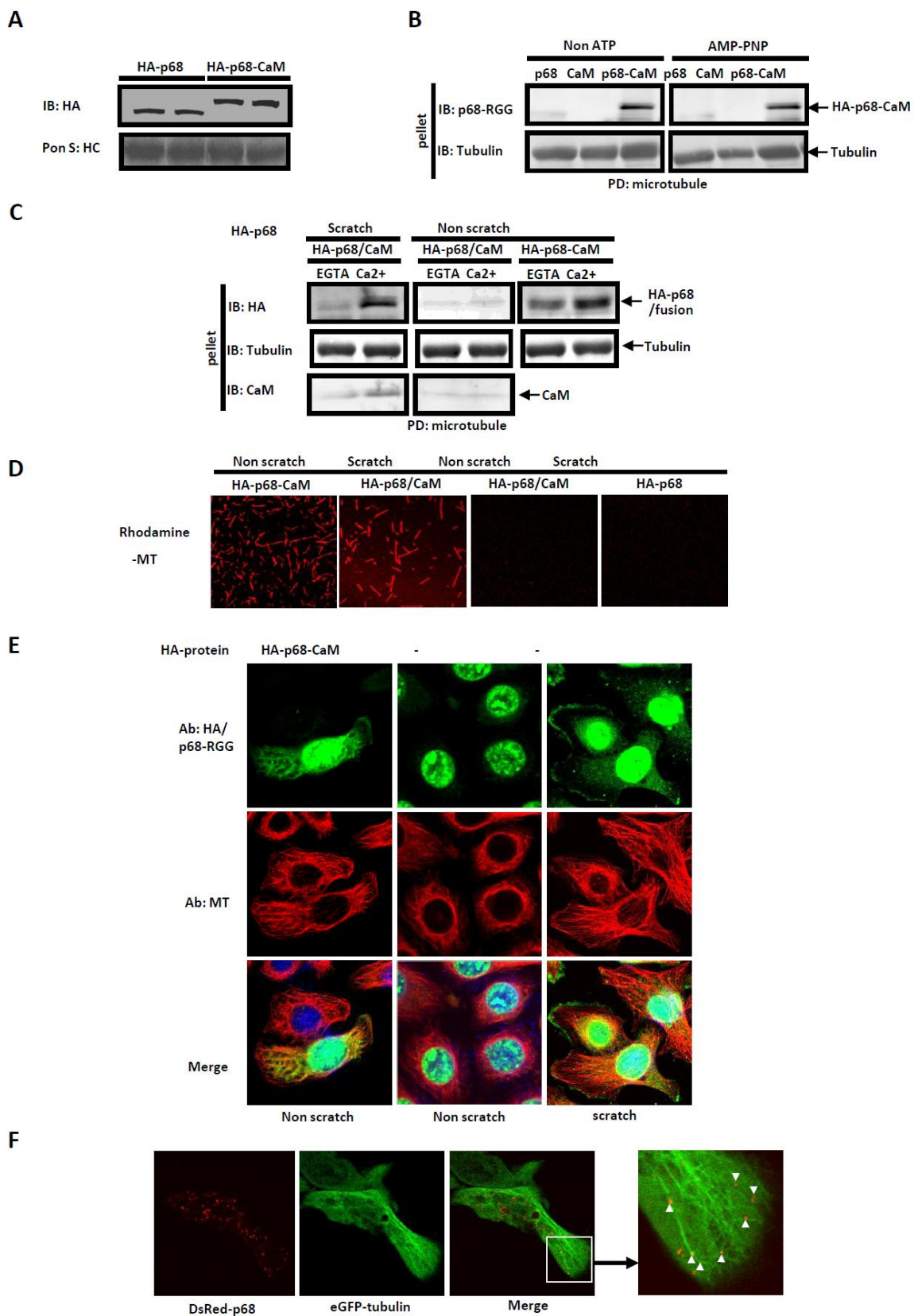
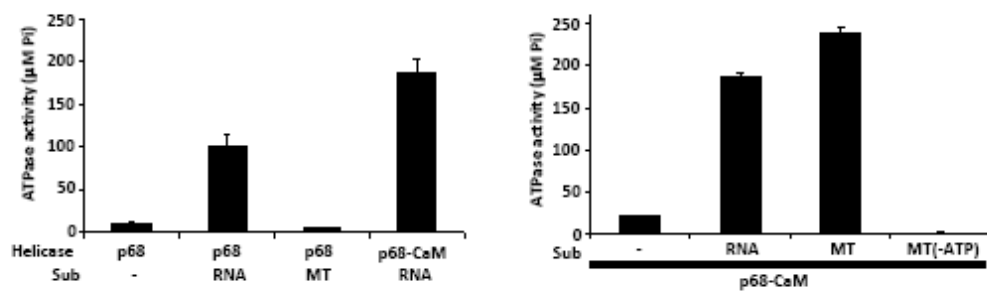


Figure 4.5 P68 and calmodulin interact with microtubule

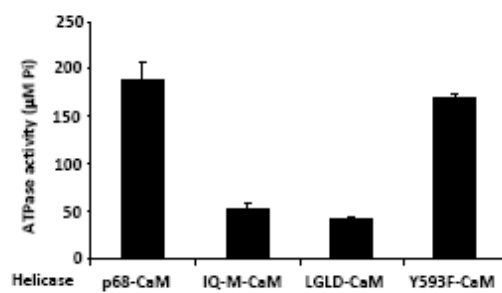
(A) HA-p68 and HA-p68-calmodulin immunopurified from SW480 cells that were treated/untreated with multiple scratch-wounds were analyzed by immunoblot using the anti-HA antibody. PonS:HC is the ponceau S stain of antibody heavy chain. (B) Precipitation of purified HA-p68-calmodulin (p68-CaM) with *in vitro* assembled microtubule (PD: Microtubule) by ultracentrifugation in the absence of ATP or in the presence of non-hydrolysable ATP analogue AMP-PNP was probed by immunoblot of the precipitated pellets using the antibody p68-RGG (IB:p68-RGG). Immunoblot analyses of α -tubulin (IB:Tubulin) is the loading control indicating amounts of precipitated microtubule. (C) Precipitation of purified HA-p68-calmodulin (HA-p68-CaM) and HA-p68 in the presence of calmodulin (HA-p68/CaM) with *in vitro* assembled microtubule (PD:Microtubule) in the presence of 0.5 mM CaCl_2 (Ca^{2+}) or 5 mM EGTA (EGTA) was probed by immunoblot of the precipitated pellets using the anti-HA antibody (IB:HA). The HA-p68 was purified from SW480 cells treated by multiple scratch-wounds (left, Scratch). The HA-p68 and HA-p68-calmodulin were purified from SW480 cells without scratch-wound treatment (middle, Non scratch and right). Immunoblot analyses of α -tubulin (IB:Tubulin) is the loading control indicating amounts of precipitated microtubule. Immunoblot of calmodulin (IB:CaM) in the microtubule precipitates indicated the co-precipitation of calmodulin with HA-p68 and microtubule. (D) Bindings of Rhodamine labeled microtubule (Rhodamine-MT) to the glass slides on which the HA-p68-calmodulin or HA-p68 (in the presence of calmodulin and Ca^{2+} [HA-p68/CaM-Ca] and absence of calmodulin [HA-p68]) that was immunopurified from SW480 cells were revealed by fluorescence microscopy. The cells from which HA-p68 was purified were treated by either 20 scratch-wound (Scratch) or no scratch-wound (No nscratch) in the culture plate. (E) Immunofluorescence staining of exogenously expressed HA-p68-

calmodulin (Ab:HA, green) or endogenous p68 (Ab:p68-RGG, green) and microtubule (Ab:MT, red) in SW480 cells. The cells were treated by a scratch-wound (Scratch) or no scratch-wound (Non scratch) in the culture plate. **(F)** Representative fluorescence microscopy images of SW480 cells that expressed DsRed-p68 and eGFP- α -tubulin. The cells were treated by scratch-wound. The arrows indicated the DsRed-p68.

A



B



C

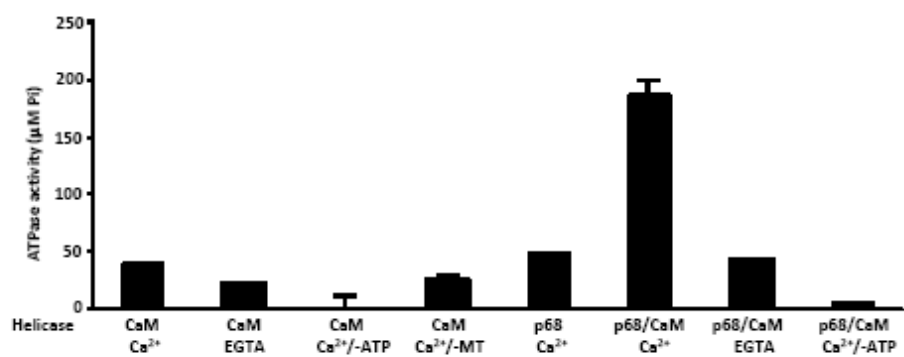
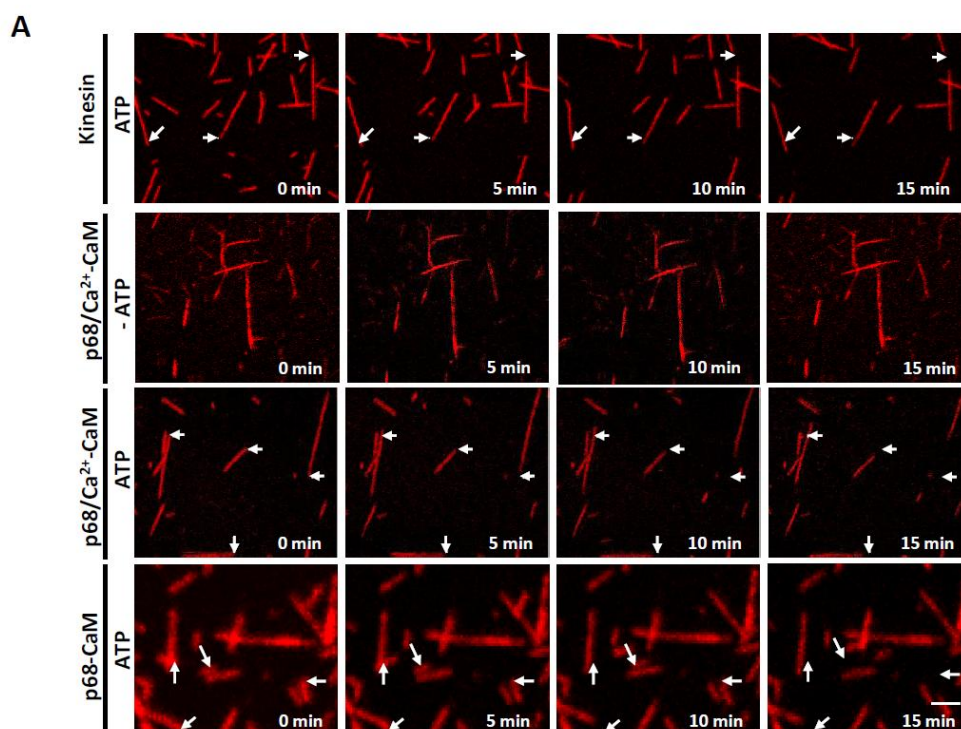


Figure 4.6 Microtubule stimulates the ATPase activity of p68

ATPase activities of **(A, left)** HA-p68 (p68) and HA-p68-calmodulin (p68-CaM) in the presence of various different substrates (Sub, indicated), **(A, right)** the p68-calmodulin in the presence of various different substrates (Sub). **(B)** the HA-p68-calmodulin (wild type and indicated mutants) with microtubule as substrate, and **(C)** the recombinant calmodulin and/or the HA-p68 immunopurified from scratch-wound treated SW480 cells in the presence of 0.5 mM CaCl_2 (Ca^{2+}), 5 mM EGTA (EGTA) were analyzed by measuring inorganic phosphate released from ATP hydrolysis. In the ATPase assays, 4 mM ATP was always added unless specified (-ATP). The ATPase activity was expressed as μmole of inorganic phosphate hydrolyzed from ATP. In **(A)** and **(C)**, MT is *in vitro* assembled microtubule. RNA is total RNA extracts from yeast.



B

	Kinesin (ATP)	p68/Ca ²⁺ -CaM (-ATP)	p68/Ca ²⁺ -CaM (ATP)	His-p68-CaM (ATP)
% of gliding microtubules [#] (n=50)	89.20 ± 1.13	5.79 ± 3.13	74.15 ± 1.20	85.48 ± 2.40
Mean gliding speed* (μm/min)	0.17 ± 0.06	0.00 ± 0.00	0.16 ± 0.12	0.09 ± 0.03
Maximum gliding speed (μm/min)	0.27 ± 0.12	0.01 ± 0.00	0.52 ± 0.14	0.13 ± 0.02

[#] Only MTs with gliding speed > 0.025 μm/min were counted.

* Mean gliding speed only measure the MTs with the motility > 0.05 μm/min.

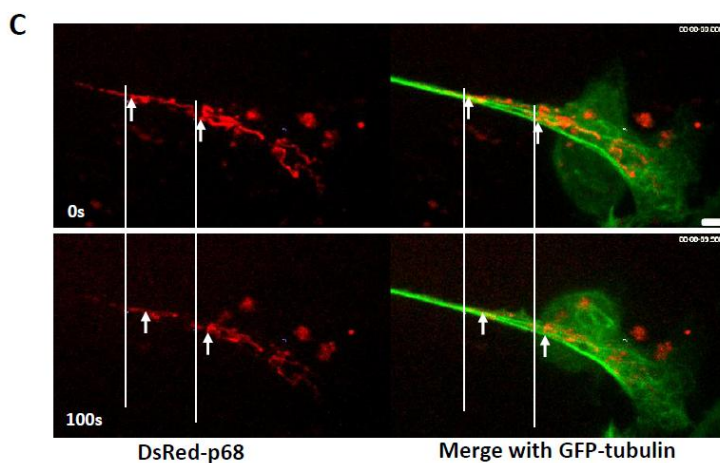


Figure 4.7 P68-calmodulin has a microtubule dependent motor activity

(A) The movements of Rhodamine labeled microtubules on kinesin, p68/Ca²⁺-CaM, or His-p68-CaM (0.5mM CaCl₂) were recorded by the time lapse photography with confocal fluorescence microscopy. p68 with HA tagged was immunopurified from scratch-wound treated SW480 cells. His-p68-CaM was purified from *E. coli*. (B) Summary of quantitative (statistical) analyses of the movements of Rhodamine labeled microtubules in the gliding assays. 50 microtubules per each group was counted. The mean gliding speed was the average of speed of the randomly selected 50 microtubules per each group. The standard deviation was obtained from examinations of three randomly selected groups of microtubules. (C) Movements of DsRed-p68 along eGFP labeled microtubules in SW480 cells that were treated by scratch-wound were recorded by time lapse photography with confocal fluorescence microscopy.

A GFP-IQ: eGFP-FVSAGIQTSFRTGNPTGAYG
 GFP-MA: eGFP-FVSAGMATSFRTGNPTGAYG

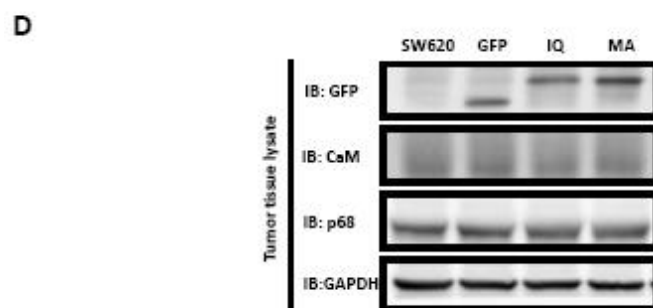
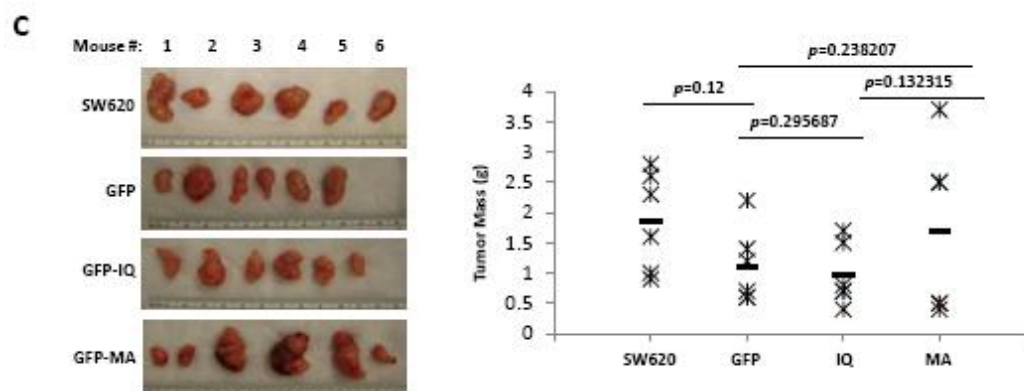
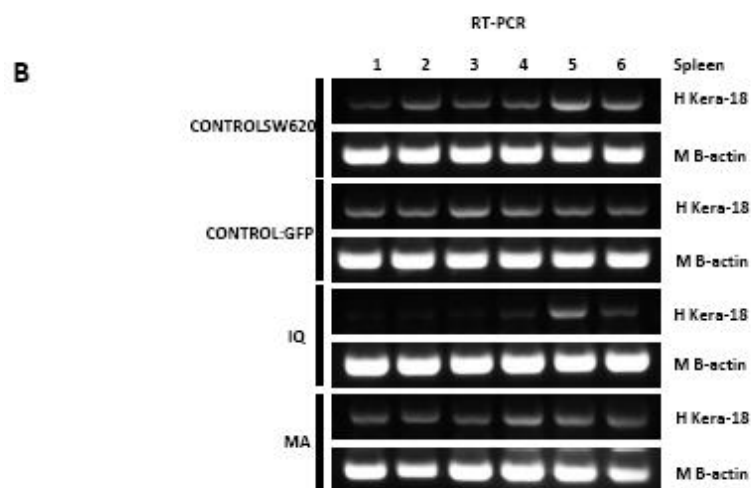


Figure Supplement 4.1 eGFP-IQ expression affected SW620 cells metastasize to spleen

(A) Schematic illustration of the eGFP-IQ and eGFP-MA fusion proteins. (B) RT-PCR indicated the spleen metastasis of different cell lines (including SW620 and eGFP/eGFP-IQ/eGFP-MA stably expressing SW620 cells) which were subcutaneously implanted to the nude mice at the right flank. H Kera-18 referred to the mRNA level of human keratin 18 marker protein; M B-actin referred to the mRNA level of mouse beta-actin which was used as the loading control. (C) The sizes of the tumors at the end point. Left images were the tumors which grew from four different cell lines. Right graph was the tumor weights at the end point. The tumor mass were statistically analyzed by T-test. (D) The expression level of eGFP or eGFP fusion proteins in the tumor mass. The expression level of p68 and calmodulin was tested in the different tumors. The IB of GAPDH was used as the loading control.

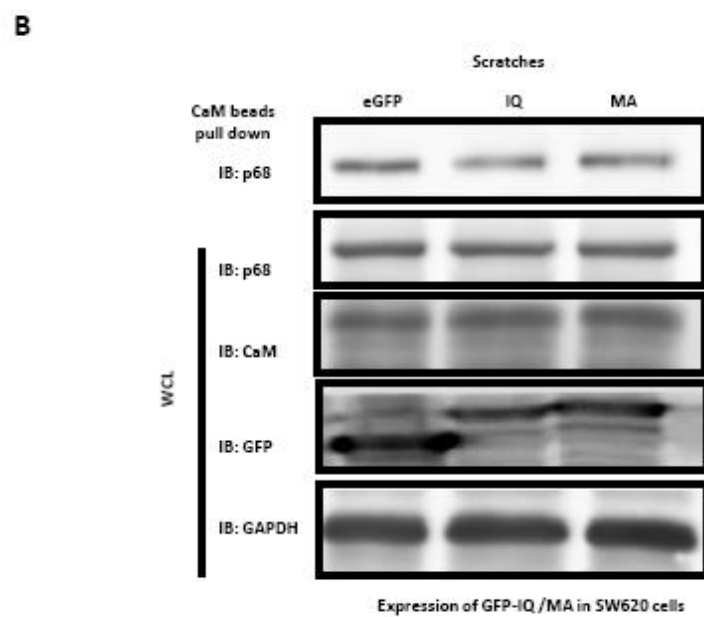
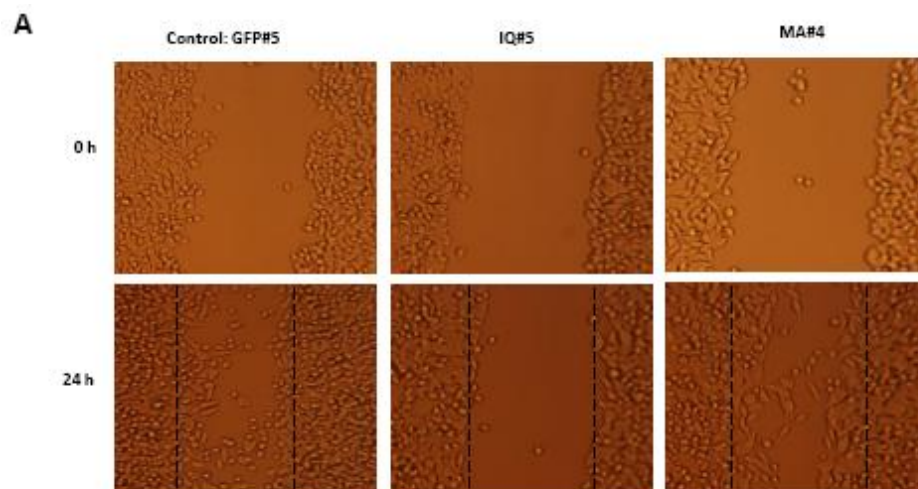
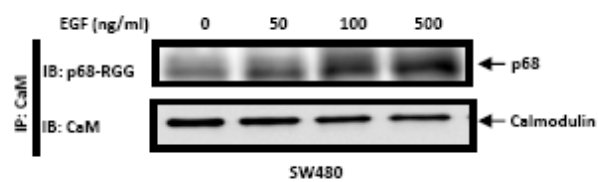


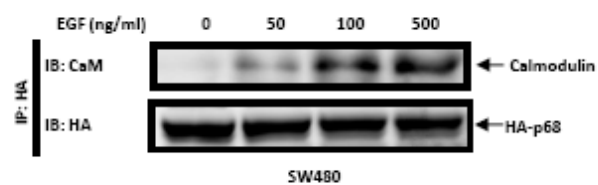
Figure Supplement 4.2 eGFP-IQ expression affected the interaction between p68 and calmodulin and cell migration

(A) The scratch induced cell migration was affected by stably expressing eGFP-IQ. # indicated the clone number of the stable cells. (B) The interaction between p68 and calmodulin was affected by transiently expressing eGFP-IQ. The interaction was examined by employing calmodulin beads pull down assay. IB: GFP indicated the expression level of the eGFP/eGFP-IQ proteins in the cells. The endogenous expression level of p68 and calmodulin were illustrated by the IBs of p68 and calmodulin. IB of GAPDH was used as the loading control for the whole cell lysate.

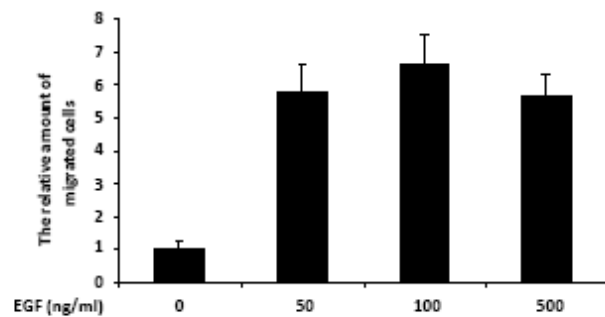
A



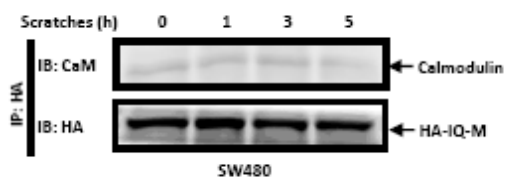
B



C



D



E

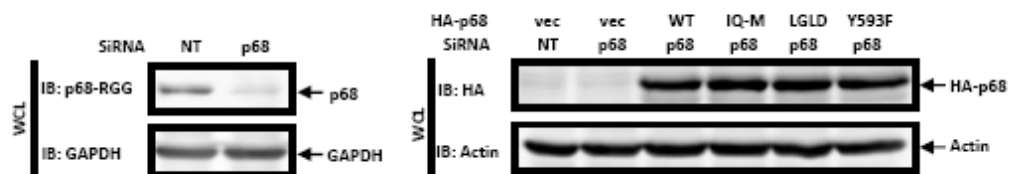
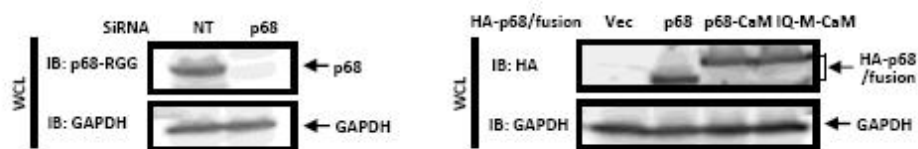


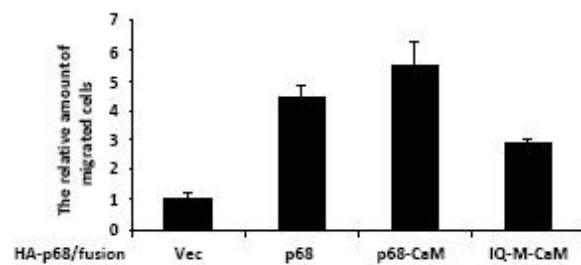
Figure Supplement 4.3

(A) The interaction between p68 and calmodulin was increased when the cells were treated EGF for 3 hours. The interaction was confirmed by the Co-IP. Poly Ab of calmodulin was used to pull down the protein complex. Mono Ab of p68 was used to indicate the amount of p68 interacted with calmodulin. The interaction between p68 and calmodulin was further confirmed in (B). SW480 cells were first exogenously expressed with HA-p68. Poly Ab of HA was used to pull down the protein complex this time. Mono Ab of calmodulin was used to indicate the amount of calmodulin interacted with HA-p68. The cell migration capability was tested under the treatment of different dose of EGF by carrying with Boyden Chamber Assay (C). The interaction between p68 and calmodulin was found to depend on the IQ motif of p68 as the interaction between the IQ mutant of p68 and calmodulin no longer increased when the cells were stimulated with the scratch (D). In order to test how the different mutant of p68 functions in cell migration, the endogenous p68 was knocked down and different mutant p68 was expressed in the p68 knock-down cells. The knock down efficiency of p68 was examined by the IB of the whole cell lysate showed in the left panel in (E). The expression levels of the different mutant of p68 in the cells were examined in the right panel in (E).

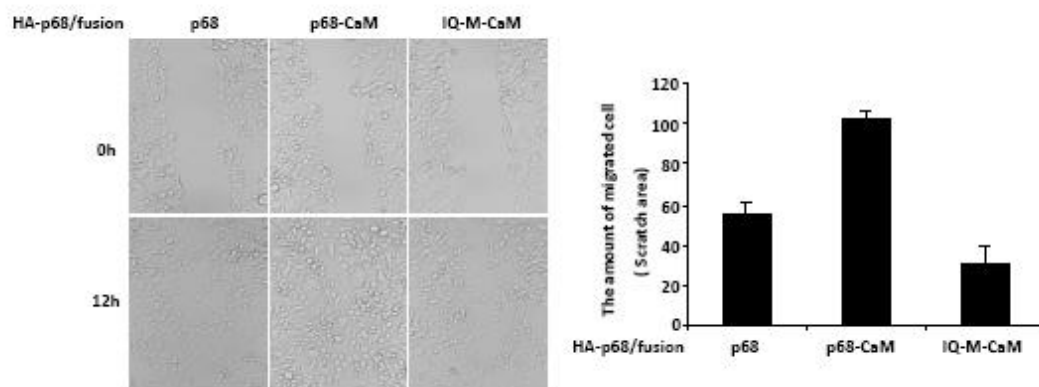
A



B



C



D

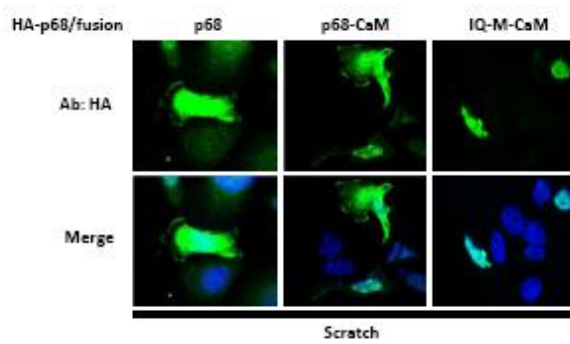


Figure Supplement 4.4

Overexpression of the fusion protein of p68 and calmodulin promoted the cell into migration status. In order to test how the fusion protein functions in cell migration, the endogenous p68 was knocked down and the knock down efficiency was illustrated in the left panel in **(A)**, and the expression levels of p68-calmodulin fusion protein and IQ-M-calmodulin fusion protein were illustrated in the right panel in **(A)**. The cell migration capabilities were then tested by the Boyden Chamber Assay **(B)**. The cell migration capabilities of those cells were also tested by the monolayer scratch assay **(C)**. The image showed the migration results which were stimulated by the monolayer scratch. The graph was the statistically analyzed result. The cellular location of p68/fusion protein (green) in scratch induced migrating cells was illustrated in **(D)**.

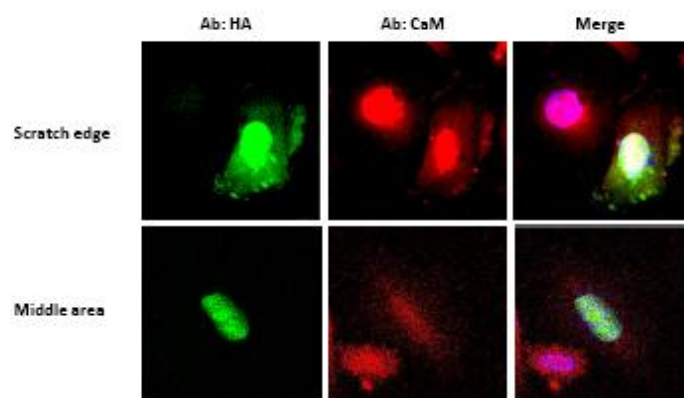
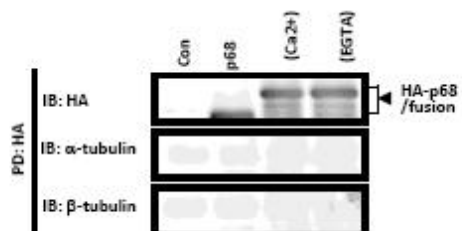
A**B**

Figure Supplement 4.5

(A) The cellular location of HA-p68 (green) and calmodulin (Red) in migrating cells (located at the scratch edge) and in resting cells (located at the middle region of the scratch area). The interaction between HA-p68/HA-fusion protein and subunits of microtubule were tested (B).

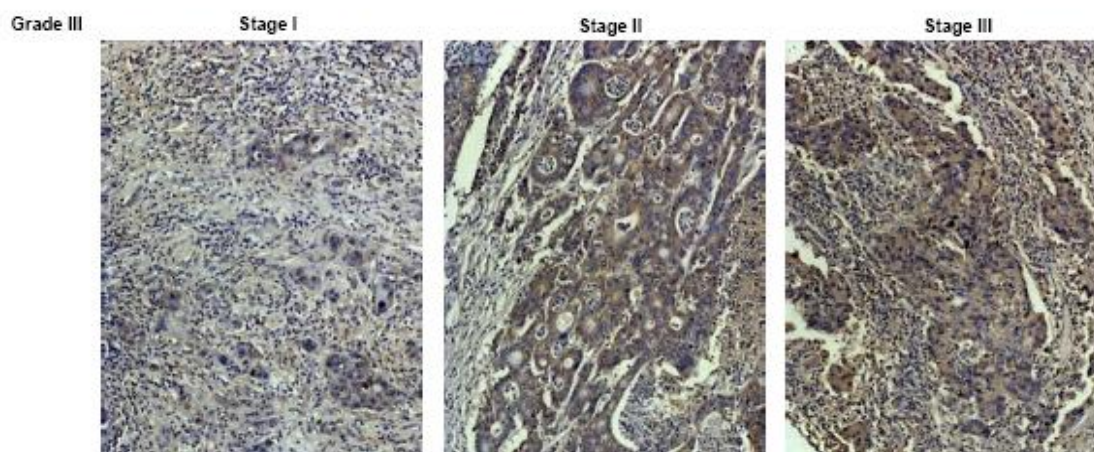
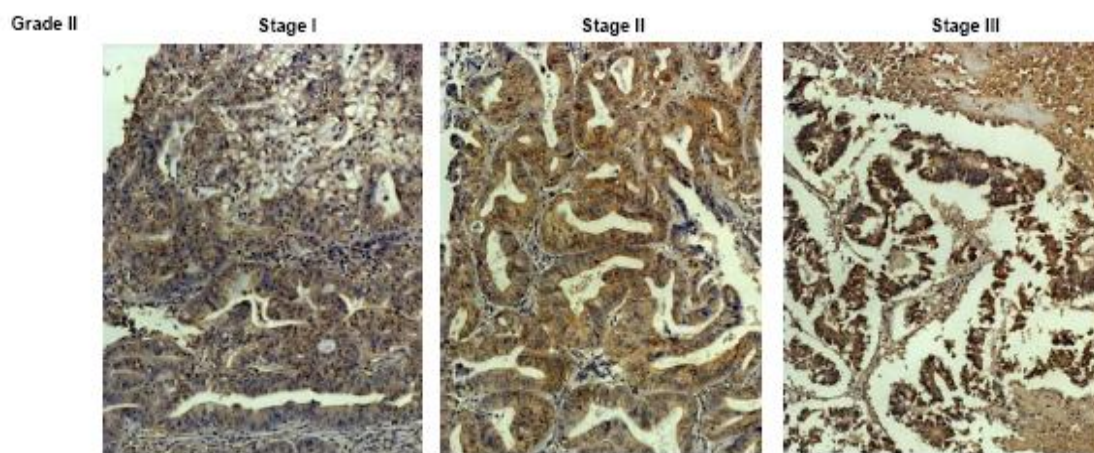
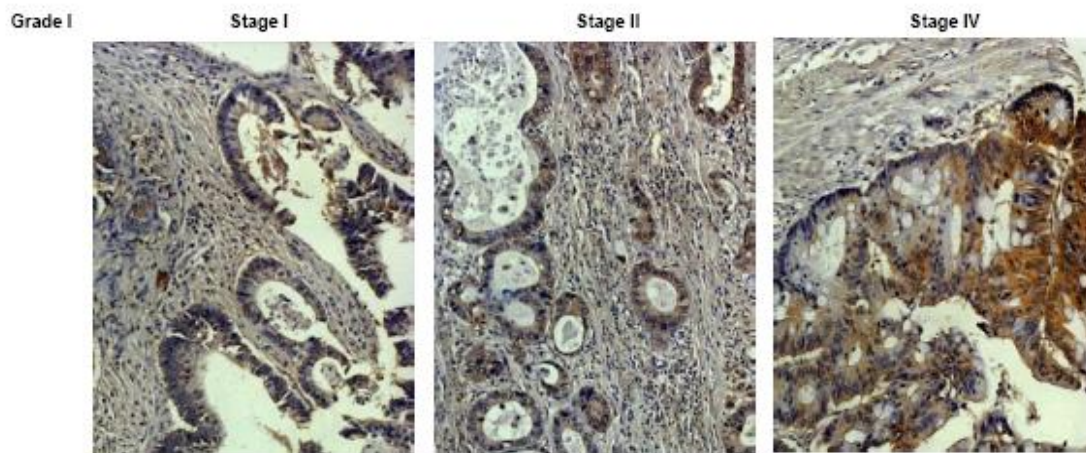


Figure Supplement 4.6

IHC staining of the human colon cancer tissues in the arrays. The cytoplasmic levels of p68 (brown color) at the different stages but in the same grade were compared.

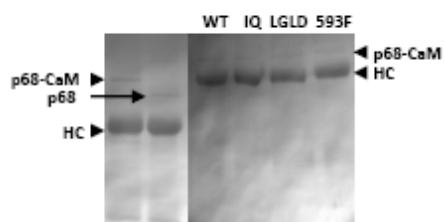
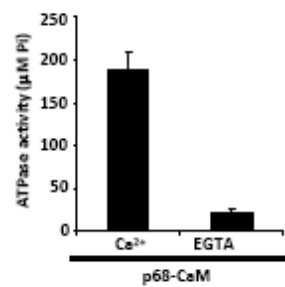
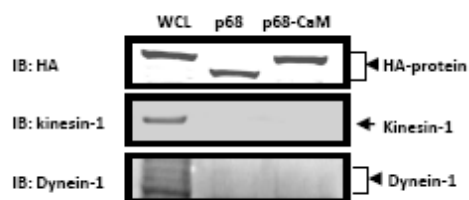
A**B****C**

Figure Supplement 4.7

The purity of the HA-p68/fusion proteins was illustrated in **(A)**. HC indicated the heavy chain of poly Abs for HA and was used as the loading control. The ATPase activity of HA-p68-calmodulin was tested in the presence of the Ca²⁺/EGTA **(B)**. Whether the HA-p68/HA-fusion proteins interact with two classical microtubule motors (kinesin-1 and dynein-1) were tested **(C)**.

CHAPTER 5

PYRUVATE KINASE M2 REGULATES GENE TRANSCRIPTION BY ACTING AS A PROTEIN KINASE

5.1 Abstract

Pyruvate kinase isoform M2 (PKM2) is a glycolysis enzyme catalyzing conversion of phosphoenolpyruvate (PEP) to pyruvate with transferring a phosphate from PEP to ADP. We report here that PKM2 localizes to the cell nucleus. The levels of nuclear PKM2 correlate with cell proliferation. PKM2 activates transcription of MEK5 by phosphorylating stat3 at Y705. *In vitro* phosphorylation assays show that PKM2 is a protein kinase using PEP as phosphate donor. The protein substrate is bound at the ADP binding site. Our experiments suggest that PKM2 dimer is an active protein kinase, while the tetramer is an active pyruvate kinase. Expression a PKM2 mutant that exists as a dimer promotes cell proliferation, indicating that protein kinase activity of PKM2 plays a role in promoting cell proliferation. PKM2 interacts with tyrosine phosphorylated p68. Binding of the tyrosyl phosphorylated proteins at the FBP binding site converts the tetrameric PKM2 to a dimer, and reciprocally regulates the pyruvate kinase and protein kinase activities of PKM2. Growth factor stimulations significantly increase the dimer/tetramer PKM2 ratio in cells and consequently activate the protein kinase activity of PKM2. Our study reveals an important link between metabolism alteration and gene expression during tumor transformation and progression.

5.2 Introduction

An important molecular feature of tumor development is the expression of pyruvate kinase isoenzyme M2 (PKM2) (Elbers, van Unnik et al. 1991; Hacker, Steinberg et al. 1998). The glycolysis catalytically active PKM2 exists as a tetramer and associates with a glycolytic

enzyme complex (Altenberg and Greulich 2004; Dombrauckas, Santarsiero et al. 2005; Spoden, Morandell et al. 2009). In tumor cells, PKM2 forms a dimer, and appears to be catalytically inactive for conversion of PEP to pyruvate (Ashizawa, Willingham et al. 1991; Mazurek, Boschek et al. 2005). It is believed that the inactive PKM2 actually provides growth advantage for tumor progression as it helps to channel the carbon source from glycolytic intermediates to biosynthesis, especially syntheses of nucleic acids, lipids, and proteins, to meet the demands for tumor cell proliferation. Recent studies have suggested that PKM2 changes its pyruvate kinase activity, consequently facilitating cell proliferation by binding to tyrosine phosphor-peptide (Christofk, Vander Heiden et al. 2008; Christofk, Vander Heiden et al. 2008), indicating that growth signals regulate the activity of PKM2 in glucose metabolism.

5.3 Results

5.3.1 Nuclear PKM2 activates transcription of MEK5 by phosphorylating stat3

We and others have observed that the PKM2 localizes to the cell nucleus (Schneider, Neu et al. 2002; Hoshino, Hirst et al. 2007; Stetak, Veress et al. 2007). To understand the functional significance of nuclear localization of PKM2, we examined nuclear PKM2 levels in ten different cancer cell lines by immunoblot using an antibody raised against a peptide spanning aa 399 – 412 of PKM2 (PabPKM2). These ten different cell lines represent different cancer progression stages and are derived from cancers of different organs/tissue types. Cell proliferation analyses demonstrated that M4C1, SW620, WM266, and H146 are more proliferated than their corresponding lines in the matched pairs (Fig. S4.1A). Immunoblot analyses indicated much higher nuclear levels of PKM2 in the more proliferated cancer cells than those in the corresponding less proliferated cells (Fig. 5.1A), The higher nuclear PKM2 levels were not because of differences in PKM2 expression, as shown in figure 5.1A whereas no significant

differences were observed in total PKM2 in cell lysates. The detection of PKM2 in the nuclear extracts was not due to contamination of cytoplasmic proteins as demonstrated by lack of GAPDH in the immunoblot analyses of the nuclear extracts.

To explore a possibility that nuclear PKM2 is involved in regulation of gene expressions, we carried out gene expression array analyses with SW620 cells expressing HA-PKM2. Expressions of 350 genes were upregulated, and expressions of 359 genes were downregulated, by at least two fold (Table S1). Among those affected genes, expression of MEK5 was affected by over six fold. We verified the role of PKM2 in expression of MEK5 by RT-PCR. Consistent with the gene array analyses, RT-PCR demonstrated a dramatic change in the MEK5 expression in SW620 cells, while only a marginal increase in SW480 cells, following the expression of PKM2 (Fig. 5.1B). Similar patterns were also observed with another pair of cell lines, WM115 and WM266. The effects PKM2 on the expressions of MEK5 were further confirmed by immunoblot analyses of cellular MEK5. It was clear that the cellular MEK5 levels increased subsequent to expression of PKM2. The more proliferated cancer cells experienced more dramatic increases in MEK5 levels (Fig. 5.1C). Interestingly, immunoblot of MEK5 using antibody against the phosphorylated MEK5 revealed a strong increase in the cellular levels of phosphorylated MEK5 in more proliferated cancer cells compared to the less proliferated cancer cells upon exogenous expression of PKM2 (Fig. 5.1C). To further verify the role of PKM2 in transcriptional regulation of MEK5, PKM2 was knocked down in SW620 and SW480 cells (Fig. 5.1D). It was evident that MEK5 expression was slightly reduced in SW480. However, the reduction in cellular levels of MEK5 in SW620 cells was dramatic upon knockdown of PKM2 (Fig. 5.1D). We also analyzed the MEK5 mRNA levels in SW620 and WM266 cells upon PKM2 knockdown. Quantitative RT-PCR analyses demonstrated a strong reduction in cellular MEK5

mRNA (Fig. 5.1E). We further used chromatin immunoprecipitation (ChIP) to probe whether PKM2 interacted with the MEK5 promoter. We carried out the ChIP experiments with SW620 cells using the PCR primer pair that spanned the region of nt -1,621 – -1,366 of MEK5 promoter. Our ChIP assays clearly demonstrated that PKM2 indeed interacted with the MEK5 promoter (Fig. 5.1F). We next sought to test whether up-regulation of MEK5 by PKM2 contributed to cell proliferation. MEK5 was first knocked down in SW620 and WM266 cells. As a result, the cell proliferation rate was dramatically reduced (Fig. S5.1B). The proliferation rate increases stimulated by expression of HA-PKM2 in the MEK5 knockdown SW620 and WM266 cells were also largely reduced (Fig. S5.1B), suggesting that up-regulation of MEK5, at least partially, mediated the effects of HA-PKM2 overexpression on cell proliferation. Moreover, we analyzed the MEK5 expression levels in these ten different cancer cell lines. MEK5 was expressed in all ten cell lines, but there were substantially higher levels of MEK5 in the more proliferated cancer cells than in the less proliferated cancer cells. Strikingly, the levels of phosphorylated MEK5 were also consistently higher in more proliferated cells than in less proliferated cells among the selected cancer cell line pairs (Fig. S5.1C). Clearly, there is a close correlation between cellular MEK5 expression levels and nuclear PKM2 levels, and both were correlated closely with the cell proliferation status of the cells (comparing Fig. S5.1C with Fig. 5.1A). We concluded from these studies that up-regulation of MEK5 by nuclear PKM2 contributed to cell proliferation. How would PKM2 function in regulation of gene transcription? Sequence analyses did not reveal any known DNA binding domain/motifs in PKM2. One possibility is that PKM2 may activate particular transcription factors. Thus, we attempted to probe the interaction of PKM2 with several known transcription factors in nuclear extracts of SW620 and SW480 cells by immunoprecipitation, such as Oct-1, Oct-4, Gadd45, SOX4-1, and stat3. Among these selected

targets, stat3 and SOX4 were involved in transcription of MEK5 (Song, Jin et al. 2004; Aaboe, Birkenkamp-Demtroder et al. 2006), while Oct-4 was reported to interact with PKM2 in extracts made from ESC (Lee, Kim et al. 2008). Our experiments showed that stat3 was the only transcriptional factor among the selected targets that interacted with PKM2 (Data not shown, Fig. 5.2A, and Fig. S5.2 A&B). It was likely due to the differences between ESC and cancer cells, we did not detect the PKM2 and Oct-4 interaction in the extracts prepared from cancer cells of several cell lines. We noted that stat3 interacts with MEK5 promoter at -1776 nt – -1520 nt region by ChIP (Song, Jin et al. 2004). Interestingly, PKM2 also interacts with MEK5 promoter at the same region by ChIP (Fig. 5.1F). To address whether the activation of stat3 mediates the effects of PKM2 on upregulation of MEK5 transcription, we first knocked down stat3 in SW620/SW480 and WM266/WM115 cells, and HA-PKM2 was subsequently expressed. It was clear that expression of HA-PKM2 could no longer upregulate MEK5 as measured by cellular levels of both mRNA and protein of MEK5 (Fig. 5.2 B&C, D&E). To further test the role of stat3 in mediating the effects of PKM2 on upregulation of MEK5 transcription, we used a dominant-negative mutant stat3 (Y705F) (Xie, Huang et al. 2006). The mutant was co-expressed with HA-PKM2 in SW620/SW480 and WM266/WM115 cells. It was evident that expression of the dominant-negative mutant largely diminished the effects of PKM2 on upregulating MEK5 transcription (Fig. S5.2 C&D, E&F). As a control, expression of stat3-DN in PKM2 knockdown SW480/SW620 cells did not result in upregulation of MEK5 expression (Fig. S5.2C). It is well documented that the activity of the active stat3 can be inhibited by specific inhibitor (Xu, Cole et al. 2008). We therefore tested the effects of a stat3 inhibitor on the upregulation of MEK5 by expression of HA-PKM2 in SW620 and WM266 cells. Treatment of the HA-PKM2 expressing cells with the inhibitor resulted in a decrease in MEK5 transcription (Fig. S5.2 G&H). Thus, we

concluded that activation of stat3 mediated the regulatory effects of PKM2 on MEK5 transcription.

We next investigated whether expression of PKM2 affected the stat3 binding to its target DNA at the MEK5 promoter. To probe whether knockdown or expression of PKM2 affected the interaction of stat3 with the MEK5 promoter, we performed ChIP experiments in SW620 cells in which the endogenous PKM2 was knocked down or HA-PKM2 was expressed. Clearly, the stat3 and MEK5 promoter interaction was strengthened by HA-PKM2 expression and was weakened by PKM2 knockdown (Fig. 5.3A). We then analyzed the effects of PKM2 on the interaction between stat3 and its target DNA by gel mobility shift assays using a ³²P-labeled oligonucleotide duplex containing a stat3 binding sequence (Xie, Huang et al. 2006). The gel-shift experiments were carried out with nuclear extracts of SW620 cells with/without PKM2 knockdown or with/without HA-PKM2 expression. Autoradiography indicated that a slow migration complex was assembled with the labeled oligonucleotide and addition of the antibody against stat3 resulted in a supershift complex (Fig. 5.3B). Interestingly, knockdown of PKM2 substantially decreased the assembly of the oligo-protein complex and assembly of stat3 in the complex (the weak supershift) (Fig. 5.3D), while expression of HA-PKM2 dramatically increased assembled complex and assembly of stat3 in the complex (Fig. 5.3C).

Stat3 is a transcription activator that is activated by phosphorylation at Y705 mainly by JAK or Src kinase. The phosphorylation increased the stat3 and DNA binding affinity (Sehgal 2008). We observed that PKM2 increased the stat3 binding to its target sequence both *in vitro* and *in vivo*. We suspected that PKM2 may play a role in stat3 phosphorylation at Y705. To test this conjecture, we analyzed the stat3 phosphorylation at Y705 in the nuclear extracts prepared from SW620 cells in which the HA-PKM2 was expressed using an antibody against the Y705

phosphorylated stat3 (P-y705/stat3). Clearly, a significant increase in Y705 phosphorylation of stat3 in the nuclear extracts was evident. Examination of the cellular levels of stat3 indicated that the expression levels of stat3 were not affected by the PKM2 expression (Fig. 5.3E). We also observed a significant reduction in the stat3 phosphorylation in SW620 cells upon PKM2 knockdown (Fig. 5.3F). It is known that JAK2 and c-Src are the most common protein tyrosine kinases that phosphorylate stat3. We therefore probed whether JAK2 and c-Src were activated by the HA-PKM2 expression. Using antibodies against JAK2, the phosphorylated JAK2, c-Src, and the phosphorylated c-Src, our experiments showed that JAK2 and c-Src were not activated upon the HA-PKM2 expression (Fig. S5.3 A&B). Furthermore, treatment of cells with JAK2 inhibitors did not lead to any significant changes of the PKM2-dependent stat3 phosphorylations (Fig. S5.3C), suggesting that stat3 phosphorylation was not due to activation of JAK2 or c-Src.

5.3.2 Dimeric PKM2 is the active protein kinase

Expression of PKM2 increased stat3 phosphorylation at Y705. We sought to verify whether PKM2 could act as a protein kinase that directly phosphorylated stat3. An *in vitro* phosphorylation assay using both the *E. coli* expressed recombinant PKM2 (rPKM2) and the HA-PKM2 immunopurified from nuclear extracts of SW620 cells in the presence of ATP did not yield phosphorylation of a commercially available GST-stat3. Since PKM2 use PEP as phosphate donor to phosphorylate ADP in the glycolysis, we reasoned that the protein may use the same phosphate donor to phosphorylate a protein substrate. Thus, we replaced ATP by PEP in our *in vitro* phosphorylation reaction. Immunoblot using the antibody P-y705/stat3 demonstrated that the GST-stat3 was phosphorylated by the HA-PKM2 in the presence of PEP. Consistently, stat3 was not phosphorylated in the presence of ATP (Fig. 5.4 A&B). These experimental results indicated that PKM2 is a protein kinase using PEP as the phosphate donor.

The kinase activity of the nuclear HA-PKM2 in phosphorylation of stat3 was substantially higher than that of the rPKM2 expressed in *E. coli*. The results led us to compare the protein kinase activity of the nuclear PKM2 and the cytoplasmic PKM2. The HA-PKM2 was immunopurified from nuclear or cytoplasmic extracts of SW620 cells. The same *in vitro* phosphorylation reactions were performed with the immunopurified HA-PKM2 in the presence of PEP or ATP. It was evident that both the HA-PKM2 purified from the nuclear extracts and the cytoplasmic extracts were active in phosphorylating stat3. However, it was also clear that the HA-PKM2 from the nuclear extracts had much higher activity than that of protein from the cytoplasmic extracts (Fig. 5.4 C&D).

It was reported that the catalytically active tetramer and inactive dimer of PKM2 co-exist in cells with high proliferation rate (Mazurek, Boschek et al. 2005). We therefore questioned whether the differences in the protein kinase activity of nuclear/cytoplasmic HA-PKM2 and the rPKM2 were due to dimer or tetramer of the protein. To investigate whether PKM2 is a dimer or a tetramer both in the nucleus and in the cytoplasm, we first fractionated the nuclear extracts and cytoplasmic extracts of SW620 cells by size exclusion chromatography. Non-specific protein-protein interactions were disrupted by treatment of the extracts with 600 mM 6-aminocaproic acid (6-ACA). The levels of PKM2 in each chromatography fraction were examined by immunoblot using the antibody PabPKM2. Nuclear PKM2 was only detected in fractions 14 – 16, while cytoplasmic PKM2 was mainly detected in fractions 11 – 16 with the highest concentrations in fractions 11 – 13. Based on the molecular weight calibration standard (Fig. S5.4 A&B), fraction 11 co-elutes with a molecular weight near 240 kDa, while fraction 14 co-elutes with a molecular weight near 120 kDa (Fig. 5.4E). The gel-filtration chromatography suggested that nuclear PKM2 was completely dimer (120 kDa), while the cytoplasmic PKM2

existed in both dimer and tetramer with a higher population of tetramers. The same chromatography procedure was also employed to analyze whether the rPKM2 is a dimer or tetramer. It was evident that the rPKM2 was detected in the fractions 11 – 14, which indicated that the bacterially expressed rPKM2 is mostly tetramer with very small amount of dimer (Fig. 5.5B). To further probe the dimer/tetramer status of nuclear and cytoplasmic PKM2, nuclear extracts and cytoplasmic extracts of SW620 cells were separated by a non-denaturing PAGE (8% acrylamide:bisacrylamide= 40:1) and subjected to immunoblot analyses using the antibody PabPKM2. It was clear that the nuclear PKM2 migrated slightly faster than the BSA dimer (132 kDa). Conversely, the majority of the cytoplasmic PKM2 approximately co-migrated with Urease (272 kDa) (Fig. S5.4C). Thus, we concluded that PKM2 is a dimer in the nucleus and a dimer/tetramer mix in the cytoplasm. The rPKM2 mainly exist as tetramer.

Based on the proceeding observations, we speculated that the dimer form of PKM2 is the active protein kinase, while tetramer is an active pyruvate kinase. Close examination of the crystal structure of the tetramer human PKM2 (Dombrauckas, Santarsiero et al. 2005) reveals that a positive charged residue R399 may plays a critical role in forming the tetramer of PKM2. It is notable that the R399 forms stable charge-charge interactions with residues E418 and E396 of PKM2 located on the other dimer of the tetramer PKM2 (Fig. 5.5A). We therefore created a mutant R399E to disrupt the charge-charge interaction. Size exclusion chromatography analyses demonstrated that the R399E mutant was mostly dimer (Fig. 5.5B). We reasoned that the dimeric R399E mutant would be more active in phosphorylating stat3 compared to the wild-type rPKM2. Thus, the *in vitro* phosphorylation reactions were carried out with the wild-type rPKM2 and the R399E mutant. It was evident that the protein kinase activity of the R399E mutant was substantially higher than that of the wild-type rPKM2 (Fig. 5.5C), while the pyruvate kinase

activity of the mutant was dramatically lower than that of the rPKM2 (Fig. 5.5D). The results supported our speculation that dimeric PKM2 is an active protein kinase.

To further verify the phosphorylation of stat3 by PKM2, we prepared [³²P]-labeled PEP according to the report by Roossien FF. and co-workers (Roossien, Brink et al. 1983). The same *in vitro* phosphorylation reaction was carried out with the rPKM2, the rPKM1, and the R399E mutant using the [³²P]-PEP. The phosphorylation reaction mixture was separated by SDS-PAGE and subjected to autoradiography. It was clear that the GST-stat3 was phosphorylated by the R399E mutant. The phosphorylation of the GST-stat3 by the rPKM2 was very weak (can only be visualized by a substantial overexposure in autoradiograph). The GST-stat3 was not phosphorylated by the rPKM1 in the presence of the [³²P]-PEP (Fig. S5.5A). No phosphorylation can be detected even under very high overexposure in the autoradiograph. To ensure that the *in vitro* phosphorylation of stat3 by PKM2 and the R399E mutant was at comparable physiological conditions, we compared the phosphorylation of the GST-stat3 by JAK2 and R399E. Clearly, similar levels of stat3 phosphorylations were observed by both kinases (Fig. S5.5B). The same phosphorylation reaction could not phosphorylate other protein substrates, such as stat5 and BSA (Fig S5.5 C&D), indicating that PKM2 only phosphorylates specific protein substrate(s). Extensive analyses of enzyme kinetic of pyruvate kinase in various tissue samples ($K_m = 0.07 - 1.2$ mM range) indicate that the physiological concentration of PEP likely to be at $\mu\text{M} - \text{mM}$ (van Veelen, Verbiest et al. 1978)(To test whether PKM2 and the R399E mutant would phosphorylate stat3 at the physiological PEP concentrations, we carried out the *in vitro* phosphorylation at various PEP concentrations. The levels of phosphorylated stat3 remained almost constant down to 100 μM of PEP. However, there was a clear decrease in stat3 phosphorylation when PEP

concentration fell below 10 μ M (Fig. S5.5E). These experiments indicated that phosphorylation of stat3 by PKM2 and the mutant were at physiological comparable conditions.

5.3.3 Expression of R399E increased stat3 phosphorylation in cells and promoted cell proliferation

We employed a PKM2 mutant R399E. Our experiments showed that the recombinant R399E existed mostly as a dimer and the mutant exhibited strong activity in phosphorylation of GST-stat3. We therefore questioned whether the R399E mutant would be active in phosphorylation of stat3 in cells. To this end, the HA-R399E was exogenously expressed in SW480 cells. Immunoblot of the nuclear extracts indicated a significant increase in the levels of phosphorylated stat3. This increase was not due to increase in cellular levels of stat3 (Fig. 5.5E). Size exclusion chromatography of cell lysate showed that, unlike the wild-type HA-PKM2, the HA-R399E was almost complete dimer (Fig. S5.5F) *In vitro* phosphorylation assays indicated that the purified HA-R399E phosphorylated GST-stat3 (Fig. 5.5F). We also tested here if expression of R399E in SW480 cells would lead to MEK5 up-regulation and cell proliferation. RT-PCR analyses clearly demonstrated that the cellular levels of mRNA of MEK5 increased significantly (Fig. 5.5G). Examination of cell proliferation using a commercial kit demonstrated that expression of R399E led to a strong increase in cell proliferation (Fig. 5.5H). To further verify the role of PKM2 protein kinase activity in promoting cell proliferation, we created a cell line by stable expression of R399E in SW480 cells (Fig. 5.6E). The derived cells were implanted to nude mice by s.c. Tumors were grown for four weeks. Clearly, the R399E mutant expressing tumors grew substantially bigger than the wild type PKM2 expression tumors did (Fig. 5.6 A&B&C). Histology analyses using anti-Ki-67 antibody indicated that the R399E expressing tumors had much higher proliferation rate than that of the wild type PKM2 expressing tumors

(Fig. 5.6D). The results strongly support our hypothesis that protein kinase activity of PKM2 promotes tumor/cell proliferation.

5.3.4 PKM2 protein kinase substrates bind to the ADP binding site

PKM2 directly phosphorylates stat3. One interesting question is how the protein substrate is bound to PKM2. Our results showed that PEP was used as phosphate donor. It is established that in the catalysis of ADP phosphorylation in the glycolysis, PKM2 binds phosphate donor PEP at one site and substrate ADP at the other. Thus, a very logic assumption is that the protein substrate may bind to the ADP site. To test this conjecture, we carried out competition binding analyses. The R399E mutant and stat3 interaction was analyzed in the presence and absence of ADP, PEP, and FBP. The GST-stat3 was immobilized on the glutathione-agarose beads. Recombinant R399E in mixing with buffer, ADP, PEP, or FBP were incubated with the beads. Binding of the R399E to the immobilized GST-stat3 was then analyzed by SDS-PAGE followed by immunoblot of R399E and stat3. It was clear that the interaction of R399E with GST-stat3 was not affected in the presence of 5 mM FBP, while the interaction was almost not detectable in the presence of 5 mM ADP. The R339E and stat3 interaction was also weakened in the presence of 5 mM of PEP. This was most likely due to phosphorylation of stat3, as the reduction in stat3 and R399E interaction was not PEP concentration dependent, while the R399E and GST-stat3 interaction showed a clear ADP concentration dependent reduction (Fig. 5.5I), indicating the competition of ADP with stat3 in binding R399E. The notion that protein kinase substrate is bound at the ADP binding site of PKM2 was also supported by our early observations that addition of ADP decreased the activity of PKM2 in phosphorylation of stat3, while addition of FBP did not (see Fig. 5.4C/D and 5.5C).

5.3.5 Reciprocal regulation of protein kinase and pyruvate kinase activities of PKM2 by tyrosine phosphor-proteins

Christofk and co-workers reported that PKM2 interacts with phosphor-tyrosine peptide and the interaction plays an important role in promoting cell proliferation (Christofk, Vander Heiden et al. 2008; Christofk, Vander Heiden et al. 2008), suggesting a possible pathway that growth signals promotes proliferation via protein tyrosine phosphorylation and subsequent action on PKM2. We previously demonstrated that P68 RNA helicase is phosphorylated in cancer cells, and tyrosine phosphorylation of p68 correlates with cancer progression (Yang, Lin et al. 2005). Phosphorylation of p68 at Y593 promotes EMT (Yang, Lin et al. 2006), while phosphorylation of p68 at Y593 and Y595 mediated resistance to apoptotic-induction (Yang, Lin et al. 2007). In an effort to probe interacting protein with the tyrosyl phosphorylated p68, we used a 14 amino acid segment that includes the Y593 or Y593/595 phosphorylation site (a.a. 587 to 600). The peptides either carried no phosphorylation (PepY593), Y593 phosphorylation (PhosPepY593), or Y593/595 double phosphorylations (D-PhosPepY593). We also used another control peptide that span different region of p68 (aa 561 – 574) with Y567 phosphorylation (PhosPepY567). The peptides were conjugated to agarose beads. Precipitation experiments with nuclear extracts of T98G cells demonstrated that the D-PhosPepY593 pulled-down a nuclear protein that migrated at ~60 kDa. The interacting protein was identified by MALDI (tof/tof) as PKM2 (Fig. 5.7A). The interaction between p68 and PKM2 was first verified by a peptide pull-down with recombinant PKM2 (rPKM2) and the pull-down with nuclear extracts of T98G cells using the rPKM2 as bait (Fig. 5.7B and S5.6A). We also verified the interaction by co-immunoprecipitation with nuclear extracts of T98G cells (Fig. 5.7C and Fig S5.6B). To test whether the PKM2 and p68 interaction is the p68 phosphorylation dependent, we carried out co-immunoprecipitation experiment with

the nuclear extracts of T98G cells in which HA-p68, wt or Y593F (a p68 mutant that cannot be phosphorylated), was expressed. It was clear that wt HA-p68 co-precipitated with PKM2, while the Y593F mutant did not (Fig. 5.7C), suggesting that p68 tyrosine phosphorylation is required for PKM2 and p68 interaction.

We reasoned what is the function of the interaction between the phosphor-p68 and PKM2. It is believed that PKM2 exists as tetramer and dimer mixture in cells (Ashizawa, Willingham et al. 1991; Mazurek, Boschek et al. 2005). We speculated whether the interaction of PKM2 with the phosphor p68 might promote the conversion of PKM2 from a tetramer to a dimer. To test this conjecture, we employed three phosphorylated/unphosphorylated peptides, the D-PhosPepY593, the PhosPepY567, and the PepY593. We first examined the interaction of the selected peptides with the rPKM2 by monitoring the Trp fluorescence changes of the rPKM2 upon interaction. It was clear that the D-PhosPepY593 interacted with the rPKM2 with K_d around 30 μ M, while the PhosPepY567 and the PepY593 did not (Fig. S5.7 A, B, and C). It was suggested that the tyrosine phosphor-peptide interacts with PKM2 at FBP binding site (Christofk, Vander Heiden et al. 2008). We therefore examined whether the D-PhosPepY593 interacts with the rPKM2 at FBP binding site by testing the interaction in the presence of excessive amounts of FBP. It was clear that FBP competed with the D-PhosPepY593 (Fig. S5.7 A, B, and C). The competition of FBP with p68 for binding to PKM2 was also revealed by co-immunoprecipitation experiment showing that coprecipitation of p68 with HA-PKM2 in T98G cell extracts decreased by supplementing the extracts with different concentrations of FBP (Fig. 5.7D). The similar co-immunoprecipitation experiment was also carried out with the rPKM2 and the HA-p68 immunopurified from T98G cell extracts in the presence of various concentrations of FBP. High concentration of FBP decreased the HA-p68 and the rPKM2 interaction (Fig. S5.7D). It is

reported that W515–G520 located at the activating loop of C-terminal of PKM2 is critical for the FBP binding (Dombrauckas, Santarsiero et al. 2005). Thus, we created a truncation mutant with deletion of W515 – G531. The interaction of the phosphor-p68 with the PKM2 truncation was examined by the coimmunoprecipitation procedure. It was evident that the deletion of the FBP binding activating loop abolished the interaction between p68 and PKM2 (Fig. 5.7E). Meanwhile, a mutation (K270M) that affects the glycolytic substrate binding (Dombrauckas, Santarsiero et al. 2005) did not affect the interaction between p68 and PKM2 (Fig. 5.7E). These results are consistent with the observations by Christofk and co-workers (Christofk, Vander Heiden et al. 2008), indicating that the phosphopeptides D-PhosPepY593 and phosphor-p68 interact with PKM2 at the FBP binding site. We next examined the effects of binding the phosphor-peptides on the tetramer and dimer formation. We used size exclusion chromatography method to analyze the molecular sizes of the rPKM2 in the presence or absence of the three tyrosine phosphor/unphosphor-peptides and compared to the chromatography profile of molecular size standard. It was evident that there were substantially more dimeric PKM2 in the presence of D-PhosPepY593, while the tetramer and dimer ratio of the rPKM2 was not affected in the presence of the PhosPepY567 and the non-phosphor-peptide PepY593 (Fig. 5.7F). The experiments apparently suggested that binding the tyrosyl phosphorpeptide converts tetramer PKM2 to a dimeric form.

We then asked whether binding of the tyrosyl phosphor-protein//peptide would activate the protein kinase activity and inactive pyruvate kinase activity of PKM2. To this end, the *in vitro* phosphorylation reactions using GST-stat3 as substrate and PEP as phosphate donor were carried out with the rPKM2 in the presence of the different peptides. Examination of phosphorylation of stat3 by the immunoblot using the anti-phospho-stat3 antibody indicated that

phosphorylation of stat3 by the rPKM2 was dramatically increased in the presence of DPhosPepY593 (Fig. 5.8A). The phosphorylations of stat3 by the rPKM2 were not affected in the presence of the PepY593. The phosphorylation of stat3 was also not affected in the presence of peptide PhosPepY567 that did not bind to PKM2 (Fig. 5.8A). As a control, the peptide DPhosPepY593 did not affect the phosphorylation of GST-stat3 by R399E, and the peptide alone did not lead to stat3 phosphorylation (Fig S5.8A). We next tested whether indeed presence of phosphor-p68 would activate the protein kinase activity of PKM2. To this end, HA-p68 was immunopurified from nuclear extracts of T98G cells. Phosphorylation of GST-stat3 by the rPKM2 in the presence or absence of the immunopurified HA-p68 was examined. Clearly, stat3 was much strongly phosphorylated by the rPKM2 in the presence of the purified HA-p68 (Fig. 5.8B). On the other hand, the protein kinase activity of PKM2 purified from p68 knockdown cells was significantly decreased (Fig S5.8B). The results support the notion that binding of the tyrosyl phosphor-protein activates the protein kinase activity of PKM2.

PKM2 is a glycolysis enzyme. It is believed that the tetramer form of the protein is catalytic active in catalyzing the conversion of PEP to pyruvate in the glycolysis. Since the binding of the tyrosine phosphor-protein promoted the conversion from tetramer to dimer, we reasoned that binding the tyrosine phosphor-protein/peptide to PKM2 should result in protein that is less active in catalyzing the conversion of PEP to pyruvate. We used the method similar to that is described by Christofk and coworkers (Christofk, Vander Heiden et al. 2008) to monitor the pyruvate kinase activity of the rPKM2 in the presence of the tyrosine phosphor-peptides. The rPKM2 catalytic activity was dramatically reduced in the presence of D-PhosPepY593, while the activity was not affected in the presence of the peptides PhosPepY567 and PepY593 (Fig. 5.8C), which indicate that binding of PKM2 to the tyrosine phosphor-proteins converted the protein to

dimer and consequently reduced the glycolytic enzyme activity. The notion was further supported by the experiments that the pyruvate kinase activity of the R399E was dramatically decreased compared to that of recombinant wild-type (Fig. 5.5D). In addition, examination of p68 and stat3 phosphorylation levels in different cancer cells revealed a correlation (Fig S5.8 C&D), suggesting a potential role of phosphor-p68 in activating the PKM2 protein kinase activity in phosphorylation of stat3 in cancer cells.

Our experiments thus far demonstrate that tyrosine phosphor-p68 interacts with PKM2 at the FBP site and strengthen the protein kinase activity of the protein. We therefore predict a three ways interaction among the phosphor-p68, PKM2, and stat3. To test this possible protein interaction, we carried out the GST-pull down using the GST-stat3, the rPKM2 and HA-p68 that were immunopurified from T98G cell extracts. Immunoblot demonstrated that both the rPKM2 and HA-p68 were co-precipitated with GST-stat3 (Fig. 5.8D). The three ways interaction was also probed by co-immunoprecipitation experiments using anti-HA antibody. The rPKM2 and GSTstat3 were co-precipitated with HA-p68 that was immunopurified from cellular extracts of T98G cells (Fig. 5.8E). These results provided additional support for the notion that interaction with tyrosyl phosphor-protein increase protein kinase activity of PKM2. The results also provide additional support for the notion that protein kinase substrate binds to the ADP binding site of PKM2.

It is well documented that stimulation of cells by growth factors and cytokines results in activation of various protein tyrosine kinases that subsequently phosphorylates many protein substrates (Hunter and Cooper 1985). For instance, we previously demonstrated that PDGF or EGF stimulation led to tyrosine phosphorylation of p68 RNA helicase (Yang, Lin et al. 2005; Yang, Lin et al. 2007). Presently our experiments demonstrated that binding to tyrosine

phosphor-protein converted PKM2 from tetramer to dimer therefore activated the protein kinase activity. We reason whether treatment of cells with growth factors would affect PKM2. Thus, SW480 cells were treated with EGF. The same chromatography procedure used for detecting the PKM2 tetramer vs dimer in crude cell extracts was employed here to analyze the tetramer and dimer ratio of PKM2 in cells under the stimulation of EGF. It was clear that the levels of dimer PKM2 in growth factor stimulated cells were significantly higher than that in corresponding unstimulated cells (Fig. 5.9A). Immunoblot analyses of PKM2 in nuclear and cytoplasmic extracts suggested that growth factor stimulation led to increase in nuclear PKM2 levels (Fig. 5.9B). Analyses of protein tyrosine phosphorylation and p68 tyrosine phosphorylation revealed that there was a substantial increase in protein tyrosine phosphorylation and tyrosine phosphorylation of p68 at tyrosine residue (Fig. 5.9C). These experiments suggested that indeed there is a clear correlation between the levels of protein tyrosine phosphorylations and dimeric PKM2 in cells, which is inducible by growth factors and cytokines.

5.4 Discussion

During tumor progression, growth signals stimulate the conversion of glycolytically active PKM2 to an inactive form, consequently regulating the glycolysis pathway to channel the carbon source from glucose for biosynthesis (Mazurek and Eigenbrodt 2003; Garber 2006; Christofk, Vander Heiden et al. 2008; Deberardinis, Sayed et al. 2008). It is conceivable that tumor cells need to coordinate the metabolism alterations with expression of genes that are related to cell proliferation. PKM2 has long been recognized as a so-called ‘moonlight’ enzyme that plays a very important role in tumor progression (Sriram, Martinez et al. 2005). Clearly, the protein kinase activity of PKM2 and subsequent activity in transcription regulation is an important ‘moonlight’ activity. The functions of PKM2 in regulating expression of genes fulfill

the role of feedback signaling from metabolic alterations to gene regulation during tumor malignancy transformation (see model in Fig. 5.9D).

We show that protein kinase activity of PKM2 is associated with proliferation. Thus, it is conceivable that the growth signals must also regulate protein kinase activity of PKM2. Our studies demonstrate here that tyrosine phosphorylations of various cellular proteins under growth stimulations facilitate the interaction between tyrosine phosphor-protein and PKM2, which will result in tetramer to dimer conversion of PKM2. This conversion leads to inactivation of pyruvate kinase and activation of protein kinase activities of PKM2 (Fig. 5.9D). The reciprocal and reversible regulation of pyruvate kinase and protein kinase activities of PKM2 functions in altering cell metabolism and coordinating the metabolism adjustments with other cellular processes in response to growth stimulations. It is intriguing that interaction with FBP facilitates PKM2 to form a tetramer, while binding to tyrosine phosphor-proteins promotes a dimer formation. Why these phosphor-molecules have just opposite effects is an open question. It is intriguing that a glycolytic enzyme can function as a protein kinase and translocate to the nucleus acting on gene transcription. It was revealed from x-ray crystallography structural analyses of the tetramer PKM2 that the ADP binding site is formed by a large hydrophobic hole, indicating a great flexibility for nucleotide binding (Muirhead, Clayden et al. 1986; Dombrauckas, Santarsiero et al. 2005). The large hydrophobic hole at the nucleotide binding site is almost completely buried in a tetramer structure, while it would be completely accessible with the dimeric form. Thus, it is conceivable that the nucleotide binding site may be able to accommodate a protein substrate when PKM2 is converted to a dimer. It should be pointed out that our results could not exclude a possibility that ADP and stat3 do not bind at the same site. The competition is due to binding of ADP cause conformational changes at the stat3 binding site.

Stat3 is a transcription activator that is activated in response to inflammatory cytokines, such as IL-6 (Gao, Mark et al. 2007; Watson and Neoh 2008). Strikingly, activation of stat3 represents probably one of the most important molecular signatures involved in promoting cancer progression. It has been observed that activation of stat3 is detected in almost all cancer types (Frank 2007; Huang 2007; Kim, Chan et al. 2007; Groner, Lucks et al. 2008). However, it is generally believed that activations of stat3 in response to growth factor and cytokines are usually transient. A long standing question is “How do the malignant cancer cells maintain constitutive activation of stat3?” Currently, mutation(s) that lead to constitutive activation of stat3 have not been identified. Thus, activation of stat3 by PKM2 in malignant cancer cells potentially provides a very attractive explanation for this long-standing question. Whether stat3 is the only PKM2 substrate for its protein kinase activity is an open question. PKM2 interacts with several other proteins (Garcia-Gonzalo, Cruz et al. 2003; Lee, Kim et al. 2008; Spoden, Morandell et al. 2009). It was also speculated that PKM2 purified from hepatoma tumour cells may be able to phosphorylate histone H1 (Ignacak and Stachurska 2003). Thus, it will be very interested to identify other PKM2 protein kinase substrates and uncover the putative cellular function of the corresponding protein phosphorylations.

5.5 Materials and methods

5.5.1 Reagents, cell lines, antibodies, and plasmids construction

The KLH conjugated peptide spans a.a. 399 – 412 of PKM2 (IYHLQLFEELRRLAPI) was synthesized by Global Peptide Services. PKM2 polyclonal antibody and anti-HA antibody was raised in the animal facility of Georgia State University. The peptides, D-PhoPepY593, PepY593, and PhosPepY567, were synthesized by AnaSpec. Antibodies against stat3, stat3(pY705), HA-tag, GAPDH, Lamin A/C, and β -actin were purchased from Cell Signaling,

Abnova, SantaCruz, Abcam, and AnaSpec respectively. Recombinant GST-stat3 was purchased from Abcam. Cell lines SW480, SW620, T98G were purchased from ATCC and cultured by following the vendor's instructions. Human full length cDNA of PKM2 and PKM1 were purchased from OriGene Technologies. The cDNA of PKM2 and PKM1 was subcloned into bacteria expression vector pET30a (+) as well as mammalian expression vectors pHM6. The PKM2 or its mutants were fused at the C-terminal of HA protein tag in pHM6 mammalian expression vector. Site directed mutagenesis were performed using QuikChange® Multi Site-Directed Mutagenesis Kit (Stratagene). All the DNA clones and mutations were verified by auto-DNA sequencing at GSU. The HA-tagged full length p68 (wild type, Y593F mutant) expression plasmids were constructed in pHM6 vectors as indicated in the previous papers from our lab (Yang et al., 2006).

5.5.2 Expression and purification of recombinant PKM2 and PKM1

The recombinant 6×his-PKM2, 6xhis-PKM1, or 6xhisPKM2 mutant was expressed in bacterial BL21-CodonPlus (DE3)-RIPL. The recombinant protein was expressed and accumulated in the bacterial inclusion body. After extensive washes, the bacterial inclusion bodies were dissolved into 8 M Urea pH = 7.5. The protein was then purified over a HiTrap® his-affinity column. The purified recombinant PKM2, PKM1, and PKM2 mutants was then refold by slow dilution into 10 folds refolding buffer (10 mM tris pH=7.5, 20% glycerol, 0.1 M KCl, 0.1 M EDTA, 1 mM DTT) and dialysis against refolding buffer. Purified protein was verified by immunoblotting using antibody against PKM2.

5.5.3 In vitro protein kinase and pyruvate kinase assays

The bacterially expressed recombinant rPKM2/R399E or HA-PKM2/HA-R399E immunopurified from cellular extracts (10 µg/ml) were incubated with GST-stat3 (10 µg/ml)

under various conditions (indicated in the figure legends) with kinase buffer (50 mM Tris-HCl pH = 7.5, 100 mM KCl, 50 mM MgCl₂, 1 mM Na₃VO₄, 1 mM PMSF, and 1 mM DTT) in 100 µl at room temperature for 1 hours. The phosphorylation reactions were carried out in the presence either 5 mM ATP or 5 mM PEP. The phosphorylation reactions were terminated by addition of 20 µl of 4 x SDS-PAGE loading buffer and heated to 100 °C for 8 minutes. The reaction mixtures were then subjected to 10% SDS-PAGE separation and subsequent analyses. Pyruvate kinase activity was analyzed by following the experimental procedure similar to that was described by Christofk and co-workers (Christofk et al., 2008b). Briefly, the rPKM2 or the mutant R399E (at 1 µM) was incubated with the buffer (100 mM Tris-HCl, pH=7.5, 100 mM KCl, 5 mM MgCl₂) containing 1 mM ADP and 0.5 mM PEP. The reaction also contained 200 µM NADH and 10 µM FBP. After incubation at room temperature for 30 minutes, 8 units of LDH (Calbiochem) were added to the reaction. The reactions were then subsequently analyzed by measuring the absorbance at 340 nm. The pyruvate kinase activity was presented as relative pyruvate kinase activity by define the activity of the rPKM2 as 100.

5.5.4 Gel-mobility shift and super-shift assays

The mobility shift assays were carried out with oligonucleotide that harbors a stat3 binding sequence 5'-GATCCTTCTGGGAATTCCTAGATC-3' (Xie et al., 2006). The oligonucleotide was 5'-end ³²P-labeled. The labeled oligonucleotide (100 pmole) was incubated with 15% nuclear extracts (20 µl) prepared from appropriate cells as indicated in the figure legends for 30 minutes at room temperature in the binding buffer (5% glycerol, 1mM MgCl₂, 0.5mM EDTA, 0.5mM DTT, 50mM NaCl, 10mM Tris-HCl, 0.05mg/ml poly(dI-dC)). The protein-oligonucleotide complexes were separated in 4% native polyacrylamide gel (acrylamide: polyacrylamide 59:1). For supershift analyses, a monoclonal antibody against stat3 (invitrogen)

or the antibody PabPKM2 was added to the oligonucleotide-nuclear extracts mixture and incubated for additional 45 minutes. The complexes in gel were transferred to a membrane and subjected to autoradiography.

5.5.5 Size-exclusion chromatography and non-denaturing gel electrophoresis

Size exclusion chromatograph was performed with a Superdex 200 10/300GL column using the Akta purifier 100 FPLC system. The samples of cytoplasmic extracts, nuclear extract, the rPKM2, the recombinant PKM2 mutants, and the immunopurified HA-PKM2/HA-R399E were prepared in tris-HCl buffer (50 mM tris, 0.15 M NaCl pH 7.2). 6-AcA (600 mM) was added to the protein samples to disrupt the non-specific protein-protein interactions. For the crude cellular extracts, the samples were prepared in 5 – 7 mg/ml of total protein. For the recombinant or the immunopurified proteins, the samples were prepared in concentration of 15 μ M. 100 μ l of prepared sample was loaded into the Superdex 200 10/300GL column and eluted with elution buffer (50 mM phosphate, 0.15M NaCl pH7.2). The fraction of 300 μ l was collected, and 50 μ l of each fraction was analyzed by 10 % SDS-PAGE and followed by immunoblot using appropriate antibody. The elution profiles were compared to that of a size exclusion chromatograph calibration kits (GE Healthcare) under identical conditions. The elution profile was recorded based on the absorbance of elution fractions at 280 nm. The elution profile was plotted against LogMW according to vendor's instructions. The treated cytoplasmic or the nuclear extracts (6 μ l) were loaded on an 8% nondenaturing polyacrylamide gel (40:1 – acrylamide: bis-acrylamide). The gel was subject to immunoblot using the antibody PabPKM2. The molecular weight markers, BSA and Urease (Sigma), were loaded on the same gel and were visualized by ponceau S staining.

5.5.6 PKM2 and peptide interaction

Interactions between the rPKM2 and its derived mutants were analyzed by monitoring the changes of tryptophan fluorescence of the recombinant protein PKM2 or the mutants ($\lambda_{\text{ex}} = 285$ nm, $\lambda_{\text{em}} = 310\text{-}410$ nm). The binding analyses were carried out with protein concentration 4 μM in the reaction buffer (50 mM tris, pH7.5, 100 mM KCl). Different peptides (100 μM) were titrated into the protein solution. All spectra were recorded at ambient temperature using a PTI spectrofluorimeter with a 1 cm path length cuvette. FBP was added in the protein solution with a final concentration of 2 mM.

5.5.7 Nude mice xenograft

Nude mice (nu/nu, 5 to 6 weeks old, Harlan Laboratory) were subcutaneously injected with 5×10^6 SW480 cells stably expressing PKM2 wild type, R399E mutant, or vector alone (6 mice each group). Tumor formation and volumes were assessed every 2 days. Tumor volumes were measured by two perpendicular diameters of the tumors over a 4-week time course with the formula $4\pi/3 \times (\text{width}/2)^2 \times (\text{length}/2)$. The tumors were collected and weighed at the end of the experiments. Tissue sections were prepared from harvested tumors, and stained using a commercially available antibody for Ki-67. Statistical analyses were done in comparison to the control group with a paired Student's t test.

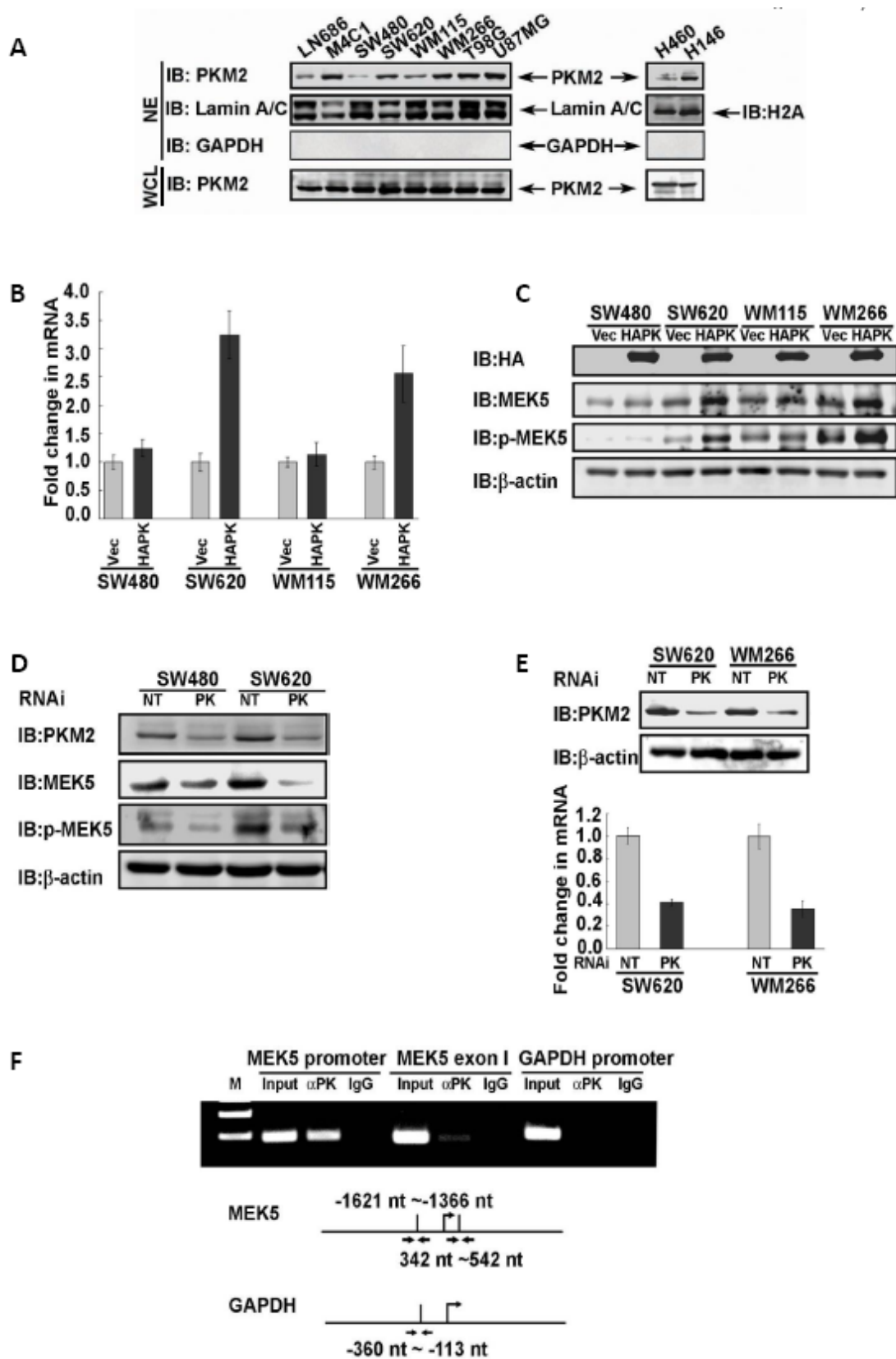


Figure 5.1 PKM2 regulates MEK5 transcription

(A) Nuclear localization of PKM2 in different cancer cells. Immunoblot analyses of PKM2 using the antibody PabPKM2 (IB:PKM2) in nuclear extracts (NE) and whole cell lysates (WCL) of ten different cell lines (indicated). Blot of GAPDH (IB:GAPDH) is a control indicate no cytoplasmic protein contaminations in nuclear extracts. Blots of lamin A/C and H2A are loading controls. (B) RT-PCR analyses of cellular MEK5 mRNA levels in two pairs of cancer cells (indicated) in which PKM2 was exogenously expressed using the adeno-viral expression kit. The results are presented as fold increase in PCR products before and 48 hours after PKM2 exogenous expression in the same cells. The level of PCR product from each cell line before PKM2 exogenous expression was defined as 1. (C) Expressions (IB:MEK5) and phosphorylation (IB: p-MEK5) of MEK5 in different cancer cells (indicated on top) were analyzed by immunoblot using antibodies against MEK5 and phosphorylated MEK5. HA-PKM2 was expressed (HAPK) in the cells using the adeno-viral expression kit (IB:HA). **Vec** were the cells infected with virus that carry the empty vector. (D) Expressions (IB:MEK5) and phosphorylation (IB:p-MEK5) of MEK5 in SW480 and SW620 cells (indicated) in which PKM2 was knocked down (PK) using the smart pool RNAi were analyzed by immunoblot using antibodies against MEK5 and phosphorylated MEK5. The cellular levels of PKM2 were analyzed by immunoblot of PKM2 (IB:PKM2). (E) (**Bottom panel**) RT-PCR analyses of cellular MEK5 mRNA levels in SW620 and WM266 cells (indicated) in which PKM2 was knocked down using a smart-pool RNAi (PK). NT represents the cells treated with non-target RNAi. The results are presented as fold changes in PCR products before and 48 hours after PKM2 knockdown in the same cells. The level of PCR products from each cell line that was treated with non-target RNAi was defined as 1. (**Upper panel**) Immunoblot analyses of cellular PKM2 in SW620 and WM266 cells (indicated) in which PKM2 was knocked down using a smart-pool RNAi (PK). (F) ChIP of the

MEK5 promoter (MEK5 promoter) using antibody against PKM2 in SW620 cells (α PK). ChIP using rabbit IgG was a negative control. ChIP using PCR primer pair targeting a region of exon 1 (MEK5 exon 1) of MEK5 gene (nt 342 – nt 542) is a negative control. ChIP targeting GAPDH promoter (GAPDH promoter) using antibody against PKM2 was another negative control. The primer pair positions are indicated. Inputs were PCR products from DNA extracts without ChIP. In **(C)**, **(D)**, and **(E)**, Immunoblot of β -actin (IB: β -actin), and immunoblot of Lamin A/C (IB:Lamin A/C) in **(A)** are loading controls. Error bars in **(B)** and **(E)** are standard deviations of three measurements.

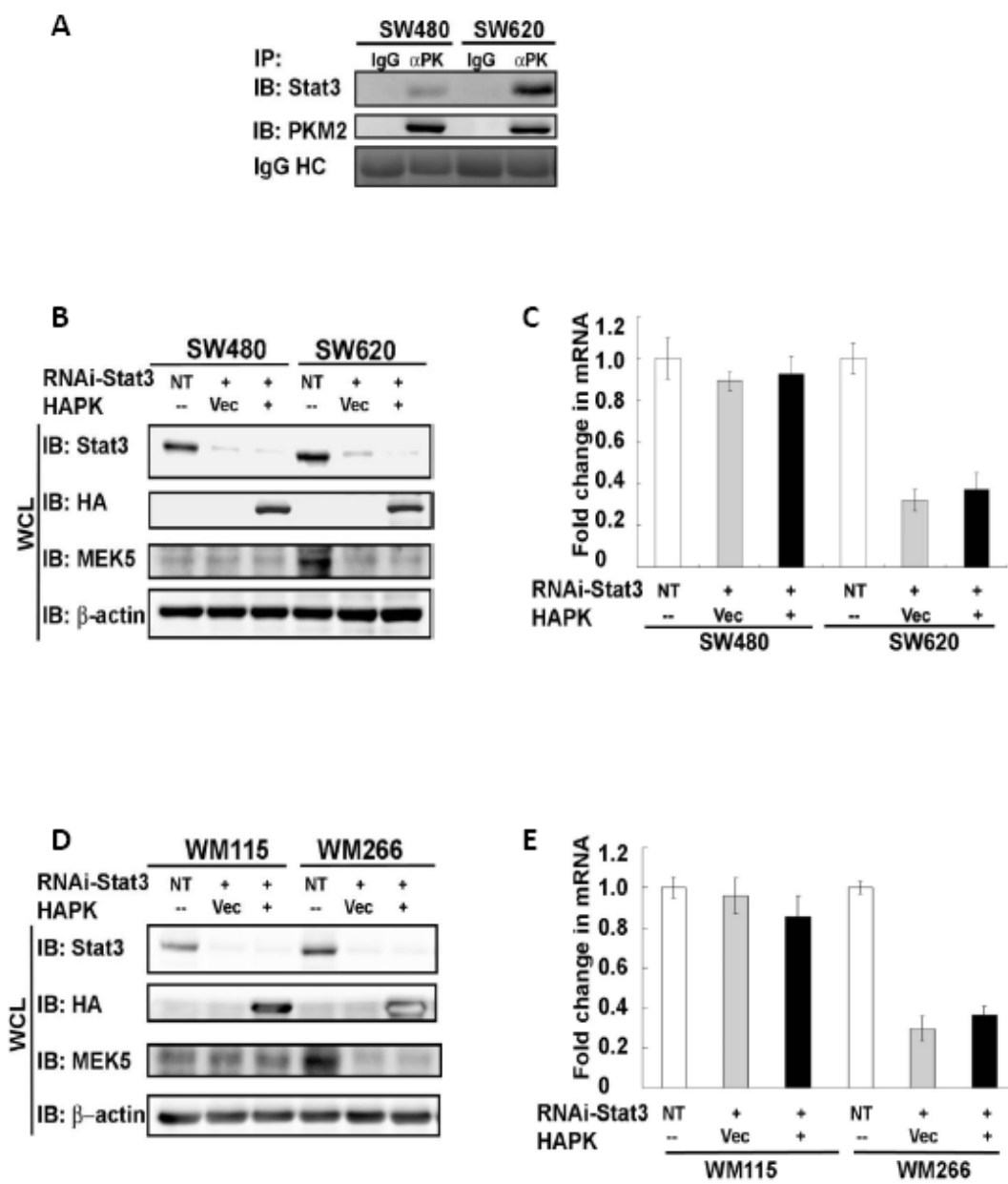


Figure 5.2 PKM2 upregulates MEK5 transcription via activation of Stat3

(A) Co-immunoprecipitation of PKM2 with stat3. PKM2 was immunoprecipitated from nuclear extracts prepared from SW620 and SW480 cells using the antibody PabPKM2 (IP: α PK). The immunoprecipitates were analyzed by immunoblot using antibodies against stat3 (IB:Stat3) or PKM2 (IB:PKM2). Ponceau S staining of IgG heavy chain (IgG HC) in the immunoprecipitates is the loading control. Immunoprecipitation using rabbit IgG (IP:IgG) was the control immunoprecipitation. (B) & (D) Expressions of MEK5 (IB:MEK5) in SW620/SW480 (B) and WM115/WM266 cells (D) (indicated) were analyzed by immunoblot the cell lysate (WCL) prepared from the cells in which stat3 was knocked down by RNAi (stat3, IB:Stat3). HA-PKM2 was exogenously expressed in the stat3 knockdown cells (IB:HA). The blot of β -actin (IB: β -actin) are the loading controls. (C) & (E) RT-PCR analyses of cellular MEK5 mRNA levels in SW620/SW480 (C) and WM266/WM115 cells (E) (indicated) in which stat3 was knocked down by RNAi (stat3, IB:Stat3). HA-PKM2 was exogenously expressed in the stat3 knockdown cells (IB:HA). The results are presented as fold changes in PCR products before and 48 hours after stat3 knockdown and HA-PKM2 expression in the same cells. The level of PCR products from each cell line that was treated with non-target RNAi was defined as 1. In (B), (C), (D), and (E), NT represents the cells treated with non-target RNAi. Vec were the cells infected with virus that carry the empty vector. Error bars in (C) and (E) are standard deviations of three measurements.

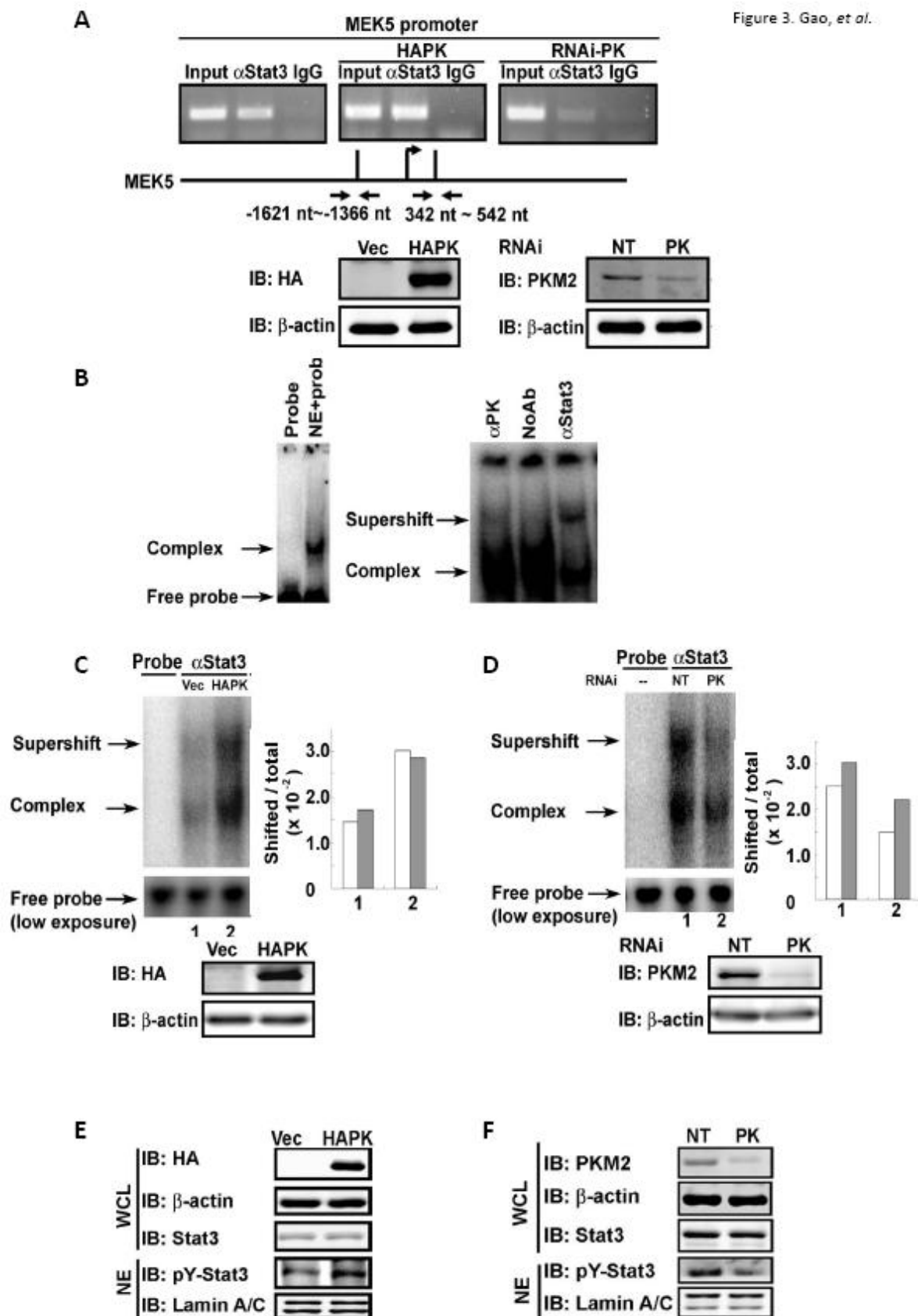


Figure 5.3 PKM2 upregulates MEK5 transcription by promoting Stat3 DNA interaction and phosphorylation of Stat3

(A) (Upper panels) ChIP of the MEK5 promoter (MEK5 promoter) using antibody against stat3 in SW620 cells (α Stat3). The cells were treated non-target RNAi (left, NT) or with RNAi target PKM2 (right, RNAi-PK), or HA-PKM2 was exogenously expressed in the cells (middle, HAPK). ChIP using rabbit IgG (IgG) was a negative control. Inputs were PCR products from DNA extracts without ChIP. The primer pair positions are indicated. **(Lower panels)** the cellular PKM2 (right) and HA-PKM2 (left) levels in SW620 cells that were treated with RNAi target PKM2 (PK) or with non-target RNAi (NT), or infected with virus that carry HA-PKM2 expression vector (HAPK) or vector alone (Vec). **(B)** DNA-protein complex (Complex) assembled on a 32 P-labeled oligonucleotide containing the stat3 targeting sequence in nuclear extracts prepared from SW620 cells (left panel) was detected by gel-shift and autoradiography. Probe indicates the free 32 P-labeled oligonucleotide probe without addition of nuclear extracts. The antibodies against PKM2 (α PK), stat3 (α Stat3), or no antibody (NoAb) was added to the complex to create supershift (Supershift) (right panel). **(C) & (D)** Supershift complex assembled with the 32 P-labeled oligonucleotide and antibodies (indicated) in the nuclear extracts prepared from SW620 cells in which **(D)** PKM2 was knocked down by RNAi (PK) or **(C)** HA-PKM2 was exogenously expressed (HAPK) was detected by gel-shift and autoradiography. Probe only is the free probe without addition of nuclear extracts. The free probe (low exposure) is the loading control with 1/10 of exposure time in autoradiography. The quantification of the assembled complex and super shift complex were presented as percentage (Shifted/total $\times 10^2$) of probe in the shift complex calculated by Intensities of complex [complex (grey bars) or supershift (open bars)] divided by Intensities of total [free probe + complex + supershift).

Immunoblots at bottom of each panel indicate cellular levels of HA-PKM2 (IB:HA) and endogenous PKM2 (IB:PKM2). **(E) & (F)** The levels of Y705 phosphorylated stat3 (IB:p-Tyr-Stat3) in the cell nucleus were analyzed by immunoblot of nuclear extracts (NE) prepared from SW620 cells in which HAPKM2 was expressed (**E. HAPK**) or endogenous PKM2 was knocked down using the smartpool RNAi (**F, PK**). The total cellular stat3 levels were analyzed by immunoblot analyses of stat3 (IB:Stat3) in whole cell lysate (WCL). In **(E)**, immunoblot of HA-tag (IB:HA) indicates the HA-PKM2 expression levels in the cells. In **(F)**, immunoblot of PKM2 (IB:PKM2) represents cellular PKM2 levels in the cells. Immunoblot of lamin A/C in **(E)** and **(F)**, and β -actin in **(A)**, **(C)**, **(D)**, **(E)**, and **(F)** are the loading controls. NTs in **(A)**, **(C)**, **(D)**, **(E)**, and **(F)** mean the cells were treated with non-target RNAi. Vec in **(A)**, **(C)**, **(D)**, **(E)**, and **(F)** means the cells were infected with virus that carry the empty vector.

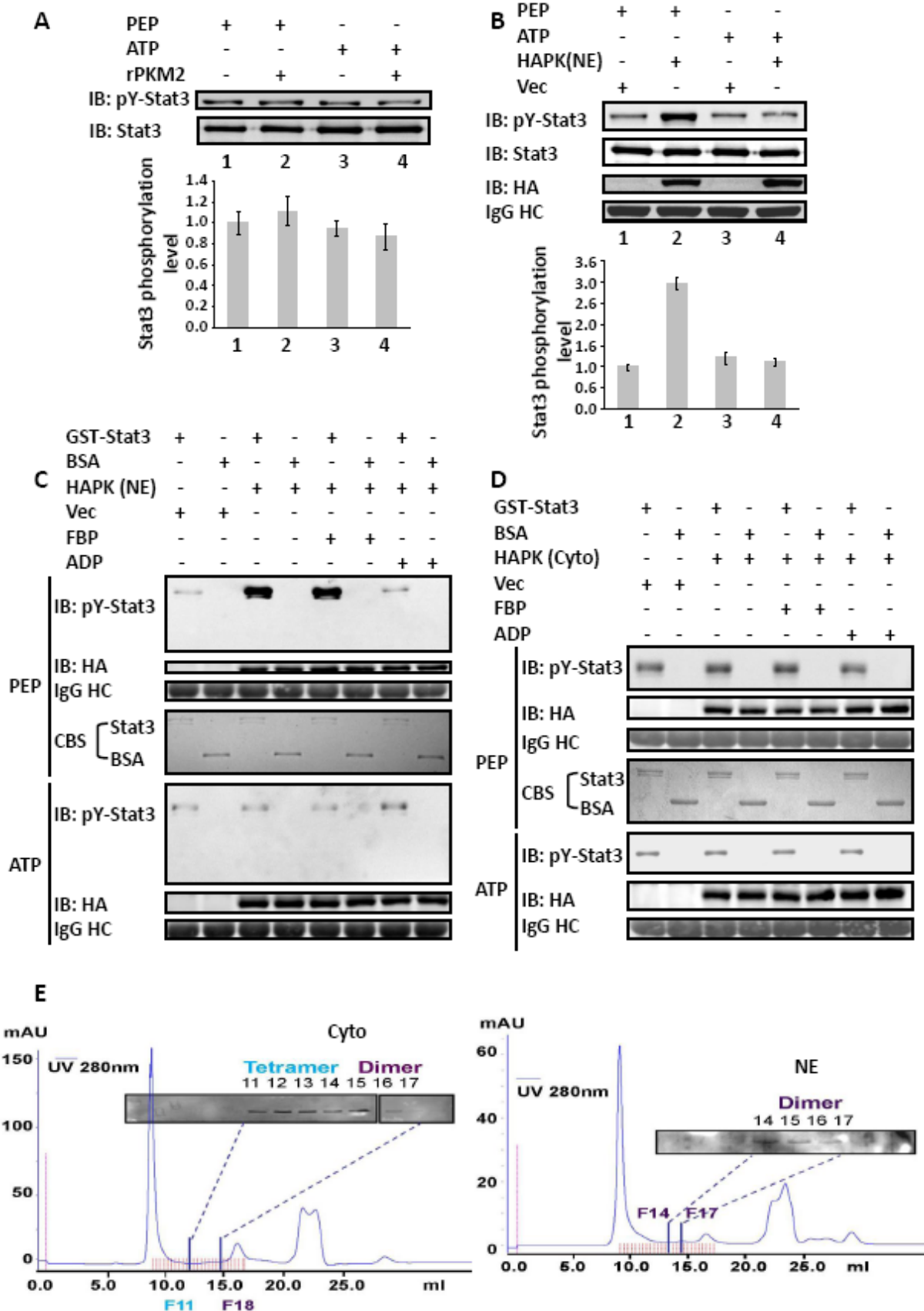


Figure 5.4 Phosphorylation of GST-Stat3 by the rPKM2

Phosphorylation of GST-stat3 by the rPKM2 (**A**) and HA-PKM2 immunopurified from nuclear extracts of SW620 cells (**B**) in the presence of 5 mM ATP (ATP) or 5 mM of PEP (PEP) was revealed by immunoblot assays using antibody against Y705 phosphorylated stat3 (IB:pY-stat3). Immunoblot analyses using antibody against stat3 (IB:Stat3) indicates the amounts of GST-stat3 used in each phosphorylation reaction. The bottom panels in (**A**) & (**B**) are the quantitative analyses of immunoblot signals. The error bars represent the standard deviations of four measurements. Phosphorylation of GST-stat3 by the HA-PKM2 (HA-PK) immunopurified from the nuclear (**C**) and the cytoplasmic (**D**) extracts of SW620 cells in the presence of 5 mM ATP (ATP) or 5 mM of PEP (PEP) was revealed by immunoblot assays using antibody against Y705 phosphorylated stat3 (IB:pY-stat3). The phosphorylation reactions were also carried out in the presence/absence of 5 mM of FBP (FBP), or 5 mM of ADP (ADP). The immunoblot of HA (IB:HA) indicates the amounts of HA-PKM2 used in each reaction. IgG HC is the ponceau S stain of antibody heavy chain, representing the amounts of antibody used in immunopurification of HA-PKM2 from the extracts. Coomassie blue staining (CBS) indicates the amounts of GSTstat3 and BSA used in each phosphorylation reaction. **Vec** were the cells infected with virus that carry an empty vector. (**E**) Size exclusion chromatography fractionation of nuclear (NE) and cytoplasmic (Cyto) extracts (100 μ l) from SW620 cells. The fractions were collected using a FPLC at 300 μ l per fraction. The collected fractions 6 to 17 from cytoplasmic extracts and fraction 9 to 18 from nuclear extracts were immunoblotted using the antibody PabPKM2. Fraction 11 (F11) co-eluted with 240 kDa and fraction 14 (F14) co-eluted with 120 kDa on the same column under identical conditions determined by size exclusion chromatography molecular weight calibration standard (see on-line supplementary Fig. S5 C&D).

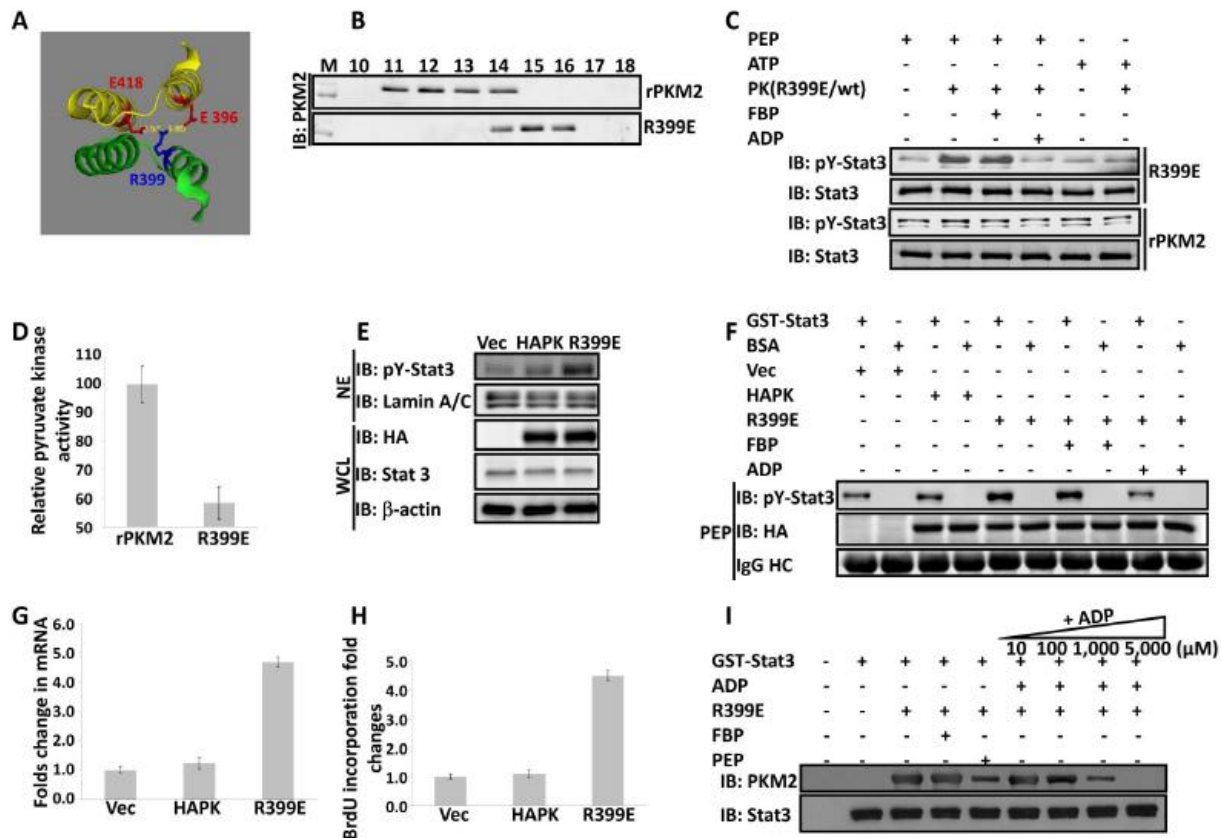


Figure 5.5 Dimeric PKM2 is active protein kinase and expression of the R399E mutant promotes cell proliferation

(A) Part of x-ray crystal structure of human PKM2. The structure was obtained from PDB bank DOI: 10.1021/bi0474923. The residue R399 and its interactive residues E418, D357, and E396 are high lighted in color. (B) Size exclusion chromatography fractionation of the wild-type rPKM2 and R399E mutant. The recombinant proteins 100 μ l in 1.5 μ M were loaded onto column. The chromatography fractions F10 – F18 were collected using a FPLC at 300 μ l perfraction. The collected fractions were analyzed by immunoblot using the antibody PabPKM2 (IB:PKM2). (C) Phosphorylation of GST-stat3 by the rPKM2 (10 μ g/ml) (rPKM2) and R399E mutant (10 μ g/ml) (R399E) in the presence of 5 mM ATP (ATP), 5 mM of PEP (PEP), 5 mM of FBP (FBP), and/or 5 mM ADP (ADP) was revealed by immunoblot assays using antibody against Y705 phosphorylated stat3 (IB:pY-stat3). Immunoblot analyses using antibody against stat3 (IB:Stat3) indicates the amounts of GST-stat3 used in each phosphorylation reaction. (D) Pyruvate kinase activity of the rPKM2 or R399E mutant (5 μ g/ml) was analyzed by the method described by Christofk and co-workers. The pyruvate kinase activity was expressed as relative pyruvate kinase activity by define the activity in the rPKM2 as 100. (E) Phosphorylation of stat3 in SW480 cells was examined by immunoblot analyses of the nuclear extracts (NE) using antibody against the Y705 phosphorylated stat3 (IB:pY-Stat3). PKM2 wild-type (HAPK) or the R399E (R399E) mutant was expressed in the cells by transient transfection. Immunoblots using anti-HA antibody (IB:HA) and anti-stat3 antibody (IB:Stat3) in the whole cell lysate (WCL) indicate the levels of stat3 and HA-PKM2/HA-R399E in the cells. Immunoblot of lamin A/C (IB:Lamin A/C) and β -actin (IB: β -actin) are loading controls. (F) Phosphorylation of GST-stat3 by the HA-p68 and the HA-R399E mutant that were immunopurified from cell lysate of SW480

cells in the presence of 5 mM of PEP was revealed by immunoblot analyses using antibody against the Y705 phosphorylated stat3 (IB:pY-Stat3). The phosphorylation reactions were also carried out in the presence/absence of 5 mM of FBP (FBP), or 5 mM of ADP (ADP). The immunoblot of HA (IB:HA) indicates the amounts of HA-PKM2 or HA-R399E used in each reaction. IgG HC is the ponceau S stain of antibody heavy chain, representing the amounts of antibody used in immunopurification of the HA-PKM2 or the HA-R399E mutant from the extracts. **(G)** Expression of MEK5 mRNA in SW480 cells was analyzed by RT-PCR. HA-PKM2(HAPK) or HA-R399E (R399E) was exogenously expressed in the cells. The results are presented as fold changes in PCR products before and 48 hours after HA-PKM2 or HA-R399E expression. **(H)** Cell proliferations of SW480 cells were measured using the cell proliferation kit. Cell proliferations were presented as fold changes in BrdU incorporation before and 48 hours after HA-PKM2 (HAPK) or HA-R399E (R399E) expression. The BrdU incorporation of the cells that were transfected with the empty vector (Vec) was defined as 1. **(I)** Interaction of GSTstat3 and R399E mutant in the presence of FBP (5 mM), PEP (5 mM), or various concentrations of ADP (10, 100, 1000 and 5000 μ M) was analyzed by GST-pull-down using the glutathione beads. The co-precipitation of R399E with GST-stat3 was detected by immunoblot using the antibody against PKM2 (IB:PKM2). Immunoblots of precipitates using antibody against stat3 (IB: Stat3) indicate the amounts of GST-stat3 that was pulled-down by the glutathione beads. Error bars in **(D)**, **(G)**, and **(H)** are standard deviations of three independent measurements. **Vec** in **(E)**, **(F)**, **(G)**, and **(H)** are the cells transfected with the empty vector.

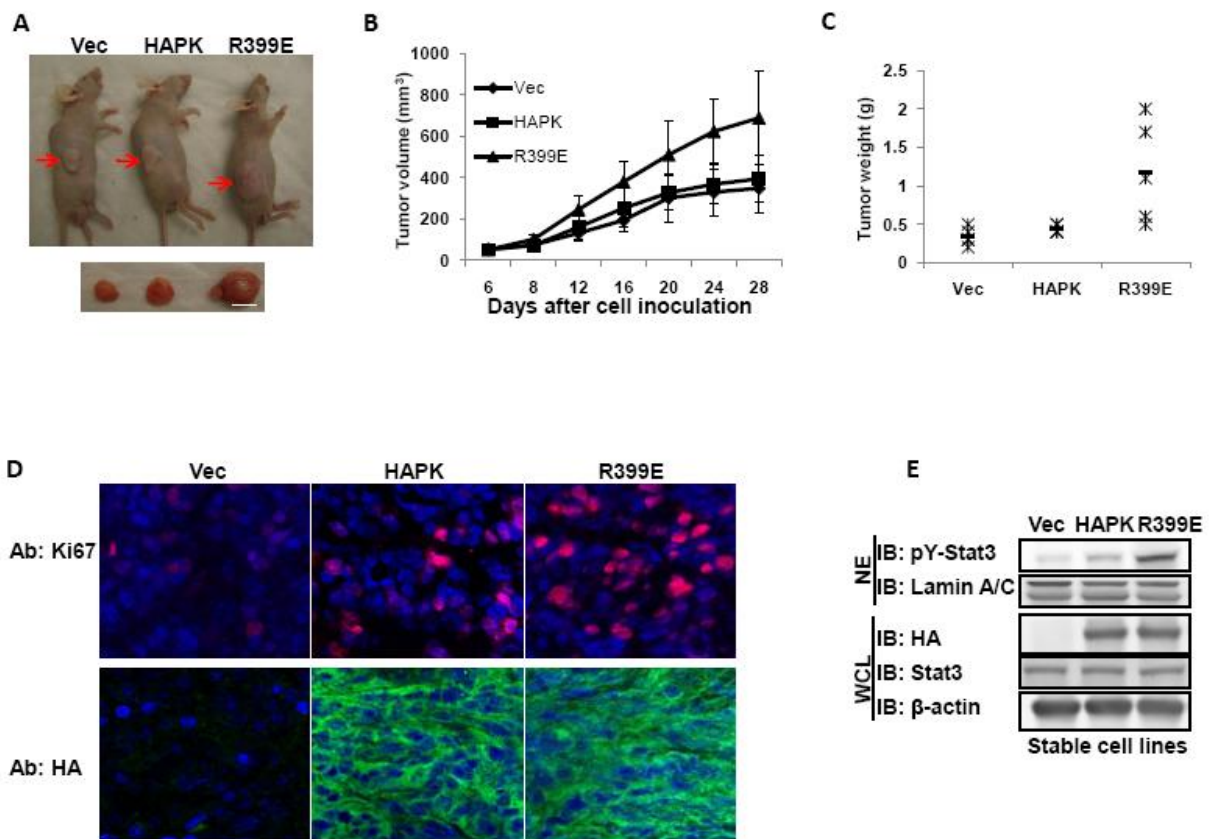


Figure 5.6 The effects of PKM2 protein kinase activity on tumor growth

PKM2 wild type (HAPK) or R399E mutant (R399E) was stably expressed in SW480 cells (IB:HA) and stat3 was phosphorylated in R399E mutant expressing cells (IB: pY - stat3) **(E)**. The derived cells were implanted to nude mice (six mice per group). The R399E tumors (R399E) grew substantially faster than that of PKM2 WT tumors (HAPK) in four weeks **(A)**. Tumor growth was monitored by measuring tumor volumes every four days and the tumor volumes were calculated by formula $\text{Tumor volume} = \pi/6 \times (\text{width})^2 \times \text{length}$ **(B)**. At end of four weeks growth, tumors were sliced out and weighted **(C)**. Tissue sections were prepared from the harvested tumors and immune fluorescence stained with antibodies against Ki67 (Ab: Ki67, Red) and HA (Ab:HA, Green). The blue is DAPI stain of cell nucleus **(D)**. In **(A)**, **(B)**, **(C)**, **(D)**, and **(E)**, the Vec means the vector alone was expressed in the cells. The error bars in **(B)** are standard deviations from the measurements of six mice.

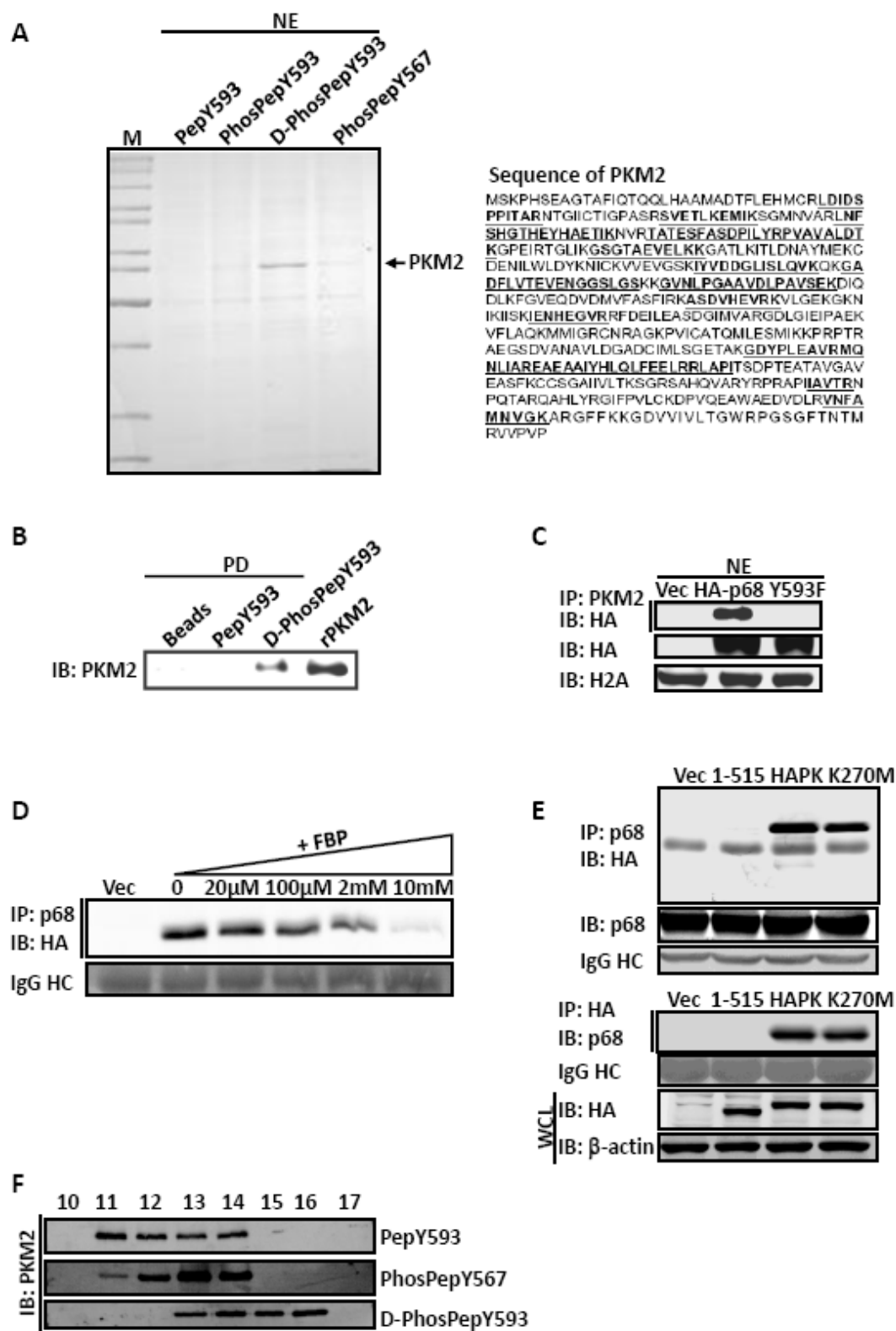


Figure 5.7 Tyrosine phosphorylated p68 interacts with PKM2

(A) (**Left panel**) GelCode staining SDS-PAGE analyses of proteins pulled down from nuclear extracts of T98G cells by different peptides coupled to agarose beads. The peptides used are: the PepY593, the PhosPepY593, the D-PhosPepY593, and the PhosPepY567. The arrow indicates the protein band that was cut out and subjected to trypsin digestion followed by MALDI-tof/tof analyses. M is molecular weight markers. (**Right panel**) The amino acid sequence of PKM2. The bold and underlined sequence indicates the peptide fragments identified by MALDI-tof/tof. (B) Interaction of the peptides, the PepY593 and D-PhosphPepY593 with recombinant PKM2 (rPKM2). The recombinant PKM2 pulled-downs (PD) by the peptides were examined by immunoblot using antibody against PKM2 (IB:PKM2). PD by rPKM2 is a control without peptide pull-down. Beads are the control pull-down using agarose beads alone. (C) Coimmunoprecipitations of exogenously expressed HA-p68s (WT and Y593F, Vec is vector alone) with endogenous PKM2 from nuclear extracts (NE) of T98G cells were examined by immunoblot with anti-HA (IP:PKM2, IB:HA). IBs of the nuclear extracts using anti-HA indicate the expression of HA-p68 (IB:HA). IBs of histone 2A (IB:H2A) are the loading controls. (D) Co-immunoprecipitation of p68 (IP:p68) with exogenously expressed HA-PKM2 in cellular extracts of T98G cells supplementary with various concentrations of FBP was examined by immunoblot using the anti-HA antibody (IB:HA). IgG HC is the ponceau S stain of antibody heavy chain, representing the amounts of antibody used in immunopurification of p68. (E) Coimmunoprecipitation of p68 with the exogenously expressed HA-PKM2 and mutants (indicated) in the cellular extracts prepared from T98G cells. In (**upper panel**), the antibody p68-RGG was used as immunoprecipitation antibody (IP:p68). Co-immunoprecipitations of HA-PKM2 and mutants with p68 were examined by immunoblot using antibody against PKM2. Immunoblot of p68 (IB:p68) indicated amounts of p68 that was immunoprecipitated down. In

(lower panel), the anti-HA antibody was used as immunoprecipitation antibody (IP:HA). Co-immunoprecipitations of p68 with HA-PKM2 and mutants were examined by immunoblot using antibody against p68 (IB:p68). IgG HC is the ponceau S stain of antibody heavy chain, representing the amounts of antibody used in immunoprecipitations. **(F)** Size exclusion chromatography fractionation of the wild-type rPKM2 in the presence of different peptides (3 μ M) D-phosPepY593 (upper panel), PepY593 (middle panel), and phosPepY567 (lower panel). The rPKM2 100 μ l in 15 μ M were loaded onto column. The chromatography fractions F10 – F18 were collected using a FPLC at 300 μ l per fraction. The collected fractions were immunoblotted using the antibody PabPKM2 (IB:PKM2).

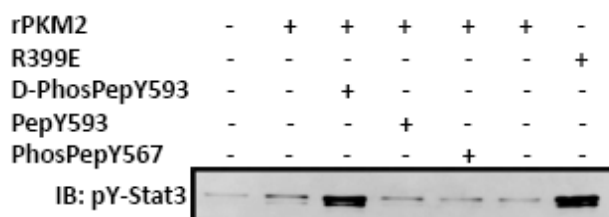
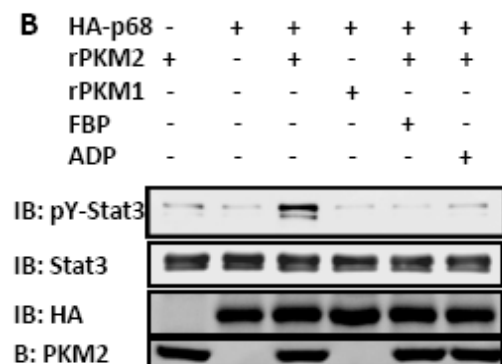
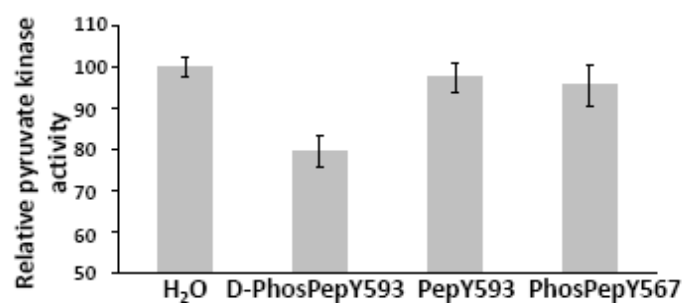
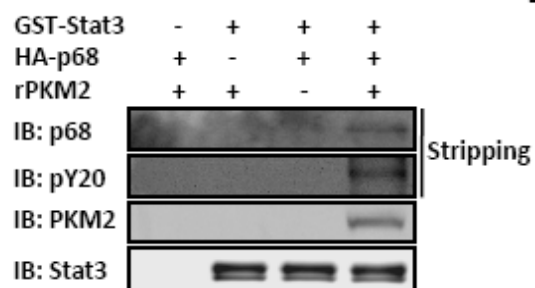
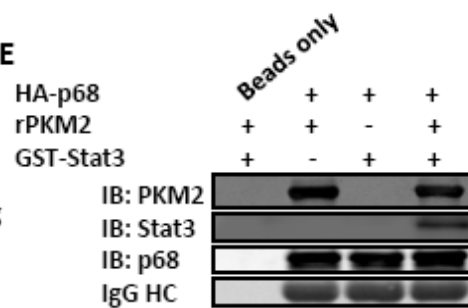
A**B****C****D****E**

Figure 5.8 Tyrosine phosphor-protein/peptide reciprocally regulates protein kinase and pyruvate kinase activity of PKM2

(A) Phosphorylation of GST-stat3 by the rPKM2 (10 $\mu\text{g/ml}$) and the R399E mutant (10 $\mu\text{g/ml}$) in the presence of different peptides (3 μM) D-phosPepY593, PepY593, and phosPepY567 was revealed by immunoblot assays using antibody against Y705 phosphorylated stat3 (IB: pY-stat3). (B) Phosphorylation of GST-stat3 by the rPKM2 (10 $\mu\text{g/ml}$) or the rPKM1 (10 $\mu\text{g/ml}$) in the presence of HA-p68 that was immunopurified from nuclear extracts of T98G cells and 5 mM of PEP was revealed by immunoblot assays using antibody against Y705 phosphorylated stat3 (IB:pY-stat3). In some phosphorylation reactions, 5 mM of FBP (FBP) or 5 mM ADP (ADP) was added to the reaction. Immunoblots of stat3 (IB:Stat3), HA-p68 (IB:HA), and PKM2 (IB:PKM2) indicate the amounts of GST-stat3, HA-p68, and the rPKM2 used in each phosphorylation reaction. (C) Pyruvate kinase activity of the rPKM2 (5 $\mu\text{g/ml}$) in the presence of different peptides (2 μM) D-phosPepY593, PepY593, phosPepY567, or buffer was analyzed by the method described by Christofk and co-workers. The pyruvate kinase activity of the rPKM2 was expressed as relative pyruvate kinase activity by define the activity in the presence of Buffer as 100. The error bars represent the standard deviations of four measurements. (E) Interaction of GST-stat3, the bacterially expressed rPKM2, and the HA-p68 immunopurified from T98G cells was analyzed by GST-pull-down using the glutathione beads. The GST-stat3 (2 $\mu\text{g/ml}$), the rPKM2 (2 $\mu\text{g/ml}$), and the HA-p68 were incubated in 500 μl at room temperature. The GSTstat3 was precipitated by the GST beads. Co-precipitations of the HA-p68 and the rPKM2 from the mixture were analyzed by immunoblot using antibodies against p68 (IB: p68) and PKM2 (IB:PKM2). The strip blot using anti-phosphor-tyrosine indicates the tyrosine phosphorylation of the precipitated HA-p68. Immunoblot of stat3 (IB: Stat3) indicates the amounts of GST-stat3 that

were precipitated by GST beads. (E) Co-immunoprecipitations of PKM2 and stat3 with HA-p68 in the cellular extracts of T98G cells. The exogenously expressed HA-p68 was immunoprecipitated using anti-HA antibody. The amounts of p68 precipitated from the extracts were examined by immunoblot using antibody against p68. The co-precipitation of PKM2 and stat3 were probed by immunoblot using antibodies against PKM2 (IB:PKM2) and against stat3 (IB:Stat3). IgG HC is the ponceau S stain of antibody heavy chain, representing the amounts of antibody used in immunoprecipitation of HA-p68 from the extracts.

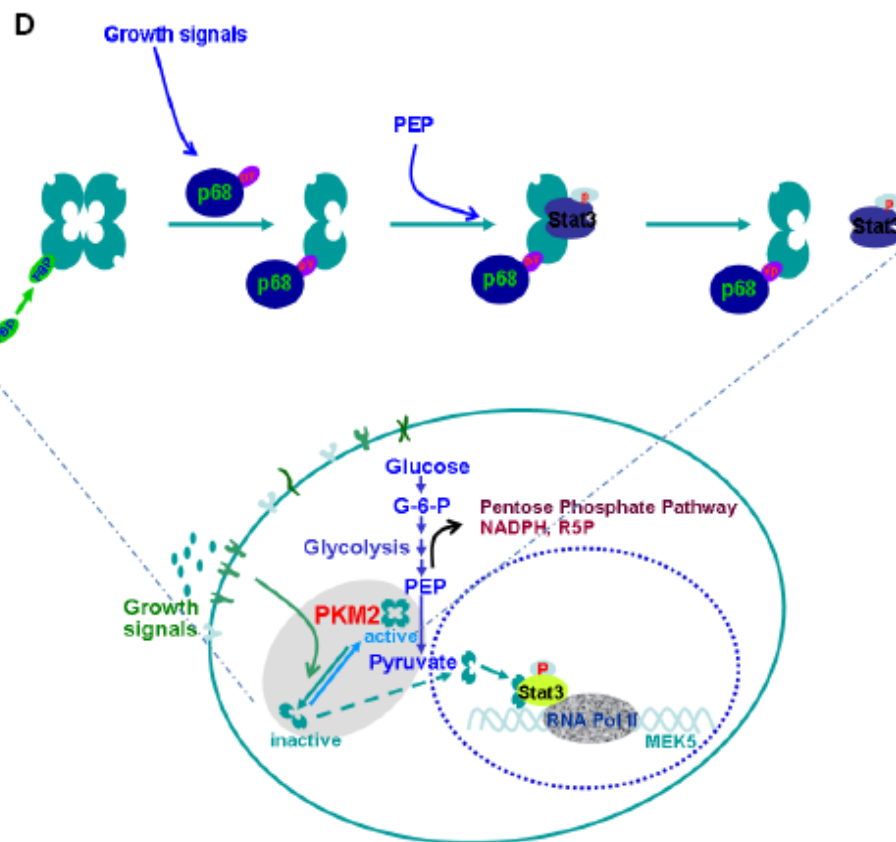
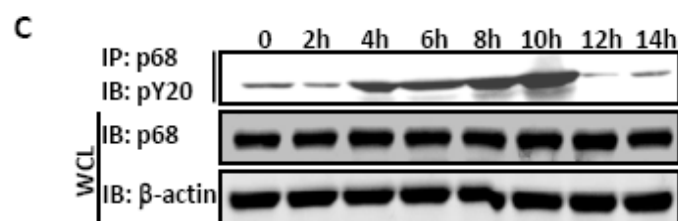
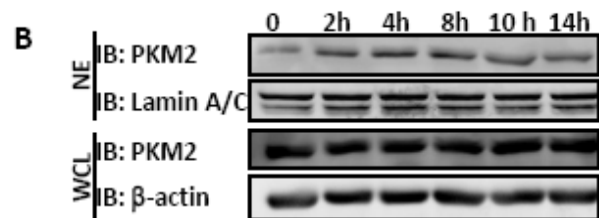
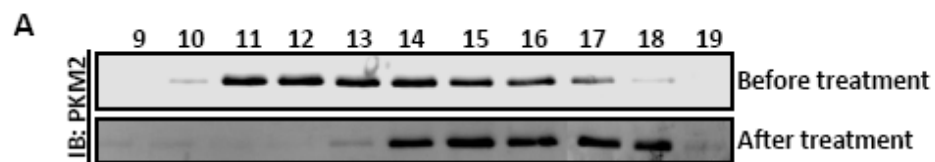


Figure 5.9 Growth stimulation activates protein kinase activity of PKM2

(A) Size exclusion chromatography fractionation of cell lysate prepared from SW480 cells that were treated/untreated by 25 ng/ml EGF for 8 hours. The cell lysate (100 μ l) were loaded onto the column. The chromatography fractions F9 – F20 were collected using a FPLC at 300 μ l per fraction. The collected fractions were immunoblotted using the antibody against PKM2 (IB: PKM2). (B) The PKM2 levels in the nuclear extracts (NE) of SW480 cells that were treated with EGF (25ng/ml) at different time points (indicated) were examined by immunoblot of the nuclear extracts using antibody against PKM2 (IB: PKM2). Immunoblot analyses of PKM2 (IB: PKM2) in the whole cell lysate (WCL) indicate the cellular levels of PKM2. Immunoblot of β -actin (IB: β -actin) and lamin A/C (IB:Lamin A/C) were the loading controls. (C) Tyrosine phosphorylation of p68 in the in the nuclear extracts (NE) of SW480 cells that were treated with EGF (25 ng/ml) at different time points (indicated) were examined by immunoblot analyses of p68 that was immunoprecipitated (IP:68) from the extracts using the anti-phosphor-tyrosine antibody (IB:pY20). Immunoblot analyses of p68 (IB:p68) in the whole cell lysate (WCL) indicate the cellular levels of PKM2. Immunoblot of β -actin (IB: β -actin) was the loading control. (D) A hypothetical model that illustrates the functional role of PKM2 in gene transcription and the regulation of protein kinase and pyruvate kinase activities of PKM2.

Figure 3

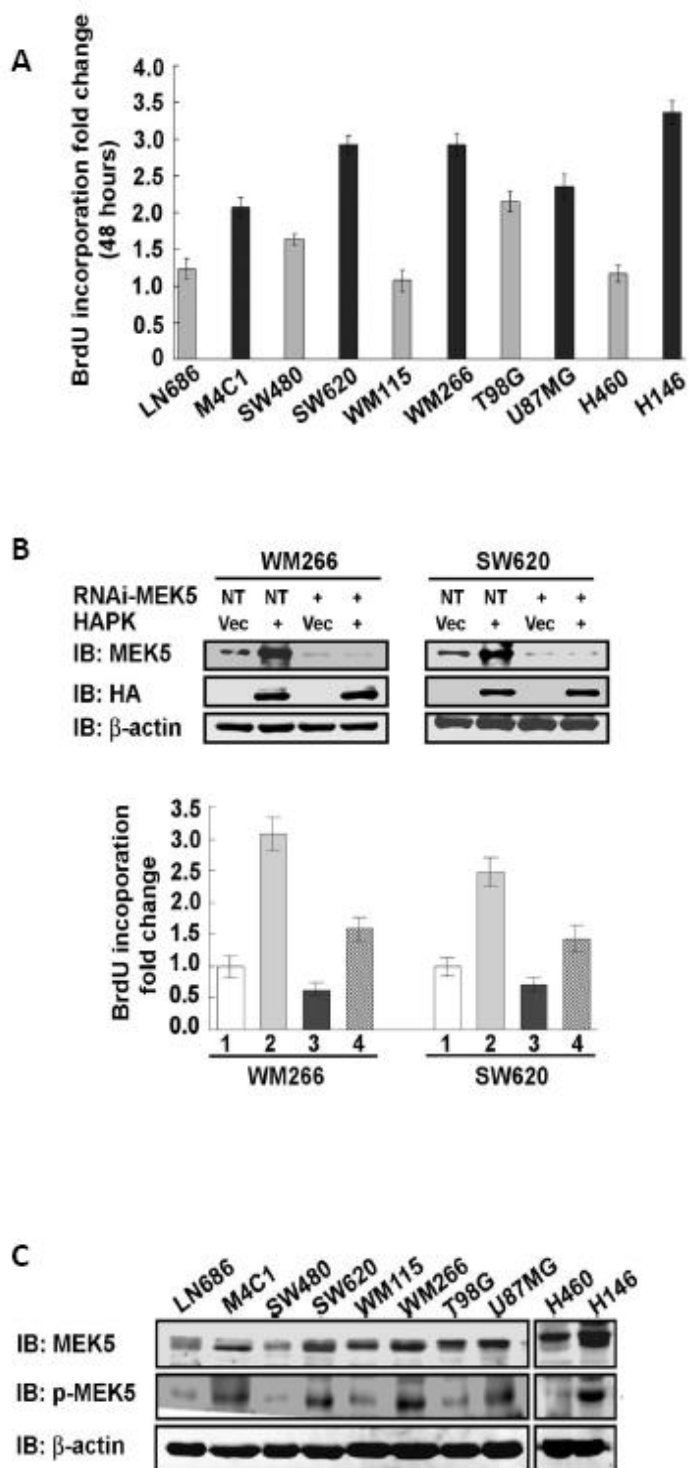


Figure Supplement 5.1

(A) Cell proliferations of ten cancer cell lines (indicated) were measured using a commercial cell proliferation kit. The proliferation rates are presented as fold changes of BrdU incorporation of the same cultured cells before and after 48 hours culturing by defining the initial BrdU incorporation as 1. (B) (**Upper panel**) Cellular levels of MEK5 and exogenously expressed HA-PKM2 in WM266 and SW620 cells were analyzed by immunoblot using antibodies against MEK5 (IB:MEK5) and HA (IB:HA). MEK5 in the cells was knocked down by RNAi (PK). PKM2 was exogenously expressed in the cells using the adeno-viral expression kit. (**Bottom Panel**) Cell proliferations of WM266 and SW620 cells were measured using the cell proliferation kit. Proliferations of WM266 (1 – 4) or SW620 (5 – 8) cells were measured under following conditions: 1) and 5) Open bars, HA-PKM2 expression and no MEK5 knockdown; 2) and 6) Gray bars, HA-PKM2 was expressed and no MEK5 knockdown; 3) and 7) Black bars, no PKM2 expression and MEK5 knockdown; and 4) and 8) Striped bars, PKM2 expression and MEK5 knockdown. The proliferations are presented as fold changes of BrdU incorporation before and after indicated treatments. NT represents the cells treated with nontarget RNAi. **Vec** were the cells infected with virus that carry the empty vector. (C) Cellular MEK5 levels and phosphorylation of the protein in ten different cell lines (indicated at top) were examined by immunoblot of whole cell lysate using antibodies against MEK5 and phosphorylated MEK5. Immunoblots of β -actin (IB: β -actin) in (B) and (C) are loading controls. Error bars in (A) and (B) are standard deviations of three measurements.

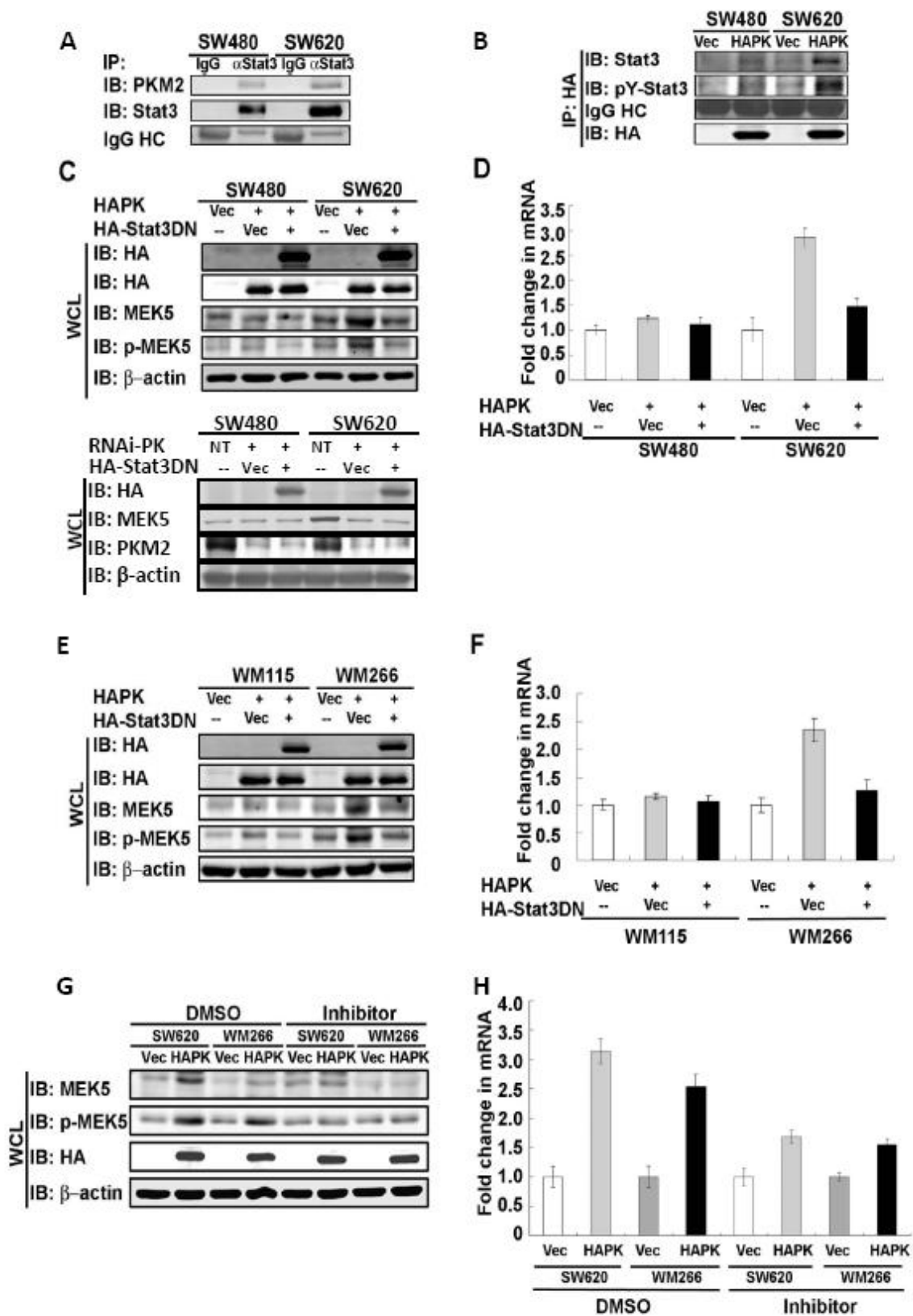


Figure Supplement 5.2

(A) & (B) Co-immunoprecipitations of endogenous PKM2 **(A)** and exogenous HA-PKM2 **(B)** with stat3 were analyzed by immunoprecipitation using antibody against stat3 (IP: α -stat3 in **A**) and anti-HA antibody (IP:HA in **B**) from nuclear extracts prepared from SW620 and SW480 cells. The immunoprecipitates were analyzed by immunoblot using antibodies against stat3 (IB:Stat3) or PKM2 (IB:PKM2). Ponceau S staining of IgG heavy chain (IgG HC) in the immunoprecipitates is the loading control. Immunoprecipitation using rabbit IgG (IP:IgG) was the control immunoprecipitation. In **(B)**, the immunoblot using anti-HA antibody was an additional loading control. **(C) & (E)**, Expressions of MEK5 (IB:MEK5) in SW620/SW480 **(C)** and WM115/WM266 **(E)** cells were analyzed by immunoblot the whole cell lysate (WCL) prepared from the cells in which a stat3 dominant negative mutant (stat3-DN) and HA-PKM2 (HAPK) were expressed (**C, Upper**) or PKM2 was knocked down (RNAi-PK) (**C, Bottom**). Immunoblot of HA-Stat3DN (IB:HA-stat3DN) and HA-PKM2 (IB:HAPK) indicated the exogenous expression levels. Immunoblot of PKM2 indicated the cellular levels of PKM2. The cellular levels of phosphorylated MEK5 were also examined by immunoblot using the antibody against phosphorylated MEK5 (IB:p-MEK5). **(D) & (F)** RT-PCR analyses of cellular MEK5 mRNA levels in SW620/SW480 **(D)** and WM266/WM115 **(F)** cells in which a stat3 dominant negative mutant (DNST) and HA-PKM2 (HAPK) were expressed. The results are presented as fold changes in PCR products before and 48 hours after the dominant negative stat3 mutant and HA-PKM2 expression in the same cells. The level of PCR products from each cell line that was infected with virus that carry the empty vector (Vec) and no stat3 mutant expression was defined as 1. **(G)** Expressions of MEK5 (IB:MEK5) in SW620/WM266 cells (indicated) were analyzed by immunoblot the whole cell lysate (WCL) prepared from the cells in which HAPKM2 was exogenously expressed (HAPK) and that were treated with the stat3 inhibitor (Inhibitor). Cells

treated with DMSO (the same amounts as used in inhibitor treatments as solvent for dissolve the inhibitor) are the control treatments. **(H)** RT-PCR analyses of cellular MEK5 mRNA levels in SW620/WM266 cells. The results are presented as fold changes in PCR products before and 48 hours after the dominant negative stat3 mutant and HA-PKM2 expression in the same cells. The level of PCR products from each cell line that was infected with virus that carry the empty vector (Vec) and no stat3 mutant expression was defined as 1. In **(C)**, **(E)**, and **(G)**, immunoblot of β -actin (IB: β -actin) is the loading control. Error bars in **(D)**, **(F)**, and **(H)** are standard deviations of three measurements.

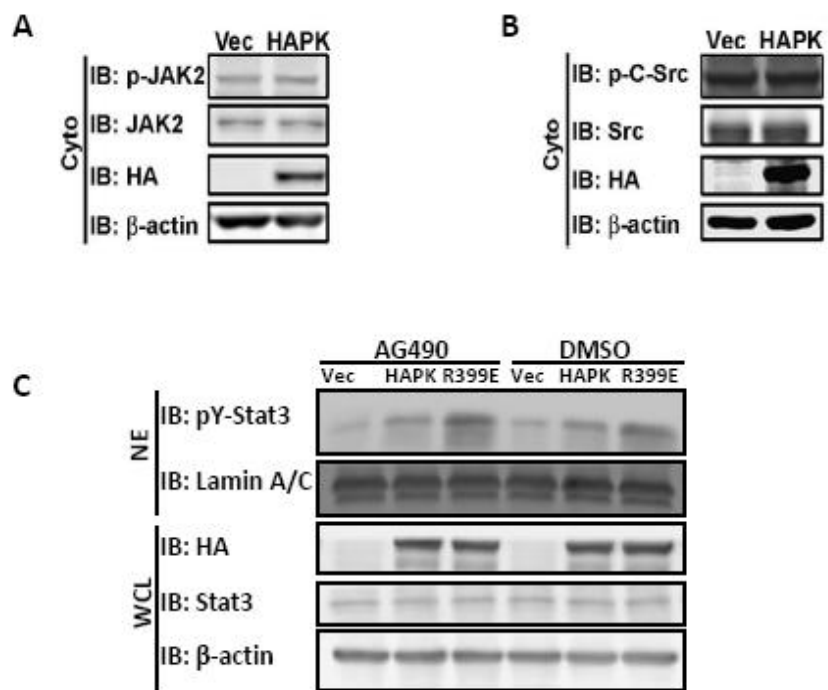


Figure Supplement 5.3

(A) & (B) Activation JAK2 **(A)** or c-Src **(B)** in SW620 cells in which HA-PKM2 was expressed (**HAPK**) was analyzed by immunoblot of cytoplasmic extracts (Cyto) using antibody against phosphorylated JAK2 **(A, IB:p-JAK2)** or antibody against phosphorylated c-Src **(B, IB:p-c-Src)**. Vec means the cells were infected by virus carry the empty vector. Immunoblots of JAK2 **(IB;JAK2)** in **(A)** and c-Src **(IB:Src)** in **(B)** are loading control. Immunoblot of β -actin is another loading control. The expression levels of HA-PKM2 were examined by immunoblot of HA-tag.

(C) Phosphorylation of stat3 was examined by immunoblot analyses of nuclear extracts (NE) prepared from SW620 cells that were treated by JAK2 (AG490) inhibitor or solvent DMSO (DMSO) using the antibody against Y705 phosphorylated stat3 **(IB:pY - stat3)**. Wild type (**HAPK**) or R399E mutant (**R399E**) was expressed in the cells. Vec represent the cells were transfected with empty vector. Immunoblot of lamina **(IB:Lamin A/C)** in nuclear extracts and immunoblot of stat3 **(IB:stat3)** and β - actin **(IB: β - actin)** in the whole cell lysate (WCL) are the loading controls. Immunoblot of HA indicates the exogenously expressed HAPK or R399E.

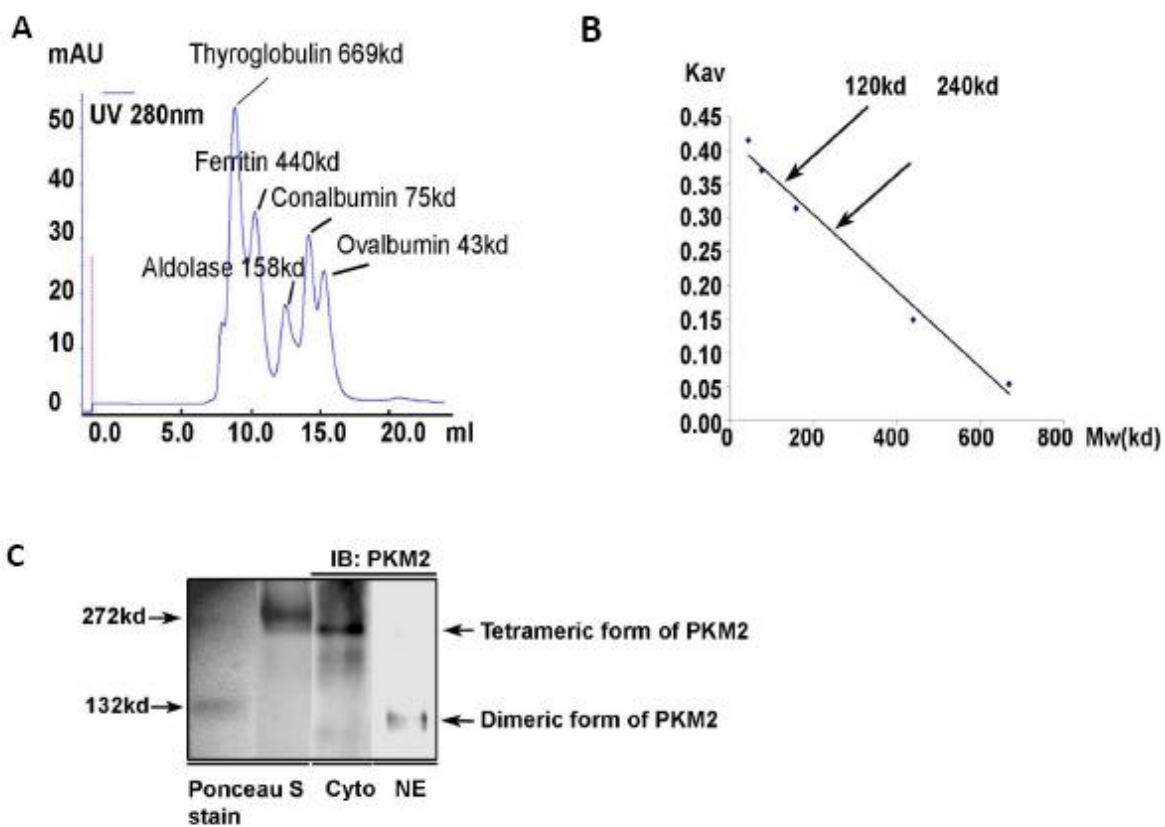


Figure Supplement 5.4

(A) Chromatographic elution profile of the molecular weight calibration kit proteins (indicated) on the Superdex 200 10/300GL column. The x-axis is the elution volume. The y-axis is the absorbance of the elution at 280 nm. (B) The standard curve of elution of the molecular weight calibration kit proteins on the Superdex 200 10/300GL column. The elution volumes were plotted against LogMW. (C) Immunoblot analyses of PKM2 in the cytoplasmic (Cyto) and nuclear (NE) extracts of SW620 cells. The extracts (6 μ l) were treated and loaded on an 8% non-denaturing gel electrophoresis. The gel was subjected to immunoblot using the antibody PabPKM2 (IB:PKM2). The molecular weight markers, BSA (dimer) and Urease (trimer), were loaded on the same gel and were visualized by ponceau S staining (ponceau S stain).

Figure Supplement 5.5

(A) Phosphorylation of GST-stat3 by the rPKM2 (10 μ g/ml), the rPKM1 (10 μ g/ml), or the R399E mutant (10 μ g/ml) in the presence of 32 P-PEP (~0.002 μ Ci) and unlabeled PEP (5 mM). The reaction mixture were separated by 10 SDS-PAGE and subjected to autoradiograph. (B) Phosphorylation of GST-stat3 by a recombinant JAK2 (JAK2, 10 μ g/ml) in the presence of 3 mM ATP or the bacterially expressed R399E mutant (R399E, 10 μ g/ml) in the presence of 5 mM PEP (PEP) was revealed by immunoblot assays using antibody against Y705 phosphorylated stat3 (IB:pY-stat3). Phosphorylation of recombinant stat5 (C) and BSA (D) by the recombinant R399E were analyzed by immunoblot using antibody against phosphorylated stat5 (IB:pY - stat5 in (C)) and antibody against phosphor - tyrosine antibodies (IB: pY10 and IB:pY100). Ponceau stain of stat5 (stat5) and BSA (BSA) indicate the amounts recombinant stat5 and BSA used in the phosphorylation reactions. (E) Phosphorylation of GST-stat3 by the bacterially expressed R399E mutant (R399E, 10 μ g/ml) in the presence of different concentrations of PEP (indicated) was revealed by immunoblot assays using antibody against Y705 phosphorylated stat3 (IB:pY-stat3). (F) Size exclusion chromatography fractionation of the wild-type HA-PKM2 (HAPK) or HA-R399E (R399E) that were immunopurified from SW480 cell lysate. The HA-PKM2 or HA-R399E (100 μ l in 0.4 μ g/ μ l) was loaded onto the column. The chromatography fractions F9 – F18 were collected using a FPLC at 300 μ l per fraction. The collected fractions were immunoblotted using the anti-HA antibody (IB:HA). Immunoblot analyses using antibody against stat3 (IB:Stat3) in (B) and (E) indicates the amounts of GST-stat3 used in each phosphorylation reaction.

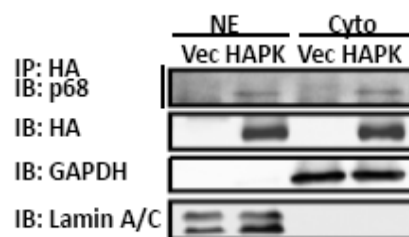
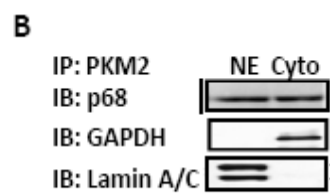
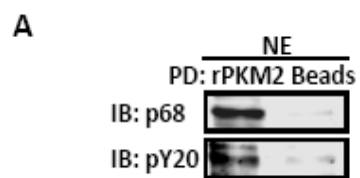
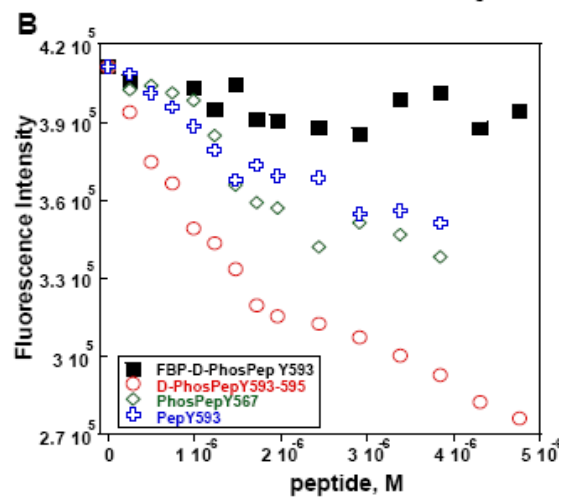
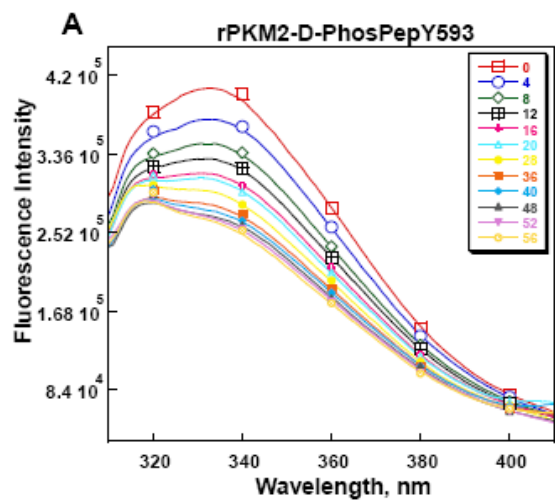


Figure Supplement 5.6

(A) Pull-down (PD) of p68 from nuclear extracts (NE) of T98G cells by recombinant PKM2 (rPKM2) was examined by immunoblot using antibody p68-RGG (IB:p68-RGG). The tyrosine phosphorylation of p68 was indicated by strip-blot of the pulldown using antibody against phospho-tyrosine (IB:PY20). Beads is the control pull-down using agarose beads alone. **(B) (Up panel)** Co-immunoprecipitations of p68 with endogenous PKM2 from nuclear (NE) and cytoplasmic (Cyto) extracts of T98G cells were examined by immunoblot with antibody p68-RGG (IP:PKM2, IB:p68-RGG). **(Lower panel)** Co-immunoprecipitations of p68 with exogenously expressed HA-PKM2 from nuclear (NE) and cytoplasmic (Cyto) extracts of T98G cells were examined by immunoblot with antibody p68-RGG (IP:HA, IB:p68-RGG). IBs of HA-PKM2 indicate the immunoprecipitated HA-PKM2 from the extracts. IBs of GAPDH (IB:GAPDH) and lamin A/C (IB:Lamin A/C) are the loading controls.



C

	rPKM2-D-PhosPep Y593	rPKM2-PepY593	rPKM2-PhosPepY567	rPKM2-FBP-D-PhospepY593
K_d (μM)	34.6	$\cong 328$	$\cong 163$	ND

D

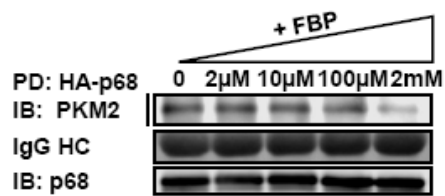


Figure Supplement 5.7

(A) Trp fluorescence emission spectrum of the rPKM2 (4 μ M) with the titration of various different concentrations (indicated) of peptide D-PhosPepY593. Binding of the peptide to the rPKM2 was indicated by the decrease in fluorescence intensity at 334 nm. (B) Trp fluorescence emission intensity of the rPKM2 at 334 nm in the presence of various peptides (2 μ M) D-PhosPepY593 (red circles), PepY593 (blue crosses), PhosPepY567 (green diamonds), and D-PhosPepY593 + 2 mM FBP (black squares). Y-axis is the fluorescence intensity at 334 nm. X-axis is peptide concentrations. (C) The dissociation constant (K_d) of the rPKM2 with the peptides D-PhosPepY593, PepY593, and PhosPepY567 were determined by the data fitting to langmuir equation (assume 1:1 binding). The K_ds were determined based on data fitting on three independent measurements. (D) Pull-down of the rPKM2 by the HA-p68 immunopurified from T98G cellular extracts (PD:HA-p68) was analyzed by immunoblot using antibody against PKM2 (IB:PKM2). The Pull-down experiments were performed in the presence of various concentrations of FBP (indicated in figure). IgG HC is the ponceau S stain of antibody heavy chain, representing the amounts of antibody used in immunopurification of HA-p68. IB:p68 indicate amounts of HA-p68 used in the pull-down.

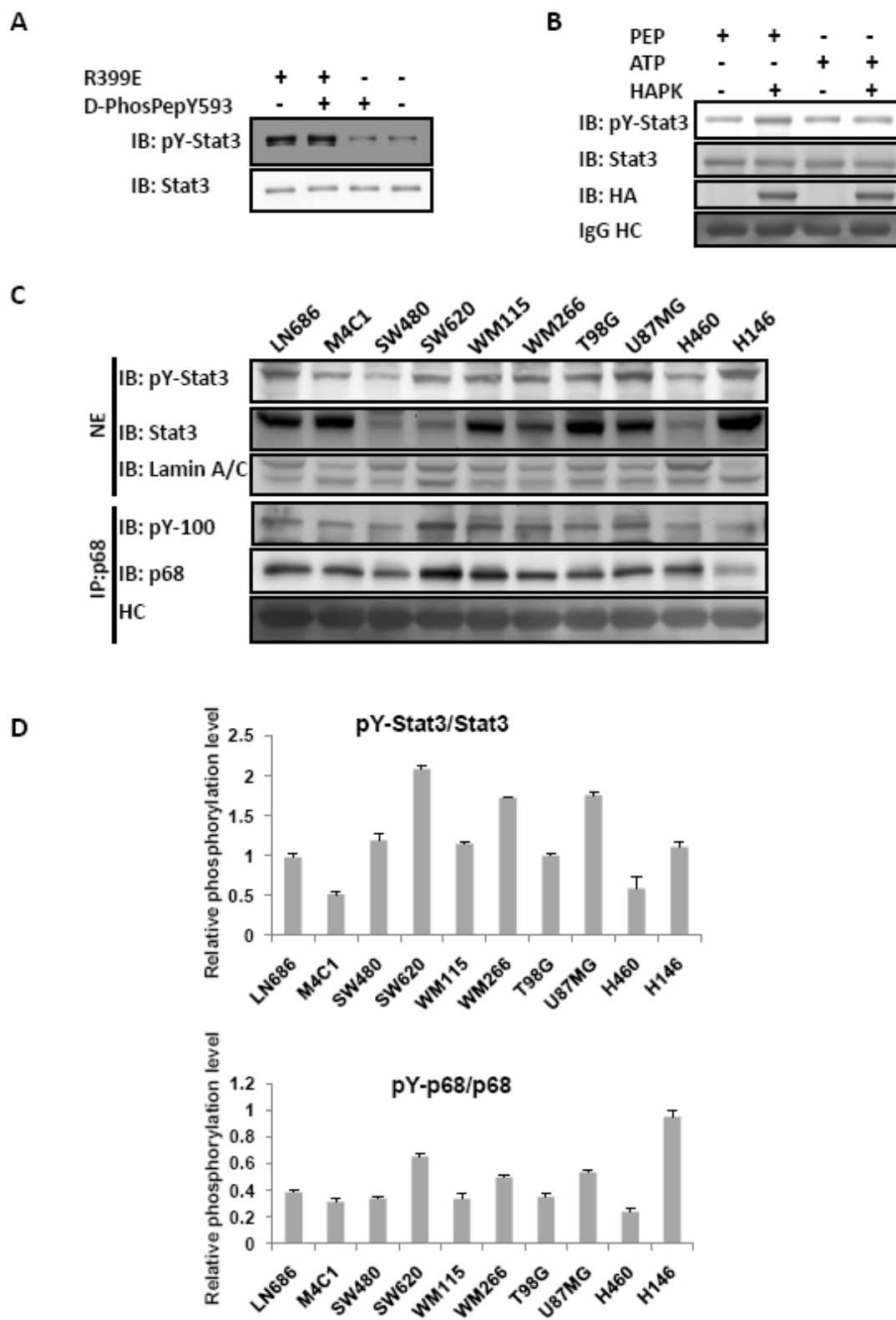


Figure Supplement 5.8

(A) Phosphorylation of GST - stat3 by the rPKM2 (10 μ g/ml) and the R399E mutant (10 μ g/ml) in the presence of different peptides (3 μ M) D - phosPepY593, PepY593, and phosPepY567 was revealed by immunoblot assays using antibody against Y705 phosphorylated stat3 (IB:pY - stat3). (B) Phosphorylation of stat3 by immunopurified HA - PKM2 from nuclear extracts (HAPK) of SW620 cells in the presence of ATP or PEP was analyzed by immunoblot using the antibody against the Y705 phosphorylated stat3 (IB:pY - stat3). P68 was knocked down by duplex RNAi. Immunoblot of stat3 (IB:stat3) shows the amounts of stat3 that were immunoprecipitated from the nuclear extracts. Immunoblot of HA (IB:HA) indicate the expression levels of HA - PKM2. Ponceau S stain of IgG heave chain (IgG:HC) indicate the amounts of antibody used in each PKM2 purification from nuclear extracts. (C) (Upper panels) Phosphorylation of nuclear stat3 was analyzed by immunoblot using antibody against Y705 phosphorylated stat3 (IB:pY - stat3) in the nuclear extracts prepared from different cells. immunoblot of stat3 (IB:stat3) indicate the stat3 levels in the nuclear extracts. Immunoblot of lamin (IB:Lamin A/C) is a loading control. (Bottom panels) Phosphorylation of p68 in nuclear extracts was analyzed by immunoblot of the immunoprecipitated p68 (IP:p68) using the antibody pY10 (IB:pY10). Immunoblot of p68 (IB:p68) indicate the amounts of p68 that was immunoprecipitated from nuclear extracts (IB:p68). Pansaus stain of IgG heave chain (HC) indicate the amount of antibody used in each immunoprecipitation reaction. (D) Quantization of phosphorylation levels of stat3 (Upper panel) and the immunoprecipitated p68 (Bottom panel) in nuclear extracts of different cells. The phosphorylation levels of stat3 and immunoprecipitated p68 were presented as relative phosphorylation levels (pY - stat3/stat3) and (pYp68/p68) respectively. The error bars in are standard deviations from four independent experiments.

CHAPTER 6

CONCLUSION AND DISCUSSION

6.1 Shuttling and translocation of p68 in cell migration

6.1.1 P68 is a nucleocytoplasmic shuttling protein and calmodulin binding regulated the nuclear exportation of p68 in migrating cells

P68 RNA helicase (p68) is a well known DEAD box family of RNA helicase protein. P68 is found to be dominantly located in the nucleus. However, studies indicate the existence of p68 in the cytoplasm. In this study, we found that p68 is a nucleocytoplasmic shuttling protein (Wang, Gao et al. 2009). Two functional nuclear localization signals (NLSs) and two functional nuclear export signals (NESs) were demonstrated to mediate the nucleocytoplasmic shuttling activity of p68. We found that the shuttling of p68 was mediated by a typical RanGTPase dependent pathway. However, the detail regulation mechanism behind the shuttling of p68 is not fully understood. P68 is dominantly located inside the nucleus in most of the cancer cells. We reasoned that the nuclear localization of p68 may be due to its functional NLSs that target p68 into the nucleus after the protein has been translated. The nuclear localized p68 might be arrested by forming complex with some nuclear proteins or trapping in a particular nuclear structure, which leads to the residence of p68 in the nucleus. However, how p68 is exported to the cytoplasm and what is the function of p68 in the cytoplasm becomes an important question as more and more studies detected the existence of cytosol p68. In the initial experiment, calmodulin was fused to the C-terminal of p68 to artificially form the interaction between p68 and calmodulin. Interestingly, high levels of the fusion protein localized into the cytoplasm when the cells expressed this fusion protein. Most importantly, the cells easily gained the migration status. We further found that the interaction between p68 and calmodulin was increased in

migrating cells. Meanwhile, there was transient increase in the levels of p68 and calmodulin in the cytoplasm in migrating cells than in the resting cells. We reasoned that binding of calmodulin to the IQ motif of p68 might promote the export of p68 to the cytoplasm, as the mutation at the IQ motif of p68 abolished the binding with calmodulin and the mutant no longer localized in the cytoplasm under the migration stimuli.

6.1.2 Working model for the cytosol translocation of p68 through binding with Ca^{2+} -calmodulin

P68 is predominantly located in the nucleus even though p68 is a nucleocytoplasmic shuttling protein. Many proteins localize at specific regions because of their interaction with a specific cellular structure or proteins. We reasoned that p68 retained in the nucleus may be due to the interaction of p68 with RNA (or RNA complex) in the nucleus, as p68 co-immunoprecipitates with RNAs at physiological salt concentration (Iggo and Lane 1989). Several evidences showed that C-terminal of p68 may be involved in the binding of p68 to RNA. C-terminal of p68 is found to bind with ssRNA *in vitro*. Meanwhile, phosphorylation of C-terminal of p68 can abolish the interaction between p68 and RNA (Yang, Yang et al. 2004). Under the stimulation of PDGF, more p68 is phosphorylated at Y593 in the cells. The phosphorylated p68 may be released from the RNA complexes and exported to the cytosol. The cytosolic translocated phosphorylated p68 subsequently carry beta-catenin back to the nucleus in order to regulate the EMT related gene expression. IQ motif exists in the C-terminal of p68. Interestingly, IQ motif of p68 is also believed to be involving in RNA binding. The IQ motif also harbors the site of PKC (serine/threonine kinase) phosphorylation of p68 (Buelte, Glidden et al. 1994). It is known that p68 alone has no ATPase activity. The RNA dependent ATPase activity of p68 requires the interaction with RNA. Interestingly, RNA dependent ATPase activity of p68

is decreased when p68 is phosphorylated by PKC at the IQ motif. This might be due to that the serine/threonine phosphorylated p68 at the IQ motif has lower affinity (or no) for RNA than the non-phosphorylated p68. Meanwhile, the phosphorylation rate of p68 by PKC can be dramatically increased when p68 is pretreated with RNase. The removal of bound RNA may expose the IQ motif, which leads to the increase of the phosphorylation by PKC. All these evidences strongly support the idea that the IQ motif is the key site in regulating the binding of p68 to RNA (or RNA complex), which may determine the localization of p68 in the cell.

Interestingly, we found that more p68 exists in the cytosol of migrating cells than in the resting cells. Correspondingly, there is more cytosolic p68 in the highly metastatic colon cancer cells than in low metastatic cancer cells. P72 is a homologous protein of p68. P72 has a high similar sequence at the helicase core domain (91.8%) with p68 and has a low similar sequence (54.5%) at the C-terminal, specifically lacking of IQ motif. Interestingly, p72 is found to be dominantly located in the nucleus in both metastatic and non-metastatic cancer cells. The nuclear location of p72 seems not due to the absence of NESs in p72, as p72 carries similar functional NESs (sequence alignment and analysis). This further supports the idea that nuclear export of p68 in migrating cells might be regulated at the IQ motif of p68.

We reasoned that p68 may interact with RNA complexes and retained inside the nucleus when there is neither calmodulin binding nor phosphorylation at the IQ motif. P68 may be released from the RNA complexes when calmodulin binds to p68. This leads to the export of p68/calmodulin to the cytoplasm. Overall, Ca^{2+} -calmodulin dissociates the p68/RNA complex is very possible, as the addition of Ca^{2+} -calmodulin to the mixture of ATPase assay can abolish the RNA-dependent ATPase activity of p68 (Buel, Glidden et al. 1994). PKC is activated in migrating cells. The dissociation of p68 from RNA complex could be maintained if PKC

phosphorylates the serine/threonine residue(s) at the IQ motif of p68 in migrating cells. The phosphorylation by PKC may require the binding of calmodulin to the IQ motif of p68.

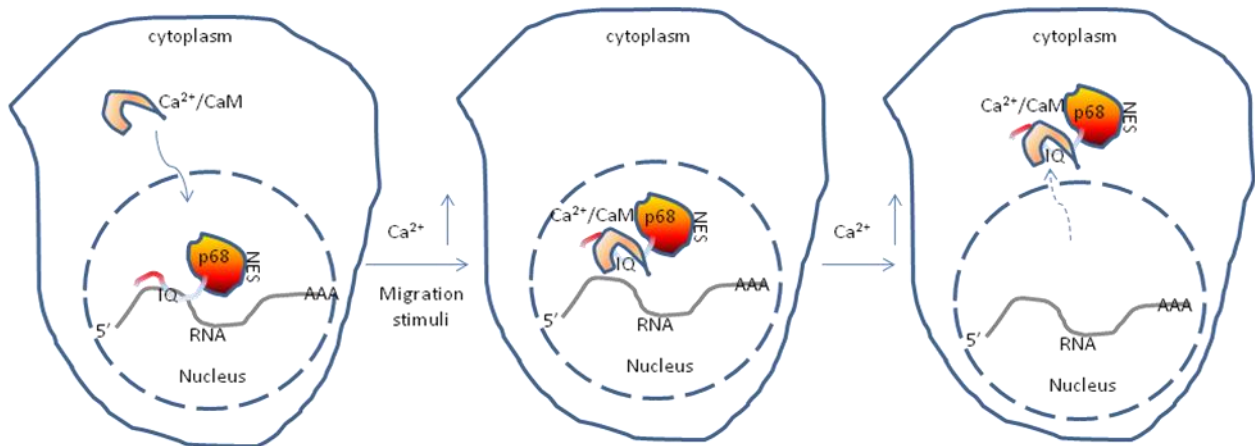


Figure 6.1 Working model about p68 cytosol exportation under the binding of Ca²⁺-calmodulin

IQ motif locates at the C-terminal of p68. The binding of CaM at the IQ motif of p68 may not affect the helicase core structure of p68, as the p68/CaM complex has the RNA dependent ATPase activity. C-terminal of p68 is very dynamic according to the structure prediction of p68. We reasoned that the binding of CaM at IQ motif may regulate the C-terminal structure of p68. This may lead to the change of the binding affinity of C-terminal of p68 to RNA or other nuclear structure. Meanwhile, CaM binding at the C-terminal of p68 may expose the NESs of p68. The exposure of NESs of p68 may lead to the exportation of p68 to the cytoplasm.

6.1.3 Nucleocytoplasmic shuttling p68 facilitated the translocation of its binding proteins

Nuclear pore complex (NPC) is considered as the place to allow the molecules to get in or go out of the nucleus. It was reported that molecules smaller than 45-60 kDa can get through NPC by passive diffusion. The larger molecules or protein complexes require receptors to

mediate the transportation across NPC by carrying NES/NLS (Allen, Cronshaw et al. 2000). The large proteins can get through the NPC without their own NES/NLS. Their translocation depends on the association with other proteins which have NES/NLS. The permeability of NPC can be regulated. The passive diffusion of molecules larger than 10kDa but smaller than 45kDa can be prevented when the Ca^{2+} stores, such as endoplasmic reticulum (ER) or nuclear store, are emptied (Stehno-Bittel, Perez-Terzic et al. 1995; Perez-Terzic, Gacy et al. 1999). Therefore, the translocation of the molecules between 10kDa and 45kDa may still need to associate with other NES/NLS carrying proteins to get through the NPC.

6.1.3.1 P68 shuttled calmodulin out of nucleus and functions in cell migration

Calmodulin is a calcium sensor protein that exists as a monomer of 16.8 kDa. Calmodulin can regulate processes both in the cytoplasm and in the nucleus by transducing a Ca^{2+} signal into a cellular response. This biological process includes changes in cytoskeletal structure and gene expression. However, how the calmodulin move into or out from the nucleus is still controversial. Even though the molecular size of calmodulin is less than 45 kDa; the simple diffusion of calmodulin in/out of the nucleus through the NPC is unlikely. This is because most of the calmodulin is always associated with other protein in a Ca^{2+} dependent/independent manner. The binding of calmodulin to other proteins will make the molecule size too big to pass through NPC. There are less than 5% of the total calmodulin free in smooth muscle cells at resting status (Luby-Phelps, Hori et al. 1995). The facilitated transportation of Calmodulin is an effective way to translocate calmodulin to the nucleus as the facilitated transport of Ca^{2+} /calmodulin into the nucleus was about 25-fold more rapid than passive diffusion (Thorogate and Torok 2004). Therefore, the facilitated transportation of calmodulin across the NPC is very important in mediating its cellular functions.

In this study, we found that p68 interacted with calmodulin in migrating cells. Both p68 and calmodulin were found to be accumulated in the cytosol of migrating cells. The cytosolic localized p68 as well as p68-calmodulin fusion protein depend on the NES(s) of p68. Since calmodulin itself has no NES, we concluded that the cytosolic translocation of p68 together with calmodulin depends on the shuttling function of p68. Interestingly, we observed that calmodulin started to translocate and accumulate in the cytoplasm at one hour post migration stimulation. Calmodulin is known to be redistributed from cytosol to the nucleus in response to a rise of cellular Ca^{2+} (Luby-Phelps, Hori et al. 1995). When the intracellular Ca^{2+} is increased, the nuclear translocation of calmodulin is initiated at around 40 seconds (Thorogate and Torok 2004). The nuclear translocation of calmodulin can be completed in 260-300 seconds (Craske, Takeo et al. 1999; Teruel, Chen et al. 2000). We reasoned that when the cell received the stimuli to migrate, the cytoplasmic Ca^{2+} was upregulated and calmodulin was accumulated in the nucleus initially. Ca^{2+} /calmodulin is shown to inhibit several nuclear events, such as transcription by direct interaction with the transcription factor (Corneliussen, Holm et al. 1994). We reasoned that the nuclear translocation of calmodulin might inhibit the binding of p68 to RNA, and might also inhibit the function of p68 as a transcription cofactor. Therefore p68/calmodulin was able to be relocated to the cytoplasm. This process allowed the cell to enter into the process of migration.

The calcium oscillation in the cell can lead to the binding switch of calmodulin to different proteins which are Ca^{2+} dependent or independent. The Ca^{2+} oscillation may also lead to the translocation of the calmodulin between the cytoplasm and the nucleus. This is important for a number of cellular functions. However, most of the studies have been focused on understanding the mechanism governing the nuclear translocation of calmodulin. How does calmodulin move back to the cytoplasm is not clear. Here, we provided a model to explain how

calmodulin is exported from the nucleus by interacting with nuclear protein p68 under the stimulation of cell migration. Since the interaction between p68 and calmodulin is Ca^{2+} dependent, we reasoned that the cytoplasmic transportation of calmodulin by p68 depends on the nuclear level of Ca^{2+} . Our preliminary data showed that the distribution pattern of p68/593F-calmodulin fusion proteins was similar to p68/WT-calmodulin fusion proteins. We speculated that Ca^{2+} -calmodulin could be exported by both WT and Y593 phosphorylated p68 to the cytoplasm.

6.1.3.2 P68 shuttled PKM2 and beta-catenin to the nucleus

PKM2 plays important roles in tumor progression. Most of the studies on PKM2 are focused on the cytosolic pyruvate kinase function. Interestingly, PKM2 is found to exist in the nucleus. How does PKM2 translocalize into the nucleus, and what is the function of PKM2 in the nucleus are not known. PKM2 has a function in regulation of the transcription of OCT-4 proteins. Our lab found that PKM2 could regulate the activity of the transcription factor Stat3. Therefore, PKM2 may function as a transcription cofactor. Previous studies showed that PKM2 can interact with tyrosine phosphorylated peptide. In the present study, we found that double tyrosine phosphorylated p68 can bind to PKM2. No classical NLSs are found in PKM2 by sequence analysis. Interestingly, we found that PKM2 could accumulate in the nucleus by binding to double phosphorylated p68 but not to the 593F mutant of p68 (a mutant no longer be double phosphorylated at Y593 and Y595). We reasoned that PKM2/p68 complex could translocate to the nucleus due to the nucleocytoplasmic shuttling activity of p68. Previous study from our laboratory (Yang, Lin et al. 2006) showed that Y593 phosphorylated p68 could be exported to the cytoplasm and interact with beta-catenin by replacing axin. Beta-catenin could be finally transported to the nucleus by p68. The nuclear beta-catenin then functioned as a transcription

factor. We later demonstrated that p68 did shuttle between the cytoplasm and the nucleus (Wang, Gao et al. 2009). We found that overexpression of Y593E did increase the nuclear beta-catenin. The Y593E mutant may mimick the Y593 phosphorylated p68. We further found that 593E and 593/595E shuttle between the cytoplasm and the nucleus by the heterokaryon assay. All these information indicated that shuttling p68 can carry different transcription factors (co-factors) into the nucleus to regulate the specific gene transcriptions. And the transportation of different transcription factor (co-factors) to the nucleus seems to depend on the post-translational modification of p68.

6.2 P68/calmodulin functioned as a microtubule motor in migrating cells

In the present study, we found that the interaction between p68 and calmodulin increased in migrating cells. The interaction between p68 and calmodulin was found to be required for the cell migration as disruption of the interaction could inhibit the cell migration as well as cancer cell metastasis. Interestingly, high levels of p68 and calmodulin were found in the cytosol of migrating cells than in the resting cells. The cytosolic location of p68 was found to depend on the binding to calmodulin.

6.2.1 P68/calmodulin functioned as a motor in migrating cells

We presented evidence to show that p68/calmodulin functioned as a microtubule motor in migrating cells. We found that p68/calmodulin that was purified from the migrating cells interacted with microtubule directly. The p68/calmodulin complex had microtubule dependent ATPase activity. When we added the microtubule onto the p68/calmodulin complex, we observed that microtubule moved on the protein complex in the presence of ATP in the microtubule gliding assay. We further demonstrated that p68 moved on the microtubule in the

living migrating cells. All this results supported the notion that p68/calmodulin functioned as a microtubule motor in migrating cells.

A conventional microtubule motor, such as kinesin I, usually has two copies of heavy chains and light chains. P68 can exist as a homodimer (Ogilvie, Wilson et al. 2003). Calmodulin itself can dimerize through a domain that is external to its Ca^{2+} dependent interaction with the target proteins (Lafitte, Heck et al. 1999). We reasoned that p68/calmodulin might dimerize to form one unit of microtubule motor. The movement of p68 along the microtubule was observed by the real time imaging of the fluorescently labeled p68 and microtubule. Interestingly, the movement of p68 along the microtubule was in a discontinued way in the living cells. Two possible reasons may explain this phenomenon. First, other protein(s) may interact with the p68/calmodulin motor complex to regulate the moving complex along the microtubule in the living cells. The back and forth movement of a motor on the microtubule are common phenomena observed in other microtubule motors (Vale, Malik et al. 1992). Second, the formation of p68/calmodulin complex depended on the presence of Ca^{2+} . The oscillation of Ca^{2+} in the cytosol might affect the stability of p68/calmodulin complex, and might affect the interaction of this protein complex with microtubules, as p68 alone could not bind to the microtubule.

During cell migration, the cell is polarized by relocalizing the microtubule-organizing center and Golgi in front of the nucleus and to the leading edge. The orientation of MTOC may contribute to the polarized migration, as the microtubule should grow into the leading edge. The forward protrusion is initiated/maintained, as the microtubule mediated the delivery of vesicles and protein complex to the leading edge (Rodriguez, Schaefer et al. 2003). P68 and calmodulin formed a complex in migrating cells. The cytoplasmic p68/calmodulin was identified to play

functions as a microtubule associated motor. Therefore, p68/calmodulin may not determine the polarization of the cell. Rather, this protein complex may play a role in initiating/maintaining the protrusion during cell movement.

6.2.2 The leading edge transportation of calmodulin by motor unit of p68/calmodulin

Calmodulin has important function in cell motility. The functions of calmodulin in cell motility are known to target other proteins and then regulate the functions of the target proteins. Interestingly, a lot of proteins located near cytoplasmic membrane (edge located) are known to play roles in cell migration, and they are regulated by calmodulin. We found that calmodulin accumulated at the leading edge in migrating cells. How calmodulin was accumulated to the leading edge was not known. As we know, most of calmodulin is bound to other proteins in Ca^{2+} dependent or independent manner. Only 5% of the total calmodulins are free in the cells at resting intracellular Ca^{2+} (Luby-Phelps, Hori et al. 1995), which makes the diffusion of calmodulin in the cytoplasm less likely. The facilitated transportation of calmodulin to the edge (including leading edge) seems more effective than the diffusion manner. We observed that p68/calmodulin functioned as a motor and p68 moved towards the leading edge. We speculated that the movement of p68/calmodulin towards plus end of microtubule could lead to the translocation of p68 with its associated calmodulin to the leading edge.

6.2.3 The putative signaling pathway in regulating the interaction between p68 and calmodulin

Previous study shows that the interaction between calmodulin and neuromodulin (at the IQ domain) decrease the phosphorylation by PKC, while the phosphorylation of neuromodulin conversely prevents the interaction between calmodulin and neuromodulin (Liu and Storm 1990). P68 possesses a region that has a sequence similar to neuromodulin, which contains the

conserved protein kinase C phosphorylation site and calmodulin binding site, IQ motif. The phosphorylation of p68 by PKC has been demonstrated by an *in vitro* assay. The interaction between p68 and calmodulin has also been documented (Buel, Glidden et al. 1994). The interaction between calmodulin and p68 decreases the phosphorylation of p68 by PKC. P68 is very likely phosphorylated by PKC in the migrating cells. However, the effect of phosphorylation of p68 by PKC on the interaction between calmodulin and p68 is not clear. We observed that the p68/calmodulin interaction was strengthened in migrating cells, and there were quite high levels of p68 and calmodulin at the leading edge of migrating cells. The translocation of p68/calmodulin to the leading edge depended on the p68/calmodulin interaction and ATPase activity of p68, as IQ-calmodulin and LGLD-calmodulin fusion proteins no longer accumulated at the leading edge. We hypothesized that PKC phosphorylation may lead to the strengthened interaction between p68 and calmodulin. Under this hypothesis, when $[Ca^{2+}]$ is increased, calmodulin binds to p68 and leads to the p68/calmodulin cytosol translocation; when $[Ca^{2+}]$ is decreased, the dissociation of calmodulin from p68 may lead to the PKC phosphorylation at the IQ motif of p68 in the cytosol. The phosphorylated p68 will then bind to calmodulin in a Ca^{2+} independent way. The p68/calmodulin complex could function as a motor in migrating cells.

SW480 cells could be induced into migration status under the treatment of EGF. It is known that EGFR activation promotes cell motility through specific intracellular signaling pathways. The activation of PLC γ -1, and the subsequent hydrolysis of phosphor-inositide bisphosphate is a required signaling pathway (Chen, Xie et al. 1994). Activation of protein kinase C and the increase of cytoplasmic calcium due to the generation of inositol triphosphate and diacylglycerol are important in modulating the process of cell motility. In our study, upregulated cytoplasmic calcium may induce the calmodulin nuclear translocation initially. Ca^{2+} -

calmodulin binding might promote the release of p68 from the RNA complexes. The p68/calmodulin would then be exported from the nucleus and function as a motor in migrating cells. The model of EGF-mediated cell motility can be divided into at least two divergent pathways. One is cytoskeletal reorganization, and the other is to destabilize cell-substratum interactions (the loss of focal adhesions leads to the reduction of the cell adhesiveness to substratum) (Xie, Pallero et al. 1998). Currently, we do not know whether p68/calmodulin has a function in the stabilization of the microtubule. P68/calmodulin may play a role in the cell-cell attachment, or cell-substratum interaction, as p68 is known to interact with beta-catenin. We further observed that p68 could interact with GrB2. GrB2 can bind to EGFR. EGF can stimulate the cell migration. The leading edge translocation of p68 may be involved in the feed back on signaling pathway by binding to GrB2. In general, growth factor-induced cell motility requires three coordinated processes: lamellipodial extension, establishment of cell-substratum adhesions at the leading edge, and detachment of the substratum at the rear side (Xie, Pallero et al. 1998). We observed translocation of p68/calmodulin to the leading edge in present study. Whether the p68/calmodulin complex or single protein plays a role in the lamellipodial extension or establishment of cell-substratum adhesions at the leading edge is unknown. Further study is required to identify the detail function of p68 or p68/calmodulin at the leading edge.

Interestingly, other migration-inducing growth factors, such as PDGF, also utilize signaling pathway similar to that of EGF (Bornfeldt, Raines et al. 1994). This might provide the explanation for why the cytosolic export of p68 occurs in cells that are treated by EGF or PDGF.

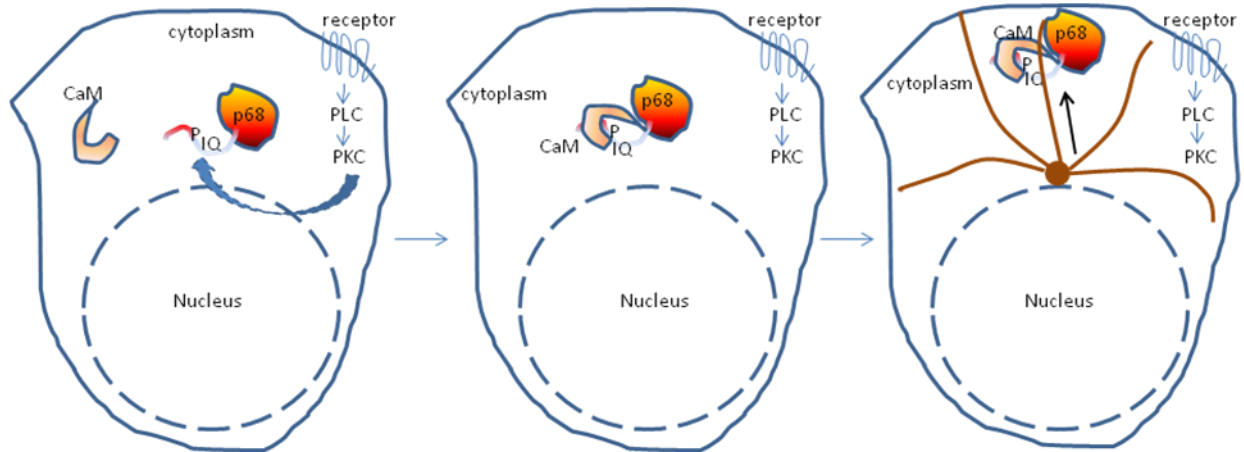


Figure 6.2 Putative signaling pathway in the regulation of the interaction between p68 and calmodulin

We found that the interaction between p68 and CaM was also increased in migrating 4T1 cells (mouse breast cancer cell). The metastasis capability of 4T1 cells to the lung and liver was decreased under the treatment of IQ peptide (data not shown). This supports the idea about that the interaction between p68 and CaM may be critical in other cancer cell lines too. We are not sure whether the intracellular Ca^{2+} level is the only regulation factor controls the binding of p68 and CaM. And the function of p68/CaM in cell migration may specifically apply to some cancer cells as different signaling pathway may be involved in different cell lines.

On the other hand, the expression levels of p68 and CaM are different in different cell line as we screened. This may indicate that the significance of the interaction between p68 and CaM in cell migration might be different in different cell lines. In normal colon tissue, the RNA level of p68 is extremely low [Am J Transl Res. 2010; 2(3): 223–234.]. We reasoned that the interaction between p68 and CaM may not function in the process of cell migration in normal colon cells.

6.2.4 Other putative cytoplasmic function of p68

As we proposed previously, transiently cytosolic localized p68 can transport the cytosolic proteins, including beta-catenin and PKM2, into the nucleus. We observed that the cytosolic p68 together with calmodulin acted as microtubule dependent motor to facilitate cell migration. We concluded that the leading edge translocation of calmodulin was facilitated by the action of p68/calmodulin motor. Whether other cargos or proteins can be transported by the p68/calmodulin motor actions is not known. Interestingly, we also found p68 interacted with Grb2 other than calmodulin translocation, which indicated that p68 may have functions at the leading edge of the migrating cells.

6.3 Colon tissue array and mouse xenograft model for cancer metastasis

6.3.1 Colon tissue array

In the tissue array analyses, we found that the cytoplasmic levels of p68 in the colorectal cancer cells were higher than in the cells of normal tissues. This observation is consistent with the Sook Shin et al's observation that p68 RNA helicase overexpression level is higher in adenocarcinomas. P68 has an important function in organ differentiation during development. P68 is overexpressed in the differentiated adipocyte and skeletal muscle cells (Fuller-Pace and Ali 2008). Interestingly, we also detected higher p68 levels in highly differentiated (grade 1) colon cancer tissue than in the poorly differentiated tissue (grade 3). The cancer cells in the poorly differentiated tumor tissue have much stronger metastatic capability than the cells in the high differentiated tumor tissue. We concluded that the migration capability was not directly linked to the cellular level of p68 in the cancer cells. The cytoplasmic level of p68 can be affected by the total cellular level of p68 in the cells. We reasoned that the ratio of p68 between the cytoplasm and the nucleus might be critical in migrating cells. In other word, higher ratio of

p68 between the cytoplasm and the nucleus may indicate higher migration capability. It is possible that the serine/threonine phosphorylated p68 in the cytoplasm may be the portion of p68 that plays a role in cell migration, as the serine/threonine phosphorylated p68 may form the stable p68/calmodulin motor complex and function in cell migration. Simply analysis of the cytoplasmic level of p68 in the colon cancer tissue may not reflect the metastasis status. One may need to analyze the ratio between cytoplasmic and nuclear p68 in the tissue. How the serine/threonine phosphorylated p68 functions in the migrating cells is an open question.

In order to find out whether there is a pattern of cytoplasmic level of p68 in different tumor tissues, we analyzed the cytoplasmic p68 in tumors at different stages but in the similar differentiation level (same grade). Interestingly, we found that there were more cytoplasmic p68 in higher stages of the tumor than that in the lower stage of the tumor. The cancer cells in higher stage tumor have higher capability of cell migration. This observation supported the notion that cancer cells with higher migration capability have higher levels of p68 in the cytoplasm.

We also found that there was high level of p68 in the cytoplasm of the tumor cells compared to that in the surrounding normal cells. In the subcutaneously implanted tumor, we also found there was a high level of p68 in the cytoplasm of the tumor cells. This phenomenon was not observed in the *in vitro* cultured colon cancer cells, such as SW480, HT29 and SW620 cells. It is known that most of the cancer cells within the tumor tissue are under the hypoxia condition (normally below 3%-5% O₂), while the cultured cells under normal culture condition are under normoxia conditions. We speculated that the colon cancer cells under hypoxia conditions have higher migration capability than the cells under normoxia condition have. P68 was observed to be dominantly localized in the nucleus (primary data from Dr. Shiyong Sun) in the lung cancer tissue. This observation provided further support for the idea that hypoxia

conditions might induce the cytoplasmic translocation of p68. The hypoxia condition may not exist in the lung cancer tissue as the lung tissue is provided with high concentration of O₂. Cytoplasmic translocation of p68 might depend on tissue environments.

6.3.2 *Mouse xenograft model for cancer metastasis*

6.3.2.1 The subcutaneous implantation to study the colon cancer metastasis to spleen is a suitable system.

Many genetic mouse models of benign adenoma have been established. However, very few models of colon cancer, excluding the locally invasive models, have been developed. Unlike in humans, there are no genetic mouse models in which cancer can spontaneously form tumors in the intestines and become invasive and metastasize to the other organs. Since mortality of most of the colon cancer is due to cancer metastasis, it is very important to study the colon cancer metastasis. The transplantation (xenograft) models are therefore becoming the primary model system to study the colon cancer metastasis currently (Taketo and Edelman 2009). Study of the colon cancer metastasis using model systems of the colon cancer includes intrarectal implantation of the colon cancer cells (Tsutsumi, Kuwano et al. 2001), orthotopic implantation of the tumor tissue (Sun, Sasson et al. 1999) or tumor cells (Cespedes, Espina et al. 2007), and subcutaneously implantation of tumor cells. In this study, we employed the model system of subcutaneous implantation of the colon cancer cells to study metastasis. This procedure is very simple. Even though the distant organ metastasis was not directly observed (not macrometastasis) in this xenograft model, trace amounts of the tumor cells that metastasized to spleen can be detected by RT-PCR (micrometastasis). The purpose of this study is to elucidate the function of p68/calmodulin complex in the cancer cell migration. The generation of the macrometastasis from micrometastasis at the distant organ involves multiple process, including cell proliferation,

cell apoptosis, dormancy, and angiogenesis (Steeg 2006). The formation of the micrometastasis in spleen by subcutaneously xenograft is an approximate model system for our study.

6.3.2.2 Microscopic spleen metastasis was detected in spleen

Tumor metastasis involves several processes which allow the tumor cells to move from the primary site to a distant organ. Tumor cells need to invade the surrounding tissue at the primary site, get into the lymph stream or the bloodstream, survive and arrest in the blood circulation, extravasate into a new tissue, and grow at the new place. Whether a tumor can metastasize to a distant organ or not depends on all these processes. When tumor cells successfully land in a distant organ, the formation of a macrometastasis tumor (observable) from a micrometastasis tumor at the new site depends on many conditions, including proliferation, apoptosis, and dormant situation of the tumor cells at the new sites. The primary tumor (implanted) may release some systemic suppressor factor(s) to prevent the growth of micrometastasis (Demicheli, Retsky et al. 2008). The angiogenesis at the new site provides the nutrition to the tumor cells and is also very important for the growth of the tumor (Steeg 2006). According to the study in model of melanoma metastasis, the survival rate of the tumor cells in the blood circulation is high (80%). However, the rate for formation of micrometastasis is low (1 in 40 cells); and the rate for formation of macrometastasis from micrometastasis is even lower (1 in 100 micrometastasis in 10 days) (Luzzi, MacDonald et al. 1998).

Although very few colon cancer cells metastasize to the spleen as well as other organs (such as liver and lung) by subcutaneous injection, the micrometastatic tumors in distant organs are likely to exist when the highly metastatic cancer cells are subcutaneously implanted. The technique of RT-PCR can detect the trace amount of the tumor cells. The trace amount of tumor cells metastasizing to the distant organ (spleen) is clinically important. As the tumor cells had

succeeded to metastasize to the distant organ, it may colonize to form a macrometastasis tumor eventually. Whether the metastasized tumor cells can grow to a big tumor in distant organs depends on many conditions. The metastasized tumor cells at distant organs may not grow to form big tumor in a short time. Those cells may get into the dormant condition when it reaches the distant organ site. The regular survival rate of the tumor cells through the blood circulation is around 1/100 (orthotopic tumor). The survival rate of the metastatic cells by subcutaneous injection would be much less, as the nearby lymph nodes are not available. Also, the metastasis may take longer time to occur, as it requires the generation of blood vessels (angiogenesis) near by or into the tumor before the metastasis can take place.

The tumor can form when SW620 cells are directly injected into the spleen (Zhang, Halder et al. 2010). The metastatic SW620 did not grow to a clinical detectable size tumor in studies in our and other laboratory. This might be due to the following reasons. First, the time for the tumor growth at the metastatic site (spleen) was not long enough. Second, the primary tumor at the SC site might secrete some inhibitory factors that affect the metastatic tumors. Third, the spleen metastatic tumor cells might have lost the growth capability during the metastatic selection.

Spleen is a large lymphoid organs, it has functions similar to lymph nodes. Spleen filters blood stream and engulfs dead cells and foreign particles. Therefore, the detection of SW620 cells in the spleen may be due to the simple engulfment of the cells by the spleen. The human SW620 cells might be regarded as foreign particles by the spleen, or these cells were already dead when the cells reached the spleen. One thing that is certain is that SW620 cells did migrate through the primary subcutaneous boundary and reached the blood circulation.

When the cancer cells colonize at the distant organ, they may further disseminate to the other organ as the primary site for second metastasis (Hanahan and Weinberg 2011). If we consider the subcutaneously implanted colon tumor as the metastatic tumor, the cancer cells likely disseminate back to the colon. Therefore, examining the metastasis of the subcutaneously implanted colon cancer cells at the colon site would also be a useful test. Liver and Lung are the main metastasis organs for the colon cancer. Therefore, examination of the metastasis trace (RT-PCR) in the liver and lung could be additional tests in our future study.

6.3.2.3 About the structure of SW620 generated tumor

We found that SW620 tumor grew fast; however, the tumor was poorly glandularly differentiated. The possible reason is that SW620 is derived from a metastatic tumor (isolated from lymphometric metastatic site. Broderss' grade IV). Highly metastatic tumors usually are less well differentiated than the primary tumors do. The parental tumor for SW620 has no glandular differentiation. SW620 produces very low differentiated glandular structure when the cells are injected into the spleen (Hewitt, McMarlin et al. 2000). Therefore, it was reasonable to see the poor glandular differentiation structure with the SW620 xenograft tumor.

Most of the metastatic tumors invade and migrate through the blood vessel to metastasize to the distant organs. We expected that there would be more migrating cells in the blood vessels site, which means that the area with high density of blood vessels would have more migrating cells. Interestingly, microvessels are dense in the periphery area of the SC tumors and less dense in the middle area. Therefore, we compared the cytoplasmic level of p68 between those two typical regions. We observed that there were more p68 in the cytoplasm in the periphery area than that in the middle area, which supported our notion about the migrating cells had more cytoplasmic p68 than that in the resting cells.

Previous study demonstrated an infiltrative pattern of invasion in the periphery area of the implanted SW620 tumor (Hewitt, McMarlin et al. 2000). We also observed an infiltrative pattern of SW620 cells relative to the mouse stromal cells (nuclei staining, data not shown). SW620 tumor was found firmly attached to the thoracic wall due to the tumor invasion underlying skeletal muscle, which is consistent with the previous study (Hewitt, McMarlin et al. 2000).

6.3.2.4 IQ peptide inhibited the cytosolic translocation of p68 and tumor growth

There was high level of p68 in the cytosol of cells in the periphery area. The IQ peptide could compete to bind to calmodulin to disrupt the interaction between p68 and calmodulin. We found that the amount of cytosolic p68 at the periphery area of the tumor was decreased when the mice were treated with IQ peptide. This phenomenon was not observed in the mice which were treated with a control peptide. This result supported our speculation that disruption of the interaction between p68 and calmodulin could inhibit the cytoplasmic export of p68. Interestingly, a calmodulin binding peptide M13 (amino acid residues are corresponding to the smMLCK to prevent Ca^{2+} -calmodulin binding) can prevent calmodulin nuclear translocation (Mermelstein, Deisseroth et al. 2001). This study indicates that the nucleus translocation of calmodulin requires its interaction with smMLCK. We were not able to exclude the possibility that the cytoplasmic accumulation of calmodulin was due to that the IQ peptide affecting the calmodulin nuclear translocation. It is possible to resolve the issue by measuring the nuclear levels of calmodulin under the treatment of IQ peptide in the future study. Further more, we can use the NLS-tagged IQ peptide to test what would happen when the interaction between p68 and calmodulin is specifically disrupted in the nucleus.

We demonstrated that IQ peptide could inhibit the spleen metastasis of the SW620 xenograft tumors. We observed that the growth of the SW620 tumor was affected by the treatment of IQ peptide. There were several explanations. First, the interaction between p68 and calmodulin might have a function in the cell proliferation *in vivo*, even though our study showed that the proliferation of SW620 cells was not affected by the IQ peptide *in vitro*. Second, the IQ peptide might function as a calmodulin antagonist, as calmodulin antagonist is known to inhibit the proliferation of the cells (Rasmussen, Lu et al. 1992). However, this is less likely. The binding of calmodulin to other proteins (result) were not affected in the presence of IQ peptide. Third, the IQ peptide could disrupt the interaction between p68 and calmodulin in mice stromal cells (including the endothelial cells), which could affect the migration of stromal cells. As a consequence, the tumor growth would be inhibited. The sequence alignment showed that the sequence of calmodulin is identical in human and in mouse. The IQ motif is identical for p68 from mouse and human. Thus, the IQ peptide may affect the migration of the endothelial cells to form the new blood vessel to provide the nutrients for the growth of the tumor. This is very likely as knockout of p68 in mice causes the malformation of blood vessels (Fukuda, Yamagata et al. 2007).

Colon cancer metastasis is the major cause that leads to the death of the cancer patient. The FDA approved drugs for treatment of colon cancer and metastasis have strong side effects. The IQ peptide derived from the p68 IQ motif can inhibit the cancer metastasis. However, the effect on metastasis inhibition was not so dramatic when compared to that in the cells in which IQ peptide fusion protein is (GFP-IQ) stably expressed. We reasoned that the circulation time of a peptide is short, and the peptide is unstable in circulation. Designing a new compound to

disrupt the interaction between p68 and calmodulin could be used to prevent the cancer metastasis in future.

6.4 Cell proliferation contributed by shuttling function of phosphorylated p68

The expression level of p68 is known to be correlated with the growth of cells. Interestingly, our laboratory observed that p68 was highly phosphorylated at Y593 in highly proliferating cancer cells. The phosphorylation of p68 at Y595 was also observed. The phosphorylation of Y595 depended on the phosphorylation of Y593. All these observations supported the notion that Y593-Y595 double phosphorylated p68 might have a function in cell proliferation. The phosphor Y593-Y595 peptide was synthesized. It is found that the peptide binds PKM2. P68 was identified to be a nucleocytoplasmic shuttling protein. The shuttling of p68 did not depend on the phosphorylation, as both the Y593E and Y593F mutants shuttled between the cytoplasm and the nucleus. We speculated that PKM2 could be transported to the nucleus by shuttling activity of the Y593-Y595 phosphorylated p68. The Y593F mutant can no longer be phosphorylated. The mutant was not able to bind PKM2. Correspondingly, we observed that PKM2 accumulated in the nucleus to a less degree when Y593 of p68 was mutated to Y593F.

Nuclear PKM2 play a role in cell proliferation (Hoshino, Hirst et al. 2007). It is speculated that nuclear PKM2 may participate in the phosphorylation of Histone 1. In our study, we observed that nuclear PKM2 functions as a transcription co-activator. Nuclear PKM2 could phosphorylate Stat3 and regulate the expression of its target genes, including MEK5. Since nuclear PKM2 can act as a protein kinase, other transcription factors or cofactors may also be targets of PKM2 in the nucleus.

6.5 Phosphorylated p68 may promote the dimer transformation of PKM2 and regulate the metabolism in the cancer cells.

Y593-Y595 phosphorylated p68 interacted with PKM2 (in submission). Interestingly, phosphor-p68 bound to PKM2 but not PKM1. The segment with different sequence between PKM2 and PKM1 is located at the interface of two dimeric subunits. There are 23 amino acids difference at the carboxy terminus (a.a. 378-434) between PKM2 and PKM1. The binding of p68 to the interface of two dimeric subunit of PKM2 might promote the dimerization of PKM2. This is very likely, as dimerization of PKM2 in tumor cells can be induced by direct interaction of PKM2 with other oncoproteins, including pp60v-src, HPV-16 E7, and A-Raf. Dimeric PKM2 are known to have less glycolytic activity, as the dimeric PKM2 has low affinity for PEP and dimeric PKM2 is almost inactive at physiological PEP concentration. Therefore, the binding of p68 to PKM2 might down-regulate the pyruvate kinase activity, upregulate the glucose transporters, and increase glucose import, which eventually facilitates the metabolic switch to glycolysis in cancer cells. On the other hand, the reliance on glycolysis can be further accentuated under the hypoxic condition. We also observed that there were more p68 in the cytoplasm under hypoxic condition (implanted tumor tissue verse to the cultured SW620 cells). Further studies will be performed to test whether p68 is more serine/threonine phosphorylated under the hypoxia condition, and how phosphorylation of p68 functions in the cancer metabolism.

REFERENCES

- Aaboe, M., K. Birkenkamp-Demtroder, et al. (2006). "SOX4 expression in bladder carcinoma: clinical aspects and in vitro functional characterization." Cancer research **66**(7): 3434-3442.
- Adams, M. R., R. Sears, et al. (2000). "Complex transcriptional regulatory mechanisms control expression of the E2F3 locus." Mol Cell Biol **20**(10): 3633-3639.
- Akao, Y., O. Marukawa, et al. (1995). "The rck/p54 candidate proto-oncogene product is a 54-kilodalton D-E-A-D box protein differentially expressed in human and mouse tissues." Cancer Res **55**(15): 3444-3449.
- Alahari, S. K., P. J. Reddig, et al. (2002). "Biological aspects of signal transduction by cell adhesion receptors." Int Rev Cytol **220**: 145-184.
- Alber, F., S. Dokudovskaya, et al. (2007). "Determining the architectures of macromolecular assemblies." Nature **450**(7170): 683-694.
- Allen, T. D., J. M. Cronshaw, et al. (2000). "The nuclear pore complex: mediator of translocation between nucleus and cytoplasm." Journal of cell science **113** (Pt 10): 1651-1659.
- Altenberg, B. and K. O. Greulich (2004). "Genes of glycolysis are ubiquitously overexpressed in 24 cancer classes." Genomics **84**(6): 1014-1020.
- Aratani, S., T. Oishi, et al. (2006). "The nuclear import of RNA helicase A is mediated by importin-alpha3." Biochemical and biophysical research communications **340**(1): 125-133.
- Ashizawa, K., M. C. Willingham, et al. (1991). "In vivo regulation of monomer-tetramer conversion of pyruvate kinase subtype M2 by glucose is mediated via fructose 1,6-bisphosphate." The Journal of biological chemistry **266**(25): 16842-16846.
- Askjaer, P., A. Bachi, et al. (1999). "RanGTP-regulated interactions of CRM1 with nucleoporins and a shuttling DEAD-box helicase." Molecular and cellular biology **19**(9): 6276-6285.
- Bates, G. J., S. M. Nicol, et al. (2005). "The DEAD box protein p68: a novel transcriptional coactivator of the p53 tumour suppressor." EMBO J **24**(3): 543-553.
- Bates, G. J., S. M. Nicol, et al. (2005). "The DEAD box protein p68: a novel transcriptional coactivator of the p53 tumour suppressor." The EMBO journal **24**(3): 543-553.
- Beier, R., A. Burgin, et al. (2000). "Induction of cyclin E-cdk2 kinase activity, E2F-dependent transcription and cell growth by Myc are genetically separable events." EMBO J **19**(21): 5813-5823.
- Bolsover, S. R. (2005). "Calcium signalling in growth cone migration." Cell calcium **37**(5): 395-402.
- Bonifaci, N., J. Moroianu, et al. (1997). "Karyopherin beta2 mediates nuclear import of a mRNA binding protein." Proc Natl Acad Sci U S A **94**(10): 5055-5060.
- Bonnet, S., S. L. Archer, et al. (2007). "A mitochondria-K⁺ channel axis is suppressed in cancer and its normalization promotes apoptosis and inhibits cancer growth." Cancer Cell **11**(1): 37-51.
- Borer, R. A., C. F. Lehner, et al. (1989). "Major nucleolar proteins shuttle between nucleus and cytoplasm." Cell **56**(3): 379-390.
- Bornfeldt, K. E., E. W. Raines, et al. (1994). "Insulin-like growth factor-I and platelet-derived growth factor-BB induce directed migration of human arterial smooth muscle cells via signaling pathways that are distinct from those of proliferation." The Journal of clinical investigation **93**(3): 1266-1274.

- Bouchard, C., K. Thieke, et al. (1999). "Direct induction of cyclin D2 by Myc contributes to cell cycle progression and sequestration of p27." EMBO J **18**(19): 5321-5333.
- Boulikas, T. (1994). "Putative nuclear localization signals (NLS) in protein transcription factors." J Cell Biochem **55**(1): 32-58.
- Brahmbhatt, A. A. and R. L. Klemke (2003). "ERK and RhoA differentially regulate pseudopodia growth and retraction during chemotaxis." J Biol Chem **278**(15): 13016-13025.
- Bretscher, M. S. (1996). "Getting membrane flow and the cytoskeleton to cooperate in moving cells." Cell **87**(4): 601-606.
- Bretscher, M. S. (2008). "Recap on cell migration." Traffic **9**(2): 198-199.
- Brunet, A., F. Kanai, et al. (2002). "14-3-3 transits to the nucleus and participates in dynamic nucleocytoplasmic transport." J Cell Biol **156**(5): 817-828.
- Buelt, M. K., B. J. Glidden, et al. (1994). "Regulation of p68 RNA helicase by calmodulin and protein kinase C." J Biol Chem **269**(47): 29367-29370.
- Buelt, M. K., B. J. Glidden, et al. (1994). "Regulation of p68 RNA helicase by calmodulin and protein kinase C." The Journal of biological chemistry **269**(47): 29367-29370.
- Buszczak, M. and A. C. Spradling (2006). "The Drosophila P68 RNA helicase regulates transcriptional deactivation by promoting RNA release from chromatin." Genes & development **20**(8): 977-989.
- Cambien, B., B. F. Karimjee, et al. (2009). "Organ-specific inhibition of metastatic colon carcinoma by CXCR3 antagonism." Br J Cancer **100**(11): 1755-1764.
- Caretti, G., R. L. Schiltz, et al. (2006). "The RNA helicases p68/p72 and the noncoding RNA SRA are coregulators of MyoD and skeletal muscle differentiation." Dev Cell **11**(4): 547-560.
- Cartwright, P. and K. Helin (2000). "Nucleocytoplasmic shuttling of transcription factors." Cellular and molecular life sciences : CMLS **57**(8-9): 1193-1206.
- Cartwright, P. and K. Helin (2000). "Nucleocytoplasmic shuttling of transcription factors." Cell Mol Life Sci **57**(8-9): 1193-1206.
- Causevic, M., R. G. Hislop, et al. (2001). "Overexpression and poly-ubiquitylation of the DEAD-box RNA helicase p68 in colorectal tumours." Oncogene **20**(53): 7734-7743.
- Cavallaro, U. and G. Christofori (2004). "Cell adhesion and signalling by cadherins and Ig-CAMs in cancer." Nat Rev Cancer **4**(2): 118-132.
- Cespedes, M. V., C. Espina, et al. (2007). "Orthotopic microinjection of human colon cancer cells in nude mice induces tumor foci in all clinically relevant metastatic sites." The American journal of pathology **170**(3): 1077-1085.
- Cespedes, M. V., C. Espina, et al. (2007). "Orthotopic microinjection of human colon cancer cells in nude mice induces tumor foci in all clinically relevant metastatic sites." Am J Pathol **170**(3): 1077-1085.
- Chambers, A. F., A. C. Groom, et al. (2002). "Dissemination and growth of cancer cells in metastatic sites." Nat Rev Cancer **2**(8): 563-572.
- Chan, K. T., D. A. Bennin, et al. (2010). "Regulation of adhesion dynamics by calpain-mediated proteolysis of focal adhesion kinase (FAK)." J Biol Chem **285**(15): 11418-11426.
- Chen, P., H. Xie, et al. (1994). "Epidermal growth factor receptor-mediated cell motility: phospholipase C activity is required, but mitogen-activated protein kinase activity is not sufficient for induced cell movement." The Journal of cell biology **127**(3): 847-857.

- Chin, D. and A. R. Means (2000). "Calmodulin: a prototypical calcium sensor." Trends Cell Biol **10**(8): 322-328.
- Chin, D. and A. R. Means (2000). "Calmodulin: a prototypical calcium sensor." Trends in cell biology **10**(8): 322-328.
- Christofk, H. R., M. G. Vander Heiden, et al. (2008). "The M2 splice isoform of pyruvate kinase is important for cancer metabolism and tumour growth." Nature **452**(7184): 230-233.
- Christofk, H. R., M. G. Vander Heiden, et al. (2008). "Pyruvate kinase M2 is a phosphotyrosine-binding protein." Nature **452**(7184): 181-186.
- Chrzanowska-Wodnicka, M. and K. Burridge (1996). "Rho-stimulated contractility drives the formation of stress fibers and focal adhesions." J Cell Biol **133**(6): 1403-1415.
- Clapham, D. E. (2007). "Calcium signaling." Cell **131**(6): 1047-1058.
- Clark, E. L., A. Coulson, et al. (2008). "The RNA helicase p68 is a novel androgen receptor coactivator involved in splicing and is overexpressed in prostate cancer." Cancer Res **68**(19): 7938-7946.
- Cohen, A. A., N. Geva-Zatorsky, et al. (2008). "Dynamic proteomics of individual cancer cells in response to a drug." Science **322**(5907): 1511-1516.
- Cokol, M., R. Nair, et al. (2000). "Finding nuclear localization signals." EMBO Rep **1**(5): 411-415.
- Collins, S. R. and T. Meyer (2009). "Calcium flickers lighting the way in chemotaxis?" Developmental cell **16**(2): 160-161.
- Corneliussen, B., M. Holm, et al. (1994). "Calcium/calmodulin inhibition of basic-helix-loop-helix transcription factor domains." Nature **368**(6473): 760-764.
- Cory, G. O. and A. J. Ridley (2002). "Cell motility: braking WAVES." Nature **418**(6899): 732-733.
- Cotton, M. and A. Claing (2009). "G protein-coupled receptors stimulation and the control of cell migration." Cell Signal **21**(7): 1045-1053.
- Craig, E., Z. K. Zhang, et al. (2002). "A masked NES in INI1/hSNF5 mediates hCRM1-dependent nuclear export: implications for tumorigenesis." EMBO J **21**(1-2): 31-42.
- Craske, M., T. Takeo, et al. (1999). "Hormone-induced secretory and nuclear translocation of calmodulin: oscillations of calmodulin concentration with the nucleus as an integrator." Proceedings of the National Academy of Sciences of the United States of America **96**(8): 4426-4431.
- Craske, M., T. Takeo, et al. (1999). "Hormone-induced secretory and nuclear translocation of calmodulin: oscillations of calmodulin concentration with the nucleus as an integrator." Proc Natl Acad Sci U S A **96**(8): 4426-4431.
- Crawford, L., K. Leppard, et al. (1982). "Cellular proteins reactive with monoclonal antibodies directed against simian virus 40 T-antigen." Journal of virology **42**(2): 612-620.
- Cuff, J. A., M. E. Clamp, et al. (1998). "JPred: a consensus secondary structure prediction server." Bioinformatics **14**(10): 892-893.
- Dang, C. V. (1999). "c-Myc target genes involved in cell growth, apoptosis, and metabolism." Mol Cell Biol **19**(1): 1-11.
- Dasso, M. and R. T. Pu (1998). "Nuclear transport: run by Ran?" Am J Hum Genet **63**(2): 311-316.
- Davis, B. N., A. C. Hilyard, et al. (2008). "SMAD proteins control DROSHA-mediated microRNA maturation." Nature **454**(7200): 56-61.

- de Curtis, I. (2001). "Cell migration: GAPs between membrane traffic and the cytoskeleton." EMBO reports **2**(4): 277-281.
- de Curtis, I. (2001). "Cell migration: GAPs between membrane traffic and the cytoskeleton." EMBO Rep **2**(4): 277-281.
- de la Cruz, J., D. Kressler, et al. (1999). "Unwinding RNA in *Saccharomyces cerevisiae*: DEAD-box proteins and related families." Trends Biochem Sci **24**(5): 192-198.
- Deberardinis, R. J., N. Sayed, et al. (2008). "Brick by brick: metabolism and tumor cell growth." Current opinion in genetics & development **18**(1): 54-61.
- Deisseroth, K., E. K. Heist, et al. (1998). "Translocation of calmodulin to the nucleus supports CREB phosphorylation in hippocampal neurons." Nature **392**(6672): 198-202.
- Demicheli, R., M. W. Retsky, et al. (2008). "The effects of surgery on tumor growth: a century of investigations." Annals of oncology : official journal of the European Society for Medical Oncology / ESMO **19**(11): 1821-1828.
- Deprez, J., D. Vertommen, et al. (1997). "Phosphorylation and activation of heart 6-phosphofructo-2-kinase by protein kinase B and other protein kinases of the insulin signaling cascades." J Biol Chem **272**(28): 17269-17275.
- Devreotes, P. and C. Janetopoulos (2003). "Eukaryotic chemotaxis: distinctions between directional sensing and polarization." J Biol Chem **278**(23): 20445-20448.
- Dietrich, K. A., C. V. Sindelar, et al. (2008). "The kinesin-1 motor protein is regulated by a direct interaction of its head and tail." Proc Natl Acad Sci U S A **105**(26): 8938-8943.
- Dombrauckas, J. D., B. D. Santarsiero, et al. (2005). "Structural basis for tumor pyruvate kinase M2 allosteric regulation and catalysis." Biochemistry **44**(27): 9417-9429.
- Elbers, J. R., J. A. van Unnik, et al. (1991). "Pyruvate kinase activity and isozyme composition in normal fibrous tissue and fibroblastic proliferations." Cancer **67**(10): 2552-2559.
- Elliott, K., K. Ge, et al. (2000). "The c-Myc-interacting adaptor protein Bin1 activates a caspase-independent cell death program." Oncogene **19**(41): 4669-4684.
- Endoh, H., K. Maruyama, et al. (1999). "Purification and identification of p68 RNA helicase acting as a transcriptional coactivator specific for the activation function 1 of human estrogen receptor alpha." Molecular and cellular biology **19**(8): 5363-5372.
- Endoh, H., K. Maruyama, et al. (1999). "Purification and identification of p68 RNA helicase acting as a transcriptional coactivator specific for the activation function 1 of human estrogen receptor alpha." Mol Cell Biol **19**(8): 5363-5372.
- Etiemble, J. and P. Boivin (1976). "Pyruvate kinase isozymes among human organs and blood cells." Enzyme **21**(4): 296-303.
- Etienne-Manneville, S. and A. Hall (2003). "Cell polarity: Par6, aPKC and cytoskeletal crosstalk." Curr Opin Cell Biol **15**(1): 67-72.
- Evan, G. I. and K. H. Vousden (2001). "Proliferation, cell cycle and apoptosis in cancer." Nature **411**(6835): 342-348.
- Evans, J. H. and J. J. Falke (2007). "Ca²⁺ influx is an essential component of the positive-feedback loop that maintains leading-edge structure and activity in macrophages." Proceedings of the National Academy of Sciences of the United States of America **104**(41): 16176-16181.
- Fairman, M. E., P. A. Maroney, et al. (2004). "Protein displacement by DExH/D "RNA helicases" without duplex unwinding." Science **304**(5671): 730-734.

- Fan, X. C. and J. A. Steitz (1998). "Overexpression of HuR, a nuclear-cytoplasmic shuttling protein, increases the in vivo stability of ARE-containing mRNAs." The EMBO journal **17**(12): 3448-3460.
- Fischer, U., J. Huber, et al. (1995). "The HIV-1 Rev activation domain is a nuclear export signal that accesses an export pathway used by specific cellular RNAs." Cell **82**(3): 475-483.
- Ford, M. J., I. A. Anton, et al. (1988). "Nuclear protein with sequence homology to translation initiation factor eIF-4A." Nature **332**(6166): 736-738.
- Fornerod, M., M. Ohno, et al. (1997). "CRM1 is an export receptor for leucine-rich nuclear export signals." Cell **90**(6): 1051-1060.
- Frank, D. A. (2007). "STAT3 as a central mediator of neoplastic cellular transformation." Cancer letters **251**(2): 199-210.
- Fried, H. and U. Kutay (2003). "Nucleocytoplasmic transport: taking an inventory." Cellular and molecular life sciences : CMLS **60**(8): 1659-1688.
- Friedl, P. and K. Wolf (2003). "Tumour-cell invasion and migration: diversity and escape mechanisms." Nat Rev Cancer **3**(5): 362-374.
- Fukuda, T., K. Yamagata, et al. (2007). "DEAD-box RNA helicase subunits of the Drosha complex are required for processing of rRNA and a subset of microRNAs." Nature cell biology **9**(5): 604-611.
- Fukuda, T., K. Yamagata, et al. (2007). "DEAD-box RNA helicase subunits of the Drosha complex are required for processing of rRNA and a subset of microRNAs." Nat Cell Biol **9**(5): 604-611.
- Fuller-Pace, F. V. (1994). "RNA helicases: modulators of RNA structure." Trends Cell Biol **4**(8): 271-274.
- Fuller-Pace, F. V. and S. Ali (2008). "The DEAD box RNA helicases p68 (Ddx5) and p72 (Ddx17): novel transcriptional co-regulators." Biochemical Society transactions **36**(Pt 4): 609-612.
- Gama-Carvalho, M. and M. Carmo-Fonseca (2001). "The rules and roles of nucleocytoplasmic shuttling proteins." FEBS Lett **498**(2-3): 157-163.
- Gao, S. P., K. G. Mark, et al. (2007). "Mutations in the EGFR kinase domain mediate STAT3 activation via IL-6 production in human lung adenocarcinomas." The Journal of clinical investigation **117**(12): 3846-3856.
- Garber, K. (2006). "Energy deregulation: licensing tumors to grow." Science **312**(5777): 1158-1159.
- Garcia-Gonzalo, F. R., C. Cruz, et al. (2003). "Interaction between HERC1 and M2-type pyruvate kinase." FEBS letters **539**(1-3): 78-84.
- Gatlin, J. C. and K. Bloom (2010). "Microtubule motors in eukaryotic spindle assembly and maintenance." Semin Cell Dev Biol **21**(3): 248-254.
- Gennerich, A. and R. D. Vale (2009). "Walking the walk: how kinesin and dynein coordinate their steps." Current opinion in cell biology **21**(1): 59-67.
- Gille, H. and J. Downward (1999). "Multiple ras effector pathways contribute to G(1) cell cycle progression." J Biol Chem **274**(31): 22033-22040.
- Godbout, R. and J. Squire (1993). "Amplification of a DEAD box protein gene in retinoblastoma cell lines." Proc Natl Acad Sci U S A **90**(16): 7578-7582.
- Goh, P. Y., Y. J. Tan, et al. (2004). "Cellular RNA helicase p68 relocalization and interaction with the hepatitis C virus (HCV) NS5B protein and the potential role of p68 in HCV RNA replication." Journal of virology **78**(10): 5288-5298.

- Goldfarb, D. S., A. H. Corbett, et al. (2004). "Importin alpha: a multipurpose nuclear-transport receptor." Trends in cell biology **14**(9): 505-514.
- Goldfarb, D. S., J. Gariepy, et al. (1986). "Synthetic peptides as nuclear localization signals." Nature **322**(6080): 641-644.
- Gomes, E. R., S. Jani, et al. (2005). "Nuclear movement regulated by Cdc42, MRCK, myosin, and actin flow establishes MTOC polarization in migrating cells." Cell **121**(3): 451-463.
- Gordan, J. D., J. A. Bertout, et al. (2007). "HIF-2alpha promotes hypoxic cell proliferation by enhancing c-myc transcriptional activity." Cancer Cell **11**(4): 335-347.
- Gorlich, D. and U. Kutay (1999). "Transport between the cell nucleus and the cytoplasm." Annu Rev Cell Dev Biol **15**: 607-660.
- Gorlich, D. and U. Kutay (1999). "Transport between the cell nucleus and the cytoplasm." Annual review of cell and developmental biology **15**: 607-660.
- Gough, A. H. and D. L. Taylor (1993). "Fluorescence anisotropy imaging microscopy maps calmodulin binding during cellular contraction and locomotion." J Cell Biol **121**(5): 1095-1107.
- Goulimari, P., T. M. Kitzing, et al. (2005). "Galpha12/13 is essential for directed cell migration and localized Rho-Dia1 function." J Biol Chem **280**(51): 42242-42251.
- Groner, B., P. Lucks, et al. (2008). "The function of Stat3 in tumor cells and their microenvironment." Seminars in cell & developmental biology **19**(4): 341-350.
- Hache, R. J., R. Tse, et al. (1999). "Nucleocytoplasmic trafficking of steroid-free glucocorticoid receptor." J Biol Chem **274**(3): 1432-1439.
- Hacker, H. J., P. Steinberg, et al. (1998). "Pyruvate kinase isoenzyme shift from L-type to M2-type is a late event in hepatocarcinogenesis induced in rats by a choline-deficient/DL-ethionine-supplemented diet." Carcinogenesis **19**(1): 99-107.
- Hainaut, P. and M. Hollstein (2000). "p53 and human cancer: the first ten thousand mutations." Adv Cancer Res **77**: 81-137.
- Hanahan, D. and R. A. Weinberg (2011). "Hallmarks of cancer: the next generation." Cell **144**(5): 646-674.
- Harris, D., Z. Zhang, et al. (2006). "Identification of cellular factors associated with the 3'-nontranslated region of the hepatitis C virus genome." Molecular & cellular proteomics : MCP **5**(6): 1006-1018.
- Hewitt, R. E., A. McMarlin, et al. (2000). "Validation of a model of colon cancer progression." J Pathol **192**(4): 446-454.
- Hewitt, R. E., A. McMarlin, et al. (2000). "Validation of a model of colon cancer progression." The Journal of pathology **192**(4): 446-454.
- Hill, C. S. (2009). "Nucleocytoplasmic shuttling of Smad proteins." Cell research **19**(1): 36-46.
- Hinrichsen, R. D. (1993). "Calcium and calmodulin in the control of cellular behavior and motility." Biochimica et biophysica acta **1155**(3): 277-293.
- Hirling, H., M. Scheffner, et al. (1989). "RNA helicase activity associated with the human p68 protein." Nature **339**(6225): 562-564.
- Hirokawa, N., Y. Noda, et al. (2009). "Kinesin superfamily motor proteins and intracellular transport." Nature reviews. Molecular cell biology **10**(10): 682-696.
- Ho, Y. D., J. L. Joyal, et al. (1999). "IQGAP1 integrates Ca²⁺/calmodulin and Cdc42 signaling." The Journal of biological chemistry **274**(1): 464-470.
- Horwitz, R. and D. Webb (2003). "Cell migration." Current biology : CB **13**(19): R756-759.

- Hoshino, A., J. A. Hirst, et al. (2007). "Regulation of cell proliferation by interleukin-3-induced nuclear translocation of pyruvate kinase." The Journal of biological chemistry **282**(24): 17706-17711.
- Hoshino, A., J. A. Hirst, et al. (2007). "Regulation of cell proliferation by interleukin-3-induced nuclear translocation of pyruvate kinase." J Biol Chem **282**(24): 17706-17711.
- Huang, S. (2007). "Regulation of metastases by signal transducer and activator of transcription 3 signaling pathway: clinical implications." Clinical cancer research : an official journal of the American Association for Cancer Research **13**(5): 1362-1366.
- Huang, Y. and Z. R. Liu (2002). "The ATPase, RNA unwinding, and RNA binding activities of recombinant p68 RNA helicase." J Biol Chem **277**(15): 12810-12815.
- Hunter, T. and J. A. Cooper (1985). "Protein-tyrosine kinases." Annual review of biochemistry **54**: 897-930.
- Huszar, D., M. E. Theoclitou, et al. (2009). "Kinesin motor proteins as targets for cancer therapy." Cancer Metastasis Rev **28**(1-2): 197-208.
- Iggo, R. D., D. J. Jamieson, et al. (1991). "p68 RNA helicase: identification of a nucleolar form and cloning of related genes containing a conserved intron in yeasts." Mol Cell Biol **11**(3): 1326-1333.
- Iggo, R. D. and D. P. Lane (1989). "Nuclear protein p68 is an RNA-dependent ATPase." EMBO J **8**(6): 1827-1831.
- Iggo, R. D. and D. P. Lane (1989). "Nuclear protein p68 is an RNA-dependent ATPase." The EMBO journal **8**(6): 1827-1831.
- Iglesias, P. A. and P. N. Devreotes (2008). "Navigating through models of chemotaxis." Curr Opin Cell Biol **20**(1): 35-40.
- Ignacak, J. and M. B. Stachurska (2003). "The dual activity of pyruvate kinase type M2 from chromatin extracts of neoplastic cells." Comparative biochemistry and physiology. Part B, Biochemistry & molecular biology **134**(3): 425-433.
- Ikura, M. (1996). "Calcium binding and conformational response in EF-hand proteins." Trends Biochem Sci **21**(1): 14-17.
- Insall, R. H. and L. M. Machesky (2009). "Actin dynamics at the leading edge: from simple machinery to complex networks." Dev Cell **17**(3): 310-322.
- Insall, R. H. and L. M. Machesky (2009). "Actin dynamics at the leading edge: from simple machinery to complex networks." Developmental cell **17**(3): 310-322.
- Jacobs, A. M., S. M. Nicol, et al. (2007). "SUMO modification of the DEAD box protein p68 modulates its transcriptional activity and promotes its interaction with HDAC1." Oncogene **26**(40): 5866-5876.
- Jang, D. J., M. Guo, et al. (2007). "Proteomic and biochemical studies of calcium- and phosphorylation-dependent calmodulin complexes in Mammalian cells." Journal of proteome research **6**(9): 3718-3728.
- Janknecht, R. (2002). "The versatile functions of the transcriptional coactivators p300 and CBP and their roles in disease." Histol Histopathol **17**(2): 657-668.
- Janknecht, R. (2010). "Multi-talented DEAD-box proteins and potential tumor promoters: p68 RNA helicase (DDX5) and its paralog, p72 RNA helicase (DDX17)." Am J Transl Res **2**(3): 223-234.
- Janssen, A. and R. H. Medema (2011). "Mitosis as an anti-cancer target." Oncogene **30**(25): 2799-2809.

- Jensen, E. D., L. Niu, et al. (2008). "p68 (Ddx5) interacts with Runx2 and regulates osteoblast differentiation." J Cell Biochem **103**(5): 1438-1451.
- Joyal, J. L., D. J. Burks, et al. (1997). "Calmodulin activates phosphatidylinositol 3-kinase." The Journal of biological chemistry **272**(45): 28183-28186.
- Kahlina, K., I. Goren, et al. (2004). "p68 DEAD box RNA helicase expression in keratinocytes. Regulation, nucleolar localization, and functional connection to proliferation and vascular endothelial growth factor gene expression." J Biol Chem **279**(43): 44872-44882.
- Kapeller, R., A. Toker, et al. (1995). "Phosphoinositide 3-kinase binds constitutively to alpha/beta-tubulin and binds to gamma-tubulin in response to insulin." The Journal of biological chemistry **270**(43): 25985-25991.
- Kau, T. R. and P. A. Silver (2003). "Nuclear transport as a target for cell growth." Drug Discov Today **8**(2): 78-85.
- Kau, T. R., J. C. Way, et al. (2004). "Nuclear transport and cancer: from mechanism to intervention." Nature reviews. Cancer **4**(2): 106-117.
- Kaverina, I., O. Krylyshkina, et al. (1999). "Microtubule targeting of substrate contacts promotes their relaxation and dissociation." J Cell Biol **146**(5): 1033-1044.
- Kennedy, S. G., A. J. Wagner, et al. (1997). "The PI 3-kinase/Akt signaling pathway delivers an anti-apoptotic signal." Genes Dev **11**(6): 701-713.
- Kim, D. J., K. S. Chan, et al. (2007). "Signal transducer and activator of transcription 3 (Stat3) in epithelial carcinogenesis." Molecular carcinogenesis **46**(8): 725-731.
- Kim, S. A., K. G. Heinze, et al. (2004). "Intracellular calmodulin availability accessed with two-photon cross-correlation." Proc Natl Acad Sci U S A **101**(1): 105-110.
- Kitamura, A., M. Nishizuka, et al. (2001). "Expression of p68 RNA helicase is closely related to the early stage of adipocyte differentiation of mouse 3T3-L1 cells." Biochem Biophys Res Commun **287**(2): 435-439.
- Kondoh, H., M. E. Leonart, et al. (2007). "A high glycolytic flux supports the proliferative potential of murine embryonic stem cells." Antioxidants & redox signaling **9**(3): 293-299.
- Krendel, M. and M. S. Mooseker (2005). "Myosins: tails (and heads) of functional diversity." Physiology (Bethesda) **20**: 239-251.
- Kudo, N., N. Matsumori, et al. (1999). "Leptomycin B inactivates CRM1/exportin 1 by covalent modification at a cysteine residue in the central conserved region." Proc Natl Acad Sci U S A **96**(16): 9112-9117.
- Kuge, S., M. Arita, et al. (2001). "Regulation of the yeast Yap1p nuclear export signal is mediated by redox signal-induced reversible disulfide bond formation." Mol Cell Biol **21**(18): 6139-6150.
- Kurosaka, S. and A. Kashina (2008). "Cell biology of embryonic migration." Birth defects research. Part C, Embryo today : reviews **84**(2): 102-122.
- la Cour, T., L. Kiemer, et al. (2004). "Analysis and prediction of leucine-rich nuclear export signals." Protein Eng Des Sel **17**(6): 527-536.
- Lafitte, D., A. J. Heck, et al. (1999). "Evidence of noncovalent dimerization of calmodulin." European journal of biochemistry / FEBS **261**(1): 337-344.
- Lahaye, F., F. Lespinasse, et al. (2010). "hMSH5 is a nucleocytoplasmic shuttling protein whose stability depends on its subcellular localization." Nucleic Acids Res **38**(11): 3655-3671.
- Lane, D. P. and W. K. Hoeffler (1980). "SV40 large T shares an antigenic determinant with a cellular protein of molecular weight 68,000." Nature **288**(5787): 167-170.

- Le Clainche, C. and M. F. Carrier (2008). "Regulation of actin assembly associated with protrusion and adhesion in cell migration." Physiological reviews **88**(2): 489-513.
- Le Roy, C. and J. L. Wrana (2005). "Signaling and endocytosis: a team effort for cell migration." Developmental cell **9**(2): 167-168.
- Lee, C. G. (2002). "RH70, a bidirectional RNA helicase, co-purifies with U1snRNP." J Biol Chem **277**(42): 39679-39683.
- Lee, J., H. K. Kim, et al. (2008). "Pyruvate kinase isozyme type M2 (PKM2) interacts and cooperates with Oct-4 in regulating transcription." Int J Biochem Cell Biol **40**(5): 1043-1054.
- Lee, J., H. K. Kim, et al. (2008). "Pyruvate kinase isozyme type M2 (PKM2) interacts and cooperates with Oct-4 in regulating transcription." The international journal of biochemistry & cell biology **40**(5): 1043-1054.
- Lee, J. C., G. X. Wang, et al. (2005). "Fusing DEDD with ubiquitin changes its intracellular localization and apoptotic potential." Apoptosis **10**(6): 1483-1495.
- Lee, K. K. and J. L. Workman (2007). "Histone acetyltransferase complexes: one size doesn't fit all." Nat Rev Mol Cell Biol **8**(4): 284-295.
- Lemaire, L. and U. A. Heinlein (1993). "High-level expression in male germ cells of murine P68 RNA helicase mRNA." Life Sci **52**(11): 917-926.
- Leone, G., J. DeGregori, et al. (1997). "Myc and Ras collaborate in inducing accumulation of active cyclin E/Cdk2 and E2F." Nature **387**(6631): 422-426.
- Li, Z., S. H. Kim, et al. (1999). "IQGAP1 and calmodulin modulate E-cadherin function." J Biol Chem **274**(53): 37885-37892.
- Liao, B., B. M. Paschal, et al. (1999). "Mechanism of Ca²⁺-dependent nuclear accumulation of calmodulin." Proc Natl Acad Sci U S A **96**(11): 6217-6222.
- Lin, C., L. Yang, et al. (2005). "ATPase/helicase activities of p68 RNA helicase are required for pre-mRNA splicing but not for assembly of the spliceosome." Molecular and cellular biology **25**(17): 7484-7493.
- Lin, J. and R. Arlinghaus (2008). "Activated c-Abl tyrosine kinase in malignant solid tumors." Oncogene **27**(32): 4385-4391.
- Linder, P., P. F. Lasko, et al. (1989). "Birth of the D-E-A-D box." Nature **337**(6203): 121-122.
- Lindsay, M. E., K. Plafker, et al. (2002). "Npap60/Nup50 is a tri-stable switch that stimulates importin-alpha:beta-mediated nuclear protein import." Cell **110**(3): 349-360.
- Liu, Y. C. and D. R. Storm (1990). "Regulation of free calmodulin levels by neuromodulin: neuron growth and regeneration." Trends in pharmacological sciences **11**(3): 107-111.
- Liu, Z. R. (2002). "p68 RNA helicase is an essential human splicing factor that acts at the U1 snRNA-5' splice site duplex." Molecular and cellular biology **22**(15): 5443-5450.
- Lowery, L. A. and D. Van Vactor (2009). "The trip of the tip: understanding the growth cone machinery." Nature reviews. Molecular cell biology **10**(5): 332-343.
- Loyola, A. and G. Almouzni (2004). "Histone chaperones, a supporting role in the limelight." Biochimica et biophysica acta **1677**(1-3): 3-11.
- Luby-Phelps, K., M. Hori, et al. (1995). "Ca(2+)-regulated dynamic compartmentalization of calmodulin in living smooth muscle cells." The Journal of biological chemistry **270**(37): 21532-21538.
- Luby-Phelps, K., M. Hori, et al. (1995). "Ca(2+)-regulated dynamic compartmentalization of calmodulin in living smooth muscle cells." J Biol Chem **270**(37): 21532-21538.

- Lusk, C. P., G. Blobel, et al. (2007). "Highway to the inner nuclear membrane: rules for the road." Nature reviews. Molecular cell biology **8**(5): 414-420.
- Luzzi, K. J., I. C. MacDonald, et al. (1998). "Multistep nature of metastatic inefficiency: dormancy of solitary cells after successful extravasation and limited survival of early micrometastases." The American journal of pathology **153**(3): 865-873.
- Luzzi, K. J., I. C. MacDonald, et al. (1998). "Multistep nature of metastatic inefficiency: dormancy of solitary cells after successful extravasation and limited survival of early micrometastases." Am J Pathol **153**(3): 865-873.
- Ma, C., Y. Rong, et al. (2008). "Extracellular matrix protein betaig-h3/TGFBI promotes metastasis of colon cancer by enhancing cell extravasation." Genes Dev **22**(3): 308-321.
- Marie, J., A. Kahn, et al. (1976). "Pyruvate kinase isozymes in man. I. M type isozymes in adult and foetal tissues, electrofocusing and immunological studies." Hum Genet **31**(1): 35-45.
- Marshall, C. (1999). "How do small GTPase signal transduction pathways regulate cell cycle entry?" Curr Opin Cell Biol **11**(6): 732-736.
- Martin, S. S., T. Haruta, et al. (1996). "Activated phosphatidylinositol 3-kinase is sufficient to mediate actin rearrangement and GLUT4 translocation in 3T3-L1 adipocytes." The Journal of biological chemistry **271**(30): 17605-17608.
- Mattila, P. K. and P. Lappalainen (2008). "Filopodia: molecular architecture and cellular functions." Nature reviews. Molecular cell biology **9**(6): 446-454.
- Mayer, T. U., T. M. Kapoor, et al. (1999). "Small molecule inhibitor of mitotic spindle bipolarity identified in a phenotype-based screen." Science **286**(5441): 971-974.
- Mazurek, S., C. B. Boschek, et al. (2005). "Pyruvate kinase type M2 and its role in tumor growth and spreading." Seminars in cancer biology **15**(4): 300-308.
- Mazurek, S. and E. Eigenbrodt (2003). "The tumor metabolome." Anticancer research **23**(2A): 1149-1154.
- McGuffin, L. J., K. Bryson, et al. (2000). "The PSIPRED protein structure prediction server." Bioinformatics **16**(4): 404-405.
- Merida, I. and A. Avila-Flores (2006). "Tumor metabolism: new opportunities for cancer therapy." Clin Transl Oncol **8**(10): 711-716.
- Mermelstein, P. G., K. Deisseroth, et al. (2001). "Calmodulin priming: nuclear translocation of a calmodulin complex and the memory of prior neuronal activity." Proceedings of the National Academy of Sciences of the United States of America **98**(26): 15342-15347.
- Miki, H., Y. Okada, et al. (2005). "Analysis of the kinesin superfamily: insights into structure and function." Trends Cell Biol **15**(9): 467-476.
- Miwa, S., K. Nakashima, et al. (1975). "Four new pyruvate kinase (PK) variants and a classical PK deficiency." Br J Haematol **29**(1): 157-169.
- Montell, D. J. (2008). "Morphogenetic cell movements: diversity from modular mechanical properties." Science **322**(5907): 1502-1505.
- Mooney, S. M., J. P. Grande, et al. (2010). "Sumoylation of p68 and p72 RNA helicases affects protein stability and transactivation potential." Biochemistry **49**(1): 1-10.
- Moore, M. S. and G. Blobel (1994). "A G protein involved in nucleocytoplasmic transport: the role of Ran." Trends Biochem Sci **19**(5): 211-216.
- Motohashi, N. (1991). "Phenothiazines and calmodulin (review)." Anticancer Res **11**(3): 1125-1164.
- Muirhead, H., D. A. Clayden, et al. (1986). "The structure of cat muscle pyruvate kinase." The EMBO journal **5**(3): 475-481.

- Nakagawa, Y., H. Morikawa, et al. (1999). "Overexpression of rck/p54, a DEAD box protein, in human colorectal tumours." Br J Cancer **80**(5-6): 914-917.
- Nakielnny, S. and G. Dreyfuss (1999). "Transport of proteins and RNAs in and out of the nucleus." Cell **99**(7): 677-690.
- Nicol, S. M., M. Causevic, et al. (2000). "The nuclear DEAD box RNA helicase p68 interacts with the nucleolar protein fibrillarin and colocalizes specifically in nascent nucleoli during telophase." Experimental cell research **257**(2): 272-280.
- Nicol, S. M., M. Causevic, et al. (2000). "The nuclear DEAD box RNA helicase p68 interacts with the nucleolar protein fibrillarin and colocalizes specifically in nascent nucleoli during telophase." Exp Cell Res **257**(2): 272-280.
- Niu, Y., F. Roy, et al. (2006). "A nuclear export signal and phosphorylation regulate Dok1 subcellular localization and functions." Molecular and cellular biology **26**(11): 4288-4301.
- Ogilvie, V. C., B. J. Wilson, et al. (2003). "The highly related DEAD box RNA helicases p68 and p72 exist as heterodimers in cells." Nucleic acids research **31**(5): 1470-1480.
- Okamura, H., J. Aramburu, et al. (2000). "Concerted dephosphorylation of the transcription factor NFAT1 induces a conformational switch that regulates transcriptional activity." Molecular cell **6**(3): 539-550.
- Perez-Terzic, C., A. M. Gacy, et al. (1999). "Structural plasticity of the cardiac nuclear pore complex in response to regulators of nuclear import." Circulation research **84**(11): 1292-1301.
- Pezzella-D'Alessandro, N., H. Le Moal, et al. (2001). "Calmodulin distribution and the actomyosin cytoskeleton in *Toxoplasma gondii*." The journal of histochemistry and cytochemistry : official journal of the Histochemistry Society **49**(4): 445-454.
- Plas, D. R., S. Talapatra, et al. (2001). "Akt and Bcl-xL promote growth factor-independent survival through distinct effects on mitochondrial physiology." J Biol Chem **276**(15): 12041-12048.
- Pollard, T. D. and G. G. Borisy (2003). "Cellular motility driven by assembly and disassembly of actin filaments." Cell **112**(4): 453-465.
- Pollard, T. D. and J. A. Cooper (2009). "Actin, a central player in cell shape and movement." Science **326**(5957): 1208-1212.
- Pronin, A. N., D. K. Satpaev, et al. (1997). "Regulation of G protein-coupled receptor kinases by calmodulin and localization of the calmodulin binding domain." J Biol Chem **272**(29): 18273-18280.
- Rasmussen, C. D., K. P. Lu, et al. (1992). "Calmodulin and cell cycle control." Journal of physiology, Paris **86**(1-3): 83-88.
- Rathmell, J. C., C. J. Fox, et al. (2003). "Akt-directed glucose metabolism can prevent Bax conformation change and promote growth factor-independent survival." Mol Cell Biol **23**(20): 7315-7328.
- Rehberg, S., P. Lischka, et al. (2002). "Sox10 is an active nucleocytoplasmic shuttle protein, and shuttling is crucial for Sox10-mediated transactivation." Mol Cell Biol **22**(16): 5826-5834.
- Ridley, A. J. (1994). "Membrane ruffling and signal transduction." BioEssays : news and reviews in molecular, cellular and developmental biology **16**(5): 321-327.
- Ridley, A. J., M. A. Schwartz, et al. (2003). "Cell migration: integrating signals from front to back." Science **302**(5651): 1704-1709.

- Robles, A. I., M. L. Rodriguez-Puebla, et al. (1998). "Reduced skin tumor development in cyclin D1-deficient mice highlights the oncogenic ras pathway in vivo." Genes Dev **12**(16): 2469-2474.
- Rodriguez, M. S., C. Dargemont, et al. (2004). "Nuclear export of RNA." Biol Cell **96**(8): 639-655.
- Rodriguez, O. C., A. W. Schaefer, et al. (2003). "Conserved microtubule-actin interactions in cell movement and morphogenesis." Nature cell biology **5**(7): 599-609.
- Roossien, F. F., J. Brink, et al. (1983). "A simple procedure for the synthesis of [32P]phosphoenolpyruvate via the pyruvate kinase exchange reaction at equilibrium." Biochimica et biophysica acta **760**(1): 185-187.
- Rossow, K. L. and R. Janknecht (2003). "Synergism between p68 RNA helicase and the transcriptional coactivators CBP and p300." Oncogene **22**(1): 151-156.
- Rudolph, B., R. Saffrich, et al. (1996). "Activation of cyclin-dependent kinases by Myc mediates induction of cyclin A, but not apoptosis." EMBO J **15**(12): 3065-3076.
- Russell, R. R., 3rd, R. Bergeron, et al. (1999). "Translocation of myocardial GLUT-4 and increased glucose uptake through activation of AMPK by AICAR." Am J Physiol **277**(2 Pt 2): H643-649.
- Schneider, J., K. Neu, et al. (2002). "Tumor M2-pyruvate kinase in lung cancer patients: immunohistochemical detection and disease monitoring." Anticancer research **22**(1A): 311-318.
- Schneider, J., C. Schindewolf, et al. (1988). "A mutant SV40 large T antigen interferes with nuclear localization of a heterologous protein." Cell **54**(1): 117-125.
- Schnitzer, M. J. and S. M. Block (1997). "Kinesin hydrolyses one ATP per 8-nm step." Nature **388**(6640): 386-390.
- Schwartzenberg-Bar-Yoseph, F., M. Armoni, et al. (2004). "The tumor suppressor p53 down-regulates glucose transporters GLUT1 and GLUT4 gene expression." Cancer Res **64**(7): 2627-2633.
- Sears, R., G. Leone, et al. (1999). "Ras enhances Myc protein stability." Mol Cell **3**(2): 169-179.
- Sears, R. C. and J. R. Nevins (2002). "Signaling networks that link cell proliferation and cell fate." J Biol Chem **277**(14): 11617-11620.
- Segditsas, S. and I. Tomlinson (2006). "Colorectal cancer and genetic alterations in the Wnt pathway." Oncogene **25**(57): 7531-7537.
- Seger, R. and E. G. Krebs (1995). "The MAPK signaling cascade." FASEB J **9**(9): 726-735.
- Sehgal, P. B. (2008). "Paradigm shifts in the cell biology of STAT signaling." Seminars in cell & developmental biology **19**(4): 329-340.
- Semenza, G. L. (2007). "HIF-1 mediates the Warburg effect in clear cell renal carcinoma." J Bioenerg Biomembr **39**(3): 231-234.
- Sengoku, T., O. Nureki, et al. (2006). "Structural basis for RNA unwinding by the DEAD-box protein Drosophila Vasa." Cell **125**(2): 287-300.
- Shariat-Madar, Z., A. M. Goldsmith, et al. (1997). "Effect of continuous phorbol ester treatment on muscarinic receptor-mediated calmodulin redistribution in SK-N-SH neuroblastoma cells." Journal of neurochemistry **68**(1): 40-46.
- Shen, X., C. A. Valencia, et al. (2005). "Scanning the human proteome for calmodulin-binding proteins." Proceedings of the National Academy of Sciences of the United States of America **102**(17): 5969-5974.

- Shibuya, T., T. O. Tange, et al. (2004). "eIF4AIII binds spliced mRNA in the exon junction complex and is essential for nonsense-mediated decay." Nature structural & molecular biology **11**(4): 346-351.
- Shin, S., K. L. Rossow, et al. (2007). "Involvement of RNA helicases p68 and p72 in colon cancer." Cancer Res **67**(16): 7572-7578.
- Shyu, A. B. and M. F. Wilkinson (2000). "The double lives of shuttling mRNA binding proteins." Cell **102**(2): 135-138.
- Song, H., X. Jin, et al. (2004). "Stat3 upregulates MEK5 expression in human breast cancer cells." Oncogene **23**(50): 8301-8309.
- Spoden, G. A., D. Morandell, et al. (2009). "The SUMO-E3 ligase PIAS3 targets pyruvate kinase M2." Journal of cellular biochemistry **107**(2): 293-302.
- Spoden, G. A., D. Morandell, et al. (2009). "The SUMO-E3 ligase PIAS3 targets pyruvate kinase M2." J Cell Biochem **107**(2): 293-302.
- Sriram, G., J. A. Martinez, et al. (2005). "Single-gene disorders: what role could moonlighting enzymes play?" American journal of human genetics **76**(6): 911-924.
- Steeg, P. S. (2006). "Tumor metastasis: mechanistic insights and clinical challenges." Nat Med **12**(8): 895-904.
- Steeg, P. S. (2006). "Tumor metastasis: mechanistic insights and clinical challenges." Nature medicine **12**(8): 895-904.
- Stehno-Bittel, L., C. Perez-Terzic, et al. (1995). "Diffusion across the nuclear envelope inhibited by depletion of the nuclear Ca²⁺ store." Science **270**(5243): 1835-1838.
- Stetak, A., R. Veress, et al. (2007). "Nuclear translocation of the tumor marker pyruvate kinase M2 induces programmed cell death." Cancer research **67**(4): 1602-1608.
- Stetak, A., R. Veress, et al. (2007). "Nuclear translocation of the tumor marker pyruvate kinase M2 induces programmed cell death." Cancer Res **67**(4): 1602-1608.
- Stevenson, R. J., S. J. Hamilton, et al. (1998). "Expression of the 'dead box' RNA helicase p68 is developmentally and growth regulated and correlates with organ differentiation/maturation in the fetus." J Pathol **184**(4): 351-359.
- Stevenson, R. J., S. J. Hamilton, et al. (1998). "Expression of the 'dead box' RNA helicase p68 is developmentally and growth regulated and correlates with organ differentiation/maturation in the fetus." The Journal of pathology **184**(4): 351-359.
- Sun, F. X., A. R. Sasson, et al. (1999). "An ultra-metastatic model of human colon cancer in nude mice." Clin Exp Metastasis **17**(1): 41-48.
- Sun, F. X., A. R. Sasson, et al. (1999). "An ultra-metastatic model of human colon cancer in nude mice." Clinical & experimental metastasis **17**(1): 41-48.
- Swaney, K. F., C. H. Huang, et al. (2010). "Eukaryotic chemotaxis: a network of signaling pathways controls motility, directional sensing, and polarity." Annu Rev Biophys **39**: 265-289.
- Takai, E., X. Tan, et al. (2005). "Correlation of translocation of tight junction protein Zonula occludens-1 and activation of epidermal growth factor receptor in the regulation of invasion of pancreatic cancer cells." Int J Oncol **27**(3): 645-651.
- Taketo, M. M. and W. Edlmann (2009). "Mouse models of colon cancer." Gastroenterology **136**(3): 780-798.
- Teruel, M. N., W. Chen, et al. (2000). "Differential codes for free Ca²⁺-calmodulin signals in nucleus and cytosol." Current biology : CB **10**(2): 86-94.

- Thorogate, R. and K. Torok (2004). "Ca²⁺-dependent and -independent mechanisms of calmodulin nuclear translocation." Journal of cell science **117**(Pt 24): 5923-5936.
- Tsutsumi, S., H. Kuwano, et al. (2001). "Animal model of para-aortic lymph node metastasis." Cancer Lett **169**(1): 77-85.
- Tsutsumi, S., H. Kuwano, et al. (2001). "Animal model of para-aortic lymph node metastasis." Cancer letters **169**(1): 77-85.
- Vale, R. D. (2003). "The molecular motor toolbox for intracellular transport." Cell **112**(4): 467-480.
- Vale, R. D., F. Malik, et al. (1992). "Directional instability of microtubule transport in the presence of kinesin and dynein, two opposite polarity motor proteins." The Journal of cell biology **119**(6): 1589-1596.
- Valiron, O., N. Caudron, et al. (2001). "Microtubule dynamics." Cell Mol Life Sci **58**(14): 2069-2084.
- Vallee, R. B., G. E. Seale, et al. (2009). "Emerging roles for myosin II and cytoplasmic dynein in migrating neurons and growth cones." Trends in cell biology **19**(7): 347-355.
- Vallee, R. B., G. E. Seale, et al. (2009). "Emerging roles for myosin II and cytoplasmic dynein in migrating neurons and growth cones." Trends Cell Biol **19**(7): 347-355.
- van Berkel, T. J., H. R. de Jonge, et al. (1974). "Kinetic evidence for the presence of two forms of M2-type pyruvate kinase in rat small intestine." Biochem Biophys Res Commun **60**(1): 398-405.
- van Veelen, C. W., H. Verbiest, et al. (1978). "Isozymes of pyruvate kinase from human brain, meningiomas, and malignant gliomas." Cancer research **38**(12): 4681-4687.
- Verhey, K. J. and J. W. Hammond (2009). "Traffic control: regulation of kinesin motors." Nature reviews. Molecular cell biology **10**(11): 765-777.
- Verkhovsky, A. B., T. M. Svitkina, et al. (1999). "Self-polarization and directional motility of cytoplasm." Curr Biol **9**(1): 11-20.
- Vicente-Manzanares, M., D. J. Webb, et al. (2005). "Cell migration at a glance." Journal of cell science **118**(Pt 21): 4917-4919.
- Wang, H., X. Gao, et al. (2009). "P68 RNA helicase is a nucleocytoplasmic shuttling protein." Cell research **19**(12): 1388-1400.
- Wang, H., Y. Liu, et al. (2007). "The recombinant beta subunit of C-phycoyanin inhibits cell proliferation and induces apoptosis." Cancer letters **247**(1): 150-158.
- Warburg, O. (1956). "On the origin of cancer cells." Science **123**(3191): 309-314.
- Watanabe, M., M. Fukuda, et al. (1999). "Involvement of CRM1, a nuclear export receptor, in mRNA export in mammalian cells and fission yeast." Genes to cells : devoted to molecular & cellular mechanisms **4**(5): 291-297.
- Watson, C. J. and K. Neoh (2008). "The Stat family of transcription factors have diverse roles in mammary gland development." Seminars in cell & developmental biology **19**(4): 401-406.
- Webb, D. J., J. T. Parsons, et al. (2002). "Adhesion assembly, disassembly and turnover in migrating cells -- over and over and over again." Nature cell biology **4**(4): E97-100.
- Wedlich-Soldner, R. and R. Li (2003). "Spontaneous cell polarization: undermining determinism." Nat Cell Biol **5**(4): 267-270.
- Wei, C., X. Wang, et al. (2009). "Calcium flickers steer cell migration." Nature **457**(7231): 901-905.

- Wei, Y. and M. H. Hu (2001). "[The study of P68 RNA helicase on cell transformation]." Yi Chuan Xue Bao **28**(11): 991-996.
- Weiss, L., E. Grundmann, et al. (1986). "Haematogenous metastatic patterns in colonic carcinoma: an analysis of 1541 necropsies." J Pathol **150**(3): 195-203.
- Wen, W., J. L. Meinkoth, et al. (1995). "Identification of a signal for rapid export of proteins from the nucleus." Cell **82**(3): 463-473.
- Wennstrom, S., P. Hawkins, et al. (1994). "Activation of phosphoinositide 3-kinase is required for PDGF-stimulated membrane ruffling." Current biology : CB **4**(5): 385-393.
- Wilson, B. J., G. J. Bates, et al. (2004). "The p68 and p72 DEAD box RNA helicases interact with HDAC1 and repress transcription in a promoter-specific manner." BMC Mol Biol **5**: 11.
- Wrighton, K. H., X. Lin, et al. (2009). "Phospho-control of TGF-beta superfamily signaling." Cell research **19**(1): 8-20.
- Xie, H., M. A. Pallerio, et al. (1998). "EGF receptor regulation of cell motility: EGF induces disassembly of focal adhesions independently of the motility-associated PLCgamma signaling pathway." Journal of cell science **111** (Pt 5): 615-624.
- Xie, T. X., F. J. Huang, et al. (2006). "Activation of stat3 in human melanoma promotes brain metastasis." Cancer research **66**(6): 3188-3196.
- Xu, J., D. C. Cole, et al. (2008). "Inhibition of the signal transducer and activator of transcription-3 (STAT3) signaling pathway by 4-oxo-1-phenyl-1,4-dihydroquinoline-3-carboxylic acid esters." Journal of medicinal chemistry **51**(14): 4115-4121.
- Xu, L. and J. Massague (2004). "Nucleocytoplasmic shuttling of signal transducers." Nature reviews. Molecular cell biology **5**(3): 209-219.
- Yager, J. D. and N. E. Davidson (2006). "Estrogen carcinogenesis in breast cancer." N Engl J Med **354**(3): 270-282.
- Yamakita, Y., F. Oosawa, et al. (2003). "Caldesmon inhibits Arp2/3-mediated actin nucleation." J Biol Chem **278**(20): 17937-17944.
- Yang, J. and S. Kornbluth (1999). "All aboard the cyclin train: subcellular trafficking of cyclins and their CDK partners." Trends Cell Biol **9**(6): 207-210.
- Yang, L., C. Lin, et al. (2005). "Phosphorylations of DEAD box p68 RNA helicase are associated with cancer development and cell proliferation." Molecular cancer research : MCR **3**(6): 355-363.
- Yang, L., C. Lin, et al. (2005). "Signaling to the DEAD box--regulation of DEAD-box p68 RNA helicase by protein phosphorylations." Cell Signal **17**(12): 1495-1504.
- Yang, L., C. Lin, et al. (2006). "P68 RNA helicase mediates PDGF-induced epithelial mesenchymal transition by displacing Axin from beta-catenin." Cell **127**(1): 139-155.
- Yang, L., C. Lin, et al. (2007). "A double tyrosine phosphorylation of P68 RNA helicase confers resistance to TRAIL-induced apoptosis." Oncogene **26**(41): 6082-6092.
- Yang, L., C. Lin, et al. (2007). "Phosphorylation of p68 RNA helicase plays a role in platelet-derived growth factor-induced cell proliferation by up-regulating cyclin D1 and c-Myc expression." J Biol Chem **282**(23): 16811-16819.
- Yang, L. and Z. R. Liu (2004). "Bacterially expressed recombinant p68 RNA helicase is phosphorylated on serine, threonine, and tyrosine residues." Protein expression and purification **35**(2): 327-333.

- Yang, L., J. Yang, et al. (2004). "Phosphorylation of p68 RNA helicase regulates RNA binding by the C-terminal domain of the protein." Biochem Biophys Res Commun **314**(2): 622-630.
- Yang, X. J., V. V. Ogryzko, et al. (1996). "A p300/CBP-associated factor that competes with the adenoviral oncoprotein E1A." Nature **382**(6589): 319-324.
- Zhang, B., S. K. Halder, et al. (2010). "Antimetastatic role of Smad4 signaling in colorectal cancer." Gastroenterology **138**(3): 969-980 e961-963.
- Zhu, J. and F. McKeon (2000). "Nucleocytoplasmic shuttling and the control of NF-AT signaling." Cellular and molecular life sciences : CMLS **57**(3): 411-420.
- Zoller, M. (2009). "Tetraspanins: push and pull in suppressing and promoting metastasis." Nature reviews. Cancer **9**(1): 40-55.
- Zwerschke, W., S. Mazurek, et al. (1999). "Modulation of type M2 pyruvate kinase activity by the human papillomavirus type 16 E7 oncoprotein." Proc Natl Acad Sci U S A **96**(4): 1291-1296.

APPENDICES

A. THE RECOMBINANT β SUBUNIT OF C-PHYCOCYANIN INHIBITS CELL PROLIFERATION AND INDUCES APOPTOSIS

A.1 Abstract

C-Phycocyanin (C-PC) from blue-green algae has been reported to have various pharmacological characteristics, including anti-inflammatory and anti-tumor activities. In this study, we expressed the β -subunit of C-PC (ref to as C-PC/ β) in *E. coli*. We found that the recombinant C-PC/ β has anticancer properties. Under the treatment of 5 μ M of the recombinant C-PC/ β , four different cancer cell lines accrued high proliferation inhibition and apoptotic induction. Substantially lower response occurred in non-cancer cells. We investigated the mechanism by which C-PC/ β inhibits cancer cell proliferation and induces apoptosis. We found that the C-PC/ β interacts with membrane-associated β -tubulin and glyceraldehyde-3-phosphate dehydrogenase (GAPDH). Under the treatment of the C-PC/ β , depolymerization of microtubules and actin-filaments were observed. The cells underwent apoptosis with an increase in caspase-3, caspase-8 activities. Cell cycle was arrested at the G0/G1 phase under the treatment of C-PC/ β . In addition, the nuclear level of GAPDH decreased significantly. Decrease in nuclear level of GAPDH prevents cell cycle from entering into the S phase. Inhibition of cancer cell proliferation and induction of apoptosis may potentate the C-PC/ β as a promising cancer prevention or therapy agent.

A.2 Introduction

C-Phycocyanin (C-PC) is a photoharvesting pigment that provides the intense blue color in blue-green algae. Due to its deep and intense color, C-PC is widely used as natural dye for various purposes [1]. C-PC is a non-toxic biliprotein consisting of α - and β - subunits. It exists as

a monomer, trimer, or hexamer aggregation in native conditions [2]. The α and β subunits of C-PC do not share any significant sequence homology. Expression separately in bacterial *E. coli* reveals that the α subunit of C-PC is easily self-aggregated during expression and purification at physiological conditions, indicating that interactions between the α subunits may contribute to the force for the C-PC trimeric aggregation. On the other hand, the C-PC/ β can be expressed and purified as soluble recombinant protein in *E. coli* (unpublished observation). C-PC has recently been reported to have many pharmacological characteristics. Its properties of anti-inflammatory [3, 4], anti-oxidant [4], and radical scavenging [5] are well documented. Recently, C-PC was demonstrated to have anti-tumor activity [6, 7]. It was demonstrated that C-PC inhibits cyclooxygenase-2 [8]. It was shown that C-PC induces apoptosis by promoting the changes in the Bcl-2/Bax ratio and releases of cytochrome *c* into the cytosol. Furthermore, treatment of a leukemia cell line with C-PC enhanced the cleavage of poly (ADP) ribose polymerase (PRAP), which contributes an important mechanism for apoptosis [7]. The activity of C-PC in induction of cancer cell apoptosis and relative low-toxicity toward non-cancer cells makes it a very good candidate as a cancer chemoprevention agent. However, the molecular mechanism underlying the anti-tumor and anti-cancer activities of C-PC is not well understood. In the present study, evidence that the recombinant C-PC/ β is an inhibitor for cell proliferation and an inducer for cancer cell apoptosis is presented. The C-PC/ β inhibits cell proliferation and promotes cancer cell apoptosis by depolymerizing the microtubule/microfilaments, arresting the cell cycle at G0/G1 phase, and activating caspases -3 and -8. Our studies demonstrated a new insight into molecular mechanism by which C-PC has anti-tumor activity. More importantly, our studies demonstrated that the C-PC/ β alone has anti-tumor activity. The action of β -subunit may be different from that of the whole C-PC protein.

A.3 Materials and methods

A.3.1 Cell lines and culture

Cell line 686LN was derived from a squamous cell carcinoma of the head and neck patient's metastatic tumor. Cell line 686LN-M4C1 is a high metastatic derivative of 686LN. Both 686LN and 686LN-M4C1 are gifts from Dr. George Z. Chen, at Emory University. All other cell lines were purchased from ATCC and grown by following the vendor's instructions. K562 is a chronic myelogenous leukemia cell line. HT-29 is a colorectal adenocarcinoma cell line. C5/MJ is a cell line derived from normal T lymphocytes. RPMI 1788 is a cell line derived from normal B lymphocytes and immortalized by EBNA.

A.3.2 Plasmid construction

The published gene sequence of the C-PC/ β was obtained from www.Pubmed.com (Accession No. X05239). Living alga, *Anabaena* PCC 7120 (UTEX) was obtained from the culture collection of algae at the University of Texas at Austin. The *Anabaena* pellet was centrifuged and collected when the alga reached the exponential growth phase in BG11 medium. The alga was pelleted in preparation for PCR. Primers used to amplify the C-PC/ β were: 5'-GGGGATCCATGACATTAGACGTATTTA-3' and 5'-GGGAATTCTTTAACCAACAGCAGCAGCAG-3'. The DNA code C-PC/ β was obtained via whole cell PCR [9] and was cloned into BamHI and EcoRI sites of pGEX-2T (pGEX-2T- β). The C-PC/ β expressed consists of the C-PC/ β fused at the C terminus to a GST sequence. The constructed plasmid was verified via DNA auto-sequencing.

A.3.3 Expression, purification, concentration and refolding of the recombinant C-PC/ β

The procedure for expression of the recombinant C-PC/ β is similar to that was described in our previous report [10]. Briefly, the constructed plasmid, pGEX-2T- β , was transformed into

E. coli BL-21 codonplus®, and the expression of the recombinant protein was induced by 0.1 mM IPTG for 4.5 hours. Bacteria were harvested and underwent a freeze-thaw cycle followed by sonication disruption in lysis buffer (1% N-lauroyl sarcosine, 1mM EDTA, 500uM PMSF, 10mM DTT in PBS, pH 7.3, pre-cooled to 4 oC). The GST-fusion protein (GST: C-PC/β) was purified over a glutathione-agarose column (Sigma). The C-PC/β was cleaved overnight by thrombin. The recombinant proteins (GST:C-PC/β, C-PC/β, and GST) were further purified over a Sephadex 200 gel-filtration column. The obtained recombinant proteins were dialyzed and refolded according to the method recommended by the protein refolding kit (Novagen). Finally, the expressed and purified GST:C-PC/β was analyzed by MALDI mass spectrometry.

A.3.4 Proliferation of cancer cells and non-cancer cells

Cell proliferation was determined using an MTT assay [11]. Cells were seeded into a 96-well plate (2×10⁴/ well) with appropriate fresh medium (with 10% FCS). The cultured cells were first treated with indicated concentrations of recombinant GST:C-PC/β, GST alone, or PBS buffer only (PBS buffered, pH 7.3) for 48 hours. After treatment, MTT assays were performed using a commercially available MTT kit (Roche). The absorbance was determined on a multi-well plate reader (PerkinElmer precisely 1420 multilabel counting). The value was determined by averaging triplicate sample measurements.

A.3.5 Immunofluorescent confocal microscopy

The cells were seeded on chambered microslides (Molecular Probes) and treated as indicated. The cells were washed, fixed, and permeabilized with 4% formaldehyde and 0.1% Triton X-100 in 1× PBS. The cells were then blocked with Image-iT™ FX signal enhancer (Molecular Probes), and subsequently incubated with appropriate antibodies for 1 hour. After extensive wash, the samples were incubated with Alexa Fluor 488 (Molecular Probes) (1:1000)

to stain primary antibodies. Microslides were washed and mounted in ProLong® Gold antifade reagent with DAPI (Molecular Probes) and viewed using a Zeiss LSM510 Confocal Microscope.

A.3.6 Apoptosis, caspases activities, and cell cycle analyses

Cells were inoculated into a 12-well plate (2×10⁵/well) with appropriate fresh medium and treated as indicated in figures. Apoptosis of cells were analyzed by Cell Death Detection ELISAPLUS kit (Roche). Cell apoptosis was expressed as enrichment of mono- and oligonucleosomes released into the cytoplasm. The specific enrichment of mono- and oligonucleosomes released into the cytoplasm was calculated using the formula: enrichment factor = absorbance of the sample (treated) / absorbance of the corresponding negative control (non-treated). For the caspase assays, cells were collected after treatment for 24 hours. 1×RIPA buffer with protease inhibitors was used to prepare whole cell lysates. 50µg of the protein was used in the immunoblotting. Caspase activities were detected by immunoblots using appropriate antibodies: monoclonal antibodies, anti-caspase 3 (Cell Signalling), anti-caspase 8 (Cell Signalling), and polyclonal antibody of anti-cleaved-caspase 3 (Cell Signalling). For cell cycle analyses, the cells were harvested and washed in PBS. The cells were then fixed with 1% paraformaldehyde and stored in 70% ethanol at -20 °C. Cells were stained with 0.5 ml PI/RNase staining buffer (BD Bioscience) for 15 minutes at 37 °C and analyzed by fluorescence-activated cell sorting (FACS) Becton Dickinson.

A.3.7 GST pull-down and co-immunoprecipitation

The GST tagged C-PC/β was pre-bound to the glutathione-agarose beads. The GST moiety and the column were used as controls. The beads were incubated with the membrane protein extracts made from 686LN-M4C1 cells in PBS buffer with 0.5% NP-40 overnight at 4 °C. The agarose beads were washed 5 times with PBS buffer containing 0.5% NP-40. The GST

pull-down proteins were separated by SDS-PAGE. The gels were stained with the gelcode® blue stain reagent (Pierce). The identified protein bands (pulled-down by the C-PC/ β) were sliced out. The gels slices were treated with the ProteoProfile™ Trypsin In-Gel Digest kit (Sigma). The digested samples were analyzed by TOF/TOF-MS. The pull-down proteins were further analyzed by immunoblot using antibodies against β -tubulin (Sigma) and GAPDH (Chemicon). The interactions of C-PC/ β with β -tubulin and GAPDH were also shown by co-immunoprecipitates using polyclonal antibody against GAPDH (abcam) or polyclonal antibody against β -tubulin (abcam), followed by immunoblot using antibodies against β -tubulin (Sigma), GST (CALBiochem) and GAPDH (Chemicon).

A.3.8 Soluble and assembled tubulin / actin

Soluble (depolymerized) tubulin/actin and assembled (polymerized) were analyzed by the same experimental procedure described previously [12]. Briefly, 686LN-M4C1 cells were treated as indicated in figures for 24 hours. After treatments, cells were washed with PBS containing 0.5 μ g/ml Paclitaxel (Sigma), and lysed with 100 μ L of lysis buffer (20mM Tris-HCl, 0.5% NP-40, 1mM MgCl₂, 2mM EGTA, and 0.5 μ g/ml Paclitaxel). Then the samples were vortexed and centrifuged at 12,000 \times g for 10 min at 4 oC. Supernatants containing depolymerized tubulin/actin were separated from pellets containing polymerized tubulin/actin. The pellets were resuspended in 100 μ l lysis buffer without paclitaxel. 14% SDS-PAGE gels were used to separate proteins. The relative quantity of depolymerized tubulin/actin and polymerized tubulin/actin were analyzed by immunoblot using antibodies against β -tubulin (Sigma) and actin (Santa cruz biotechnology).

A.3.9 Subcellular localization of GAPDH

686LN-M4C1 cells were grown and treated as indicated in figures. The cells were washed with pre-cooled PBS and the Nuclear Extraction kit was used to preparation of nuclear extracts. 115 μg of the nuclear proteins were used for the immunoblotting to detect the level of nuclear GAPDH. Meanwhile, 50 μg of the whole cell lysate proteins were used to measure the expression level of GAPDH. A 14% SDS-PAGE gel was utilized to separate the proteins and immunoblots were probed using monoclonal antibodies against GAPDH (Chemicon) and monoclonal antibody against β -tubulin (Sigma).

A.4 Results

A.4.1 Expression and purification of recombinant C-PC/ β in *E. coli*

Anabaena PCC 7120 is among the most primitive life forms on earth. Its cellular structure is a simple prokaryote. We carried out whole cell PCR and obtained a DNA fragment that coded for C-PC/ β . Sequencing results confirm the identity of the DNA (by comparing to the C-PC/ β in databases). The DNA fragment was cloned into the expression vector pGEX-2T and the C-PC/ β was subsequently expressed in *E. coli* BL-21 as a GST-fusion protein. High expression level of C-PC/ β was observed (Fig.A.1A). After purification over a glutathione-agarose beads column and a Sephadex 200 gel-filtration column, high purity and concentration of the recombinant proteins were obtained. The concentration of the C-PC/ β protein was estimated to be 0.9 mg/ml. Molecular weight of obtained recombinant proteins was determined by MALDI-TOF mass spectrometry (Fig.A.1B). The mass spectrometry results indicated that the obtained GST:C-PC/ β had a MW of 45.4 kDa. This molecular weights was consistent with the corresponding calculated MWs. We also attempted to express and purify the α subunit of C-PC. However, the α subunit of C-PC rapidly aggregates in bacterial inclusion body. We purified the

insoluble α subunit of C-PC under denaturing condition and refolded the protein subsequently. Nevertheless, the refolded α subunit re-aggregated shortly after elution (data not shown).

A.4.2 The C-PC/ β inhibited cell proliferation

C-PC was reported to inhibit cell proliferation in a number of cancer cell lines [6] [7]. To test whether the recombinant C-PC/ β also inhibits cell growth, we carried out MTT assays with a number of cancer cell lines and two normal cell lines. Growth of all cancer cells was largely inhibited by treatment with C-PC/ β (Fig.A.2A). The greatest inhibitory effect on cell proliferation occurred to 686LN-M4C1 cells (inhibitory ratio was 60.4%, Fig.A.2A). On the other hand, the C-PC/ β had a minor inhibitory effect on growth of non-cancer cells (inhibitory ratios of C5/MJ and RPMI 1788 cells were 29.7% and 25.2% respectively, Fig.A.2A). As a control, GST alone had no significant effects on the growth of any of the cell lines tested. The results suggested that the recombinant C-PC/ β inhibits cell growth. We noticed that the morphology of the cancer cells changed when the cells were treated with the C-PC/ β . 686LN-M4C1 cells became non-transparent and distorted (Fig.A.2B). Other cancer cell lines also changed significantly upon the treatment with C-PC/ β . The majority of K562 cells changed from a round to a spindle-like morphology. HT29 cells grew sparsely. The 686LN cells became clustered and distorted. In contrast, no significant changes in the morphology of non-cancer cells were observed under the same treatments (Fig.A.2B).

A.4.3 Recombinant C-PC/ β induces apoptosis and cell cycle arrest

We speculated that both cell growth inhibition and cell morphology changes were due to induction of apoptosis by the C-PC/ β treatment. To test the speculation, we examined apoptosis with cancer and non-cancer cells using a commercially available apoptosis kit (detection of mono- and oligonucleosomes in the cytoplasm). Our experiments demonstrated that apoptosis

was induced in three cancer cell lines upon the C-PC/ β treatment (Fig.A.3A) with the metastatic head and neck cancer cells, 686LN-M4C1, exhibiting the highest level of apoptotic induction. As a control, GST alone did not induce apoptosis in any of the cells tested (Fig.A.3A). No clear apoptosis was observed with non-cancer cells under the treatment with C-PC/ β (Fig.A.3A). Activation of different caspases is often associated with cell apoptosis. Thus, we examined the caspase activity that may be activated by the C-PC/ β treatment. Since, the metastatic head and neck cancer cells, 686LN-M4C1, suffered the highest degree of growth inhibition and apoptosis, we chose this cell line as our test system for probing caspase activity. Under the treatment of the C-PC/ β , both caspases 8 and 3 were activated as revealed by the cleavage of pre-caspase 8 and pre-caspase 3 (Fig.A.3B, Left panel). These results suggested that the C-PC/ β triggered 686LN-M4C1 cell apoptosis by activation of extrinsic cell death pathway. We also analyzed the cell cycle progression of 686LN-M4C1 cells under the C-PC/ β treatment using FACS. The cell cycle profiles were monitored 24 hours after C-PC/ β treatment. An accumulation of cells with 2N DNA contents and a decrease in cells with 4N DNA contents was evident by comparing to those of untreated cells (Fig.A.3B, Right panel). This result indicated that 686LN-M4C1 cells were mainly accumulated in the phase of G0/G1 after the cells were treated with the C-PC/ β . In addition, an increase in cells with a sub-G1 DNA content was clearly observed, which is a characteristic of cells undergoing apoptosis (Fig.A.3B, Right panel) [13]. This observation provides an additional support for our conclusion that C-PC/ β treatment induces apoptosis.

A.4.4 Recombinant C-PC/ β was accumulated on the plasma membrane

The preceding experiments suggested that C-PC/ β treatment inhibited cancer cell proliferation and induced apoptosis. C-PC/ β treatment activated caspase and led cell cycle arrest. To understand the molecular basis for the apoptotic induction and cell cycle arrest, we examined

localization of the recombinant C-PC/ β in cells after the treatment. We employed Immunofluorescent staining to detect the GST:C-PC/ β in 686LN-M4C1 cells using antibody against GST. The recombinant GST:C-PC/ β was mainly stained on the cell plasma-membrane (Fig.A.3C). While the membrane staining pattern was not observed with non-cancer cells (data not shown). Interestingly, the accumulation of membrane C-PC/ β correlated with the degree of cell apoptosis (Compare Fig.A.3A to Fig.A.3C). This observation suggested a potential role of plasma-membrane C-PC/ β in cell apoptosis.

A.4.5 C-PC/ β interacted with β -tubulin in the cell membrane promoting depolymerization of microtubules

Since the recombinant C-PC/ β was mainly accumulated on the cancer cell membrane, we attempted to probe the protein or protein complex that interacted with C-PC/ β in the plasma membrane. To this end, we carried out a GST-pull down experiment with membrane extracts made from 686LN-M4C1 cells using GST:C-PC/ β . We found that a 55 kDa and a 36 kDa protein bands were among the proteins that specifically associated with GST:C-PC/ β (Fig.A.4A). MALDI-(ms/ms) analyses (Fig.A.4B) and immunoblot results (Fig.A.4C) showed that the 55 kDa band was β -tubulin ([gi|57209813](#), NCBI) and 36 kDa band was Glyceraldehyde-3-phosphate dehydrogenase (GAPDH) ([gi|31654](#), NCBI). The interactions of C-PC/ β with β -tubulin and GAPDH were further confirmed by co-immunoprecipitation experiments using antibodies against β -tubulin and GAPDH with the cell extracts made from C-PC/ β treated 686LN-M4C1 cells. It was clear that GST:C-PC/ β co-immunoprecipitated with β -tubulin and GAPDH separately (Fig.A.4D).

C-PC/ β interacted with β -tubulin. We asked whether microtubules were affected by this interaction. We examined the ratio of depolymerized/polymerized tubulin in 686LN-M4C1 cells

by immunoblotting under C-PC/ β treatment. The ratio of depolymerized/polymerized tubulin was approximately 0.949 for C-PC/ β treated cells, and was 0.371 for PBS treated cells (Fig.A.5A, right panel). This data suggest that the microtubules were depolymerized under the treatment of the β subunit protein of C-PC. Interestingly, we found that the microfilaments were also depolymerized under the treatment of the C-PC/ β . The ratio of depolymerized/polymerized actin was approximately 0.721 for the C-PC/ β protein treated cells and was 0.211 for PBS treated cells (Fig.A.5A, right panel). Thus, our results demonstrated that C-PC/ β interacted with β -tubulin in the cell membrane promoting depolymerization of cytoskeleton, microtubules and microfilaments.

A.4.6 C-PC/ β interacted with GAPDH and promoted GAPDH redistribution

Interaction of C-PC/ β with GAPDH is intriguing. Biological functions of GAPDH are dependent upon the subcellular localization [14]. The nuclear form of GAPDH has been suggested to be a key transcriptional coactivator necessary for entry into S phase [15] [16]. We have observed the effects of C-PC/ β on cell cycle progression. The cells were arrested in the G0/G1 phase under the treatment of the C-PC/ β . We reasoned that C-PC/ β treatment might have effects on GAPDH cellular localization. To this end, we examined the level of GAPDH in the cell nucleus and cytoplasm by immunoblotting the GAPDH in the nuclear and whole cell lysate made from cells before and after C-PC/ β treatment. It was clear that the level of nuclear GAPDH was greatly decreased after the incubation with the C-PC/ β protein for 24 hours (Fig.A.5B). Interestingly, more GAPDH was expressed under the treatment of the C-PC/ β (Fig.A.5B). This might be the result of feedback from decrease in nuclear form of GAPDH. The effects of C-PC/ β treatment on the distribution of GAPDH were likely specific, since no changes in the distribution of β -tubulin and Histone H2A were observed (Fig.A.5C).

A.5 Discussion

In present study, we demonstrated that the recombinant C-PC/ β inhibited cell proliferation and induced apoptosis. We believe that the C-PC/ β inhibits cell proliferation and promotes apoptosis by promoting cytoskeleton depolymerization and activating the caspase activities that are associated with extrinsic cell death pathway. Interestingly, the C-PC/ β causes cells to arrest at G0/G1 phase of cell cycle. Our data showed that C-PC/ β treatment led to the export of GAPDH from the nucleus. It is conceivable that GAPDH nuclear exporting stimulated by C-PC/ β treatment causes the cell cycle arrest, which subsequently inhibits cell proliferation. The ability of recombinant C-PC/ β to preferentially inhibit cancer cell growth and induce cancer cell apoptosis is very important. This property may indicate a potential application of C-PC/ β as a cancer prevention and/or treatment agent. Especially, we observed in our studies that C-PC/ β exhibited the greatest effects on metastatic cancer cells compared to non-metastatic cancer cells. Thus, it is tempting to speculate and explore the potentials of using C-PC/ β as an agent for preventing tumor metastasis. The mechanism by which C-PC/ β co-precipitated with GAPDH in the GST-pull down is not clear. Previous reports show that β -tubulin is targeted to the membrane through association with GAPDH [17] [18] [19]. We suspected that the C-PC/ β interacted with β -tubulin. GAPDH was co-precipitated due to association with β -tubulin. Actin filaments were reported to be associated with GAPDH under unbeneficial (Stress) environments [20]. We reasoned the depolymerization of actin might result from the association with GAPDH under the apoptotic induction by C-PC/ β . Depolymerization of cytoskeleton, microtubules and microfilaments, also provides a good explanation for the observed cell morphology changes under the C-PC/ β treatments. How the C-PC/ β promotes reduction of nuclear GAPDH level is an open question. Our current speculation is, under the treatment of the C-PC/ β proteins, GAPDH is

indirectly targeted by the C-PC/ β and recruited to the plasma membrane. This may not only prevent the GAPDH nuclear translocation but also promote nuclear export of GAPDH. If the amount of the GAPDH in the nucleus is lowered to a certain level, it then prevent cells from entering into S phase [15]. Lower level of nuclear GAPDH will in turn activate the expression of GAPDH. It is intriguing that C-PC/ β treatment activates caspase-3 and -8, which subsequently triggers cell apoptosis. It was reported that the biliprotein α/β :C-PC purified from blue-green algae also induces cell apoptosis [6] [8] [7]. However, the mechanism by which the α/β :C-PC triggers apoptosis seems different from the mechanism by which C-PC/ β induces apoptosis. In addition, the α/β :C-PC enter cytoplasm of cancer cells [7], the recombinant C-PC/ β was mainly accumulated on the plasma membrane. Under the C-PC/ β treatment, cytoplasm GAPDH might be associated with actin and trigger the depolymerization of the actin. It is suggested that GAPDH is associated with apoptosis [21, 22]. No evidence demonstrates that α/β :C-PC has any effects on cytoplasm or nuclear GAPDH. In this regard, our studies seem to suggest that the recombinant β subunits of C-PC may be a more effective in inhibition of cell proliferation and apoptosis induction than α/β :C-PC does.

A.6 References

1. Yoshida, A., Y. Takagaki, and T. Nishimune, *Enzyme immunoassay for phycocyanin as the main component of spirulina color in foods*. Biosci Biotechnol Biochem, 1996. 60(1): p. 57-60.
2. Saxena, A.M., *Phycocyanin aggregation. A small angle neutron scattering and size exclusion chromatographic study*. J Mol Biol, 1988. 200(3): p. 579-91.
3. Romay, C., N. Ledon, and R. Gonzalez, *Further studies on anti-inflammatory activity of phycocyanin in some animal models of inflammation*. Inflamm Res, 1998. 47(8): p. 334-8.
4. Romay, C., et al., *Antioxidant and anti-inflammatory properties of C-phycocyanin from blue-green algae*. Inflamm Res, 1998. 47(1): p. 36-41.
5. Bhat, V.B. and K.M. Madyastha, *C-phycocyanin: a potent peroxy radical scavenger in vivo and in vitro*. Biochem Biophys Res Commun, 2000. 275(1): p. 20-5.

6. Pardhasaradhi, B.V., et al., *Phycocyanin-mediated apoptosis in AK-5 tumor cells involves down-regulation of Bcl-2 and generation of ROS*. Mol Cancer Ther, 2003. 2(11): p. 1165-70.
7. Subhashini, J., et al., *Molecular mechanisms in C-Phycocyanin induced apoptosis in human chronic myeloid leukemia cell line-K562*. Biochem Pharmacol, 2004. 68(3): p. 453-62.
8. Reddy, M.C., et al., *C-Phycocyanin, a selective cyclooxygenase-2 inhibitor, induces apoptosis in lipopolysaccharide-stimulated RAW 264.7 macrophages*. Biochem Biophys Res Commun, 2003. 304(2): p. 385-92.
9. Pan, H., et al., *Detection of hepatotoxic Microcystis strains by PCR with intact cells from both culture and environmental samples*. Arch Microbiol, 2002. 178(6): p. 421-7.
10. Huang, Y. and Z.R. Liu, *The ATPase, RNA unwinding, and RNA binding activities of recombinant p68 RNA helicase*. J Biol Chem, 2002. 277(15): p. 12810-5.
11. Mosmann, T., *Rapid colorimetric assay for cellular growth and survival: application to proliferation and cytotoxicity assays*. J Immunol Methods, 1983. 65(1-2): p. 55-63.
12. Sasaki, J., et al., *The anthelmintic drug mebendazole induces mitotic arrest and apoptosis by depolymerizing tubulin in non-small cell lung cancer cells*. Mol Cancer Ther, 2002. 1(13): p. 1201-9.
13. Pozarowski, P. and Z. Darzynkiewicz, *Analysis of cell cycle by flow cytometry*. Methods Mol Biol, 2004. 281: p. 301-11.
14. Sirover, M.A., *New insights into an old protein: the functional diversity of mammalian glyceraldehyde-3-phosphate dehydrogenase*. Biochim Biophys Acta, 1999. 1432(2): p. 159-84.
15. Zheng, L., R.G. Roeder, and Y. Luo, *S phase activation of the histone H2B promoter by OCA-S, a coactivator complex that contains GAPDH as a key component*. Cell, 2003. 114(2): p. 255-66.
16. Sirover, M.A., *New nuclear functions of the glycolytic protein, glyceraldehyde-3-phosphate dehydrogenase, in mammalian cells*. J Cell Biochem, 2005. 95(1): p. 45-52.
17. Tisdale, E.J., *Glyceraldehyde-3-phosphate dehydrogenase is phosphorylated by protein kinase Ciota /lambda and plays a role in microtubule dynamics in the early secretory pathway*. J Biol Chem, 2002. 277(5): p. 3334-41.
18. Glaser, P.E., X. Han, and R.W. Gross, *Tubulin is the endogenous inhibitor of the glyceraldehyde 3-phosphate dehydrogenase isoform that catalyzes membrane fusion*:

Implications for the coordinated regulation of glycolysis and membrane fusion. Proc Natl Acad Sci U S A, 2002. 99(22): p. 14104-9.

19. Muronetz, V.I., et al., *Binding constants and stoichiometries of glyceraldehydes 3-phosphate dehydrogenase-tubulin complexes.* Arch Biochem Biophys, 1994. 313(2): p. 253-60.

20. Schmitz, H.D. and J. Bereiter-Hahn, *Glyceraldehyde-3-phosphate dehydrogenase associates with actin filaments in serum deprived NIH 3T3 cells only.* Cell Biol Int, 2002. 26(2): p. 155-64.

21. Schmitz, H.D., *Reversible nuclear translocation of glyceraldehyde-3-phosphate dehydrogenase upon serum depletion.* Eur J Cell Biol, 2001. 80(6): p. 419-27.

22. Chuang, D.M., C. Hough, and V.V. Senatorov, *Glyceraldehyde-3-phosphate dehydrogenase, apoptosis, and neurodegenerative diseases.* Annu Rev Pharmacol Toxicol, 2005. 45: p. 269-90.

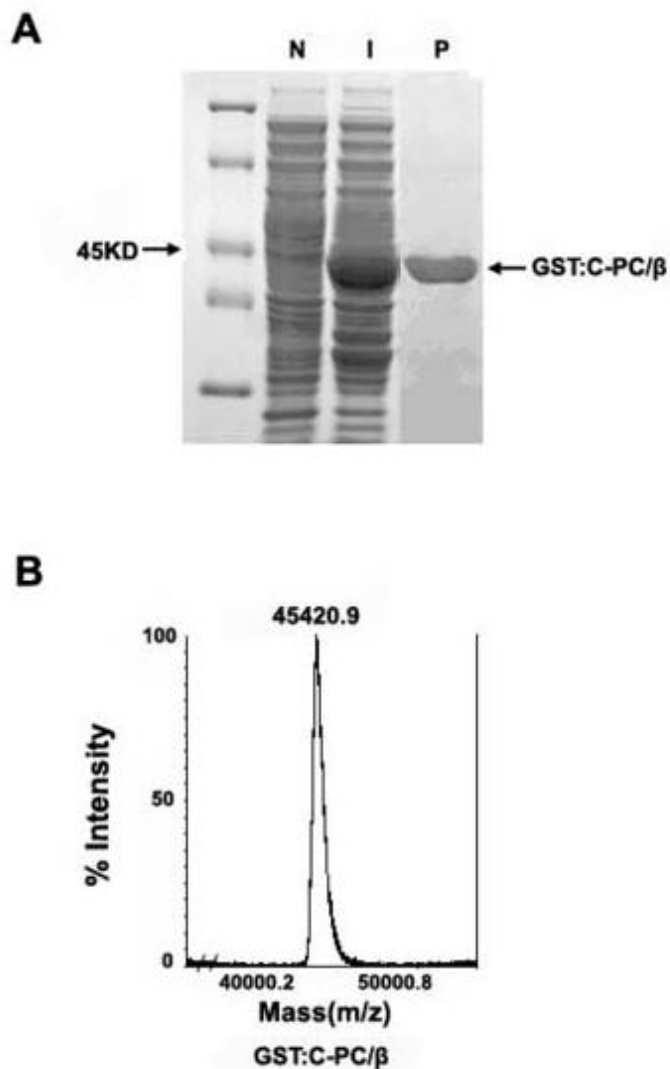


Figure A.1 (A) Expression of recombinant GST:C-PC/β expressed in *E. coli* BL 21. Bacterial cell lysates was analyzed by 10% SDS-PAGE, before IPTG induction (N), after IPTG inducing (I), and after purification (P). (B) Purified recombinant GST:C-PC/β was analyzed by mass spectrometry.

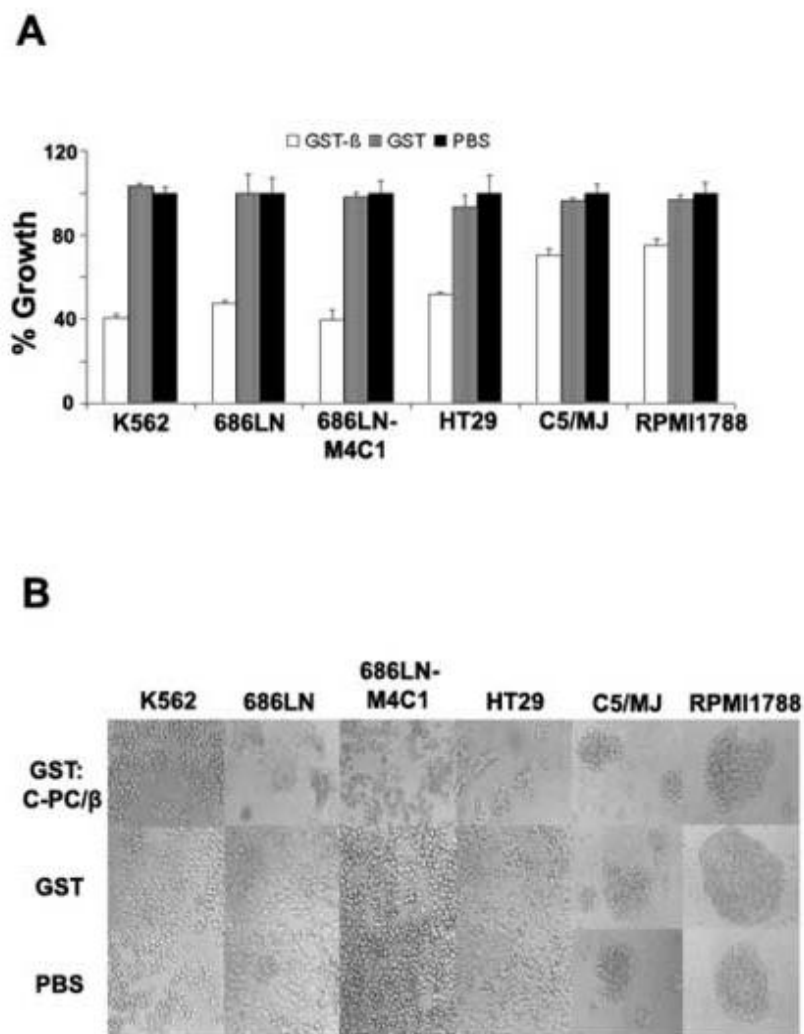


Figure A.2 (A) MTT assays of cell proliferation of different cell lines (indicated) upon treatments of different agents (indicated). The cell proliferations were expressed as percentage of growth and were calculated in comparison to PBS treated cells. Values were calculated as mean \pm S.D. of triplicate measurements ($P < 0.05$). **(B)** Morphologies of different cell lines (indicated) upon the treatments of 5 μ M of GST:C-PC/ β or other agents (indicated).

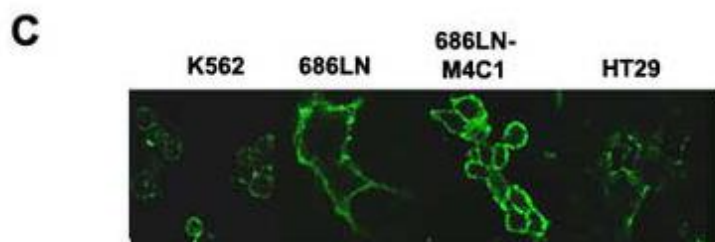
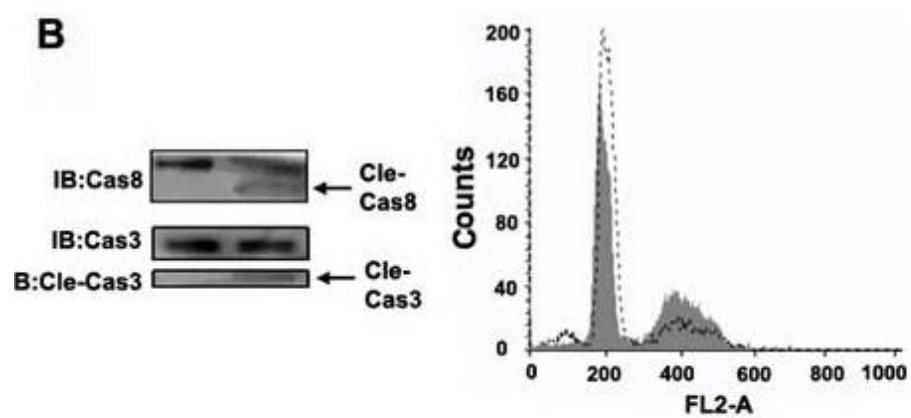
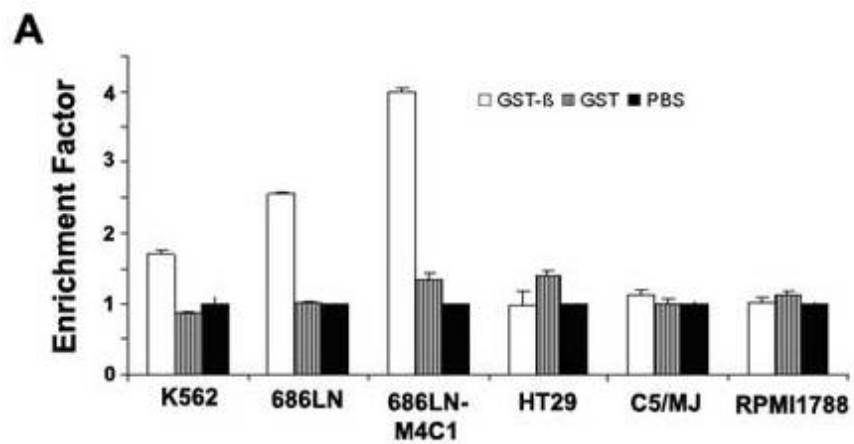


Figure A.3 (A) Apoptosis of different cell lines (indicated) upon the treatment via different agents (indicated). The apoptosis was expressed as the enrichment of mono- and oligonucleosomes released into the cytoplasm. (B, left panel) Immunoblot analyses of cellular caspase -3 and -8 (Cas3 or Cas8) in cell extracts made from 686LN-M4C1 cells that were treated with C-PC/ β or PBS using antibodies against Cas3 or 8. The arrows indicate the cleavage products of caspases (Cle-Cas8, or Cle-Cas3). (B, right panel) FACS analyses of cell cycle for 686LN-M4C1 cells upon the treatment of PBS (shaded) or C-PC/ β (dotted line). Cells were analyzed for DNA content by PI staining (FL2-A) and flow cytometry. (C) Immunofluorescence staining of GST:C-PC/ β in different cell lines (indicated) upon 5 μ M GST:C-PC/ β treatment using antibody against GST. The green signal represents staining of GST:C-PC/ β .

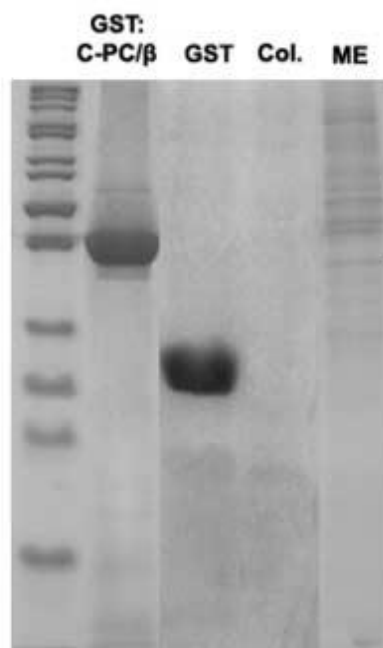
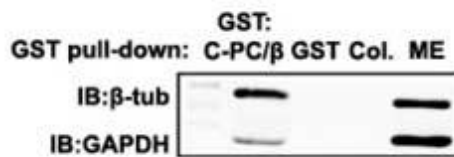
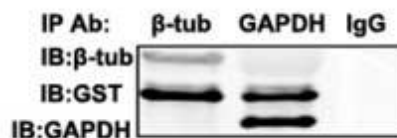
A**B****C****D**

Figure A.4 (A) SDS-PAGE analyses of the GST:C-PC/ β pull-downs from the membrane extracts made from 686LN-M4C1 cells. The GST moiety, the column (Col.), and the membrane extracts (**ME**) were used as controls. Arrows indicate the protein bands that associate with C-PC/ β . (B) MALDI/TOF/TOF-MS analyses of the C-PC/ β association proteins. Bold characters indicate the sequences identified by mass-spectroscopy. (C) Immunoblot analyses of the GST:C-PC/ β pull-downs by immunoblot using antibodies against β -tubulin (IB: β -tub) and against GAPDH (IB:GAPDH). (D) Co-immunoprecipitation of GST:C-PC/ β by the antibodies (IP:Ab) against β -tubulin (β -tub) and GAPDH (GAPDH) was analyzed by immunoblot the co-precipitates using appropriate antibodies (indicated). IP by mouse IgG was a control for the co-immunoprecipitation.

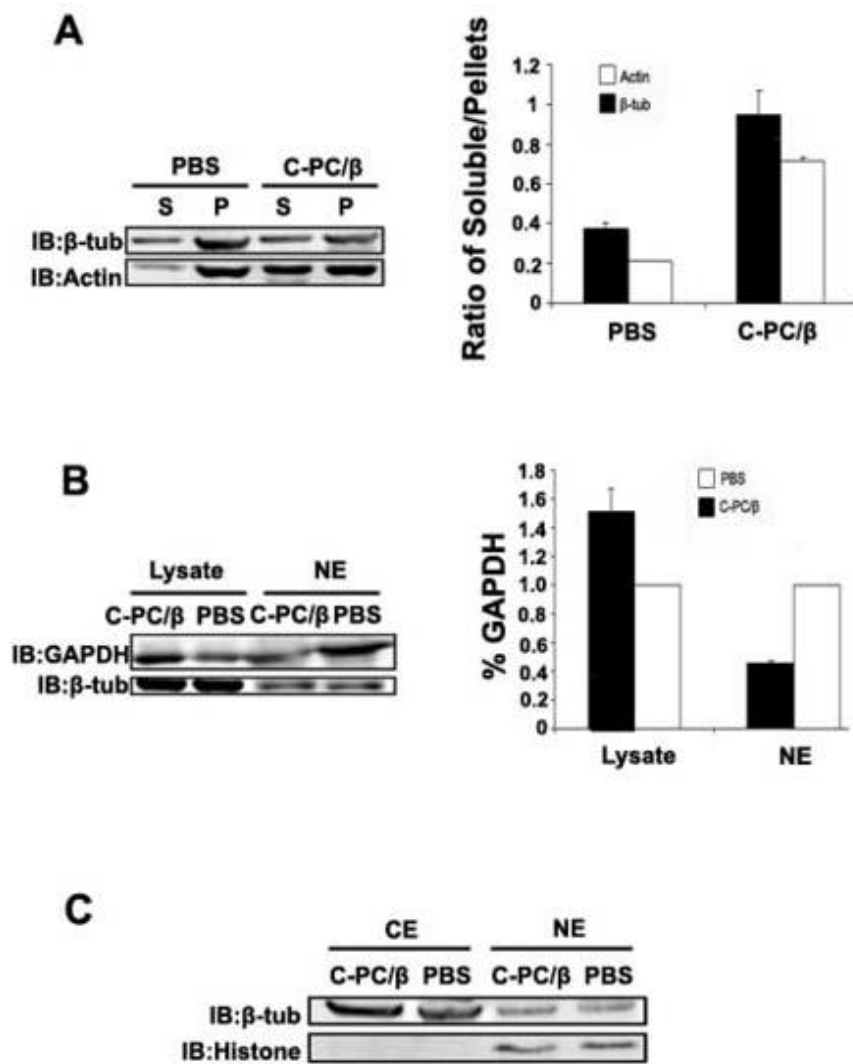


Figure A.5 (A) Immunoblot analyses of soluble (S) tubulin and actin and insoluble (P, precipitates) tubulin and actin in the soluble and insoluble extracts made from the PBS or C-PC/ β treated 686LN-M4C1 cells (**left panel**). Right panel is the quantification of the immunoblotting results expressed as the ratio of soluble/insoluble tubulin (filled bars) and actin (open bars). (B) Immunoblot analyses of cellular (**lysate**) and nuclear (**NE**) levels of GAPDH in PBS or C-PC/ β treated 686LN-M4C1 cells. IBs of β -tubulin (β -tub) was a loading control. Right panel is the quantification of the immunoblotting of GAPDH. The quantification was expressed as relative GAPDH levels in nuclear extracts or in total cell lysate by defining the GAPDH levels in nuclear extracts or in total cell lysate made from PBS treated cells as 1% (open bars). (C) Immunoblot analyses of cytoplasmic (**CE**) and nuclear (**NE**) levels of β -tubulin and Histone H2A in PBS or C-PC/ β treated 686LN-M4C1 cells.

B. P68 IS A POTENTIAL SUBSTRATE OF CASPASE 3

B.1 Materials and methods

B.1.1 Apoptosis induction of SW480 cells by Oxiplantin

10uM of Oxiplantin was added into the culture medium. Cells were cultured for additional 24 hours. Cells were then collected and the whole cell lysate was obtained. The anti-cleaved-Caspase 3 antibodies were used to examine whether Caspase 3 was activated. Antibodies recognizing N-terminal or C-terminal (RGG) of p68 were used to examine whether p68 was cleaved by the activated Caspase 3. The inhibitor for Caspase 3 (DEAD-CHO) was used to block the activity of Caspase 3. The recombinant Caspase 3 (active) was used to cleave the target proteins under *in vitro* situation.

B.1.2 Plasmids construction and truncates of p68 expression

The DNA sequences encoding four truncates of p68 were constructed into the pHM6 vector at the HindIII and NotI digestion sites respectively. The primers for F1 truncate were 5'-GGGAAGCTTATATTCGAGTGACCGAGACCG-3' and 5'-GGGCGGCCGCTTAGTCTGCTTCATCAAGGACAAGG-3'. The primers for F2 truncate were 5'-GGGAAGCTTAAGAATGCTTGATATGGGCTTTG-3' and 5'-GGGCGGCCGCTTAATCTTCCACATCTAGCCCTCT-3'. The primers for F3 truncate were 5'-GGGAAGCTTAGTGAAATTTGTCATCAATTATGAC-3' and 5'-GGGCGGCCGCTTAGTCCCGACGGTCATCCTTC-3'. The primers for F4 truncate were 5'-GGGAAGCTTACGATACTCTGCGGGCAAAGG-3' and 5'-GGGCGGCCGCTTATTGGGAATATCCTGTTGGCATT-3'. The sequences were then cloned into virus vector. SW480 cells were expressed with four different truncated proteins respectively. The activation of Caspase 3 was examined in SW480 cells two days post-transfection.

B.2 Results

B.2.1 Three putative cleavage sites of p68 by Caspase 3

There are three putative cleavage sites in p68 based on the sequence analysis (Fig.B.1.A). All putative cleavage sites in p68 are exposed for Caspase 3 according to the location of the cleavage sites in the predicted helicase core structure (Fig.B.1.B).

B.2.2 P68 can be cleaved by Caspase 3

Four truncates of p68 were detected by running western-blot when SW480 cells were induced into apoptosis. And the molecular weight of the protein bands match to the predicted truncates (Fig.B.2.A and B): F1 (~25kDa), F2+F3+F4 (~43kDa), F3+F4 (~22.8kDa), and F4 (~13kDa). Caspase 3 was activated when the cells were induced into apoptosis as we expected. Interestingly, the cleaved truncates of p68 (protein bands) were no longer observed by running western blot (Fig.B.2.B) when the cells were treated with the Caspase 3 inhibitor DEVD-CHO. The truncates of p68 were observed again on the western blot when the same cell lysates were incubated with active Caspase 3. This supports the idea about that p68 can be specifically cleaved by the active Caspase 3. The recombinant p68 was cleaved by the active Caspase 3 *in vitro* further confirmed that p68 is the substrate of active Caspase 3 (Fig.B.2.C). However, only two fragments (~55kDa and 43kDa) of p68 were observed in SDS gel according to the result of *in vitro* cleavage assay.

B.2.3 Expression of F4 truncate of p68 activates Caspase 3 in cells

The plasmids encoding F1, F2, F3, and F4 were successfully cloned into the pHM6 vector (Fig.B.3.A). The plasmids were then cloned into the virus vectors respectively and the truncates of p68 were successfully expressed in SW480 cells (Fig.B.3.B). Interestingly, Caspase 3 was activated under the expression of those four truncates at different levels (Fig.B.3C).

Caspase 3 was activated most when the cells were expressed with F4 truncate. This result indicates that the cleavage product of p68 by Caspase 3 has a positive feedback function in cell apoptosis.

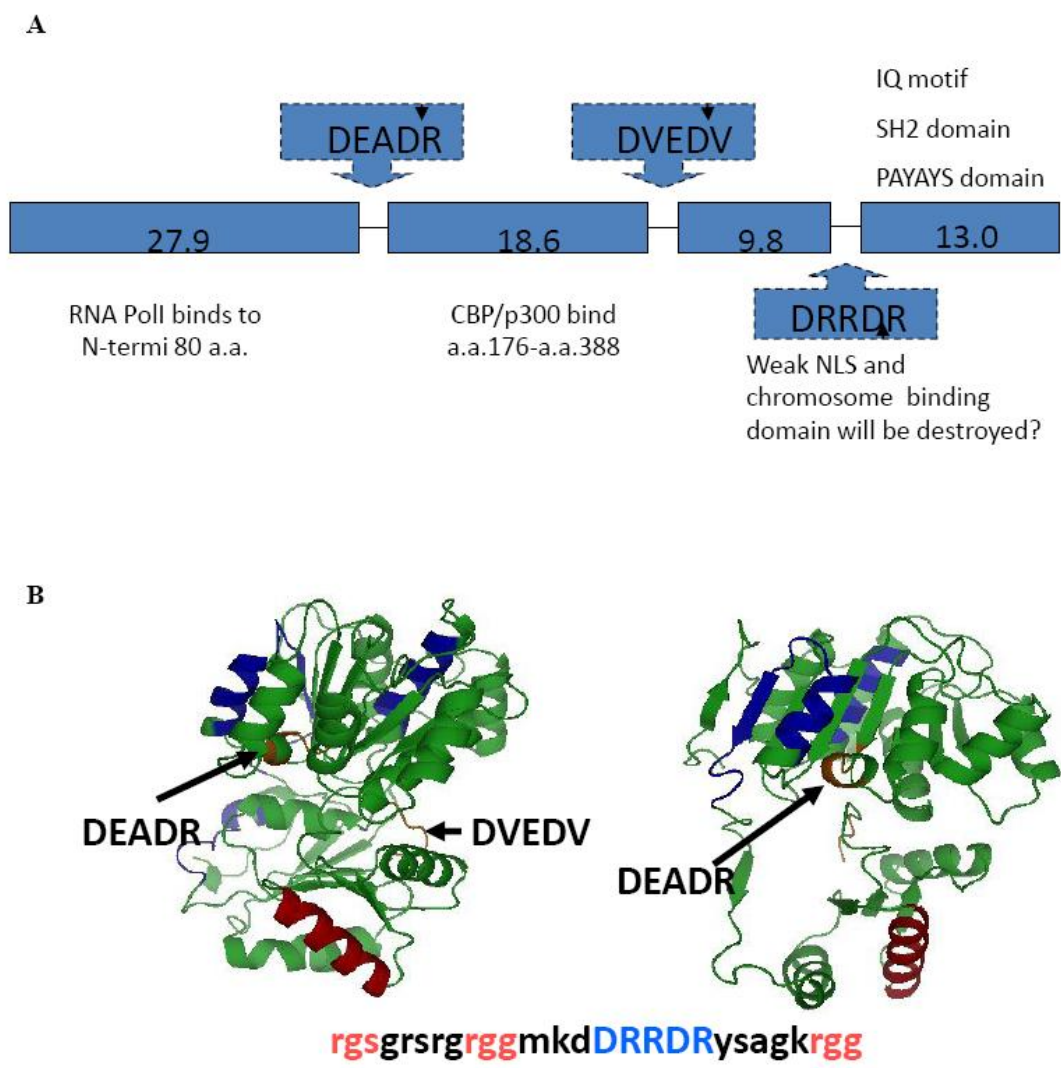


Figure B.8 Three putative cleavage sites of p68 by active Caspase 3

A) Diagram of the putative cleavage sites of p68 by Caspase 3. B) The location of predicted cleavage sites on the helicase core structure of p68.

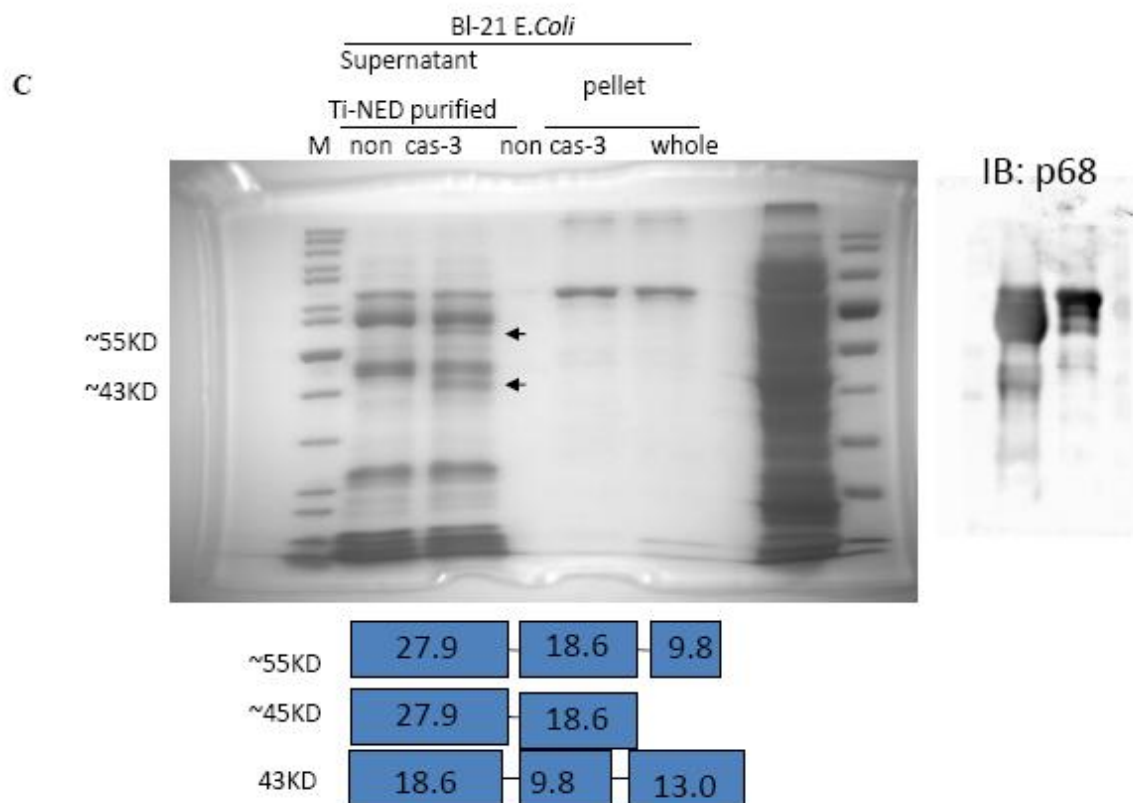
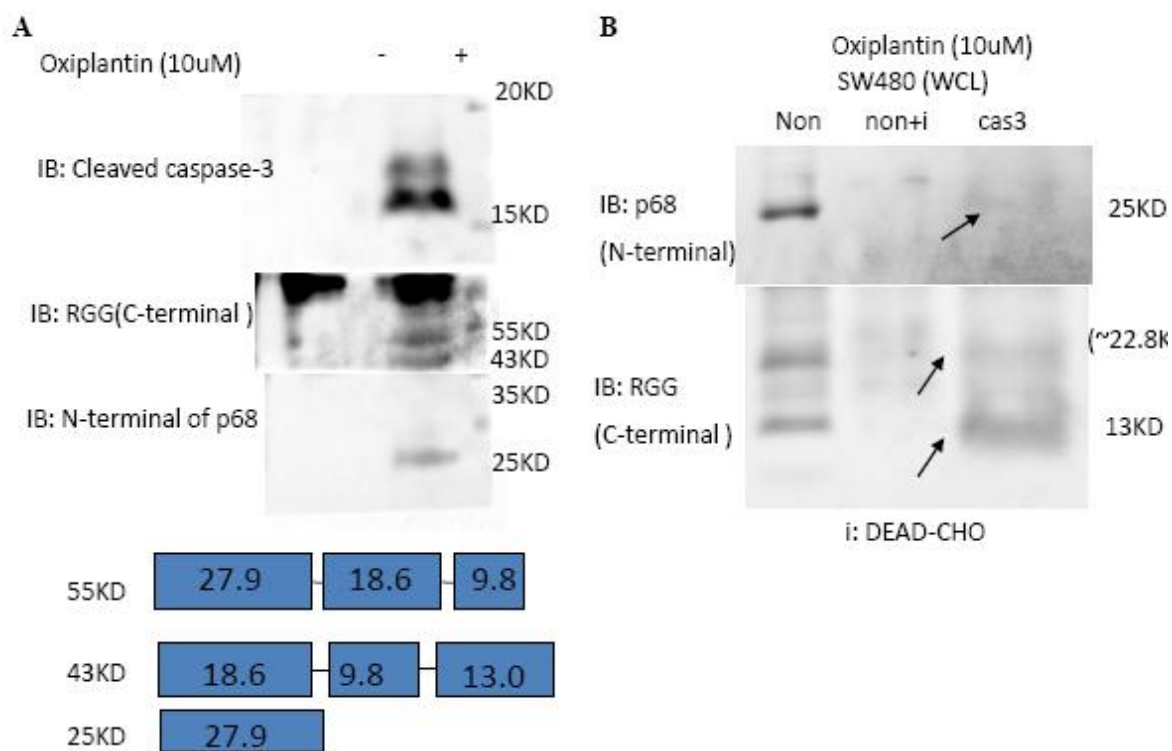


Figure B. 2 P68 was cleaved by the activated Caspase 3

A) Oxiplantin induced cell apoptosis and Caspase 3 was activated. Three truncates of p68 were detected by two different antibodies which recognize N-terminal and C-terminal of p68 respectively. B) The cleavage of p68 under the treatment of Oxiplantin was prevented when the cells were incubated with the DEAD-CHO, a Caspase 3 inhibitor. P68 was cleaved again when the cell lysate was added with the active Caspase 3. C) The protein fragments of recombinant p68 were generated under *in vitro* Caspase 3 cleavage assay. IB of p68 was used to identify that recombinant p68 was successfully pulled down by the Ti-NED beads. The blue boxes indicate the putative combination of the protein fragments of p68.

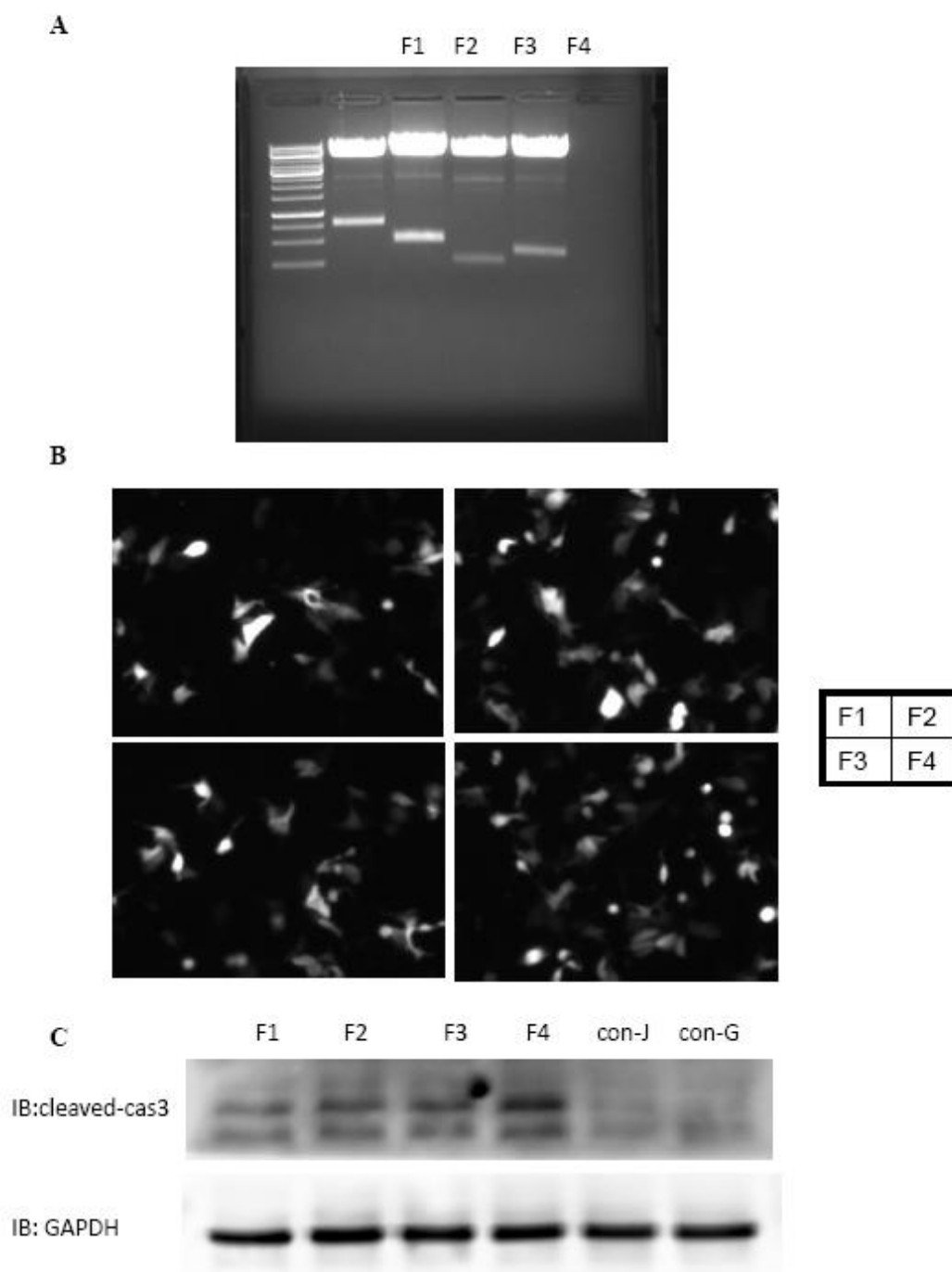


Figure B.3 Caspase 3 was activated upon the expression of truncates of p68

A) F1, F2, F3 and F4 truncates of p68 encoding plasmids was successfully constructed. The plasmids were confirmed by digestion with HindIII and NotI. B) The expression of four truncates of p68 (expressing eGFP) in SW480 cells were confirmed by fluorescent images of cells as indicated. C) Western blot showed that Caspase 3 was activated by overexpression of the four different truncates of p68 in cells.

C. P68/CAM MAY HAVE A FUNCTION IN PC-12 DIFFERENTIATION

C.1 Material and method

PC-12 cells were gifted by Dr. Keqiang Ye in Emory University. RPMI1640 medium contains 10% FBS and 5% Horse Serum was used to culture PC-12 cells for 3 days. On the fourth day, the cells were seeded with low density (~10%) in plates which had been coated with poly-L-lysine. The medium was replaced with RPMI1640 medium contains 2% FBS and 100 ng/ml NGF (CalBiochem, cat. 480352). The medium was changed everyday for 4-5 days till the cells were well differentiated. The cells were fixed on the different day as indicated in the figure. The fixed cells were penetrated by the Triton-100 as we did previously. And anti-p68 antibodies and anti-calmodulin antibodies were used to show the locations of p68 and calmodulin in the differentiated cells.

C.2 Result

C.2.1 P68 and calmodulin colocalized at the leading edge of the dendrites in PC-12 cells

PC-12 cells were successfully differentiated (Fig.C.1). Interestingly, p68 was found to be accumulated at the leading edge of the dendrites during differentiation. Calmodulin was found to colocalize with p68 at the leading edge of the dendrites. The results indicated that p68 together with calmodulin may have function in the formation of the dendrites which plays important roles during the differentiation of PC-12 as well as other neuron cells.

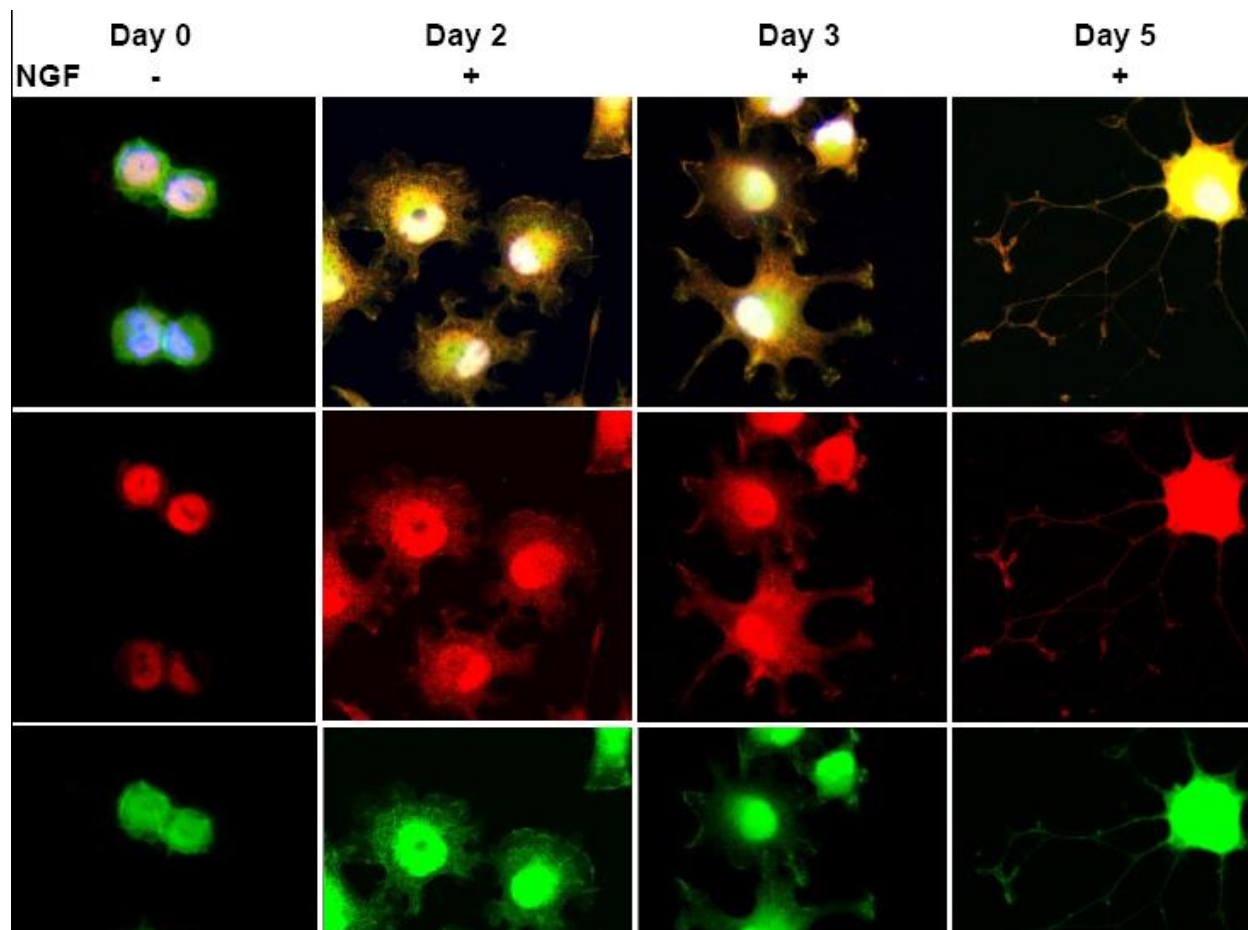


Figure C.1 P68 and calmodulin colocalized at the leading edge of the dendrites in PC-12 cells

Day 0 indicates the day the cells were seeded into the chamber but without the treatment of NGF.

Day 2 indicates the cells were treated with NGF for two days. So do the day 3 and the day 5. In

the images, red presents for p68, and green presents for calmodulin. Yellow indicates the colocalization of p68 and CaM (Red and green). Blue shows the nuclei of PC-12 cells.